Sequence stratigraphy and basin analysis of the Meso- to Cenozoic Tarfaya- Laâyoune Basins, on- and offshore Morocco

INAUGURAL-DISSERTATION
zur
Erlangung der Doktorwürde
der
Naturwissenschaftlich-Mathematischen Gesamtfakultät
der
Ruprecht-Karls-Universität
Heidelberg

vorgelegt von
Dipl.-Geol. Axel Adrian Oliver Wenke
aus der Heidelberger Altstadt

Gutachter 1: Priv. Doz. Dr. Rainer Zühlke
Institut für Geowissenschaften, Ruprecht-Karls-Universität, Heidelberg
Postanschrift:
Saudi Arabian Oil Company (Saudi Aramco)
PO Box 9261, Dhahran, 31311, Saudi Arabia

Gutachter 2: Prof. Dr. Harald Stollhofen
Geozentrum Nordbayern, Friedrich-Alexander Universität Erlangen-Nürnberg
Schloßgarten 5, D-91054, Erlangen, Deutschland

Tag der mündlichen Promotionsprüfung: 18. 12. 2014

Meinen Eltern

Abdelouahed Lmoubessine of ONHYM inspecting clastic series of the proximal Tan Tan Delta near Abteh.

Acknowledgements

This thesis is a partial outcome of the Atlantic Margin Project, a joint venture between ONHYM, RWE Dea, GeoResources STC, Heidelberg University, RWTH Aachen and Kiel University (CAU). My sincere thanks go to all project members who made both the Atlantc Margin Project as well as performing and writing this PhD thesis a great and successful experience.

First of all I am very grateful to ONHYM for the data provision, administrative support, persistent interest in the progress of the project, fruitful geological discussions, an excellent introduction to the regional geology of the Tarfaya-Laâyoune area in the field and finally the permission to publish the results of the thesis, particularly to Haddou Jabour, Driss Bouhaddioui, Lahcen Boutib, and Abdelouahed Lmoubessine.

I am very much obliged to RWE Dea for inititating, funding, and managing the project, especially to Oliver Kluth, Axel Emmerich (now at EnBW), Torge Schümann and Bastian Wirth.

I want to thank my supervisor Rainer Zühlke (now at Saudi Aramco) very much for inducing my interest in sedimentology, allocating the thesis topic, his supervision in the field and in front of the computer, as well as in pointing me in the direction of my next important career step.
My second supervisor, Thilo Bechstädt (now at Jagiellonian University, Kraków) motivated and supported me during the whole period of the preparation of this thesis. For this, I am indebted to him.

For the adoption of the second report I am very grateful to Harald Stollhofen from the Geozentrum Nordbayern, Erlangen University. For joining the Disputation my thanks go to Bernhard Höfle and Norbert Becker.

For a wonderful time and lively discussions in the field, during core screening and during project meetings I want to thank my researching project members Sajid Ali, Mohamed Aquit, Björn Heise, Victoria Sachse, Manuel Sehrt, and Martin Wipf.

The evaluation of geophysical data in basin scale needs powerful software. For the deployment and teaching of the Petrel suite I am indebted to Schlumberger, in particular Martin Neudecker, Sonat Kaya and Michel Hamers (now at Chevron). For granting access to and training in the use of OpendTect SSIS I want to thank dGB Earth Sciences, especially Paul de Groot, Eric Crepin Bouanga, Geert de Bruin (now at TNO), and Farrukh Qayyum. For the access to PHIL I am grateful to Scott Bowman at Petrodynamics.

The thesis would never had found an end without the work of my research assistents. For their efforts, entertainment in the computer lab and delivering great results I want to thank Sebastian Dedera, Lukasz Gregorczyk (now at Eriksfjord), Georg Miernik, Ludwig Mroszewski, Andreas Rittersbacher (now at Statoil),

Special thanks go to my peers at Heidelberg University Jorham Contreras (now at Xenith Pty), Dominik Hennhöfer, Ewa Patrizia Kissner (now at Exxon), Christian Lorson, Lennart Rohrer and Dominik Soyk.

For fruitful discussions during the time of writing and having a look at my written language I want to thank my colleagues Hans Aronsen, Ingebrigt Aspelund, Birgit Dietrich, Lisa Burton, Lisa Michelsen, Eric Mathey, Andrew McGill, Rudie van der Meer, Marian Morris, Grant Scott, Naoufal Sellam, and Jeremy Watt.

This thesis was performed part-time. For the flexibility, tolerance, sympathy and support during the six years of studying. I want to thank my former employer Horst Kreuter, CEO of GeoThermal Engineering GmbH and my managers in Statoil Marian Morris, Kerstin Schemmann, Noralf Steinsland and Dan Tuppen. For the permission to print Figure 10 I am very thankful to Überlandwerk Groß-Gerau.

...and last but not least many thanks to my family, Anne, Philip, Konrad, Nina, Rebekka, my parents and sisters for their patience and support. You are wonderful!

Abstract

With the initiation of rifting in the Late Permian (Kazanian; 259.3 Ma) and the onset of drifting in the Early Jurassic (Pliensbachian/Toarcian 189.6 Ma), the Tarfaya-Laâyoune Basins are part of the oldest passive continental margin segments in the Atlantic domain.

A basin analysis of the Tarfaya-Laâyoune Basins has been performed based outcrop data, well data, and a multi 2D-seismic survey dataset. Present organo-geochemical, heavy mineral, and thermochronological studies have been considered. The workflow includes: i) post-processing /filtering of seismic data, ii) outcrop and well data screening, iii) seismic interpretation, iv) sequence stratigraphy, v) time/depth conversion, and vi) numerical reverse modeling.

The Meso-/Cenozoic basin fill is bound by two superordinated unconformities. The Initial Rift Unconformity (IRU, 259.3 Ma) at the base and the seafloor at the top represents an incomplete 1st order sequence. This sequence can be subdivided into two phases, a transgressive phase and a regressive phase. The change between transgression and regression takes place during the Late Cretaceous, which marks the onset of basin inversion.

Six 2nd order tectonic sequences are bound at the top by major unconformities: i) the rift stage by the Initial Drift Unconformity (IDU, 189.6 Ma), ii) the early drift stage by the Mature Drift Unconformity (MDU, 144.2 Ma), iii) the mature drift stage by the Peak Spreading Unconformity (PSU, 112.2 Ma), iv) the mature drift stage with initial Atlasian convergence by the Initial Atlasian Unconformity (IAU, 65 Ma), v) the mature drift stage with initial Atlasian compression and uplift by the Peak Atlasian Unconformity (PAU, 28.5 Ma), and vi) the mature drift stage with peak Atlasian uplift and erosion is bounded on top by the seafloor (present day).

All 2nd order sequences are characterized by a specific sedimentary environment: the first by an alluvial, fluvial and restricted marine setting, the second by carbonate ramps and platforms, the third by deltaic environments, the fourth by open marine clastic and carbonate deposits, the fifth by the development of a clastic shelf margin wedge and the sixth by terrestrial runoff via deltas and widespread bypass sedimentation.

In total, 31 3rd order sequences and 113 4th order sequences have been identified on three key transects of the dataset. The northern transect is located in the Tan Tan Delta region, the central transect is crossing the Cap Juby oilfield and the southern transect is located at the transition between the Tarfaya and the Laâyoune Basin.

Based on the developed high resolution sequence stratigraphy in combination with well data screening, 13 potential source rock formations have been identified, their distribution circumscribed by using chronostratigraphic plots (Wheeler diagrams). Twelve of these potential source rocks have been deposited during the transgressive phase of the 1st order sequence, one, the source rock of the PETM event, after the onset of basin inversion.

Reservoirs have been identified in the Triassic rift, the Jurassic carbonate, the Early Cretaceous deltaic and the Cenozoic deep marine successions.

With the end of Late Permian to Early Jurassic rifting, subsidence and sediment flux was controlled by far-field intra-plate stresses. Persistent ridge-push during the Early to Late Jurassic with sea floor spreading (SFS) half-rates of 19 mm/y resulted in peak subsidence rates of about 150 m/m.y in outer shelf areas. Sediment supply from the hinterland was inhibited, initially resulting in unfilled accommodation space, subsequently filled by carbonate platforms,

During the Tithonian to Berriasian, the tendency of divergence of the Central Atlantic margins has been reduced by the remaining Gondwana continent. Even though rifting in the South Atlantic started in Late Tithonian/ Early Berriasian, SFS halfrates decreased stepwise to 7 mm/y. Thermo-tectonic uplift in the South Atlantic rift area and decreased ridge push-forces resulted in an uplift of the Central Atlantic passive continental margins. The Jurassic shelf was subaerially exposed during the Berriasian and early Valanginian and major erosion started in the Anti-Atlas and the Sahara Craton. Supplied sediment was transported over the Jurassic shelf and formed the Tan Tan and Boujdour delta complexes on the outer continental shelf to lower slope. Combined flexural and compaction-induced subsidence added up to 120 m/m.y. in outer shelf areas. The delta development continued until the Albian. Its end correlates with initial drifting in the South Atlantic and strongly increasing SFS half-rates up to 24 mm/y in the Central Atlantic. Although ridge-push forces were smaller than in Jurassic times, water depths on the shelf top increased to several hundred meters. Sediment supply from the continent was starved. Cenozoic subsidence and sediment flux history was controlled by Alpine convergence and Atlasian uplift.

Resumée

Avec un épisode de rifting qui a débuté au Wuchiapingien (Permien supérieur, 259.3 Ma) et un début de dérive au Pliensbachien (Jurassique inférieur, 189.6 Ma), le bassin de Tarfaya-Laâyoune (sud du Maroc) est une des plus anciennes marges continentales passives des côtes Atlantiques.

L'étude du bassin a été réalisée à partir de données d'affleurements, de puits et de plusieurs campagnes sismiques 2D. Des analyses organo-géochimiques, thermo-chronologiques, et de minéraux lourds ont été menées. Le plan de travail est le suivant : i) traitement et filtrage des données sismiques, ii) analyse des données d'affleurements et de puits, iii) interprétation sismique, iv) analyse de la stratigraphie séquentielle, v) conversion temps/profondeur et vi) inversion.

Le remplissage du bassin du Mésozoïque au Cénozoïque est délimité par deux discordances majeures : à la base, la discordance correspondant au début du rift (Initial Rift Unconformity, IRU, 259.3 Ma) et au sommet, le plancher océanique, englobant une séquence de 1er ordre incomplète. Cette séquence est subdivisée en deux phases, une transgression d'abord, puis une régression. Le changement de phase est intervenu au Crétacé supérieur, marquant le début de l'inversion du bassin.

Six séquences tectoniques de 2ème ordre sont délimitées par des discordances majeures : i) la phase de rift par l'Initial Drift Unconformity (IDU, 189.6Ma), ii) le début de dérive par la Mature Drift Unconformity (MDU, 144.2 Ma), iii) le stade de maturité de la dérive par la Peak Spreading Unconformity (PSU, 112.2 Ma), iv) le stade de maturité de la dérive au début de la phase orogénique Atlasienne par l'Initial Atlasian Unconformity (IAU, 65 Ma), v) le stade de maturité de la dérive en contexte surrectif et compressif au début de la phase orogénique Atlasienne par le Peak Atlasian Unconformity (PAU, 28.5 Ma), et vi) le stade de maturité de la dérive avec le pic de surrection de la phase orogénique Atlasienne puis l'érosion au niveau du plancher océanique (époque actuelle).

Toutes les séquences du 2ème ordre sont caractérisées par un environnement sédimentaire spécifique : la première correspond à un milieu alluvial, fluviatile et marin confiné, la deuxième à un talus et une plateforme carbonatée, la troisième au développement d'un environnement deltaïque, la quatrième par des dépôts sédimentaires clastiques dans des carbonates de zone marine ouverte, la cinquième par le développement d'un prisme de sédimentation clastique de bordure de plateforme et la sixième par une sédimentation terrigène deltaïque et un by-pass étendu de la sédimentation.

Trente-et-une séquences du 3ème ordre et 113 séquences du 4ème ordre ont été identifiées sur trois transects clefs de l'ensemble de données. Le premier transect traverse la région du delta de Tan Tan, le deuxième croise le champ pétrolifère de Cap Juby et le troisième se situe entre les bassins de Tarfaya et de Laâyoune.

C'est en combinant la stratigraphie séquentielle à haute résolution et l'analyse des données de forages, que 13 formations potentiellement roches sources ont été identifiées. Leurs distributions ont été définies en utilisant des graphes chronostratigraphiques (diagrammes de Wheeler). Douze de ces roches sources ont été déposées durant la phase transgressive de la séquence de 1er ordre. La treizième roche source a été déposée pendant le maximum thermique du passage Paléocène-Eocène (PETM), après le début de l'inversion du bassin.

Des réservoirs ont été identifies dans le rift Triasique, dans les carbonates du Jurassique, dans le delta du Crétacé inferieur et dans les formations marines profondes du Cénozoïque.

Après la phase de rift du Permien Supérieur au Jurassique Inférieur marquant la dislocation de la Pangée, la subsidence et le flux de sédiment sont contrôlés par des contraintes intra-plaques éloignées. La dorsale océanique durant le Jurassique à un demi-taux d'accrétion de 19 mm/y (Sea Floor Spreading, SFS) qui engendre des pics de subsidence d'environ 150 m/m.y sur les plateformes externes. L'apport de sédiments de terrigènes fut inhibé, entraînant un espace d'accommodation vide, ultérieurement rempli par les plateformes carbonatées.

Du Tithonien au Berriasien, la divergence des marges Atlantiques centrales a été ralentie par les restes du Gondwana. Même si la formation du rift dans l'Atlantique Sud débuta au Tithonien supérieur / Berriasien inférieur, les demi-taux d'écartement des plaques décrurent par palier jusqu'à 7 mm/y. Le soulèvement thermo-tectonique dans la zone de rift Atlantique Sud et la décroissance des forces de poussée de la dorsale dans le Centre de l'Atlantique a résulté en un soulèvement des marges continentales passives de l'Atlantique central. Le plateau Jurassique a émergé et a subi une érosion majeure dans l'Anti-Atlas et le Craton Saharien. Les sédiments ont contourné le plateau Jurassique et formé les complexes deltaïques Tan Tan et Boujdour

à l'extérieur du plateau continental avec une pente plus faible. La combinaison d'une subsidence induite par flexion et compaction a ajouté jusqu'à 120 m/m.y dans les zones externes du plateau. Le développement du delta a continué jusqu'à l'Albien. Il se corrèle avec la dérive initiale dans l'Atlantique sud et augmente fortement les demi-taux d'accrétion jusqu'à 24 mm/y dans le centre de l'Atlantique. Même si la poussée exercée par la dorsale est plus faible qu'au Jurassique, la colonne d'eau sur le plateau a augmenté de plusieurs centaines de mètres. L'apport de sédiments continentaux s'est tari. La subsidence Cénozoïque et l'histoire des flux sédimentaires ont été contrôlés par la convergence Alpine et le soulèvement Atlasien.

Zusammenfassung

Nach dem Beginn der Krustendehnung und Grabenbildung im Zechstein (Kazanium, 259.3 Ma) und mit dem Einsetzen der Kontinentaldrift im Lias (Pliensbachium/Toarcium) wurden die Tarfaya-Laâyoune Becken ein Teilstück des ältesten passiven Kontinentalrandes entlang der Atlantikküsten.
Anhand von Aufschlussdaten, Bohrlochdaten und Daten aus multi-2D seismischen Messungen wurde, unter Berücksichtigung von Untersuchungen zur organischen Geochemie, Schwermineralanalyse und Thermochronologie, eine Sedimentbeckenanalyse durchgeführt. Der Arbeitsablauf beinhaltet: i) Nachbearbeitung und filtern der seismischen Daten, ii) Auswertung von Aufschluss- und Bohrlochdaten, iii) Interpretation seismischer Daten, iv) sequenz stratigraphische Interpretation und Auswertung, v) Zeit/Tiefen Konvertierung und vi) numerische Rückwärtsmodelierung.
Die meso/känozoische Beckenfüllung ist durch zwei übergeordnete Diskordanzen abgegrenzt. Dies sind an der Basis die Initialriftdiskordanz (Initial Rift Unconformity - IRU, 259.3 Ma) sowie der Meeresboden an der Sedimentoberkante. Die Diskordanzen umfassen eine unvollständige Sequenz der 1. Ordnung. Diese Sequenz kann in zwei Phasen unterteilt werden, eine transgressive und eine regressive Phase mit einem Phasenumschwung in der Oberkreide.
Sechs tektonische Sequenzen der 2. Ordnung werden durch Hauptdiskordanzen voneinander abgegrenzt. Dies sind je an der Oberkante einer Sequenz: i) die initiale Driftdiskordanz (Initial Drift Unconformity - IDU, 189,6 Ma), ii) die Spätdriftdiskordanz (Mature Drift Unconformity - MDU - 144,2 Ma), iii) die Driftdiskordanz welche die Periode maximaler ozeanischer Spreizungsraten anzeigt (Peak-Spreading Unconformity - PSU, 112.2 Ma), iv) die die initiale atlasische Konvergenz markierende Driftdiskordanz (Initial Atlasin Unconformity - IAU, 65 Ma), v) die Basisdiskordanz der initialen atlasischen Kompression und Anhebung (Peak Atlasian Unconformity - PAU, 28.5 Ma) und vi) der Meeresboden (heute).
Alle Sequenzen der 2. Ordnung sind durch einen speziellen Ablagerungsraum gekennzeichnet. Die Permo-Triassische durch alluviale, fluviale Riftsedimente und randmarine Abfolgen, die jurassische durch karbonatische Rampen und Plattformkomplexe, die unterkretazische durch deltaisch-klastische Ablagerungssysteme, die vierte durch klastischkarbonatisch offen marine Ablagerungsräume, die paleogene durch einen klastischen Ablagerungs-

keil am Schelfrand und die neogene durch durch die Ablagerung klastischer Sedimente am Kontinentalhang und im Abyssal bei gleichzeitiger Umgehung des kompletten Schelfs.
Einunddreißig Sequenzen der 3. und 113 der 4. Ordnung wurden auf drei Schlüsseltransekten identifiziert. Der nördliche Transekt verläuft entlang des Tan Tan Deltas, der mittlere quert das Cap Juby Ölfeld, und der südliche verläuft entlang der Grenze zwischen dem Tarfaya und dem Laâyoune Becken.
Auf der Grundlage der entwickelten hochauflösenden Sequenzstratigraphie in Kombination mit der Auswertung von Bohrlochdaten konnten 13 potentielle Kohlenwasserstoffmuttergesteine identifiziert und ihre Verteilung mit Hilfe chronostratigraphischer Diagramme (Wheeler Diagramme) eingegrenzt werden. Zwölf dieser potentiellen Muttergesteine wurden während der transgressiven Phase erster Ordnung, eine , das Muttergestein des PETM events, nach dem Beginn der Beckeninversion abgelagert.
Reservoire wurden in den triassischen Rift-, den jurassischen Karbonat-, den unterkretazischen Delta und den känozoischen submarinen Sedimentfächern identifiziert.
Seit dem Ende der permojurassichen Riftphase (189.6 Ma) werden die Subsidenzraten und der Sedimenteintrag durch großräumige Spannungsfelder beeinflusst. Kontinuierlicher Schub vom mittelatlantischen Rücken im Jura mit Spreizungshalbraten von 19 mm/y resultierten in Spitzensubsidenzraten am äußeren Schelf von über 150 m/m.y. Sedimentanlieferung aus dem Hinterland blieb aus, was zur Bildung eines großen Akkomodationsraumes führte. Dieser wurde zunehmend durch das wachsen von Karbonatplattformen gefüllt.
Die Divergenztendenz der atlantischen Kontinentalränder nahm an der Grenze Tithonium - Berriasium (ca. 145 Ma) schlagartig ab, da der Süd- und der Nordteil Gondwanas noch nicht auseinander gebrochen war. Auch wenn die Grabenbildung im Südatlantik zu dieser Zeit bereits begonnen hatte, fielen die Spreizungsraten im Mittelatlantik auf 7 mm/y. Eine thermotektonisch bedingte Anhebung des Südatlantikgrabens bei rückläufigem Spreizungsschub führte zu einer Anhebung der Kontinentalränder im Zentralatlantik. Der jurassische Schelf hob sich im Barriasium und Untervalanginium aus dem Wasser während eine Periode starker Erosion im Anti-Atlas und auf dem Saharakraton einsetzte, die die gesamte Unterkreide andauern sollte. Das angelieferte Sediment wurde über den jurassichen Schelf hinweg an den Kontinentalhang und ins Abyssal transportiert, wo sich der Tan Tan und der Laâyoune Deltakomplex bildeten. Dort summierten sich die Kombination aus flexureller und kompaktionsinduzierter Subsidenz auf über 120 m/m.y. auf. Die Deltaentwicklung hielt bis zum Albium (112.9 Ma) an. Das Ende der Deltasedimentation korreliert mit dem Beginn der Kontinentaldrift im Südatlantik und stark ansteigender Spreizungsraten im Zentralatlantik mit Halbraten über 24 mm/y.Auch wenn der Spreizungsdruck aufgrund der höheren Entfernung zum mittelatlantischen Rücken geringer waren als im Jura, betrug die Wassertiefe auf dem Schelf mehrere hundert Meter. Der Sedimentnachschub vom Kontinent kam vollkommen zum erliegen.
Während dem Känozoikum (65.0 Ma - heute) zeigt sich ein erster Einfluss der alpinen Konvergenz und der atlasischen Anhebung auf die Subsidenzraten und den Sedimentfluss.

Table of content

Table of figures

Table of tables

List of abbreviations

’ - feet
°API - oil density unit (American Petroleum Inst.)
λ - wavelength
1D - one dimensional
2D - two dimensional
3D - three dimensional
AMOCO - American Oil Company
AMP - Atlantic Margin Project
API - American Petroleum Institute unit (GR-log)
AWI - Alfred Wegener Institut
BG - British Gas
BGR - Bundesanstalt für Geowissenschaften & Rohstoffe
BH - Borehole
BP - British Petroleum/Beyond Petroleum
BTR - Berriasian Terrestrial Runoff
CAMP - Central Atlantic Magmatic Province
cc - correlative conformity
CCC - Callovian Carbonate Crisis
cf. - confer/compare
CGG - Compagnie Générale de Géophysique
CMP - Common Mid Point
CO_2 - Carbon dioxide
CPU - Central Processing Unit
D - Density log
D - flexural rigidity of the crust
dGB - de Groot Bril Earth Sciences
DSDP - Deep Sea Driling Project
DSMF - Dip-Steered Median Filter
E - Young‘s modulus
E - East
e.g. - exempli gratia/for example
EM - Electro Magnetic
ENI - Ente Nazionale Idrocarburi
ESRI - Environmental Systems Research Institute
FFT - Fast Fourier Transformation
fs - flooding surface
FSST - Falling Stage Systems Tract
FZ - Fracture Zone
GOM - Gulf of Mexico
GR - Gamma Ray log hc/HC - hydrocarbons
HI - Hydrogen Index
HST - High Stand Systems Tract
IAU - Initial Atlasian Unconformity
ICS - International Commission on Stratigraphy
IDU - Initial Drift Unconformity
IFREMER - Institut français de recherche pour l‘exploitation de la mer
IRU - Initial Rift Unconformity
JMQZ - Jurassic Magnetic Quiet Zone
JT - Jurassic turnover
KB - Kelly Bushing km - kilometre
km^2 - square kilometre
KW - Kellwasser event
LSF - Low Stand Fan
LST - Low Stand Systems Tract
LVL - Low-Velocity Layer
m - meter
Ma - Megaannum/one million years
mD - milli Darcy
MD - Measured Depth
MDU - Mature Drift Unconformity
mfs - maximum flooding surface
MTC - Mass Transport Complexess
m.y. - million years (time interval)
mya - million years ago
n - Poisson‘s ratio
N - North
NE - Northeast
NSMF - Non-Steered Median Filter
NW - Northwest
OAE - Oceanic Anoxic Event
OAE-1a - Selli event (Aptian)

OAE-1b - Urbino, Paquier and Jacob events (Apt-Alb)
OAE-1c - Tollebuc event (Albian)
OAE-1d - Breistroffer event (Albian)
OAE-2 - Bonarelli event (Cenomanian/Turonian)
OAE-3 - (Coniacian-Santonian)
OCC - Oxfordian Carbonate Crisis
ODP - Ocean Drilling Project OI - Oxygen Index
OM - Organic Matter
ONAREP - Office National de Recherche et d'ExploitationsPétrolières
ONHYM - Office National des Hydrocrbures et des Mines
OS - Ordovician-Silurian
p-wave - primary/pressure wave
PAU - Peak Atlasian Unconformity
PETM - Paleocene-Eocene Temperature Maximum
PI - Productivity Index
PRU - Post Rift Unconformity
PSU - Peak Spreading Unconformity
R - Resistivity log
RKB - Rotary Kelly Bushing
RockEval - Pyrolytic analysis method
s - second
S - South
s-wave - secondary/shear wave
S1 - Magn. anomaly in the Tarfaya-Laâyoune area
S1 - volatile hydrocarbons fraction (RockEval)
S2 - kerogen fraction (RockEval)
S3 - CO_2-fraction (RockEval)
SB - Sequence Boundary
SE - Southeast
seismic surveys: see Appendix
SFS - Sea-Floor Spreading
SMST - Shelf Margin Systems Tract
SOMIP - former Italian Moroccan oil company
SP - Spontaneous Potential log
ST - Subsidence Trend
sT1
sT2
sT3
sT4
SSIS® - Seq. Stratigraphic Interpretation System
SU - Subaerial Unconformity
SW - Southwest
SWB - Storm Wave Base
TD - Total Depth
Te - effective lithospheric Thickness
TG - Total Gas
TOC - Total Organic Carbon
TR - Triassic event
ts - transgressive surface
TST - Transgressive Systems Tract
TVD - True Vertical Depth
TVDSS - True Vertical Depth Sub Sealevel
TWT - Two-Way-Travel-Time
W - West
WAC - Wets African Craton
wellnames: see Tab.2
WHA - Western High Atlas
WP - Waypoints

1. Introduction

1.1 Scientific framework

The Northwest African passive continental margin, together with its conjugate Northeast American passive continental margin, bound one of the oldest active extensional basins in the world which includes one of the oldest global oceanic crust segments (Müller et al., 2008).
Initial rifting in the Central Atlantic took place in Late Permian approximately 260 mya. During the first 60 to 80 m.y. deep graben systems developed and where filled by eroded material from the hinterland of a still bounded Pangaea. Red clastic material was deposited in an arid, desert like region. First marine ingressions during the Late Triassic/ Early Jurassic (Norian-Sinemurian) associated with subsequent evaporation resulted in the development of a huge salt province.
With the onset of drift approx. 184 m.y. ago, Northwest Africa and North America were fully separated (e.g. Sahabi et al., 2004) and continuous production of oceanic crust at the new oceanic rift drives incipient sea-floor spreading. Since then, marine to coastal depositional environments dominated the West African margin, its conjugate margin, respectively. The basin fill has reached a maximum thickness of more than 14 km (Ranke et al., 1982; cf. chapter 3.3.4, Fig. 26a). Its structure, composition and succession is of both scientific and economic interest.
The basin fill of the Tarfaya-Laâyoune Basins as a sedimentary archive contain a huge amount of information which can be used to understand the local, regional and super regional development of the southern Moroccan continental margin. In addition it contains information about the Central Atlantic and the adjacent on- and offshore regions (Hafid et al., 2008). The basin fill provides information about the depositional history, the local environment at time of deposition (including paleoclimate and structure of paleobiospheres) as well as local, regional and global coherences of cycles and sediments.
Passive margins are more stable than active margins, on which the development of coastal cordilleras or island arches continuously reshape the coastal topography and contourline (Moucha et al., 2008). Since the opening of the Atlantic, the coastlines of the eastern Americas and West-Africa have kept their physical appearance. It was Alfred Wegener (1915; 1929) who did the first integrative study on passive margins comparing the shapes of the Atlantic coastlines and the composition of the paleobiospheres (*Glossopteris*-distribution) in the hinterland. This resulted in his continental drift theory, including heat convection in the sublithosphere as its driving force. Bullard (1950) found the origin of sea-floor

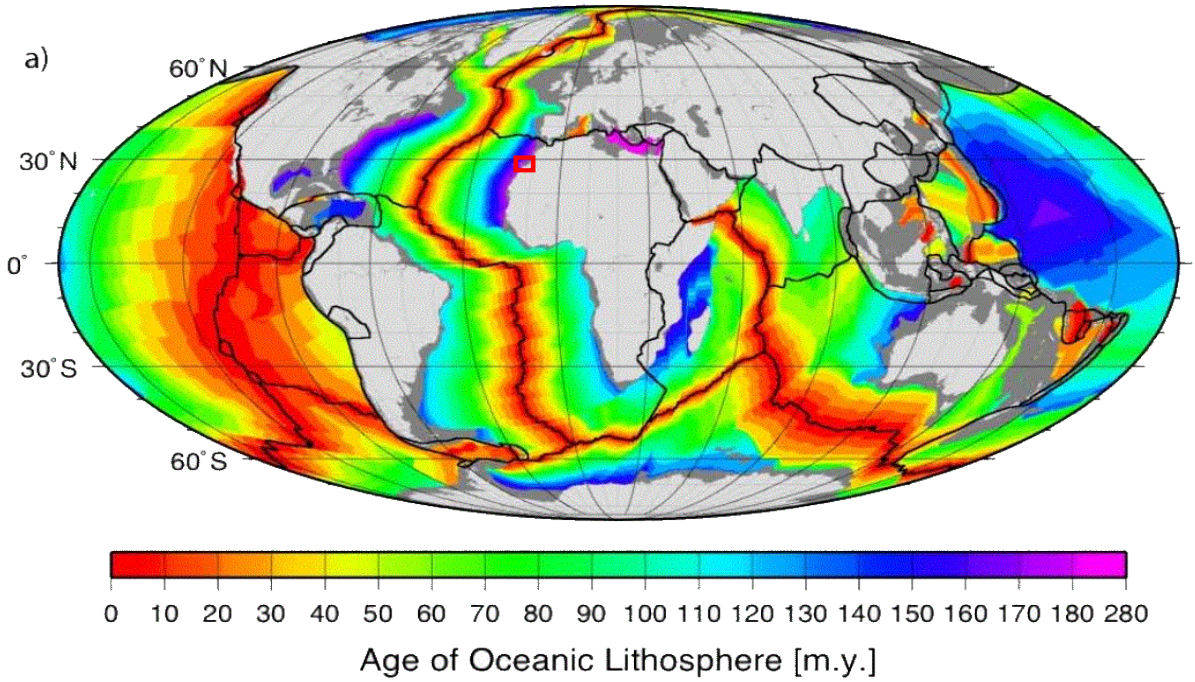

Fig.1: Age area distribution of the ocean floor (Mollweide projection). Continental margins in dark, continents in light grey (Müller et al. 2008). The red square marks the location of the study area.

spreading and rift push.
A systematic scientific exploration campaign, the Deep-Sea-Drilling Project (DSDP) started in 1969 and continued until 1983, finding its continuation in the Ocean Drilling Project (ODP, 1983-2003) and International Ocean Drilling Project (IODP, 2003-2013). This has helped to understand the structure of the sea-floor, the mechanism of sea-floor spreading, marine paleoenvironments and sedimentation processes.
A contribution of significant impact changing the understanding of sedimentation in marine environments was the article compilation of Vail et al. (1977) introducing the concept of sequence stratigraphy. This global comparison of (former) marine basin fills resulted in the theory that eustatic sea-level changes induce the development of repetitive sedimentation patterns. These include, the depositional sequence containing a low stand sea-level, a rising sea-level and a high stand sea-level subsequence, the systems tract. A cross-section from the Tarfaya Basin was chosen, along with examples from the Gulf of Mexico (GOM), the Joaquin Basin and the North Sea, as a kind of „locus-typicus“ for (seismic) sequence stratigraphy. Since its introduction, the concept of sequence stratigraphy has been continuously developed, resulting in three schools. It is understood that eustatic sea-level change is not the only driving force of sequence stratigraphy, but also tectonic forces, sediment flux, subsidence/accommodation space development and oceanic currents.
Research facilities like the Alfred Wegener Institute (AWI) or the Institut Français de Recherche pour l'Exploitation de la mér (IFREMER) are well known for their contributions on the structural framework of passive margins of the Atlantic (e.g. Gohl & Haywood, 2009; Klingelhöfer et al., 2009).
Passive continental margins are of major economic significance. They contain more than 30% of the global conventional hydrocarbon reserves (Mann et al., 2001). Several major productive basins in a passive margin setting are located in the Atlantic domain, as well as adjacent areas including the Barents Sea, the Norwegian Sea, the Niger Delta, the Angolan and Brazilian basins, the GOM, U.S. East Coast and Nova Scotia (Horn, 2014). The basic concept of hydrocarbon generation and entrapment in the sedimentary basin fill is based on the deposition of organic matter during times of low sedimentation energy, most-likely under anoxic conditions. This is followed by the coverage through high porous media during periods of high sediment flux (carbonate production or terrestrial run off), the generation and expulsion of hydrocarbons from organic matter during burial, and the entrapment of generated petroleum during the migration of oil and gas to the sedimentary surface (e.g. Tissot & Welte, 1984; Klemme & Ulmishek, 1991; Tyson, 2005). In the Tarfaya-Laâyoune area, hydrocarbon exploration began in the late 1950s, resulting in one mentionable discovery made in 1969 by Exxon offshore Cap Juby, indicating a single or multiple productive hydrocarbon system. However, until present it was not able to start hydrocarbon production in the area as the petroleum system is not fully understood.

1.2 Project description and scope of work

This study was realized as an integrated part of the Atlantic Margin Project (AMP), a joint venture between RWE Dea, Hamburg, Office National des Hydrocarbures et des Mines (ONHYM), Rabat, and the Universities of Heidelberg, Kiel and Aachen. The AMP was initiated as a geological reconnaissance and research project with the aim to receive new indications and concepts for functional hydrocarbon play scenarios. Six subprojects carried out as PhD and post-doc projects include i) Provenance analysis (Ali, 2012), ii) Micropaleontology of the Late Cretaceous OAE2 event (Aquit, in prep.), iii) Source-to-sink analysis (Heise, unpubl.), iv) Organic Geochemistry (Sachse, 2011), v) Thermochronology (Sehrt, 2014) and iv) integrated Basin Analysis (this study).
Key objectives of the research in this monograph are: i) a basinwide stratigraphic framework integrating the available well and seismic, outcrop and literature data, ii) a high-resolution sequence stratigraphic model for three key transects, iii) the prediction of source rock/reservoir distribution, iv) flexural 2D subsidence modeling in order to quantify the sediment flux, accommodation and compaction history of the Tarfaya-Laâyoune Basins.
The workflow includes eight major steps in the following order: i) stratigraphic framework from 1D-well, outcrop and 2D-seismic data, ii) 1D-high-resolution sequence stratigraphy based on γ-ray- and R-log data, iii) 2D-seismic and sequence stratigraphy for three key transects, iv) time/depth conversion of the key transect interpretation, v) chronostratigraphic transformation (Wheeler plots), numerical modeling of subsidence and sediment flux for three key transects in the study area.

2. State of the art

2.1. Concepts in exploration

2.1.1. The acquisition and interpretation of geological, geophysical & geochemical data

2.1.1.1. Field work

Apart from a notebook, pens, pencils, appropriate clothing, footwear and a rucksack, the basic equipment of a field geologist (Fig. 2) comprises a hammer, chisel, hard lens, compass-clinometer, acid bottle, sample bags, marker pen and a GPS. Equipped with these tools, there are six aspects of sedimentary rocks to consider in the field, which should be recorded in as much detail as possible: i) the lithology, that is the composition and or mineralogy of the sediment; ii) the texture, referring to the features and arrangements of the grains in the sediment, of which the most important aspect to examine in the field is the grain-size; iii) the sedimentary structures, present on bedding surfaces and within beds, some of which record the paleocurrents which deposited the rock; iv) the colour of the sediments; v) the geometry and relationships of the beds or rock units, and their lateral and vertical changes; and vi) the nature, distribution and preservation of fossils contained within the sedimentary rocks (Tucker, 2003). Field work during this study has been performed in the sediment source area, especially the Anti-Atlas, the Bas-Draâ region and the northern Reguibat, and in the sink area, the onshore Tarfaya-Laâyoune Basins, where the Early Cretaceous to Quarternary succession is exposed. Aside from the standard data acquisition, the main focus was on sequence stratigraphic issues and hydrocarbon geology aspects (source rock, reservoir rock and seal identification).

2.1.1.2. Remote sensing

Remote sensing is the acquisition of information about an object or phenomenon without making physical contact with the object. In modern usage, the term generally refers to the use of aerial sensor technologies to detect and classify objects on Earth (on the surface, in the atmosphere and in oceans) by means of propagated signals (e.g. electromagnetic radiation emitted from aircraft or satellites) (Schowengerdt, 2007; Schott, 2007). In this study, aerial and satellite images in this study were used for orientation in the field. They also provided background data for generating maps and figures.

Fig. 2: Carl Spitzweg: Der Geologe (The Yorck Project, 2002).

2.1.1.3. Borehole evaluation

Following Walther‘s law that a vertical sequence of facies will be the product of a series of depositional environments which lay laterally adjacent to each other (Walther, 1893/94), an exposition of the deeper part of an undeformed basin fill can just be achieved by drilling a well. Exploration wells for scientific and economic purposes in general are drilled vertically, production wells can also be drilled deviated. The most common used technique is the hydraulic rotary drilling. Depending on the planned depth and the locality of the well (on- or offshore), a small mobile, a stationary (Fig. 3) or a floating rig are used for drilling (Reich, 2012). A drill string, powered by an engined rotary table which includes the Kelly Bushing (KB) or a top drive, steers a tricone roller or diamond-impregnated drill bit which drills through the rock. The developing bore hole is

filled with a fluid, the drill mud. This fluid has mainly two functions: i) transporting the destroyed rock (cuttings) to the surface, and ii) stabilizing the well (Chilingarian & Vorabutr, 1981). The mudlogger, a geologist observing the upcoming mud with the cuttings describing the just drilled section on site is the first scientist working with the „synthetic outcrop". He creates the first (litho-)stratigraphic chart of the drilled basin fill. Depth measurement of the current drilled section (counting the drill pipes), the depth assignment of the flushed cuttings (lighter particles are faster at the surface than heavier) and geological identification with this method is very imprecise. A more precise geological evaluation is possible when the rocks are cored. As this is, with increasing depth, very time consuming and expensive, cores are normally only taken in shallow scientific wells or reservoir sections of hydrocarbon bearing wells.

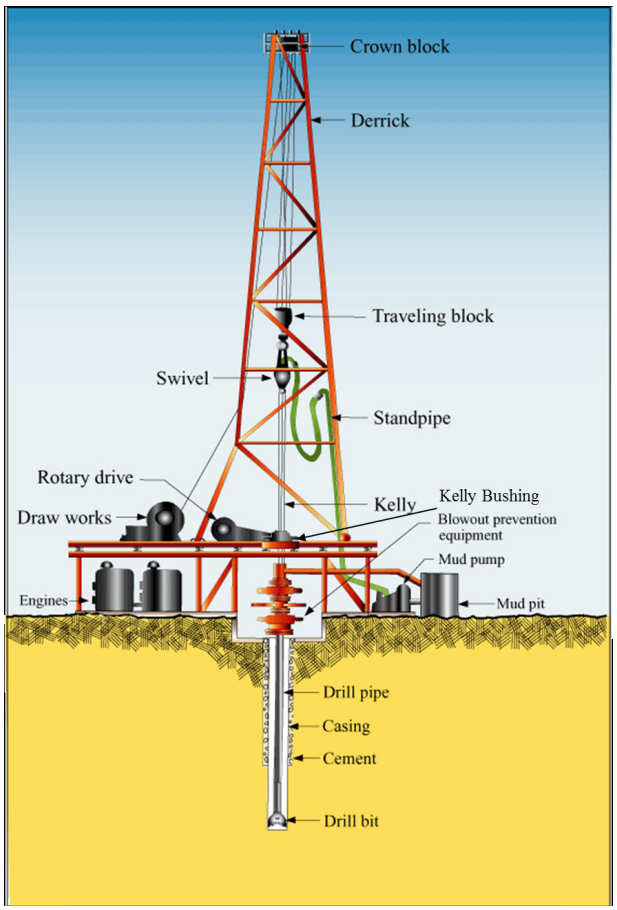

Fig.3: Schematic sketch of a drill rig and its components (State of California, 2013).

A variety of different logging tools have been developed over the decades that helps the mudloggers and well site geologists to make more correct and detailed description of the geology in the subsurface. The standard log types that are used in a hydrocarbon exploration well are: i) Caliper, ii) self-potential (SP), iii) resistivity (R), iv) conductivity, v) gamma ray (GR), vi) neutron, vii) sonic, viii) density (D), ix) dipmeter and x) temperature logs (Bjørlykke, 2010). Important log types in this study are the GR, the R, the SP, the sonic and the D log.

Based on the results from the geological description of the mudlogger and the logs, a lithostratigraphic description at the position of the well is possible. In general a hard change in the rock composition defines the top of a new formation. In sedimentary environments it can also be the shift between to different facies in one formation for instance between marine shale and an incised channel (Reading 1998). The way how a position of a formation top in the well can be mentioned varies. The first depth assignment is the so called „drillers depth" based on the amount of drill pipes in the hole. The second is the loggers depth which represents the length of the cable run into whole during wireline logging. Both depths are called measured depth, and are measured from rotary table (RKB). The unit is metre (mMD RKB) or feet ('MD RKB). AAs a drill bit is not always drilling vertically, the drill path can become deviated resulting in the MD being longer than the distance between the RKB and the bottom of the hole (Bottom Hole - BH). The corrected depth is called True Vertical Depth (mTVD) and is in general assigned to mean sea-level (mTVD MSL). If the common datum chosen for a regional evaluation is mean sea-level, the term True Vertical Depth Sub-Sea (mTVDSS) is used to include onshore wells (Theys, 1999).

The GR-tool measures the natural radiation from the formation in API (American Petroleum Institute unit). In shales a lot of radioactive elements are incorporated in the clay mineral structure and a high gamma ray reading is the result. It can be used to differentiate between reservoir (sandstone/carbonate) and source rock/seal facies (claystone/shale) (Veeken, 2007).

R and SP logs were used, when GR was not available. The R log is the result of measuring the resistance between 2, 4 or 8 electrodes which are in contact with the rock in the well wall. Resistivity is measured as a function of the cross-section (m^2) of the rock and the distance (m) between the electrodes, the unit is ohm metre. In general, hydrocarbons (hc) filled sandstones as well as carbonates show a high resistivity, whereas shales and water filled sands are good conductors. Hence, the log pattern of the R log

is comparable to the GR with the exception that a differentiation between water-filled sand and shale is not possible (Hobson & Tiratsoo 1981). The SP log measures the electric potential which develops between a moving electrode in the well and a fixed electrode near the surface. An electric current is created due to the difference in the concentrations of electrolytes in the liquid phase (Bjørlykke, 2010). The log pattern is comparable with the GR pattern with the exception that carbonates and sandy shales are not distinct in their amplitude. The three log types were used in this study for the interpretation of sequence stratigraphic pattern detection (see chapter 3.4.3.).
Well based exploration is one-dimensional as the diameter of the well is around a few inches (4 1/2“ - 33“). Lateral correlations only based on well information are potentially misleading. It is important to link 1D-data with 2D-, 3D- and in some cases of production, 4D-data.
As the common unit used for depth assignments in wells is m (or feet) and in reflection seismics it is seconds of Two-Way-Travel-Time (sTWT, see chapter 3.1.4), data from well evaluation have to be converted, or vice versa respectively. This time/depth conversion is based on the knowledge of the sonic velocities in the subsurface. In general, check shots surveys are performed to receive the relation between depth and sonic velocity in a well (Goetz et al., 1979). The generation of synthetic seismograms can compensate the lack of check shot data when a sonic and a density log is available (Veeken, 2007). For this study, check-shot surveys for five wells were available. Synthetic check-shots were generated for further key wells (see. chapter 3.3.2, table 2).

2.1.1.4. Reflection seismic

The entire basin scale exploration is dependent on the possibility to image the subsurface. The most common technology to make the subsurface visible is the reflection seismic. Waves, similar to a medical ultrasound scan, are emitted from the surface. They reflect off intervals in the subsurface and their reflection is recorded again at the surface. the setup of a reflection seismic survey includes: i) survey designing, ii) data acquisition (Fig. 4, 5 & 6), iii) data processing and iv) data interpretation. Steps i) and vi) in general are performed by geologists and/or geophysicists. For step ii) a field or ship crew is needed, often more than 100 persons. Step iii) is normally completed by a geophysicist. Experience is of high significance and is said that a full „apprenticeship“ for seismic processor is about ten years (Rybarczyk, 2012).

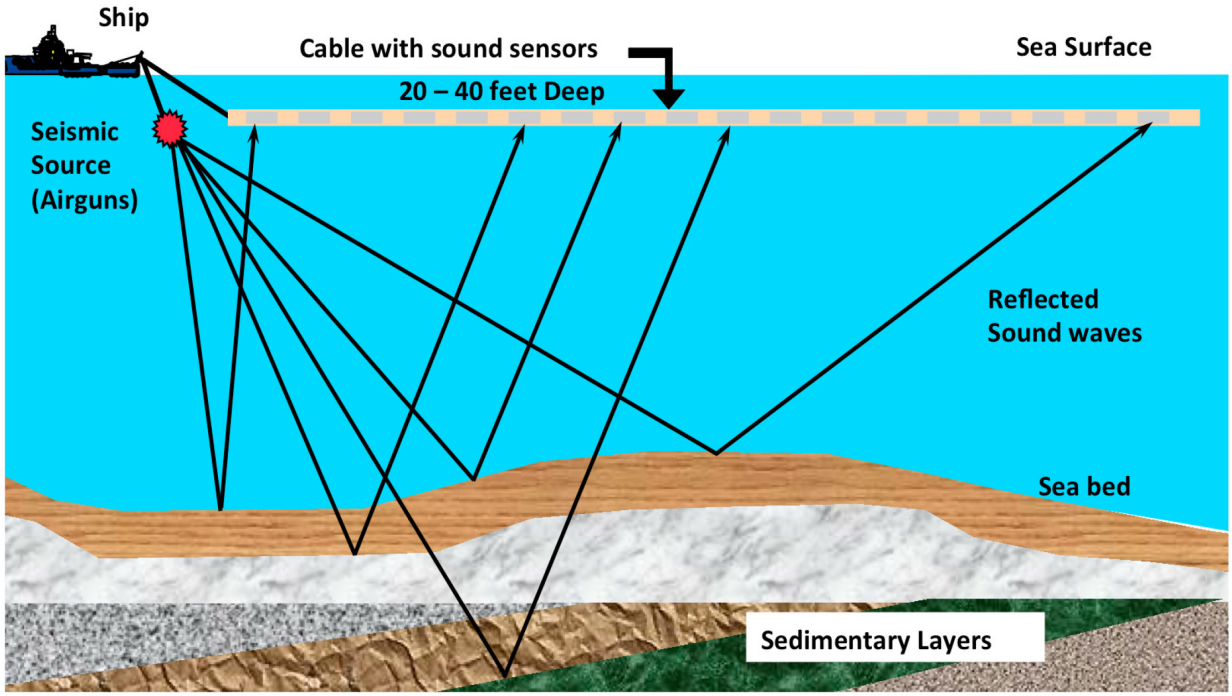

Fig. 4: Concept of seismic acquisition (energy tomorrow, 2014). A signal source, offshore in general an airgun is in use, onshore vibro-trucks emit low frequency waves into the subsurface. The reflected signal is captured with geophones which transmit the responded signal to the recorder .

2.1.1.4.1. Seismic survey designing

The acquisition of seismic data, in general performed before drilling, is the first considerable invest in basin evaluation. Onshore, the recording of 1km 2D-seismic is about 1,250 €, 1 km² 3D-seismic about 6,000-7,000 €. Therefore a seismic survey has to be planned based on the purpose of the research. 2D-transects are generally useful when a first basin scale reconnaissance should be performed. 3D-seismic is used if structures, e.g. a hydrocarbon reservoir, should be fully resolved. As the strength, the bandwidth of the emitted signal and the geometry of acquisition are relevant for the quality of the final data, geological knowledge is necessary regarding the depth of the target and the geometry of a structure (Cordson et al., 2000). High acquisition energy with low frequencies (2 - 30Hz) is needed for deep structure >3,500m, high frequencies (30-240 Hz) are important for a high resolution.

2.1.1.4.2. Acquisition of seismic data

The basic concept of seismic reflections originates from interfaces in the subsurface that show sufficient density-velocity (Rho-Vee) contrasts. Each seismic layer in the subsurface has its own acoustic impedance which is defined as:

A.I.=density * velocity.

This means, the higher the lithological contrast regarding density and sound conductivity, the more intense is the reflection (Veeken, 2007). Reflection follows Snell's law and the basic rule that the ray path is following the Pythagoras principle (cf. Fig. 4). It is founded on: i) Elastic wave propagation: rocks will transmit P and S elastic waves without major attenuation as long as the wavelength (λ) of the waves is only 2 to 3 orders of magnitude less than the path length (e.g., if λ is 10m then the useful propagation distance is 1-10km); ii) Reflectivity: spatial heterogeneity in the local elastic moduli and/or density of the rocks cause a fraction of the incident elastic energy to reflect or backscatter. The term „reflection" is used when dealing with extended interfaces and incident wavefronts, and the term „scattering" when the geometry of the heterogeneity is less regular (Nedimović, 2000). Fig. 7 shows a shotpoint gather with a signal emitted in the centre and the reflections from the subsurface in sTWT. The reflection pattern is parabolic as the travel time

Fig. 5: Four-source vibroseis pattern acquiring data in a densely populated area. 2D-seismic-survey Heidelberg 2010 (Wenke et al., 2012a).

Fig. 6: Marine seismic acquisition unit including vessel with airgun and recording and the pulled streamer (receiver) arrays (Dragoset, 2005).

to the outer geophones is longer than to the ones near the shotpoint.

The concept of seismic as an exploration tool was introduced by Ludger Mintrop. During World War I, all armies attempted to find enemy guns by using airwaves or refracted waves. As a soldier in the German army he recognized that the waves have some interaction with the subsurface. Soon after the war was over, he further developed the refraction seismic concept as a tool for geological exploration and identified the Orchard Dome oilfield in Texas in 1924 (Meunier, 2011). After this discovery, the technology of seismic exploration developed very quickly and reflection seismic was introduced just one year after, and since the middle of the 1930s seismic surveys are almost exclusively performed by the E&P industry because the necessary funds, technology, equipment and manpower exceeds the means of academic insitutions. However, if fundamental research has been granted access to industry seismic data, major advances in structural and sedimentological research could be achieved (e.g. sequence stratigraphy since the late 1970ies; e.g. Vail et al., 1977; Catuneanu et al.; 2010).

The first major discovery based on reflection seismic was in 1927 the Maud Field in Oklahoma. This was done using a sonic sounder originally developed to find icebergs and a single recording. The technology developed with increased velocity and two channel/four trace per shot recording was introduced in 1928. In 1930 six channel systems were employed. By the end of the 1930s, seismic systems typically had up to 12 channels, 6 or more geophones per channel, mixed channels and automatic volume control (Roden, 2005). The first marine survey was shot in 1944 using dynamite as the source while geophones were deployed on the seafloor offshore Louisiana (Meunier, 2011), by the end of the 1940s, 24-channel systems were standard.

After World War II, six significant developments shaped the future of exploration geophysics: i) magnetic tape recording (until then, migration and interpretation of the data was performed in the field with

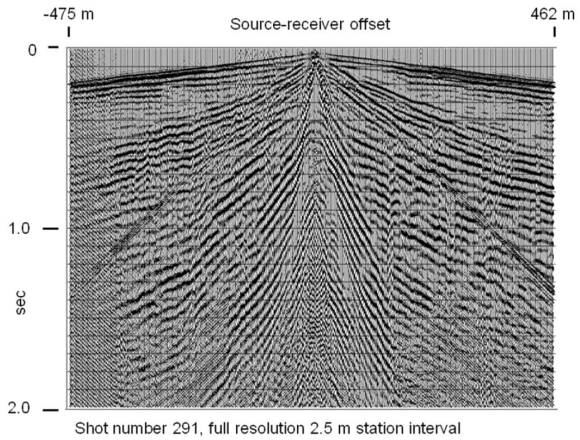

Fig. 7: Shotpoint gather with 2.5 m geophone distance on each side of the shotpoint (centre) Rybarczyk, 2012).

pen and paper), ii) the Common Midpoint method allowing multi-shot recording (Fig. 8), iii) the development of vibro-seismic (Fig. 5), iv) the development of streamers in the 1950s, v) tuned airguns in the late 1960s for marine seismic (Fig. 6) which allowed acquisition while moving, and vi) the digital revolution which allowed recording signals in milliseconds, processing of the data in datacentres as well as interpretation off the location (Dragoset, 2005; Roden, 2005; Veeken, 2007).

While 48-channel acquisition was standard in the early to mid-1970s, up to several thousand channels are in use at present day 3D-acquisition and the frequency and force control of present day airguns or vibroseis engines result in images of very high resolution and quality.

As the uppermost very few meters of sediments (e.g. soil, sea-floor mud), are often very loose and poorly lithified, seismic velocities are reduced significantly. Applying a wrong velocity model for this layer, also called low-velocity layer (LVL), can result in a misfit in depth interpretation/conversion. Onshore, small refraction seismic surveys attend a reflection

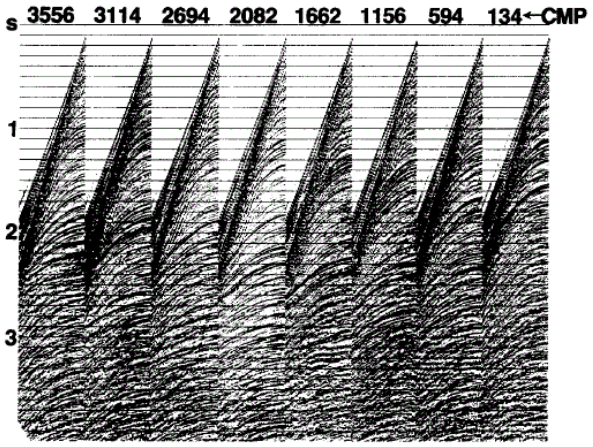

Fig. 8: Common midpoint gather as a first step of shotpoint stacking/data processing (Veeken 2007).

seismic survey to determine the velocities (in general 1400-1700m/s) in the LVL (Cordsen et al., 2000). Offshore, static corrections of travel-time anomalies due to mud sediments can be done by using variations of first break travel-times as correction time values (Zöllner & Schikowsky 2003).

In this study, seismic data from 10 seismic surveys acquired between 1969 and 1999 were used.

2.1.1.4.3. Seismic Processing

In the earliest days of reflection seismology, data processing consisted mostly of three key steps: i) static corrections (geographic relationships between shotpoints and receivers), ii) velocity determination (for time/depth conversion), and image construction.

Tab. 1: Seismic processing workflow (Cordsen et al., 2000)

Processing sequence (turnkey price):
Demultiplex and edit field data
Gain recovery
Instrument and geophone dephasing
Geometry and refraction statics analysis
Deconvolution and filter tests
Surface-consistent deconvolution and scaling
Brute stack
Velocity analysis
Automatic surface consistent statics
Intermediate stacks
Final velocity analysis
3-D trim stack with final statics
FX-decon
3-D migration after stack, one-pass
Options possible (price per unit):
3-D interpolation
Bin-borrowing or mixing
Rebinning
f-k noise attenuation
DMO
Multiple attenuation (e.g., Radon transform)
Depth migration—mainly after stack
Prestack time or depth migration
Deliverables (paper):
Selected shot records, before and after NMO
Common-offset stacks with mute displays
Decon tests
Narrow and broad-band filter tests
Brute stack
Velocity analysis displays (e.g., semblance)
Intermediate stack
Final stack
Migration
Deliverables (film):
Map of source and receiver locations
Subsurface bin and coverage maps
Migration (e.g., every tenth line, both polarities, both directions)
Deliverables (SEG-Y tape):
FX-decon—unfiltered and filtered
Migration—unfiltered and filtered

Fig. 9: Small portion the seismic processing CPU of Western Geco (Dragoset, 2005).

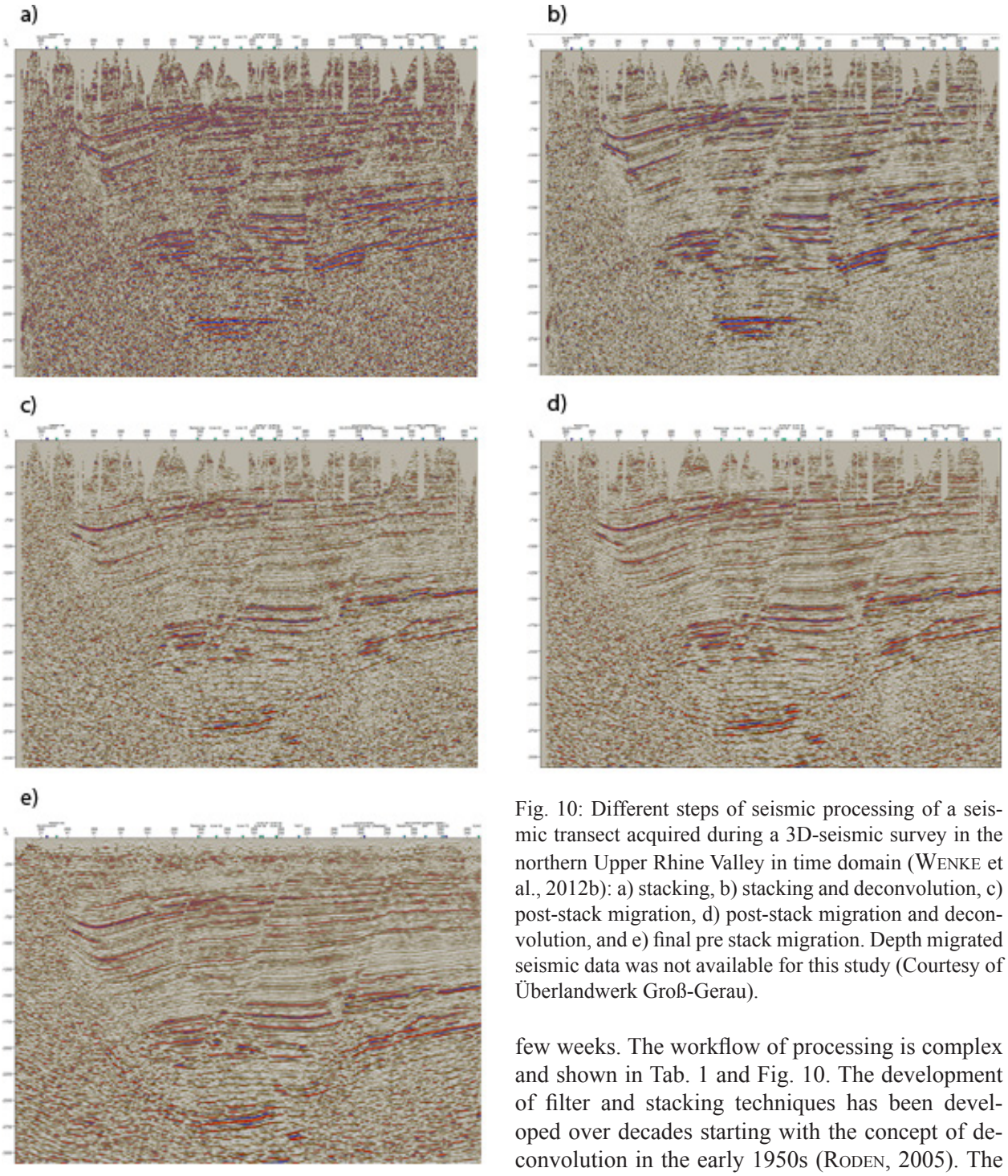

Fig. 10: Different steps of seismic processing of a seismic transect acquired during a 3D-seismic survey in the northern Upper Rhine Valley in time domain (Wenke et al., 2012b): a) stacking, b) stacking and deconvolution, c) post-stack migration, d) post-stack migration and deconvolution, and e) final pre stack migration. Depth migrated seismic data was not available for this study (Courtesy of Überlandwerk Groß-Gerau).

These were accomplished by a "computer", which was the job title of the individual on a seismic crew who performed these functions using pencil and paper (Dragoset, 2005). Not much has changed about the basic concepts of processing, but the amount of data which has to be handled has increased enormously. The first 3D-seismic survey shot in 1967 by Exxon in the Gulf of Mexico took 2-3 years of processing. At present day, three to four specialists with powerful CPUs (Fig. 9) perform this process in a few weeks. The workflow of processing is complex and shown in Tab. 1 and Fig. 10. The development of filter and stacking techniques has been developed over decades starting with the concept of deconvolution in the early 1950s (Roden, 2005). The fundamental assumption of deconvolution is that a seismic trace consists of a series of reflection events convolved with a wavelet, plus unrelated noise. The deconvolution process designs an inverse filter that compresses the wavelet, thereby enhancing the resolution of seismic data.

Digital static correction methods have been developed in the 1970s. The refraction statics correction method uses the arrival times from refracted seismic waves (head waves) that travel along the boundary between the weathering layer and the bedrock

to determine the thickness of the weathering layer and the bedrock velocity. This allows computation of a static correction that effectively "replaces" the weathering layer velocity with the bedrock velocity (Dragoset, 2005).
Further major steps in the development of processing technology concern digital CMP-detection, stacking velocity determination and velocity modelling for stacking and migration, and the different pre- and post-stack-migration techniques (Dragoset, 2005; Roden, 2005; Meunier, 2011).
Like the seismic data acquisition technology, the technology of data processing underwent several quantum leaps since its introduction. This has to be kept in mind during the interpretation of a multiple survey dataset as a high variety of data quality has to be managed.

2.1.1.4.4. Archiving of acquired data

As exploration techniques like the acquisition of seismic data or drilling and coring a well requires high financial investment, data has to be stored as they may deliver important results over decades. Cuttings and cores in general are stored in huge core sheds under dry and more or less constant temperature conditions. Well log data is stored in archives of the data owners, while seismic datasets recorded on tape are often stored by professional companies in special racks and stable climatic conditions. Paper prints from older days have to be stored dry and away from sunlight. As seismic paper prints can have sizes up to 1x10m, storage is a challenge. They have to be hung or rolled or stored on microfilm. Maintaining these conditions over decades can be a challenge as magnetic tapes should be copied every ten years, DVDs every five years.

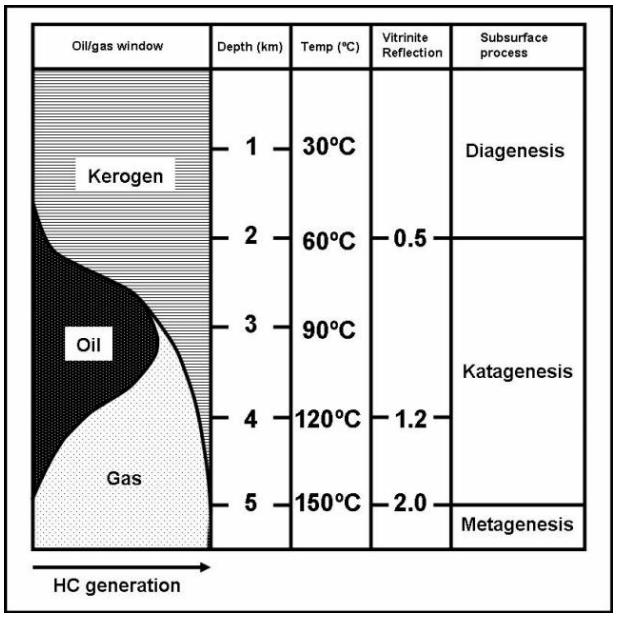

Fig. 11: Relationship between burial depth, temperature, vitrinite reflectance and oil phase generation (simplified from Tissot & Welte 1984).

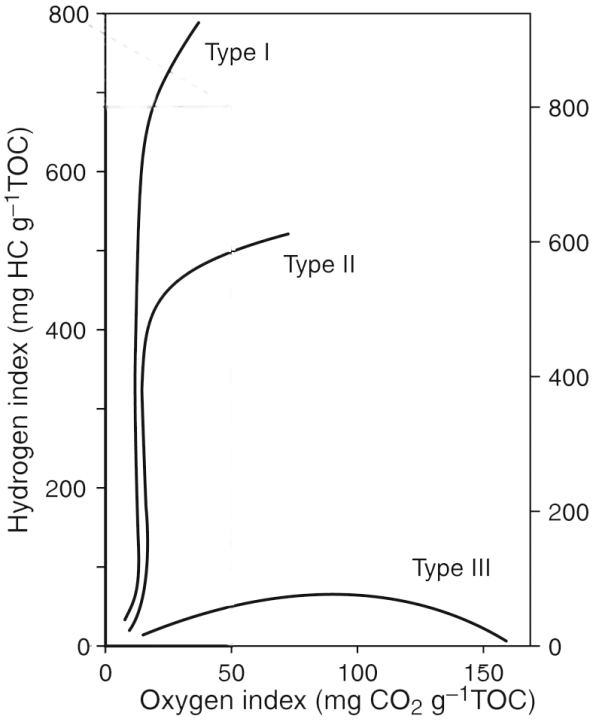

Fig. 12: Pseudo Van-Krevelen diagram illustrating the range and correlation between HI, OI and kerogen (modified from Vining & Pickering (2010).

2.1.1.5. Petroleum geochemistry

Petroleum geochemistry is the application of chemical principles to the study of the origin, migration, maturation and alteration of petroleum (Hunt, 1979) in the geosphere. The origin of hc is organic matter of dead flora and/or fauna. Once deposited it has to be buried before bacteria is able to decompose the organic material. If the thickness of high organic accumulation reached a certain amount (several meters), a source rock can be develop during further diagenetic history (e.g. Tissot & Welte, 1984).
Controlling factors steering the accumulation and preservation of organic matter are i) primary production (of biomass), ii) dysoxic to anoxic conditions in the lower water column and iii) sediment flux (Klemme & Ulmishek, 1991; Tyson, 2006). A potential source rock contains >0.5wt% of total organic carbon (TOC) per kg rock if it is part of a carbonate sediment and >1wt% TOC if it is part of a

clastic sediment (Tissot & Welte, 1984). Four different types of kerogen (organic geochemical compounds) classify the source rock type: Type I which is containing proteins and (freshwater) algae, Type II/IIS mainly of marine plankton and Type III of lipids from higher terrestrial plants (Hutton et al., 1994). Type IV kerogen contains mostly decomposed organic matter in the form of polycyclic aromatic hc and have no potential to produce petroleum (Weber & Green, 1981).

During burial, the temperature in the subsurface increases and results in the transformation of the organic matter, above 60°C the generation of oil and above 125°C the generation of gas (simplified from Tissot & Welte, 1984; Fig. 11).

The quality of a source rock can be specified by analyzing source rock samples with a pyrolysis carbon analyzer (RockEval). Between the temperatures of 20°C to 300°C the free oil or already released hc in the sample (S1) are determined, and between 300°C and 550°C the remaining hydrocarbon potential (kerogen or S2) can be recognized. 550°C is the peak temperature and during the following cooling phase CO_2 is released between 390°C to 300°C (Espitalie et al. 1977). Further parameters delivered

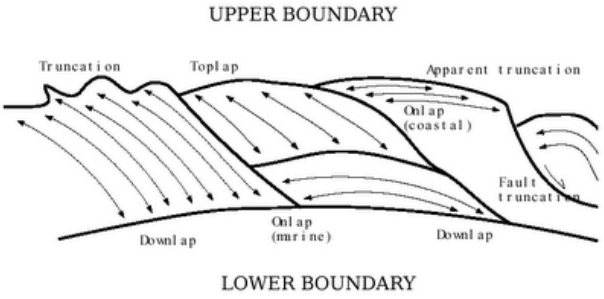

Fig. 13: Types of stratal/reflector terminations (Bertram & Milton (1996)

by RockEval analysis is the Hydrocarbon Index (HI), the Oxygen Index (OI) and the Production Index (PI) (Tissot & Welte, 1984).

The HI is used to characterize the origin of the organic matter. The HI range for kerogen type I reaches from approx. 600 to 850mgHC/gTOC, type II from 400 to 600mgHC/gTOC, type II-III from 200 to 400mgHC/gTOC and type III between 50 to 200mgHC/gTOC. Values below 50mgHC/gTOC is generally characterizing dead/inert hydrocarbon also named kerogen type IV.

A high OI indicates land plants (polysaccharide)

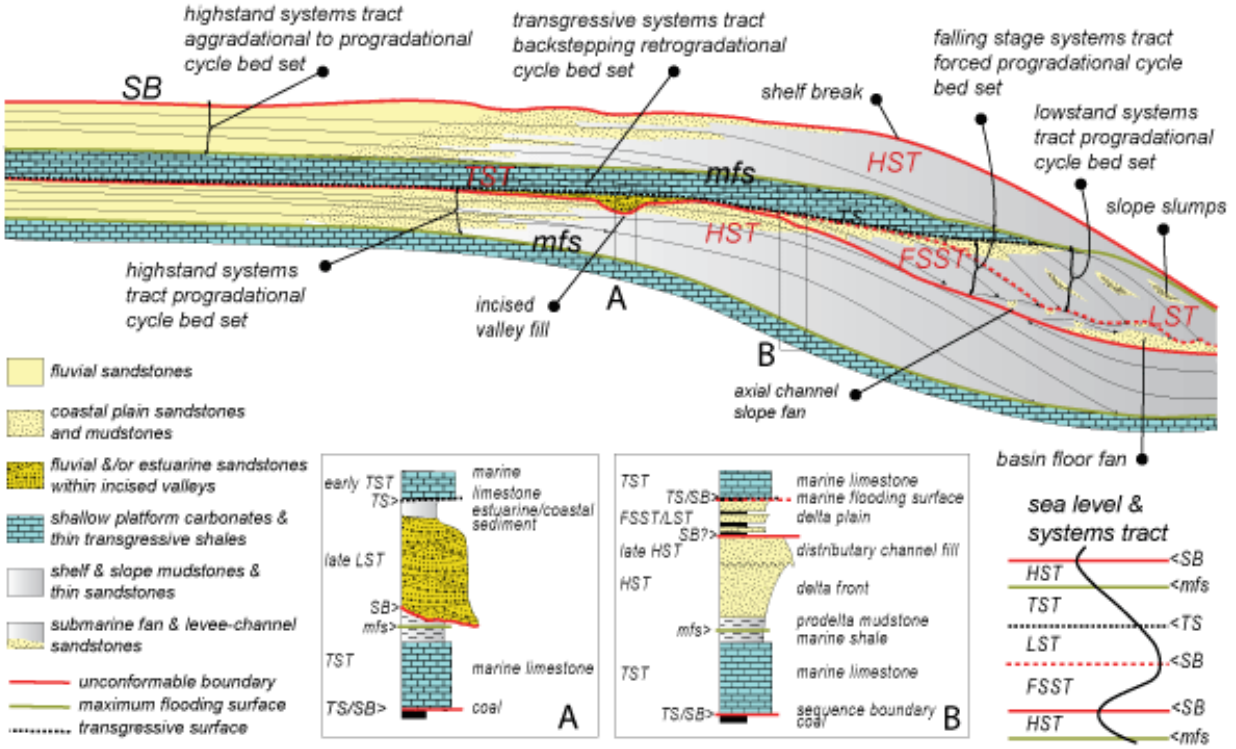

Fig. 14: Combined illustration of the Depositional Sequence II (Exxon model) & IV (Hunt & Tucker, 1992; 1995) models and its major components. The original Exxon sequence consists of three systems tract, the (early & late) LST, TST and HST. During further concept development the early LST was classified as an independent systems tract, the FSST (explanations see text). Characteristic vertical profiles are shown in A & B, the interaction between relative sea-level variations and systems tract development in the lower right corner (Kendall & Tucker, 2010).

while marine sediments show a low OI. The relation between HI and OI is often shown in the Van-Krevelen or pseudo-Van-Krevelen diagram (Fig. 12).
The state of maturation regarding generated hydrocarbon (S1) and remaining potential (S2) is given by the production index (PI = S1/S1+S2).
The main parameter used in this study to define potential source rocks is the TOC. In addition, HI, OI and PI are given when available. For detailed organic geochemistry performed in the Atlantic Margin Project read Sachse/Sachse et al. (2011; 2011; 2014).

2.1.2. Geological Concepts

2.1.2.1. Sequence stratigraphy

Sequence stratigraphy is a method to subdivide depositional systems into conformable bound units on a variety of orders. Based on the identification and mapping of characteristic surfaces, the method allows to i) increase the resolution of (chrono-)stratigraphic subdivision, ii) identify relative sea-level changes, iii) understand the lateral and vertical distribution of depositional systems. It is an important tool in the analysis of sedimentary basins and petroleum systems.
Based on a global 2D-seismic and exploration dataset including the Gulf of Mexico (GOM) and the Tarfaya Basin (EM 69 seismic survey and wells MO 1-8 & HM-1) the Exxon Production Research group around Peter Vail developed the concept of sequence stratigraphy during the early to middle 1970s (Vail & Sangree 1971, Vail 1975, Mitchum et al. 1976) and published their final definitions in AAPG Memoir 26 (Vail et. al. 1977). In this publication major definitions like stratal terminations and behaviour (erosional truncation, toplap, onlap, downlap, offlap and concordance/correlative conformity, Fig. 13), the definition of depositional sequence, their subordinated units (low stand system tract - LST, transgressive system tract - TST, and high stand system tract - HST) and the position of the sequence boundary on top of the HST were made. The concept was published together with a global sea-level chart based on the underlying assumption that eustasy is the main driving force behind sequence formation at all levels of stratigraphic cyclicality. This basic concept is also known as the Depositional Sequence I Concept (Catuneanu 2006), the Exxon Model.
With the Depositional Sequence II Concept or the revised Exxon Model terms like sequence boundary type I & II, shelf margin system tract (SMST) and low stand fan (LSF) as part of the early LST (Catuneanu 2006) were introduced while the definition of sequence boundary is still set at the top of the HST (Van Wagoner et al., Posamentier et al., Posamentier & Vail, all 1988). In addition to eustatic sea level changes, tectonic subsidence, sediment flux, climate and sea currents were named as sequence stratigraphic controlling forces.
Van Wagoner et al. (1990) noted that sequence stratigraphic interpretation can be more precise under incorporation of outcrop and well data. Stacking patterns for well log interpretations were defined. In addition to the Depositional Sequence II Concept it was suggested to reassign the LSF as a part of the late HST which shifts the position of the sequence boundary in distal basin areas.
Hunt & Tucker (1992) developed the concept of a falling stage system tract (FSST) and defined the LSF as a part of the FSST (Fig. 14). This model is named as the Depositional Sequence IV Concept (Catuneanu 2006).
The main surfaces to identify boundaries between systems tracts and sequences are i) the subaerial unconformity (SU) extended by the correlative conformity (cc) (type I sequence boundary), and ii) the maximum flooding surface (mfs) marking the end of transgression (TST-HST boundary).
Further surfaces are the flooding surfaces, within trend surfaces, transgressive ravinement surfaces and the basal surface of forced regression. They are described in detail in Catuneanu (2006).
In addition to the Exxon 'school' and following developments Galloway (1989) proposed in his Genetic Sequence model that maximum flooding surfaces, rather than subaerial unconformities, should be used as sequence boundaries mainly based on transgressive-regressive trends. Embry & Johannessen (1992) proposed a third type of stratigraphic unit named the transgressive-regressive sequence. At least, the last two concepts were not able to establish in science and industry.
According to this variety of sequence stratigraphic approaches, Catuneanu et al. (2009; 2010; 2011) proposed a standardisation of sequence stratigraphic interpretation and modelling, while Neal & Abreu (2009) introduced the concept of the accomodation succession method based on progradation, aggradation and retrogradation stacking patterns. In their opinion the key definitions for the depositional sequence concept were set by Vail et al. (1977) and

Posamentier et al. (1988) and should be used as a standard for seismic interpretation.

2.1.2.2 Subsidence analysis (backstripping)

Subsidence (or uplift) is the motion of a (time-) surface relative to a fixed datum, in general the sea-level. Sedimentary basins can be assumed to be in isostatic equilibrium in relation to the earth's crust. However, the crust has a certain rigidity, and it takes time before equilibrium is attained after loading/deloading (Bjørlykke, 2010).

The controlling factors on subsidence/uplift in extensional basins are i) crustal stretching and thinning due to horizontal extension, ii) cooling or heating of the crust, iii) isostatic balancing in response to sediment/ice loading or erosion (Einsele, 2000). The technique to calculate the subsidence rates of a sedimentary basin by stepwise retracting the sedimentary basin fill is called backstripping or reverse modeling and was first introduced by Watts & Ryan (1976).

Reverse basin modelling provides a quantitative analysis of the basin architecture and infill as controlled accommodation change and sediment flux (e.g. Emmerich et al., 2008; Contreras, 2011; Fig. 15). The genetic components of total subsidence are: i) thermo-tectonic, ii) flexural and iii) compaction-induced subsidence (e.g. Zühlke et al., 2004). The modelling approach has been applied primarily to extensional settings in order to analyze lithospheric stretching factors and subsidence/uplift histories (Nadin & Kuznir, 1995; Roberts et al., 1995; 1997; 1998; Nadin & Kuznir, 1996; Bowman & Vail, 1999; Zühlke et al. 2004; Kuznir & Karner, 2007; Veselovsky et al., 2008; Contreras et al., 2010). Flexural reverse basin modelling starts from the present basin architecture. Chronostratigraphic layers are incrementally removed down to the top of the rheological basement (Intra-Khazhanian, 259.3 Ma in this study).

The initial basin architecture is controlled by i) paleotopography, ii) structural setting, iii) the type of lithosphere and, iv) its flexural rigidity (Watts & Burov, 2003). Subsequent changes in depositional patterns and sediment and water loading of the crust result from changes in subsidence/uplift, eustatic sea-level and sediment input (cf. Zühlke et al., 2004; Contreras, 2011). The accommodation space is defined by two surfaces, i) the top of the rheologi-

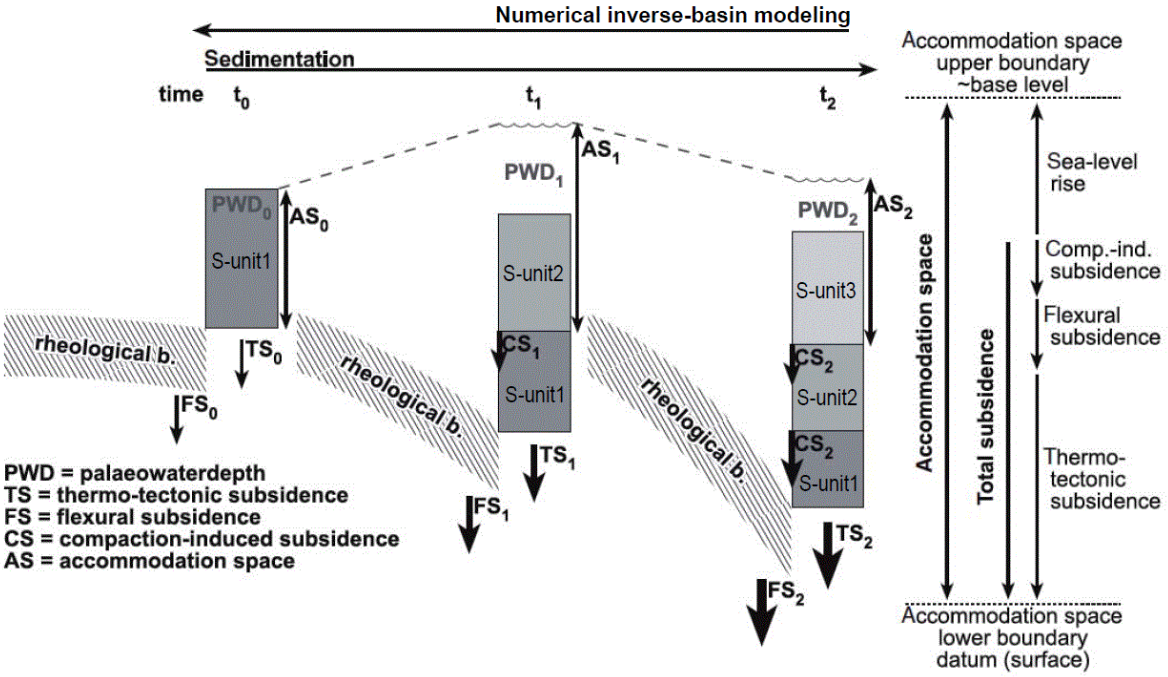

Fig. 15: Sketch illustrating the flexural inverse-basin modeling process ('backstripping'). x-axis, time; y-axis, burial depth; stratigraphic units (S-units 1 to 3) show different greyscales; arrows below the stratigraphic columns illustrate vectors of tectonic and flexural subsidence (thick arrow, high subsidence; thin arrow, low subsidence). The principle of the development of accommodation space is illustrated on the right. From Contreras (2011) after Emmerich et al. (2008).

cal basement and ii) the sea-level in approximation for base level.2.2. Geological Setting

2.2 Geological Setting

2.2.1. Passive continental margins

Passive continental margins are the boundaries of extensional or strike-slip basins after the break-up of a continent is complete. The transition from continental to oceanic crust in these basin types is not represented by a dynamic boundary like a rift or a subduction zone but an amalgamated contact (e.g. Bjørlykke, 2010).

Three types of passive margins are defined by their geometry so far: i) rifted margins, ii) sheared margins and iii) transtensional margins. Sheared margins develop after pure strike-slip movement (e.g. the Gulf of Aqaba; Scrutton, 1982), transtensional margins are a result of a mixed strike-slip and extensional movement (e.g. Czuba et al., 2011). A present day active example of a transtensional rift is the Upper Rhine Graben (Dézes et al., 2004), which is a hybrid of the types i) and ii). An example of this margin type in a drift stage is the southern Arabian/ Omanian passive margin (Robertson et al., 1990).

The passive continental margins of the Atlantic domain are in general rifted margins, but transtensional or strike-slip stages have occurred during basin evolution, resulting in a latitudinal offset of tens off kilometers between the conjugate margins. Tracing the fracture zones across the floor of the (Central) Atlantic Ocean result in a precision of +/- 100 km (Jansa & Wiedmann, 1982).

The initial stage of a true oceanic basin setting (or a proto-oceanic rift system) is established when two divergent continents separate and new oceanic crust forms in the intervening space (Einsele, 1992). All extensional basins experience a comparable development: i) brittle extension of the crust, causing extensional fault arrays and fault-controlled subsidence, and ii) thermal relaxation following ductile extension of the lithosphere, leading to regional postrift subsidence (e.g. Bjørlykke, 2010). A scheme of the geodynamic evolution from initial rift to early drift is shown in Fig. 16.

The driving force of rifting and subsequently drifting of a rifted divergent basin is often a heat accumulation or hot spot below the crust of huge continents. Before the opening of the Central Atlantic started, more or less all landmasses were concentrated in one supercontinent Pangaea (e.g. Blakey 2008). Heat accumulation results in melting of the lower lithosphere and therefore crustal thinning starts. Isostatic equilibrium results in the development of fault blocks in the rigid upper crust which slide down along listric faults (Veeken et al., 2008). This results in accomodation space om top which is filled with sediments delivered from the continents. During drift, the distance to the spreading axes increases and thermal cooling results in the development of further accomodation space which can be filled by clastic or marine sediments (e.g. Bjørlykke, 2010). Accomodation space on mature margins can be generated by flexural subsidence. If the vertical accomodation space is filled, the depositional system shifts into distal parts of the basin (cf. chapter 4&5).

The current status of an extensional basin can be described with the ß-factor and was first introduced by McKenzie (1978) together with the Pure-Shear-Model. Further models have been introduced later e.g. the Simple Shear, the pure shear or depth dependent models (e.g. Allen & Allen, 2005). Fig. 17illustrates the relationship between ß and status of divergence.

A differentiation can be made between volcanic and non-volcanic passive continental margins (e.g. Geoffroy, 2005; Wilson et al., 2001). As the passive continental margin of southern Morocco includes volcanic intrusions of the Central Atlantic Magmatic Province (CAMP) it is classified as a volcanic passive continental margin (Oyarzun et al., 1997). However, currently there is a controversy if the Tarfaya-Laâyoune segment is a volcanic passive margin or a non-volcanic passive margin with some volcanics.

The evolution of the sedimentary pattern at rifted passive continental margins follows a general trend. During the rift stage, the rift margins are filled-up by alluvial fans. At a later stage alluvial plains alternate with marine ingressions and often also with the deposition of extensive evaporite series (e.g. Bjørlykke, 2010). The transition from rift to drift is often defined by a sag basin characterized by reduced extension rate and minor faulting (e.g. Contreras, 2011). During this stage, a basinward dipping surface may develop, in general named Post Rift Unconformity, which is often the base for a continental shelf (e.g. Purser & Bosence, 1998). Drift sedimentation starts with deposition above this basinward dipping surface and often a ramp develops. With increasing maturity of the shelf, the variance of depositional environments increases and may in-

clude a huge variety, e.g. clastic/carbonate ramps, carbonate platform, river deltas or open marine non-carbonatic environments (Einsele, 1992). The sedimentary facies at passive margins include i) the sediment source with mountains, lakes and rivers, ii) the onshore/offshore transition characterized by deltas and estuaries, iii) the continental shelf, iv) the shelf break, v) the continental slope and vi) the bathyal including submarine fans which is adjacent in distal direction to the abyssal plains (Bjørlykke, 2010). Fig. 18 illustrates the erosional and depositional environments of a passive continental margin.

2.2.2. Exploration & Research history of the Tarfaya-Laâyoune Basins

Geological research of the lithosphere, asthenos-

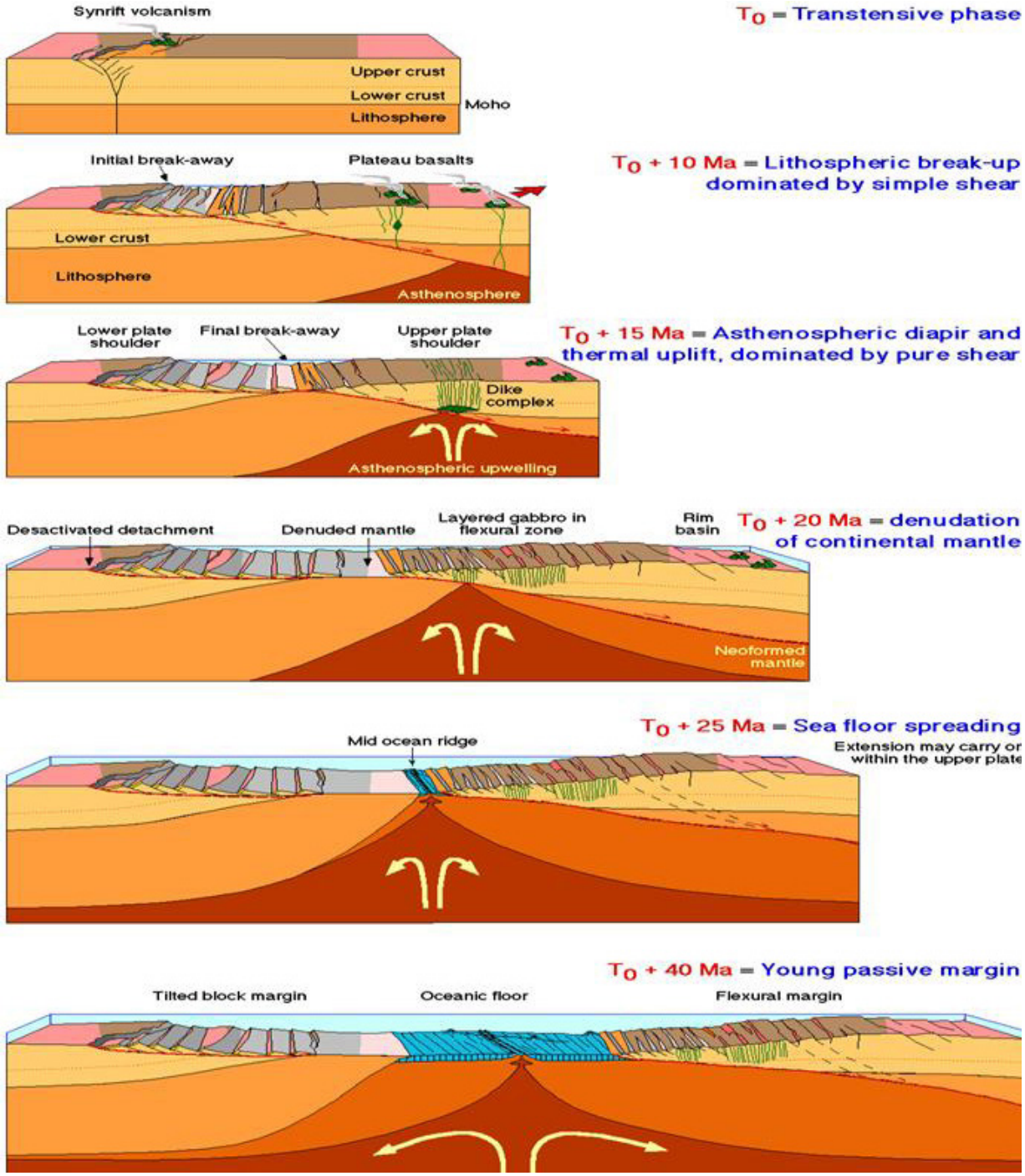

Fig. 16: Block model of the asymmetric, pure shear rift to early drift stages of a young ocean, the Red Sea (Stampfli & Merchant, 1997)

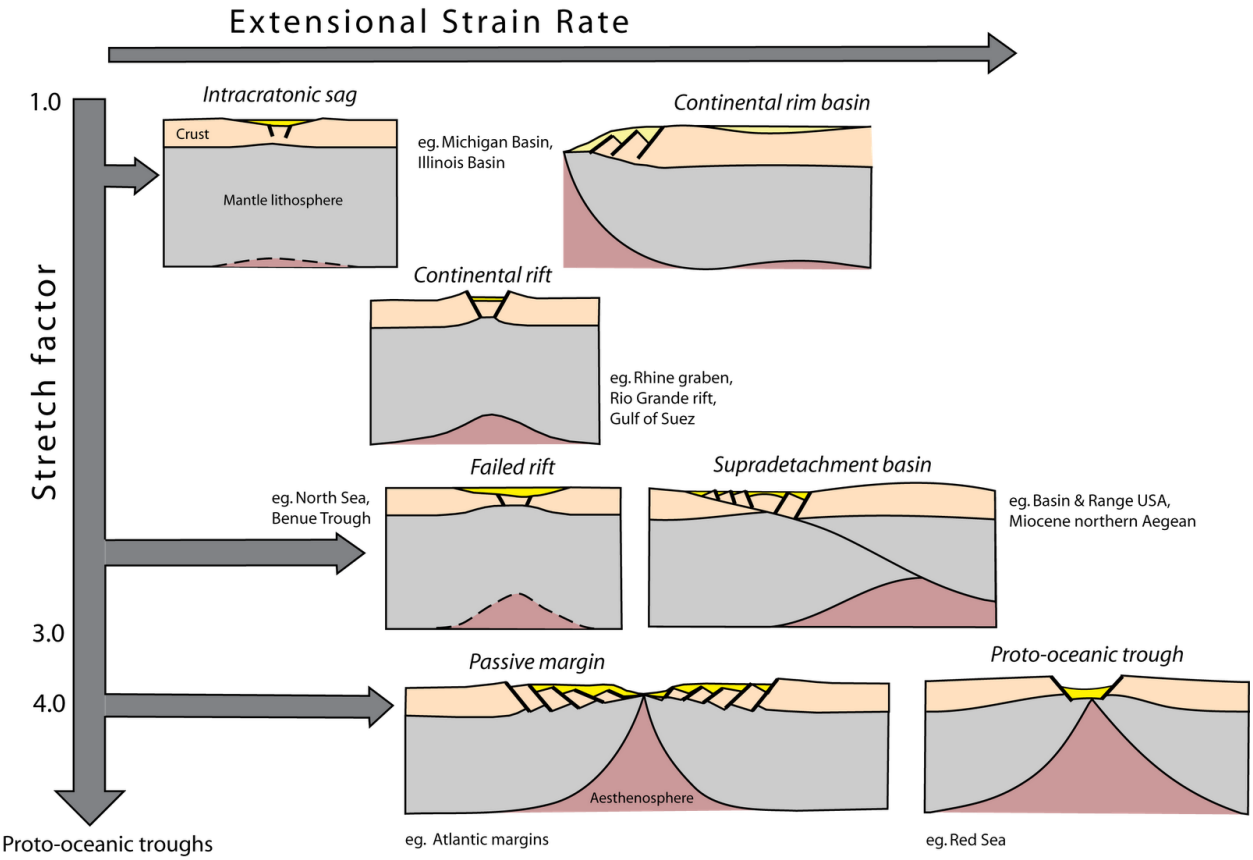

Fig. 17: Relationship between the stretching factor β and the stage of basin development. Basins with amounts around 1.5 or less are classified as active extensional basins before break-up or failed rifts. Basins with a factor >4.0 are spreading marine basins generating oceanic crust and are bounded by passive margins (Allen & Allen, 2013).

phere and in particular the mapping of the subsurface for geological interpretation and basin analysis of passive continental margins is highly dependent on the acquisition and availability of geophysical data. This can be combined with the evaluation of outcrop and well data. Collecting information in the field needs the lowest budget as a single geologist with a car is able to perform a full geological field reconnaissance. When it comes to the acquisition and evaluation of geophysical data like gravimetry, electromagnetic or reflection seismic, the amount of investment as well as man power rapidly increases. Finally the most cost intense exploration method, drilling a well, is often performed when the return of investment is above a certain probability. It is therefore hardly surprising that the highest amount of available subsurface data was and still is generated by exploration companies in the search for new resources for their product and asset portfolio. Economically driven exploration in the Tarfaya-Laâyoune Basins was always triggered by the aim to make a significant hydrocarbon discovery in the region and to understand the petroleum systems in this segment of the Moroccan margin.

Hydrocarbon exploration started in the late 1950s with a gravimetric survey of ENI (El Mostaine, 1991) resulting in the drilling of the first onshore wells in the region (CHBK, EA-1, PC-1, 1-1, 1-2 & 1-8) with promising results regarding hydrocarbon shows but no discoveries. Until present day, hydrocarbon exploration continued in batches resulting in

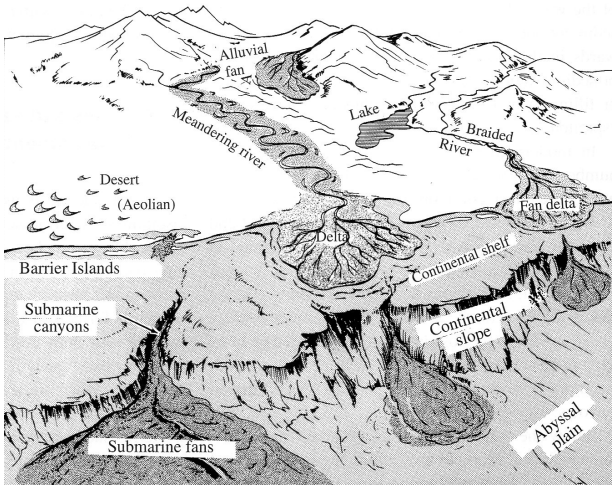

Fig. 18: Schematic representation of sedimentary facies on a passive margin (Bjørlykke, 2010).

the acquisition of several seismic surveys and drilling of some wells. The most important campaign has been performed by Exxon Morocco and lasted more than a decade. Based on 2D-seismic data acquired in the late 1960s, eight wells were drilled offshore between 1968 and 1972 (Moroccan Offshore - MO 1-8). This campaign and the follow up with Mobil Oil resulted in one major and two technical petroleum discoveries at the Cap Juby field (e.g. Davison, 2005; Wenke et al., submitted). Further mentionable campaigns have been the 1990 onshore campaigns by CGG, beicip and ONAREP (beicip, 1991), and the drilling of the wells AMBER and RAK by Shell (e.g. Whaley, 2012). After a period of more or less no exploration activity, new wells are currently drilled (Foum Draa 1) or planned by Cairn Energy, Galp Enegija and San Leon. In autumn 2013, two majors, ENI and BP returned or newly farmed in to the region.
Nevertheless, some wells in the deep offshore of the region have been drilled for scientific reasons during the DSDP and ODP projects. Wells with significant relevance for this study are DSDP 415, 369 and 397. Several scientific cruises organized by national institutions like the AWI using wide-angle seismic, gravimetry or electromagnetic collected a huge amount of information about the nature of the sediment boundary and deeper crust. Further important cruises have been performed by the Bundesanstalt für Geowissenschaften und Rohstoffe (BGR, von Rad et al., 1982) and the IFREMER (Contrucci et al., 2004; Klingelhöfer et al., 2009).
A considerable number of regional, structural and stratigraphic studies exist for the Tarfaya-Laâyoune and adjacent Moroccan Atlantic Basins. Choubert et al. (1966) and Querol (1966) presented the first synthetic litho- and biostratigraphy for the Tarfaya-Laâyoune Basins, which was revised by Ranke et al. (1982). The structural development and present basin architecture is described in Rona (1970), Uchupi (1976), Lancelot & Winterer (1980), Hinz et al. (1982), Ranke et al. (1982), Heyman (1989), Le Roy (1997), Davison (2005), and Hafid et al. (2008). Salt flow and its impact on the basin fill architecture has been discussed in Tari et al. (2003), Davison & Dailly (2010), and Tari et al. (2012).
Vail et al. (1977) developed the first 3rd order sequence stratigraphic framework for the post-rift Tarfaya Basin. Le Roy & Piqué (2001) subdivided the rift stage into four sequences. High resolution 4th order sequence stratigraphy for the Tarfaya-Laâyoune post-rift basin fill is presented in Wenke et al. (2011).
The timing and lithospheric mechanism of Atlantic rifting and continental separation in the central Atlantic have been discussed in Hinz et al. (1982), Steiner et al. (1998), Olsen et al. (2003), Contrucci et al. (2004), Knight et al. (2004), Sahabi et al. (2004), Maillard et al. (2006), Klingelhöfer et al. (2009), and Gouiza (2011).
1D subsidence models exist for the Essaouira Basin (Le Roy et al., 1998; Ellouz et al., 2003), the onshore Doukkala Basin, the northern Tarfaya Basin and southern Souss Basin (Gouiza, 2011; Bertotti & Gouiza, 2012). 2D flexural basin and compositional accommodation analyses exist for the onshore Agadir Basin in the Western High Atlas (Zühlke et al., 2004), north of the study area.

2.2.3. Tectonostratigraphic units of the Tarfaya-Laâyoune Basins and adjacent areas

The Tarfaya Basin (75.000 km^2) extends from the town of Sidi Ifni in the north to south of Daora. The Laâyoune Basin (150.000 km^2) extends south from Daora (DAO 1-1 well) to approx. 150 km north of the city of Dakhla. The study area covers the whole Tarfaya and the northern Laâyoune Basin to the town of Boujdour (cf. Chapters 3.1).
Adjacent tectono-stratigraphic units of the Tarfaya-Laâyoune Basins are the Pre-Cambrian to Paleozoic Anti-Atlas (N), the Paleozoic Bas-Drâa region, the Paleozoic-Cenozoic Zag Basin (NE and E) and the West African Craton, including the Reguibat shield (SE). To the north the Tarfaya Basin shows a gradual transition to the Agadir/Souss Basin. To the south, the Laâyoune Basin is limited by the Dakhla Fracture Zone (Hafid et al., 2008; Shaw & Roberts, 2009). To the west, the offshore basins pass over into the open Atlantic Ocean. Features in the deep basin are the Jurassic Magnetic Quiet Zone (JMQZ), the eastern Central Atlantic salt province (Tarfaya Basin) and the Canary Islands (Fig. 19). The two basins are divided by the Canary Island Fracture Zone (cf. Fig. 23)

2.2.4. Structural elements

The structural setting is controlled by the post Hercynian break-up of Pangaea and the Atlantic drift phases. The continental basement which consists in the NE of Precambrian to Cambrian crystalline rocks and Paleozoic sediments in the central and southern onshore and shelf areas dominate the pre-

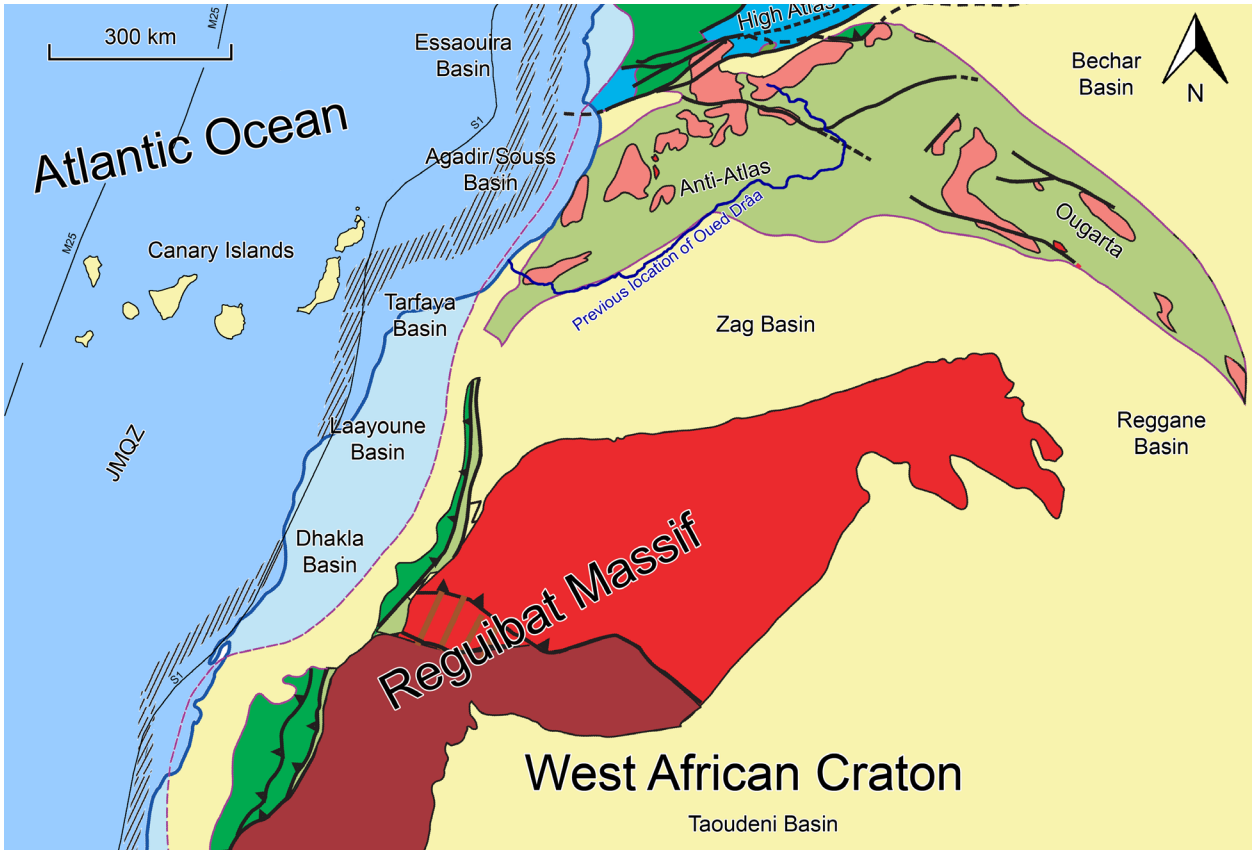

Fig. 19: Southern Moroccan Basin as a transition between continent and ocean (modified after Michard et al. 2008). From N to S: Essaouira Basin, Agadir/Souss Basin, Tarfaya Basin, Laâyoune Basin, Dakhla Basin and, at the very south, the Senegal Basin. Surrounding tectonostratigraphic units clockwise from North: (Western) High Atlas, onshore Souss Basin, Anti-Atlas, Zag Basin, Reguibat with Zemmour fault zone and West African Craton and the Atlantic Ocean with the Canary Islands. The grey hatched areas marks the oceanic margin anomaly after Sahabi (2004), the S1 magnetic anomaly is taken from Roeser (1982). The area of the Jurassic Magnetic Quiet Zone (JMGZ) and the location of the M25 anomaly are taken from Klitgord & Schouten (1986).

rift basement (Michard et al., 2008; Wenke et al., sub.). With the onset of drift, oceanic crust has been produced and defines the basement in the W of the S1 magnetic anomaly (Roeser, 1982; Contrucci et al., 2004) (Fig. 19).

The onshore part of the basin as well as the shelf are characterized by syn-rift structures (Hafid et al., 2008).

Three (half-) grabens developed striking NE-SW (Fig. 20). From proximal to distal these are the Chebeika graben, the Laâyoune graben and the Atlantic Basin. The three structures are separated by two horst blocks, the Chebeika Horst and the Juby Horst (Horst du Juby; beicip, 1991). Listric faults bound the structures, their top mark the PRU (Wenke et al., 2011, c.f. chapter 4).

Increasing lithostratigraphic pressure resulted in the movement of late rift salt deposits, ending in the development of numerous salt diapirs in the deep offshore. The diapirs are related to faulting of the overlying sediments and a collapse of the Jurassic slope with related development of growth faults (e.g. Tari et al., 2003; Wenke et al., sub.).

The regional Alpine development with the uplift of the High Atlas result in a flexural uplift of the NE-Tarfaya Basin as well as the development of a major regional unconformity, the Base Cenozoic or Initial Atlasian Unconformity (IAU; Wenke et al., sub.).

2.2.5. Basin development stages and fill

The pre-rift succession of the Tarfaya-Laâyoune Basins, which is called in this study „rheological basement“ is mainly defined by two units: i) magmatic and metamorphic rocks of the proterozoic panafrican belt (Gasquet et al., 2008) and ii) (meta-)sediments of the variscan belt (Michard et al., 2008).

The oldest rocks in the study area are exposed in the Central and Western Anti-Atlas as well as the Bas Drâa region. Magmatic rocks of three different intrusion stages are linked with so called Precambrian inliers („boutonnières“). Early intrusions have

been identified in the Bas Drâa region, as well as the Ammeln Valley (Tahala granite) and are dated to the Orosirian of the Paleoproterozoic (2,000 - 2,050 Ma, Gasquet et al., 2008). The Ifni granites are dated 614 +/-10 Ma (Early Ediacarian of Neoproterozoic). The youngest Pan-African magmatic rocks have an age of 550-580 Ma (Late Ediacarian)

The exhumation of these rocks took place during transpressional or transtensional strike-slip tectonics (Gasquet et al., 2008) further uplifts during Triassic rift and Early Cretaceous drift stages have been recognized in recent studies (Gouiza, 2011; Sehrt, 2014). These three plutonic boutonnières which are accompanied with proterozoic rocks, represent a continuous source of sand during basin evolution.

The Paleozoic is represented by a i) Cambrian rift to ramp clastic to carbonate sequence; ii) Early Ordovician post-rift/sag valley fills including mainly clay and siltstones; iii) Late Ordovician clastic ramps; iv) Silurian shales; v) Early Devonian carbonate platforms; vi) Late Devonian extension with the deposition of shale, silt and sand alternations; vii) Carboniferous carbonates. For a detailed description read Destombes et al. (1985) and Michard et al. (2008).

The Meso- to Cenozoic seismostratigraphy of the Tarfaya-Laâyoune Basins (Wenke et al., 2011) covers six major basin stages: i) rift and sag; Tatarian (Late Permian) to Pliensbachian (Early Jurassic), ii) early drift; Pliensbachian/Toarcian (Early Jurassic) to Mid/Late-Tithonian (Late Jurassic), iii) mature drift; Late Tithonian (Late Jurassic) to Late Aptian (Early Cretaceous), iv) mature drift with initial Atlasian compression; Early Albian (Early Cretaceous) to Maastrichtian (Late Cretaceous), v) mature drift with initial Atlasian uplift; Maastrichtian (Late Cretaceous) to Early Oligocene (Late Paleogene) and vi) mature drift stage with peak Atlasian uplift and erosion; Late Oligocene (Late Paleogene) to present.

Initial rifting at the Central Atlantic region started in the Late Permian (Klitgord et al., 1988; Olsen, 1997; Steiner et al., 1998; Zühlke et al., 2004) indicated by the post-Hercynian or the Initial Rift Unconformity (IRU). The early rift basin fill has been preserved in the onshore Argana Valley (Western High Atlas, onshore Agadir Basin). There, alluvial

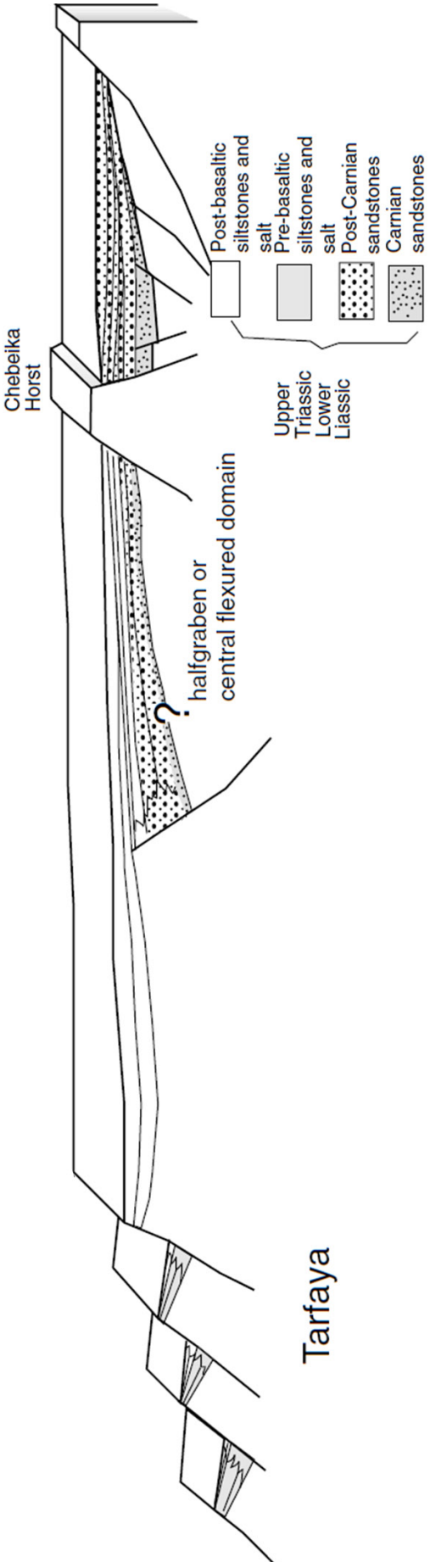

Fig. 20: Basement structure, halfgraben and graben setting of the Tarfaya basement and the Permo-Triassic graben fill of the inner to outer shelf area. The rift (half-) grabens are segmented by Horst structures. Three parallel graben developed, two failed, one ended up in the Atlantic Ocean. The direction of view is N (from Le Roy & Piqué, 2001).

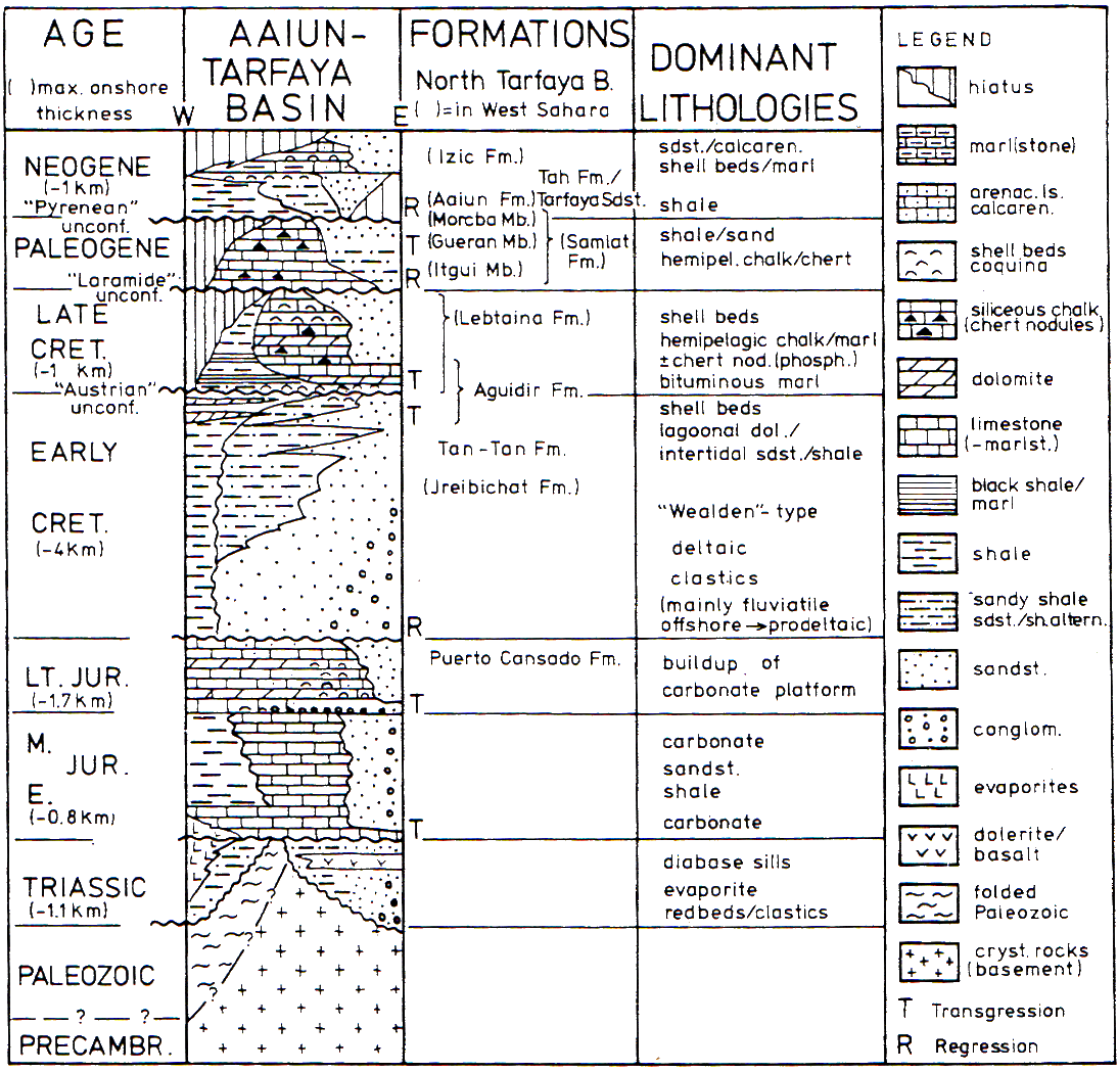

Fig. 21: Generalized lithostratigraphy of the onshore Aaiun-Tarfaya Basin. From Ranke et al. (1982), after Choubert et al. (1968), Querol (1966), AUXINI (1969), and Ratschiller (1970).

fan conglomerates and sandstone channels confined to large graben valleys reach thicknesses of up to 1,500 m (Brown, 1980; Tourani et al., 2000; Zühlke et al., 2004).

Until today, a comprehensive chrono-/lithostratigraphic subdivision of the Triassic and Jurassic for the Tarfaya-Laâyoune Basins does not exist. Basic descriptions can be found in Choubert et al. (1966), Querol (1966), Ranke et al. (1982, Fig. 21), El Khatib et al. (1995), Abou Ali et al. (2004; 2005), and Hafid et al. (2008). For the northern Tarfaya Basin, LeRoy and Piqué (2001; Fig. 20) subdivided the rift and sag basin fill into four units (sT1-sT4) based on onshore and offshore seismic and well data. The units sT1 and sT2 correlate approximately to the Ikakern Formation, sT3 to the Tadrart Ouadou Member of the Bigoudine Formation and sT4 to the Sidi Mansour and Aït Hssaine Members of the Bigoudine Formation of the Western High Atlas (cf. Zühlke et al., 2004). A comparable subdivision of the Essaouira Basin is given in Hafid (2000a; b).

The rift and sag basin fill of the Tarfaya-Laâyoune Basins have only been encountered in two proximal onshore wells (EA-1 and CHBK-1) (Choubert et al., 1966; LeRoy & Piqué, 2001). Offshore, Late Triassic salt was drilled in the wells MO-3 and CJ-1 (ONHYM, 2008; Fig. 22 & 21). The Triassic succession includes mainly coarse clastics, fine-grained intercalations and dolerite sills/dykes. Allochthonous evaporites are known from offshore wells as well as seismic imaging and extend between the Cap Juby Horst in the south (cf. Chapter 5) and the Moroccan Meseta in the north (Hafid et al., 2008). They also occur south of Laâyoune where they extend beyond the study area to Senegal (Rona, 1970; Seibold, 1982; Davison & Dailly, 2010). Dolerites

of the Central Atlantic Magmatic Province (CAMP; Knight et al., 2004; Marzoli et al., 1999) define the Tarfaya-Laâyoune Basin segment as a volcanic passive continental margin.

Like all other Moroccan passive margin segments the rift stage is bounded at the top by the Base Jurassic or Post Rift Unconformity (PRU). The end of the sag stage is defined by the Toarcian or Initial Drift Unconformity (IDU) with significant erosional topography, toplap terminations in the lower rift/sag succession and onlap to offlap of the upper early drift succession (Hafid, 2000a; b; LeRoy & Piqué, 2001; Zühlke et al., 2004; Wenke et al., 2011).

The onset of the formation of oceanic crust in the Central Atlantic is discussed in numerous contributions to have started between 150 and 210 Ma (e.g. Rothe, 1968; Rona, 1970; Lancelot & Winterer, 1980; Hinz et al., 1982; Roeser, 1982; Steiner et al., 1998; LeRoy et al., 1998; Sahabi, 2004, Zühlke et al. 2004; Contrucci et al., 2004). Studies based on litho- and biostratigraphy (Steiner et al., 1998; LeRoy et al., 1998; Zühlke et al., 2004) and magnetic data (Sahabi et al., 2004) indicate that sea-floor spreading started in the Pliensbachian/Toarcian (189 – 195 mya). In this study, the age of the IDU is assumed to be latest Pliensbachian (189.6 Ma).

The early drift stage is bounded by the IDU at the base and the Base Cretaceous or Mature Drift Unconformity (MDU) at the top. The MDU has an initial age of 144.2 Ma in the outer shelf to slope area of the Tarfaya-Laâyoune Basins and continues until 132.0 Ma on the shelf (Wenke et al., 2011). The earliest Berriasian shelf succession has been deposited or preserved only in the Tan Tan Delta (Todd & Mitchum, 1977). In the proximal Agadir Basin, the Early Cretaceous hiatus covers approx. 12 mya (Zühlke et al., 2004).

With initial sea-floor spreading Toarcian ramps switched from aggradation to progradation and encroached the African craton to the E-SE. Clastic ramps prevailed until the Bajocian. Well-developed slope clinoforms indicate increasing bathymetry of the early Central Atlantic continental margin (Todd & Mitchum, 1977; Wenke et al., 2011). Bajocian outer shelf areas experienced an intermittent regression with intertidal carbonate platform deposition, while the subtidal inner to outer shelf deposition prevailed during the Bathonian. Oolites indicate shoals and high energy conditions (Wenke & Zühlke, 2011).

The late Bathonian is overlain by mid- to inner shelf deltas and thin outer-shelf shales (Todd & Mitchum, 1977). Callovian to Oxfordian conglomerates indi-

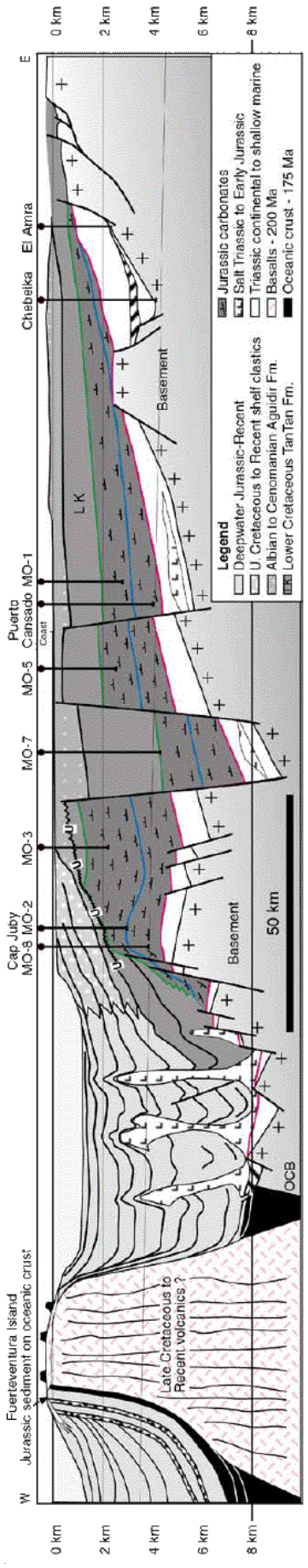

Fig. 22: Schematic cross section of the Tarfaya Basin extrapolated out to Fuertaventura. From Davison (2005), based on section in ONAREP (2003). The transition from oceanic to continental crust is illustraed in this sketch at the western most salt diapir. The Cap Juby oil field is located on an elevated Horst block (Horst de Juby, Juby Horst). The section between MO-2 and Puerto Cansado follows S to N direction, the deeper subsided block should figure the depression in which the Tan Tan Delta developed. The illustration is simplified. The part between Puerto Cansado and El Amra follows W-E direction, the position of MO-1 is „projected". The well Puerto Cansado (PC-1) is located in the Laâyoune Depression, wells Chebeika (CHBK-1) and El Amra (EA-1) were drilled into the Chebeika Depression. The two depressions are separated by the Chebeika Horst.

cate a period of tectonic/thermal relaxation followed by a major transgression (Ranke et al., 1982; Ellouz et al., 2003). During the Kimmeridgian open marine shelf carbonate platforms again prevailed on the shelf (Wenke & Zühlke, 2011). Their margins feature extended coral-algal reef tracts and high-energy oolite belts. The Kimmeridgian to Tithonian succession of the Tarfaya-Laâyoune Basin consists of the Puerto Cansado Formation. Carbonate production was terminated in the Latest Tithonian (Todd & Mitchum, 1977).

The MDU developed in response to a major eustatic sea-level fall in Late Tithonian to Early Berriasian (for mature drift definition see Bott, 1992; Zühlke et al., 2004). The Late Jurassic platform top experienced major subaerial exposure and karstification during this forced regression (Vail et al., 1977; Ranke et al., 1982; El Khatib et al., 1995). Incised valleys linked eastern source areas (Anti-Atlas, Reguibat) with regionally extensive (Tan Tan, Laâyoune) deltas on the inherited Jurassic slope (Wenke et al., 2011).

Berriasian pro-delta shales are the earliest deposits of the Tan Tan Delta (Berriasian-Aptian) which can be identified. Existing wells do not penetrate the early delta front and top. On the shelf top, which has been widely exposed since the Late Jurassic deposition returned during the Hauterivian. At the same time, increasing overburden triggered the mobilization of Triassic salt in the western deeper buried parts of the Tarfaya Basin (Hinz et al., 1982; Wenke et al., 2011). Tari et al. (2003) assign initial rafting in the Safi and Essaouira Basins to the Hauterivian to Aptian. Prominent growth faults which were triggered by salt movement and the collapse of the Jurassic continental rise developed below the outer shelf to upper slope of the Tarfaya Basin (Wenke et al., 2011). In the southern outer shelf areas of the Tarfaya Basin, rising salt diapirs led to the development of the Juby Horst structure. Due to the reduced thickness of Triassic evaporites in the northern Laâyoune Basin, salt deformation is less pronounced. Fault blocks in the outer shelf area show only minor offsets (tens of meters). Growth faulting finished during Albian times. Retrogradation of the Tan Tan Delta started in the Hauterivian and continued until the Aptian in response to high rates of subsidence and eustatic sea-level rise (Todd & Mitchum, 1977; Heyman, 1989; Hardenbol et al., 1998). In the Late Aptian, the Tan Tan Delta became inactive.

The Top Aptian erosional unconformity is related to an extended eustatic sea-level lowstand and high sea floor spreading half-rates which controlled reduced subsidence or uplift of the Moroccan margin (Zühlke et al., 2004). The unconformity can be identified by a consistent high-amplitude reflector on the shelf top and margin (Wenke et al., 2011). In this study, the Aptian Unconformity separates the tectonic stages 3 and 4 and is termed the Peak Spreading Unconformity (PSU) and has significant importance for the Tarfaya Basin development.

A long term transgressive trend starts in the Albian. Inner shelf low-energy and middle-outer shelf lagoonal envrionments prevail (Aguidir Fm.; Ranke et al., 1982; El Khatib et al., 1995; Abou Ali et al., 2004).

Apart from a regressive episode in the Cenomanian, a long-term transgressive trend prevailed throughout the Cretaceous and peaked in the Turonian. The basin fill shows comparatively thin thicknesses and is represented by hemipelagic marls and carbonates with decreasing terrigenous influx and increased plankton input (Ranke et al., 1982). Several oxygen minimum zones led to the development of black shales (OAE 1c, 1d, OAE-2 and 3) during the Albian to Santonian (Kuhnt et al., 2009; Sachse et al., 2011).

After maximum transgression, which correlates with low sediment input during the Late Cretaceous, initial plate convergence, compression and tectonic uplift. This led to the development of a major regional unconformity, the Base Cenozoic or Initial Atlasian Unconformity (IAU). Its development is controlled by: i) a minimum of sediment accumulation at the slope area during Albian to Campanian (Ranke et al., 1982; Wenke et al., 2011) or post-Campanian erosion of this succession (Uchupi et al., 1976; Heyman, 1989), ii) erosion of Upper Cretaceous succession in the northern proximal basin in Late Oligocene caused by Atlasian uplift (Arthur et al., 1979; Rad & Arthur, 1979, Zühlke et al., 2004) and/or iii) a relative sea-level fall in the post-Campanian. The IAU of the Tarfaya Basin formed at the same time as initial submarine volcanic activity of the Canary Islands began. Thermal uplift may have influenced the crustal rigidity, total subsidence/uplift history and basin architecture of the distal Tarfaya Basin.

During the Maastrichtian, the depocenter shifted basinward and slope deposition recommenced in the Paleogene (Samlat Fm.). The Santonian to Paleogene Tarfaya Basin fill is represented by shallow marine, shelfal silty marl- and claystones. In the Laâyoune Basin marlstones, interbedded siliceous-

phosphatic chalks, and chert or phosphorite horizons developed (Ranke et al., 1982). Increased Atlasian compression resulted in a moderately increased sediment input (Zühlke et al., 2004) and the development of shelf margin wedges during the Eocene and early Oligocene.
Late Oligocene continental clastics have been preserved only in the southern Laâyoune Basin (Ranke et al., 1982). Peak Atlasian deformation and uplift strongly affected the northern Tarfaya Basin, where the original Meso- to Cenozoic succession has been eroded down to the Lower Cretaceous (Choubert et al., 1966; Vail et al., 1977; Ranke et al., 1982; Wenke et al., 2011).
The Mid-Oligocene Peak Atlasian Unconformity (PAU) bounds the Paleogene shelf margin wedge. Neogene sedimentation is characterized by shelf bypass; low angle strata dip in basinal direction showing onlap against the Paleogene succession.
A schematic cross section illustrating the Meso- to Cenozoic Basin fill of the Tarfaya Basin is illustrated in Fig. 22.

2.2.6. Hydrocarbon play scenarios

With the discovery of the Cap Juby oil field in 1968/1969, the presence of a functioning petroleum system has been proven. However, the source rock never has been really identified. Restricted Triassic rift sediments, organic matter of the Toarcian turnover event (e.g. Jenkyns et al., 2002), or a potential Middle Jurassic source rock have been discussed (e.g. Jabour et al., 2000; Davison, 2005). Regionally exposed Aptian/Albian as well as late Cretaceous source rocks of the OAE 1 and 2 events have been described in various contribution, (e.g. Kuhnt et al., 2009; Sachse et al., 2014). Potential reservoir facies is described for late Jurassic bioherms, Lower Cretaceous deltaic sandstones (e.g., Heyman, 1989) or Cenozoic Mass Transport Complexes (MTCs, Lee et al., 2004).
The top seal for potential Triassic plays is believed to be represented by Early Jurassic shales of the sag stage, Late Jurassic reservoirs are potentially sealed with Lower Cretaceous shales and Cenozoic MTCs by Neogene fine clastics (e.g. Wenke et al., 2011).

3. Materials & Methods

3.1. Data base

The database available for this study includes data from outcrop analogue studies, literature data, well information (16 offshore, 14 onshore) and 4,084 km of 2D-seismic lines (Fig. 23). Outcrop, well and seismic data are of different scale. Outcrop and well cuttings allow analysis in microscope to cm-scale, well-log interpretation in m-scale while vintage 2D-seismic data as used in this study seismic scale in depth reaches 30-60m per phase (e.g. Bertram & Milton, 1996; Wenke et al., 2011; see Fig. 24).

3.1.1. Outcrop studies

The rheological basement analogue and sediment source area was studied in the Anti-Atlas, Bas-Draâ region and NW Reguibate. It comprises of Pre-Cambrian plutonites and the Cambrian - Carboniferous sedimentary succession. The Triassic rift and Jurassic early drift sediment analogues have been studied

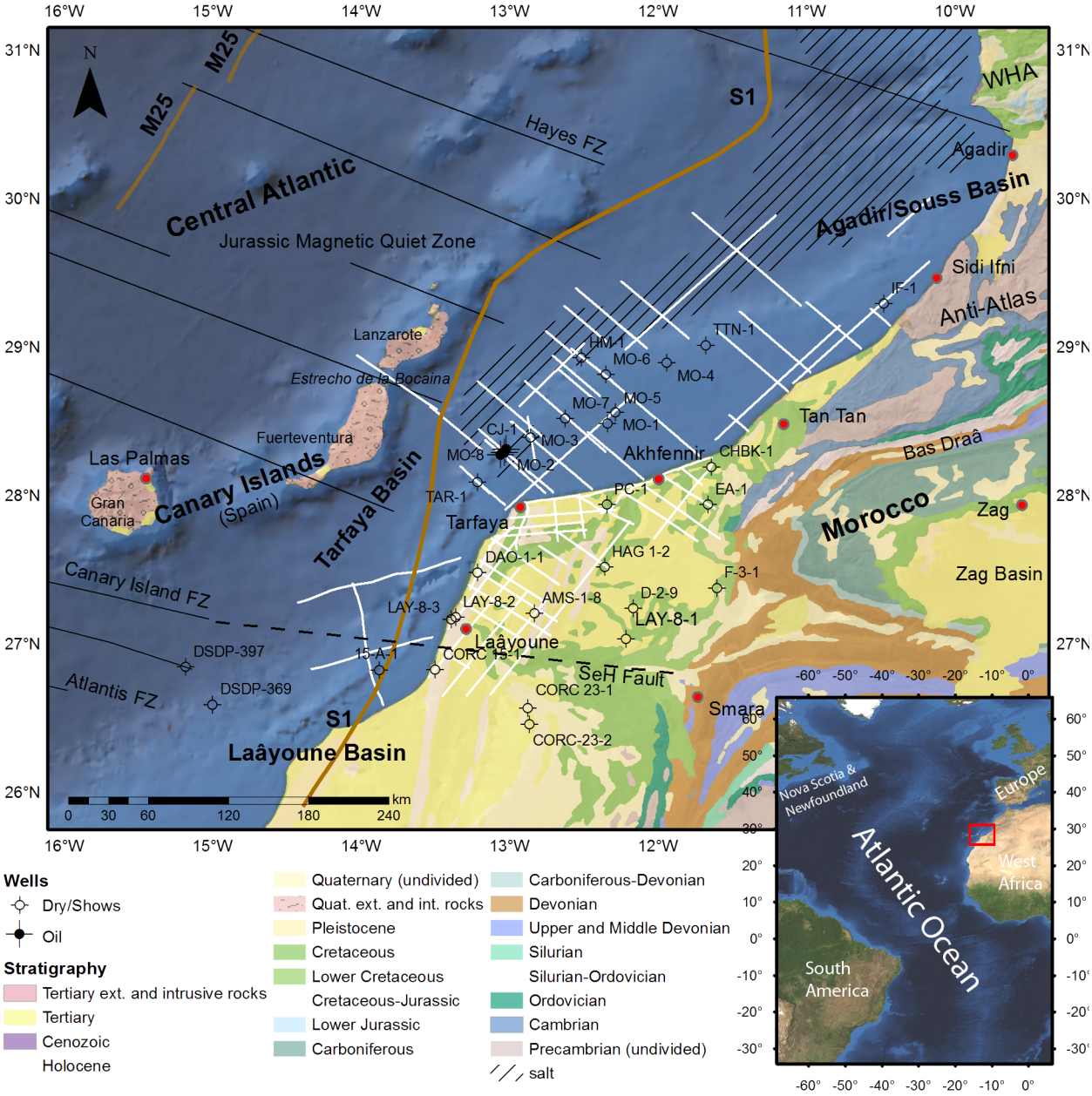

Fig. 23: Basemap with 2D-seismic lines for a) regional mapping (white lines), b) 2D flexural reverse modelling (red lines), and correlation wells. Fracture zones after Klitgord & Schouten (1986), magnetic zones after Roeser (1982) and Labails et al. (2010), Stratigraphy after Saadi et al. (1985). From Wenke et al. (subm.)

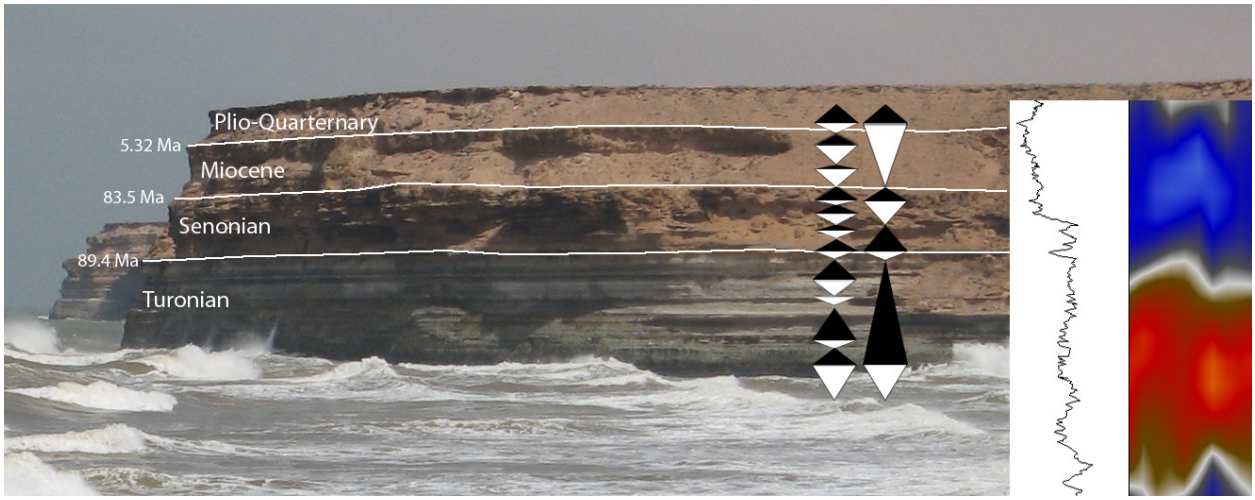

Fig.: 24: Data resolutions (rock, log and seismic reflections) compared in outcrop of Turonian black shales (Oued Ma Fatma) (Wenke et al., 2011).

in the Western High Atlas; the first is fully exposed in the Argana Valley, the latter in the Paradise Valley.
The proximal to mid shelf Early Cretaceous - Holocene succession is fully exposed in the Tarfaya-Laâyoune Basins. In addition, the westernmost Late Cretaceous succession of the Tethyan domain was studied in the Northern and Southern Zag Basin. A map of the visited outcrops can be found in Appendix 1.

3.1.2. Well data

Eleven onshore and thirteen offshore wells are located in the Tarfaya Basin. Three onshore and three offshore wells in the Laâyoune Basin. In addition, three wells drilled in the Bas-Draâ and southern Anti-Atlasian have been available for the evaluation of the stratigraphic succession of the Paleozoic „basement“. The majority of the wells in the Tarfaya-Laâyoune Basins reach the Tithonian basin fill. Four wells have their TD in Toarcian ramp units and eight wells in Triassic rift units. Only four wells encountered the Hercynian basement. Well data includes formation tops, lithofacies, biostratigraphy and standard log suites (i.e. gamma ray, resistivity, sonic, density, self potential). Check shots from borehole seismic data were available for five wells. In addition, synthetic check shots were generated during this study. An overview of the available well dataset is given in Tab. 2.

3.1.3. 2D-seismic dataset

The seismic database includes 4,084 km of 2D-seismic data in time domain from ten seismic surveys acquired between 1969 and 1999. A detailed list is given in Appendix 2.

3.1.4. Literature data (EM & gravity)

The location and extension of fracture zones (FZ) are taken from Le Pichon & Fox (1971), Klitgord & Schouten (1986). The position and extension of the magnetic anomalies including the S1 which marks the transition from continental to oceanic crust, was taken from Roeser (1982) and Labails et al. (2010). As the base of the Meso/Cenozoic sedimentary basin fill was not covered everywhere by the available reflection seismic profiles, the Top of the basement in the outer shelf to basin area was reconstructed from literature. Hinz et al. (1982) determined the thickness of the sedimentary basin fill and the top of the basement based on gravimetry, sono-buoy refraction seismic measurements and refraction seismics (Fig. 26b). Wide angle seismic was used for the northern Moroccan margin (Contrucci et al. 2004; Fig. 26c) and the Dakhla Basin (Klingelhöfer et al. 2009; Fig. 26d).

3.2. Methods & workflow

The workflow of this study is given in Fig. 25.

3.2.1. Field work

The basin analysis includes a 30 day field reconnaissance performed in spring 2009. Field work contained standard procedures after Tucker (2003, see chapter 3.1.1), including 25 vertical sections and

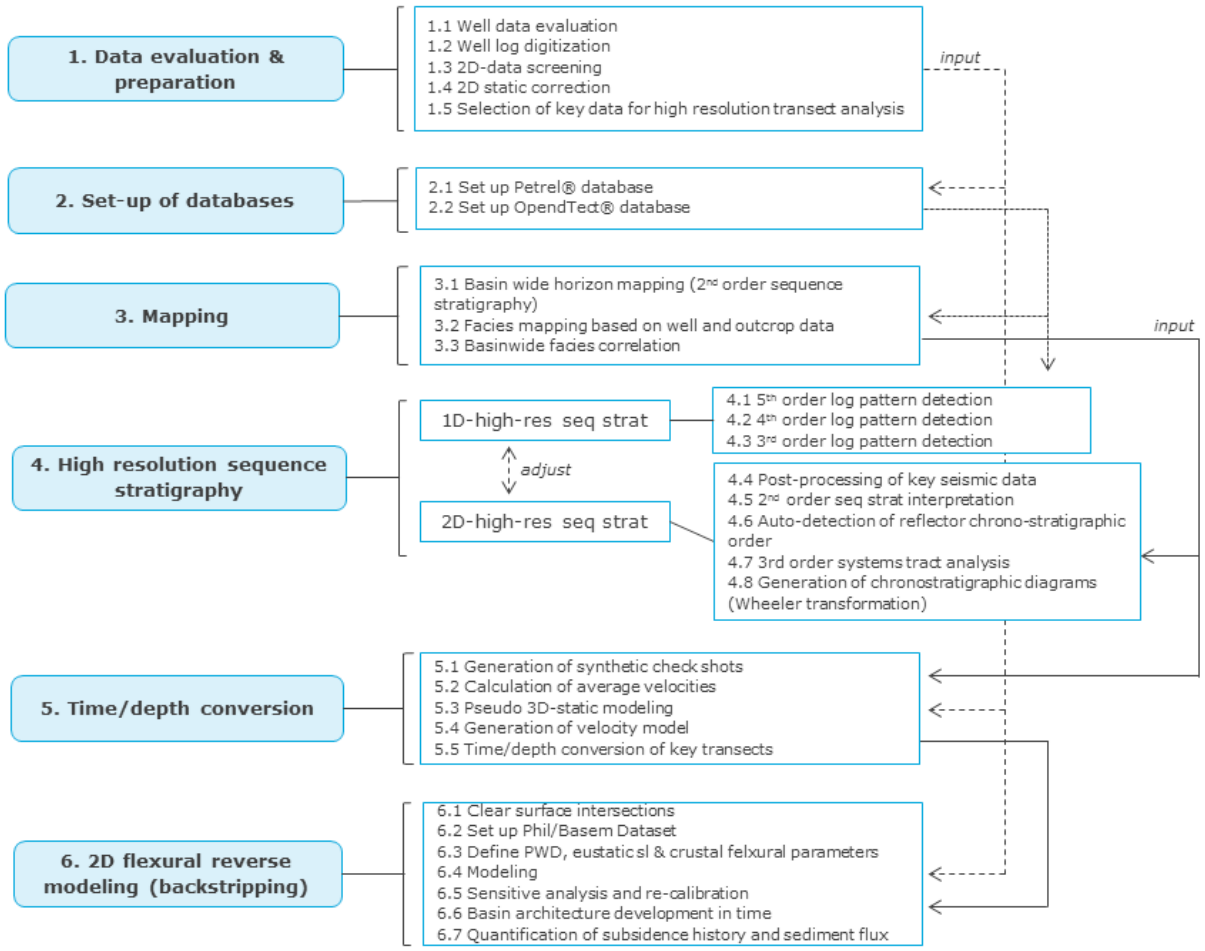

Fig. 25: Thesis workflow.

200 sample points.

3.2.2. Well evaluation

The available data was screened and evaluated (Tab.2). Well-logs were available for 17 wells in .las (6 wells) and scanned .tif file format (11 wells). Las files were loaded into the Petrel project, tif-files were digitized in GraphClick® to ASCII format and subsequently loaded. Formation tops are available from 18 onshore and 17 offshore well reports, lithostratigraphic charts and literature data. Fourteen onshore and 11 offshore wells are located in the modelling area. Check-shots for the stratigraphic tie of seismic data are available from well reports for the wells Ifni, HM-1, MO-3, MO-6, MO-7 and TAR-1. Velocity and TWT data of the wells EA-1 and CHBK-1 given in by Beicip (1990) appeared not to be reliable and have therefore been modified. The evaluation of all well information resulted in 29 formation tops which could be recognized at basinwide scale. All post-Pliensbachian stages of the Mesozoic, apart from the Aalenian have been identified.

3.2.3. Seismic interpretation

3.2.3.1 Basin wide mapping

Seismic interpretation (reflector picking) was performed basin wide on eight formation tops (Quarternary, Top Miocene, Top Eocene, IAU, Top Aptian, Top Hauterivian, Top Tithonian, and Top Pliensbachian). These are reflectors with a characteristic amplitude, geometry and good lateral consistency. Basinwide horizon maps in time domain have been generated as a base for basin wide facies mapping. Prominent seismic reflectors with clear amplitude characteristics or reflector geometries are in general the major unconformities with hard contrasts based on sudden lithological changes in the depositional succession, e.g. the Top Aptian/Tan Tan Delta.

Name	Short name	UWI	Well symbol	Surface X	Surface Y	Latitude	Longitude	KB (m asl)	TD (TVDSS)	TD (MD)	Spud date	Operator	stratigraphic chart	well report	check shot data	litera-ture	stratigra-phic depth	AMP key well	SN	SP	DT	GR	LAT	LN
Alisio 15-A-1	15-A-1	870011011	Dry	611974	2967741	26°49'34.90"N	13°52'23.60"W	10	3813	3823	5/10/1970	ENPASA	x		x	x	Valanginian	x	Yes	Yes	Yes	Yes	No	No
Amseiquir 1-8	AMS 1-8	870031011	Dry	715081	3011385	27°12'28.97"N	12°49'42.83"W	70	4047	4117	10/29/1961	Union Oil	x	x		x	Aalenian?	x	Yes	Yes	Yes	Yes	Yes	Yes
Adrar Zougar-1	AZ-1	870581011	Dry	1123970	3224675	28°59'50.53"N	8°36'4.58"W	0	10	10	12/17/1961	Petrofina		x			Precambrian		No	No	No	No	No	No
Chebeika 1	CHBK-1	870051011	gas shows	830094	3123452	28°11'42.82"N	11°38'16.37"W	70	4130	4200	5/14/1961	SOMIP	x			x	Precambrian	x	No	No	No	No	Yes	No
Cap Juby 1	CJ-1	870041011	Dry	693449	3131101	28°17'28.90"N	13°01'38.90"W	29.9	4768	4798	5/6/1984	Mobil		x		x	Triassic	x	No	No	Yes	Yes	No	No
CORC 15-1	CORC-15-1	870381011	gas shows	649345	2968439	26°49'44.99"N	13°29'49.81"W	13.53	3456	3470	2/26/1962	Champlin	x			x	Kimm/Ti		No	No	No	No	No	No
CORC-23-1	CORC-23-1	870491011	Oil	711808	2940701	26°34'14.97"N	12°52'24.85"W	179.44	4020	4199	9/29/1962	Champlin	x			x	Aalenian?		No	No	No	No	No	No
CORC-23-2	CORC-23-2	870501011	gas shows	713034	2928591	26°27'40.97"N	12°51'47.85"W	208.9	4176	4385	11/10/1962	Champlin	x			x	Callovian?		No	No	No	No	No	No
D-2-9	D-2-9	870561011	oil shows	780811	3016333	27°14'26.95"N	12°09'51.85"W	283	1781	2064	3/1/1961	Gulf/CEPSA	x				Paleozoic		No	No	No	No	No	No
Daora 1-1	DAO 1-1	870061011	Dry	676820	3041045	27°28'52.10"N	13°12'37.36"W	20	4221	4241	3/1/1961	Union	x	x		x	Oxfordian	x	Yes	Yes	Yes	No	Yes	Yes
Deep Sea Drilling Project 366	DSDP 369	870091011	Dry	500247	2941498	26°35'38.03"N	14°59'51.09"W	10	2239	2249	5/28/1975	NSF	x	x		x	Aptian		No	No	No	No	No	No
Deep Sea Drilling Project 397	DSDP 397	870071011	Dry	482234	2969477	26°50'47.05"N	15°10'43.75"W	10	4353	4363	2/1/1976	NSF	x	x		x	Hauterivian		No	No	No	No	No	No
El Amra 1	EA-1	870121011	Dry	828596	3095424	27°56'34.88"N	11°39'39.39"W	250	2323	2573	12/21/1961	SOMIP	x	x		x	Precambrian	x	No	No	No	No	Yes	Yes
F-3-1	F-3-1	870551011	Dry	836105	3033090	27°22'45.93"N	11°36'7.87"W	325	1379	1704	5/16/1961	Spanish Gulf	x			x	Precambrian		No	No	No	No	No	No
Foum El Hassane 1	-	870611011	Dry	1090564	3199974	28°47'29.49"N	8°57'18.44"W	0	10	10	8/31/1961	AGIP / ENI		x			Ordovician		No	No	No	No	No	No
Hagounia 1-2	HAG 1-2	870131011	Dry	761207	3046769	27°31'9.01"N	12°21'20.40"W	224.4	2176	2401	5/1/1962	Union Oil	x	x			Kimm/Ti	x	Yes	Yes	Yes	No	Yes	Yes
Haute Mer 1	HM-1	870141011	Dry	742162	3203054	28°55'55.70"N	12°30'57.17"W	11.3	3281	3292	1/15/1975	Shell / Exxon		x	x		Berriasian	x	No	No	Yes	Yes	No	No
Ifni 1	Ifni 1	870151011	Dry	926105	3247940	29°17'17.24"N	10°36'55.51"W	24.69	1977	2002	1/8/1976	Sunoco		x	x		Cambrian		No	No	No	No	No	No
El Aaiun 8-1	LAY 8-1	n.k.	Dry	776240	2993151	27°01'57.73"N	12°12'56.55"W	25	1379	1404	1/31/1972	ENPASA	x			x	Lower Cretac.		No	No	No	No	No	No
El Aaiun 8-2	LAY 8-2	870101011	gas shows	662577	3007458	27°10'47.34"N	13°21'32.22"W	10	1993	2003	11/25/1972	ENPASA	x	x		x	Albian	x	No	No	Yes	Yes	No	No
El Aaiun 8-3	LAY 8-3	870111011	gas shows	659812	3005961	27°09'59.89"N	13°23'13.36"W	9.4	2020	2029	1/12/1973	REPSOL	x	x		x	Albian	x	No	No	No	No	No	No
Morrocan Offshore 1	MO-1	870161011	Dry	765578	3158928	28°31'46.79"N	12°17'10.31"W	9.8	2746	2756	7/13/1968	Exxon		x			Kimmeridgian	x	No	No	No	Yes	No	No
Morrocan Offshore 2	MO-2	870171011	Oil	693742	3130891	28°17'21.90"N	13°01'28.30"W	9.8	2973	2982	11/16/1968	Exxon		x		x	Ox/Kimm	x	No	No	No	No	No	No
Morrocan Offshore 3	MO-3	870181011	oil shows	710068	3142503	28°23'29.95"N	12°51'21.76"W	10.06	2177	2187	2/13/1969	Exxon		x	x		Triassic	x	No	No	No	No	No	No
Morrocan Offshore 4	MO-4	870191011	oil shows	798502	3200323	28°53'44.28"N	11°56'21.39"W	10	3454	3464	4/6/1969	Exxon		x	x		Callovian		No	No	No	No	No	No
Morrocan Offshore 5	MO-5	870201011	Dry	750016	3153782	28°29'10.81"N	12°26'46.31"W	9.2	2476	2486	5/9/1969	Exxon		x			Kimmeridgian	x	No	No	No	Yes	No	No
Morrocan Offshore 6	MO-6	870211011	Dry	758927	3188690	28°47'57.66"N	12°20'50.43"W	9.5	3651	3661	6/30/1969	Exxon		x	x		Valanginian	x	No	No	No	Yes	No	No
Morrocan Offshore 7	MO-7	870221011	Dry	732557	3157263	28°31'15.49"N	12°37'25.33"W	10	4319	4329	10/30/1969	Exxon		x	x		Callovian	x	Yes	No	No	Yes	No	No
Morrocan Offshore 8	MO-8	870231011	Oil	690407	3129706	28°16'45.19"N	13°03'31.33"W	9.5	3819	3829	11/14/1971	Exxon		x			Bathonian	x	Yes	Yes	Yes	Yes	No	No
Oum Doul 1	-	870631011	Dry	1004812	3118216	28°05'34.72"N	9°51'55.45"W	0	10	10	3/15/1961	SOMIP		x			Silurian		No	No	No	No	No	No
Puerto Cansado 1	PC-1	870271011	gas shows	761676	3093752	27°56'33.93"N	12°20'26.36"W	16	4074	4090	1961	SOMIP	x	x		x	Toa/Aal	x	No	No	No	Yes	No	No
Tarfaya 1	TAR-1	870311011	gas shows	675390	3108916	28°05'37.41"N	13°12'53.53"W	10	2995	3005	3/9/1990	Walter Int.	x	x			Kimmeridgian	x	No	No	No	Yes	No	No
Tan Tan 1	TTN 1	870301011	Dry	823647	3214116	29°00'49.73"N	11°40'40.19"W	29.87	5039	5069	12/31/1984	AMOCO	x	x	x		Toarcian		No	No	No	No	No	No

Tab. 2: Well data available for this study.

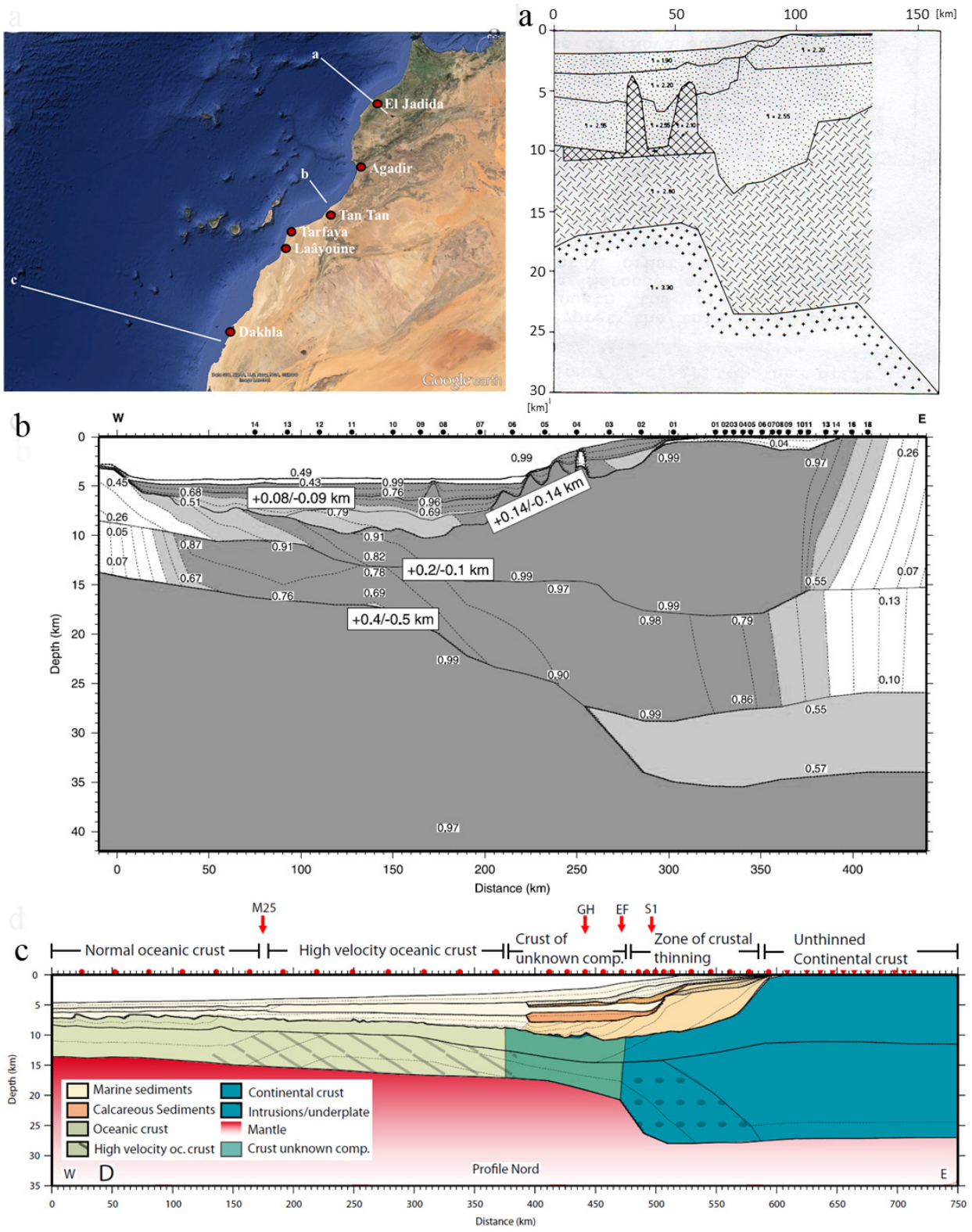

Fig. 26: Topographic map (Google Earth) of the eastern Central Atlantic margin showing the positions of the BGR combined gravimetric, refraction seismic and sono-buoy refraction seismic profile, Northern Tarfaya basin (a), the Ifremer SISMAR cruise, on- and offshore Mazagan segment (b) and the DAKHLA cruise, offshore Dakhla Basin (c). Hinz et al. (1982) determined a maximum crustal subsidence at the point of highest sediment loading of approximately 13km bsl at the Tarfaya shelf (a), KLINGELHÖFER et al. (2009) report a maximum depth for the basement of 11.5 km bsl at the lower slope area of the Dakhla Basin (c), and CONTRUCCI et al. (2004) quote the deepest point of the top basement 10km bsl (b).

3.2.3.2 3rd order sequence stratigraphy

High resolution seismic interpretation (30 formation tops) has been performed on three key transects (tr) following 3rd order sequence stratigraphic timelines and geometries. These are:

Tan Tan tr.: 87-TA-15, EM69-39 & 83MMO-15

Cap Juby tr.: 88-LA-17, 87-TA-04, 83MMO-35, FRED & SEM

Laâyoune tr.: 88-LA-03 & WMS-5

3rd order sequence stratigraphic modeling was essential to i) establish the workflow for all successive transects, ii) further develop the stratigraphic framework, iii) develop quantitative high-resolution sequence stratigraphy models and, iv) numerically model subsidence and sediment flux variations during the rift to drift basin evolution.
The integration and construction of the full stratigraphic framework including TWT and velocity data generation has been performed iteratively.

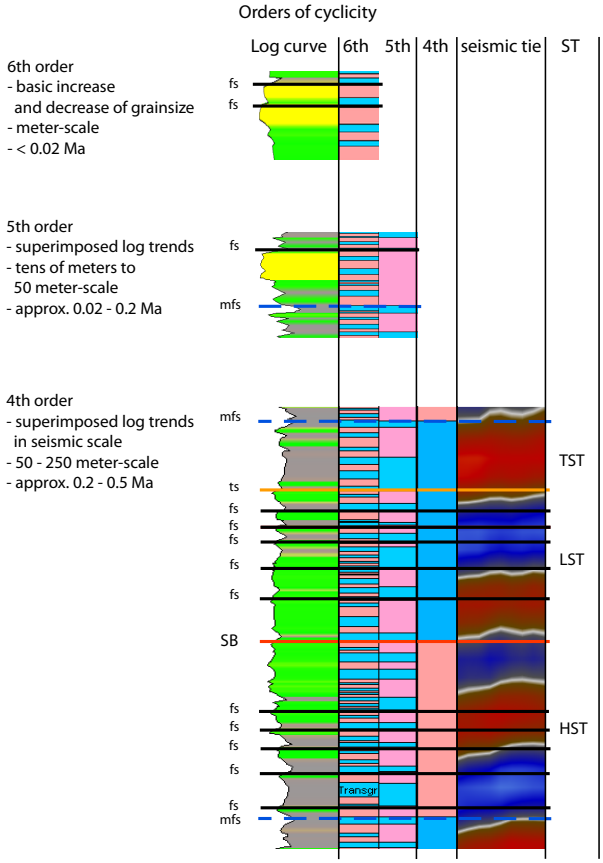

Fig. 27: Log pattern detection and sequence stratigraphy. Fourth order cycles in seismic scale (Wenke et al. 2011).

3.2.4. Facies maps

Based on the field trip data, the well evaluation and the 3rd order seismic sequence stratigraphic interpretation in the time domain, facies maps have been generated illustrating the shelf geometry, depositional environment and indirectly the paleowater-depth of the basins.

3.2.5. High-resolution sequence stratigraphy

3.2.5.1 Well correlation

1D-sequence stratigraphy is based on hierarchical sediment stacking patterns (funnel, bell, bow, symmetric, chaotic) observed in γ-ray or R-logs (Van Wagoner, 1990). Stacking patterns cover meter-scale cycles to thick coarsening/fining-upward (progradation/retrogradation) trends at a seismic scale. Stacking patterns cover metre-scale 6th order to 50 to 250 m-scale 4th order cycles. At well log and seismic scale, API peaks and trends have been interpreted as sequence boundaries (SB), maximum flooding (mfs), transgressive (ts) and flooding surfaces (fs). These define sequences, systems tracts, and parasequences. Fourth order sequence boundaries in seismic scale were aligned with high-resolution seismic (sequence) stratigraphy. Fig. 27 shows the concept of well log interpretation.
Well correlations along the three sequence stratigraphic transects have been performed:

Well Correlation 1 (Tan Tan transect):
EA-1, PC-1, MO-5 and MO-7
(GR-log or R-log).

Well Correlation 2 (Cap Juby transect):
HAG 1-2, PC-1, CJ-1 and MO-8
(GR-log or R-log).

Well Correlation 3 (Laâyoune transect):
AMS 1-8, LAY 8-2 and 15A-1
(GR-log or R-log).

3.2.5.2. Seismic (sequence) stratigraphy

2D-sequence stratigraphic interpretation in this study was performed with OpendTect SSIS® (Sequence Stratigraphic Interpretation System, dGB) for the drift basin stages. The basic concept of SSIS®

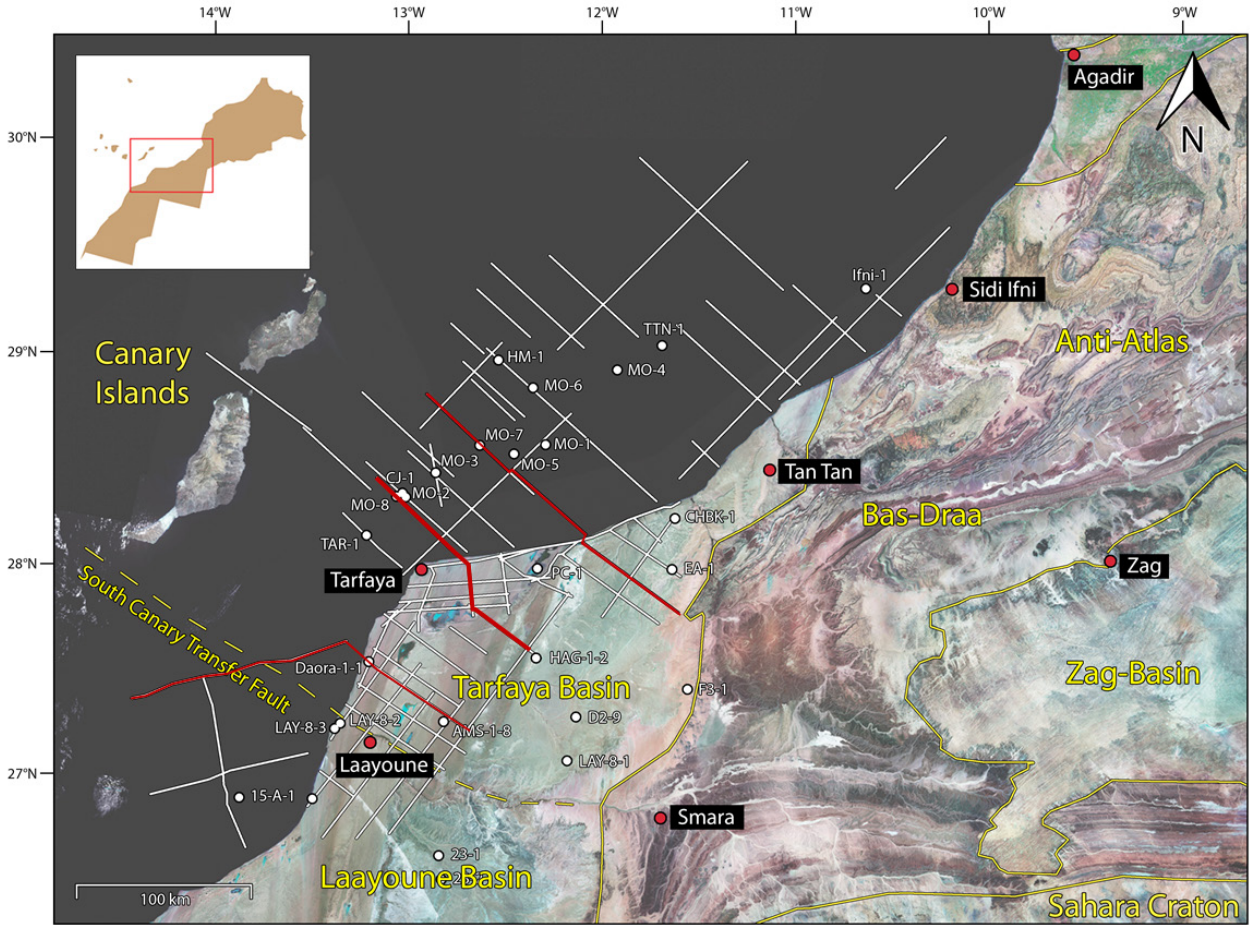

Fig. 28: Location of the three key transects on which high resolution sequence stratigraphy has been performed (red lines). From N to S: Tan Tan transect, Cap Juby transect and Laâyoune transect (Wenke & Zühlke, 2010).

is the autodetection of all reflector traces (horizons) within user-defined intervals, usually (super-)sequences, and their correct chronostratigraphic order (Ligtenberg et al. 2006, de Bruin et al. 2006 & de Groot et al. 2006a,b). Reflector traces (horizons) are analyzed at sub-seismic resolution and tracked throughout the seismic volume within the limits of manually defined interval boundaries (2D) or surfaces (3D-cube). In this study they are biostratigraphic boundaries or reflector termination surfaces following the 3rd order sequence stratigraphic interpretation.

Based on the trace analysis, systems tracts can be interpreted by using the chronostratigraphic slider (e.g. de Bruin et al. 2007). From the several sequence stratigraphic interpretation approaches which are available the Depositional Sequence II concept (revised Exxon Model, e.g. Catuneanu 2006) was used in this study. Fig. 29 and 30. show the concept of SSIS.

In addition, chronostratigraphic plots (Wheeler diagrams) were generated based on the systems tract interpretation (Figure 28). A Wheeler diagram is a stratigraphic summary chart on which geological time is plotted as the vertical scale, and distance across the area of interest as the horizontal scale. This combines a variety of stratigraphic information (Mitchum et al., 1977).

The results from the facies analysis and organochemical summarisation were integrated to map out the distribution of potential source rock and reservoir formations.

In order to receive the best possible results, internally homogenous seismic data sets (range of reflector amplitudes) are necessary. The available seismic data set is a mixture of seismic lines from six seismic surveys acquired between 1969 and 1999. Therefore, several steps of seismic post-processing, scaling and filtering were necessary in order to achieve similar amplitude ranges. For the EM and WMS lines a cut of low frequencies (8-16 Hz) was necessary and was kindly provided by the data centre. This data was originally handed out as a paper print, but later digitized from microfilm, including paper wrinkles. In order to receive a comparable vertical display of seismic reflectors, the vertical component

in depth was intensified mainly for the MMO survey. Scaling of the horizontal amplitude range was necessary to receive an adequate setup on each transect and was oriented to the amplitude ranges of the onshore CGG lines (87-TA, LA and 88-LA surveys). Additional filters have been employed in order to attenuate remnant noise (dip, conditional dip, dip-variance, similarity, azimuth and Fast Fourier Transformation).
Seismic sequence stratigraphy was interpreted in three transects (Fig. 23) which are also covered by well correlations:

Tan Tan tr.: 87-TA-15, EM69-39 & 83MMO-15

Cap Juby tr.: 88-LA-17, 87-TA-04 & 83MMO-35

Laâyoune tr.: 88-LA-03 & WMS-5

The proximal part of the Tan Tan transect is located at the northern margin of the Tarfaya Basin adjacent to the Anti-Atlas. It is oriented in NW direction and covers the whole shelf to lower slope. In terms of the basin architecture, it represents the most important transect.
The Cap Juby transect crosses the central Laâyoune depression and the Cap Juby oil field (Horst de Juby).
The Laâyoune transect is located in the south of the Tarfaya/Agadir salt province and includes parts of the Laâyoune Delta.

3.2.6. Time/depth Conversion

Basinwide velocity modelling is based on average velocity calculations carried out for a total of 19 wells. Check-shot data have been iteratively generated for 15 wells during seismic interpretation. Horizons have been defined in most of lines and survey available. An average velocity sheet was created for all 19 wells (Appendix 3) and the enclosed area (Fig. 28). Surfaces in time domain where generated for the given datum, which are sea-level offshore, ground level onshore, and the horizon tops of Miocene, Eocene, Maastrichtian, Albian, Aptian, Barremian, Hauterivian, Valanginian, Tithonian, Callovian, Toarcian and Pliensbachian.
3D interpolation of 2D data is based on a regular grid with 750 m cell spacing (Fig. 31). The 3D cube was subdivided to 27 layers. Well data were upscaled with average velocity information (Fig. 32). Point velocity data were extrapolated to the entire

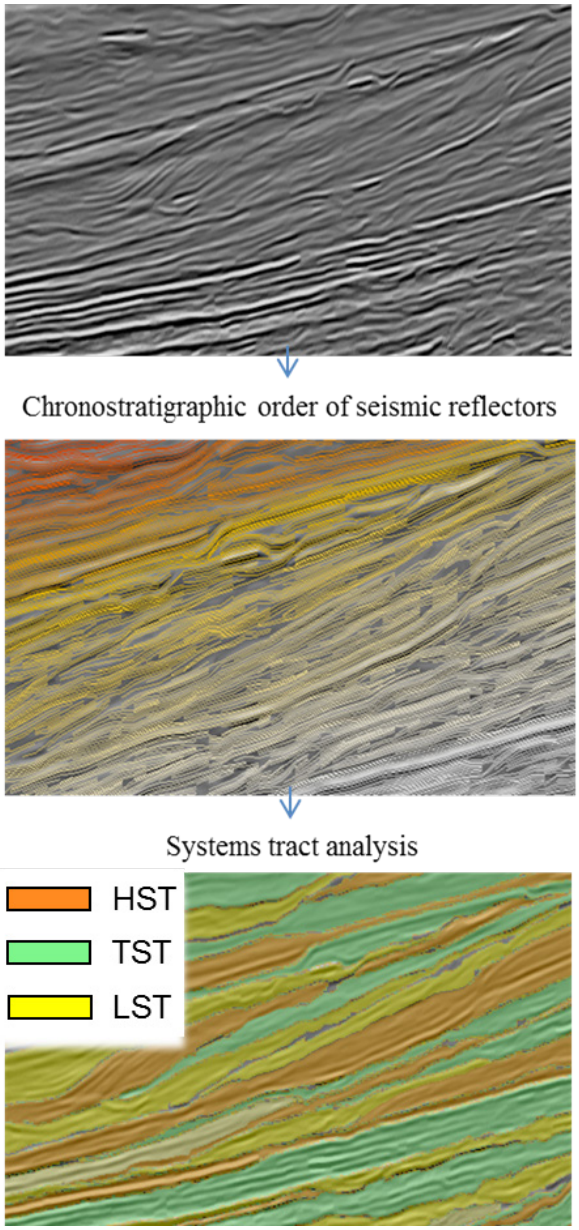

Fig. 29: Concept of SSIS®. The reflector pattern of a seismic transect (top) is analysed on the chronostratigraphic order of each reflector trace in subseismic scale. Systems tract analysis can then be performed with the chronostratigraphic slider.

3D-grid.
Time/depth conversion was carried out in the enclosing areas of each transect for computing time considerations. Polygons comprise the seismic lines of the key transects. For all transects, local surfaces on each transects have been created. Subsequently, each surface was categorized as basal, erosional, discontinuous or concordant and finally converted to depth (Fig. 33).
The final depth converted transect models are shown in Fig. 34. In preparation of flexural basin model-

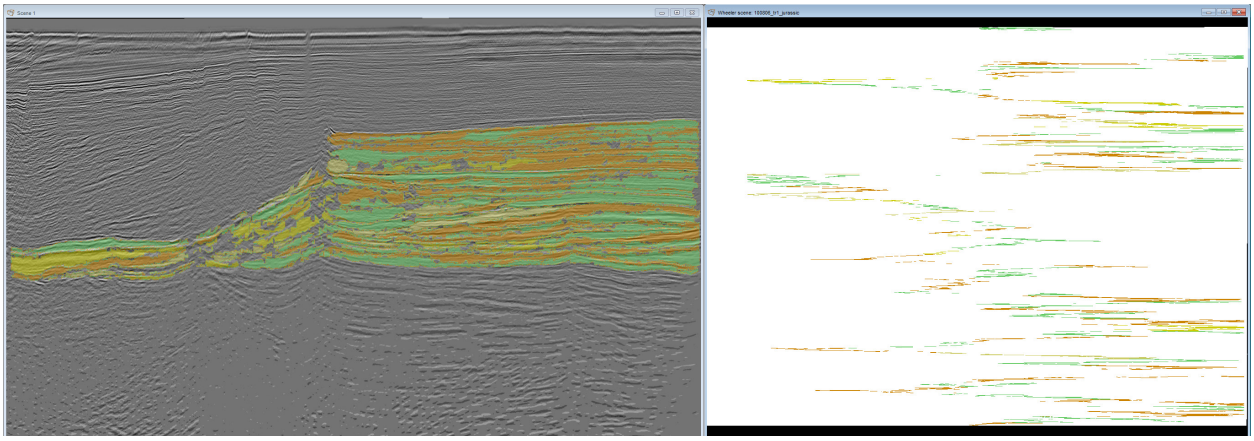

Fig. 30: Open dTect SSIS® systems tract interpretation and chronostratigraphic diagram (Wheeler plot) of the Jurassic succession of line MMO-15 (Wenke et al. 2011). The color code in this example follows the revised Exxon model (Van Wagoner et al., 1988).

ling, horizons in the three transects were exported as x-y-stratigraphic age matrices. The results are synthetic transects which represent the essential input dataset for basin modeling (Fig. 35).

3.2.7. Flexural Reverse Modeling

3.2.7.1. Approach

Reverse basin modelling has been performed with Phil/Basim® (cf. Bowman & Vail, 1999), which follows a flexural modelling approach, including key crustal parameters as opposed to 1D backstripping (Airy isostasy).

Flexural reverse basin modelling provides a quantitative analysis of the basin architecture and infill as controlled by accommodation change and sediment flux (e.g. Contreras, 2011). The genetic components of total subsidence are: i) thermo-tectonic, ii) flexural and iii) compaction-induced subsidence (e.g. Zühlke et al., 2004). The modelling approach has been applied primarily to extensional settings in order to analyze lithospheric stretching factors and subsidence/uplift histories (Nadin & Kuznir, 1995; Roberts et al., 1995; 1997; 1998; Nadin & Kuznir, 1996; Bowman & Vail, 1999; Zühlke et al. 2004; Kuznir & Karner, 2007; Veselovsky et al., 2008; Contreras et al., 2010). Flexural reverse basin modelling starts from the present basin architecture. Chronostratigraphic layers are incrementally removed down to the top of the rheological basement (Intra-Khazhanian, 259.3 Ma in this study).

The initial basin architecture is controlled by i) paleotopography, ii) structural setting, iii) the type of lithosphere and, iv) its flexural rigidity (Watts & Burov, 2003). Subsequent changes in depositional patterns and sediment and water loading of the crust result from changes in subsidence/uplift, eustatic sea-level and sediment input (cf. Zühlke et al., 2004; Contreras, 2011). The accommodation space is defined by two surfaces, i) the top of the rheological basement and ii) the sea-level in approximation for base level. The basin model fully considers the amount of incremental compaction in the buried basin fill as controlled by initial porosity, sediment density, water depth and sediment overburden. Porosity-depth paths for 12 lithologies have been individually adjusted for shallow to deep diagenesis. Numerical results include rates of total subsidence, the subsidence rate of each of the three genetic components, sediment flux for each time interval and location on the transects. Graphic modelling results include restored stratigraphic transects for each time interval, which show the evolution of basin architecture.

Input parameters include i) thickness, i) lithology, ii) compaction parameters, iii) paleobathymetry, iv) diagenetic coefficient, v) effective elastic thickness (Te) and vi) taper limit distances.

3.2.7.2. Input data to flexural modelling

In preparation of flexural basin modelling, horizons of the three depth converted transects (Fig. 35) were exported as x-y-stratigraphic age matrices. The results are synthetic transects which represent the essential input dataset for basin modeling.

Recent bathymetric profiles (Fig. 34) of the three transects vary and indicate variations in crustal configuration, tectonic evolution or (submarine) erosion. In addition, the slope to basin geometries of the Tan Tan and the Cap Juby Transects have been

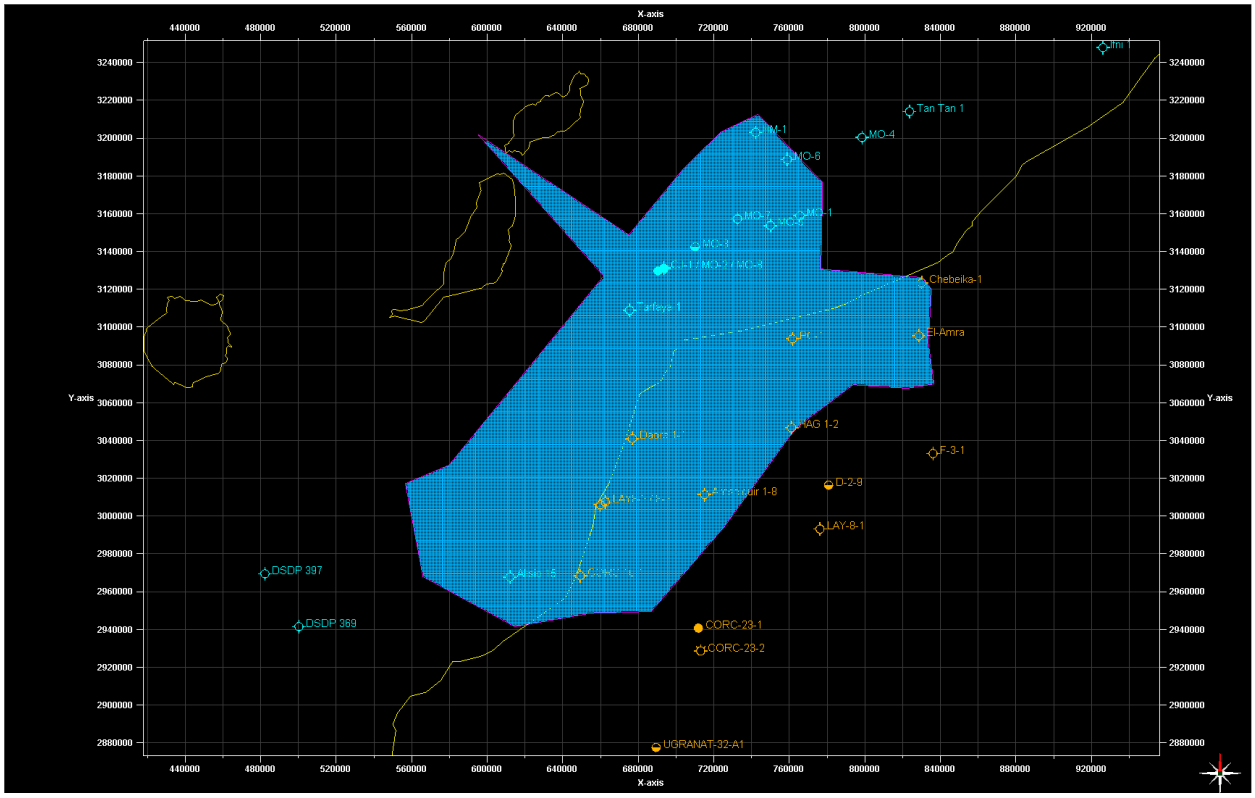

Fig. 31: Grid of the velocity modelling area. The cell size in x and y direction is 750 m.

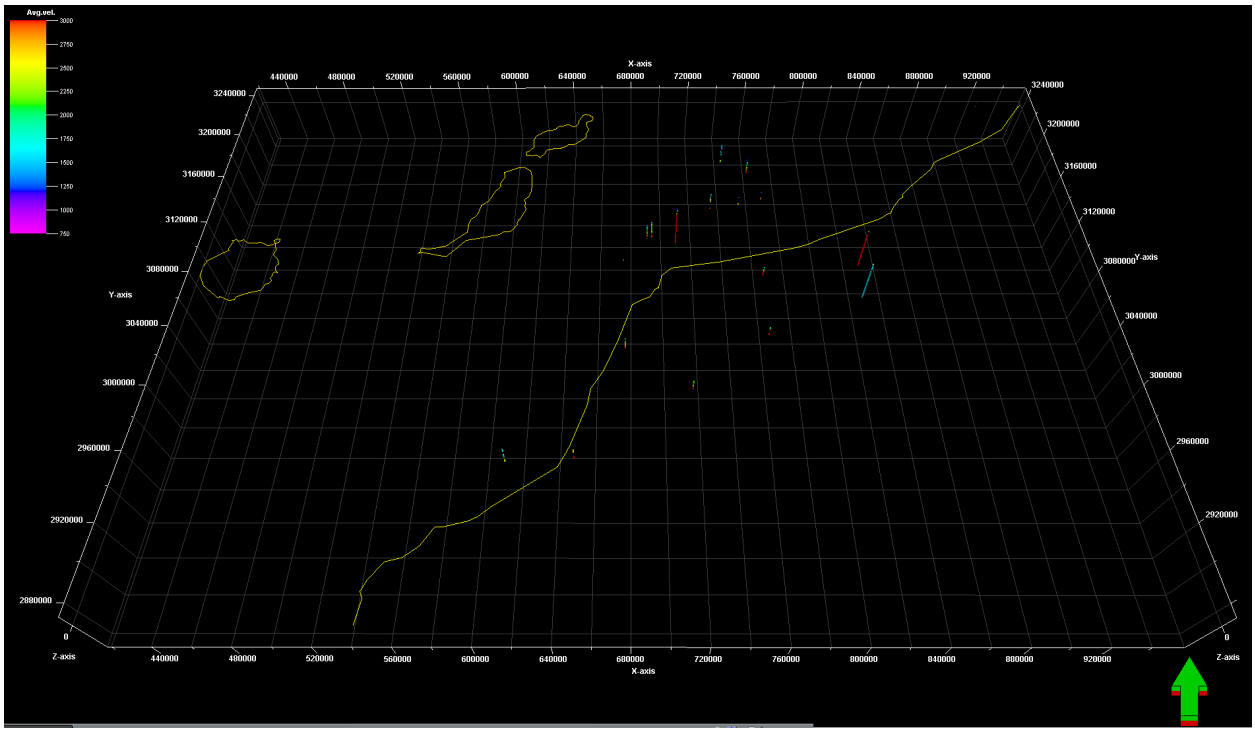

Fig. 32: With average velocities upscaled wells of the modeling area. Red: high velocity layers, violet: low velocity layers.

modified by the rise of the Canary Islands (compare Gouiza 2011 for northern Tarfaya Basin geometry). Paleobathymetric profiles have been reconstructed from seismic geometries, facies and paleoecological

Fig. 33 (next page): Depth converted formation tops of the key transects after stratal termiantion assignment.

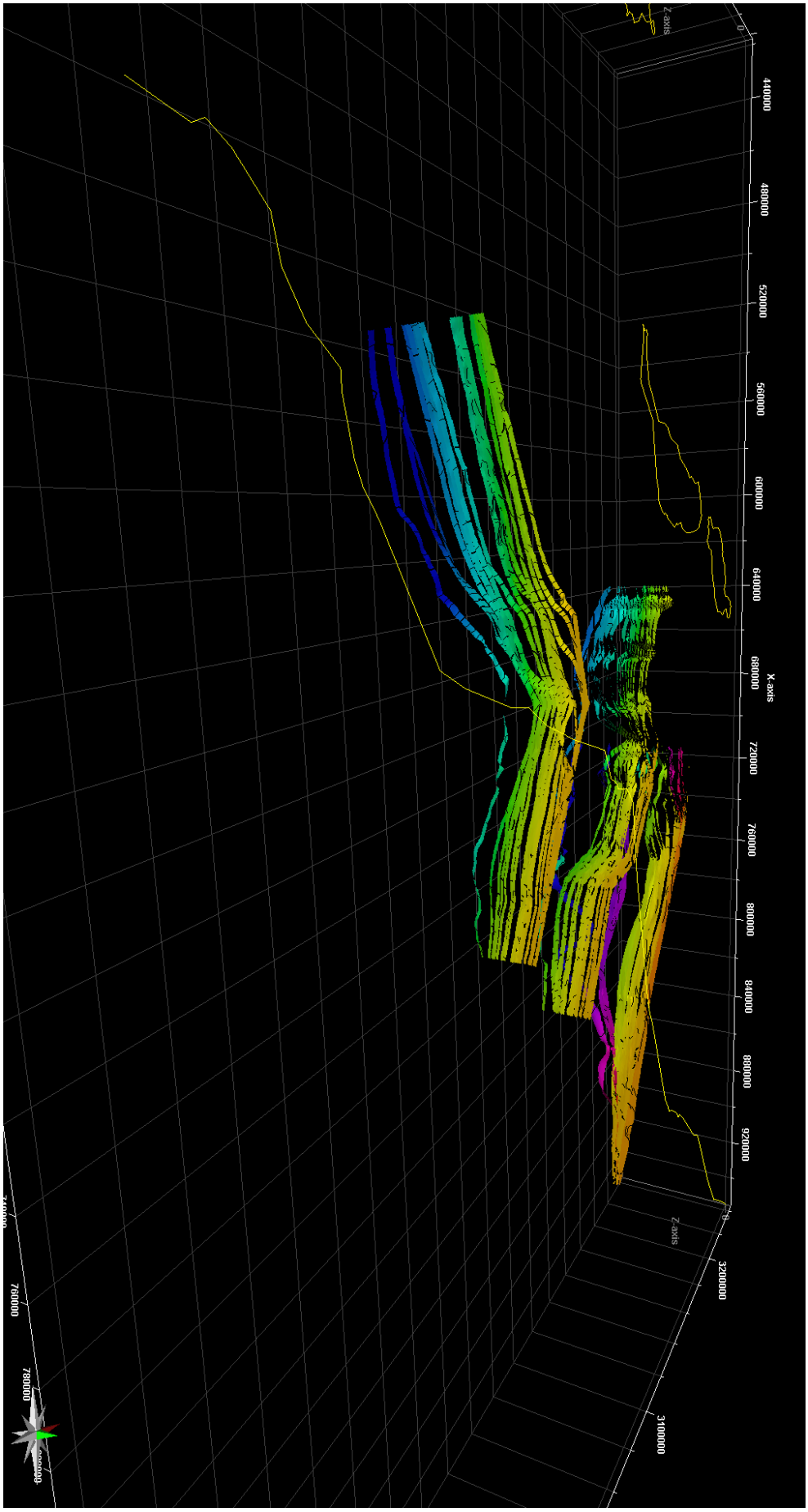
Z-axis
0
440000
480000
520000
560000
600000
640000
680000
X-axis
720000
760000
800000
840000
880000
920000
Z-axis
3200000
3100000
760000
780000

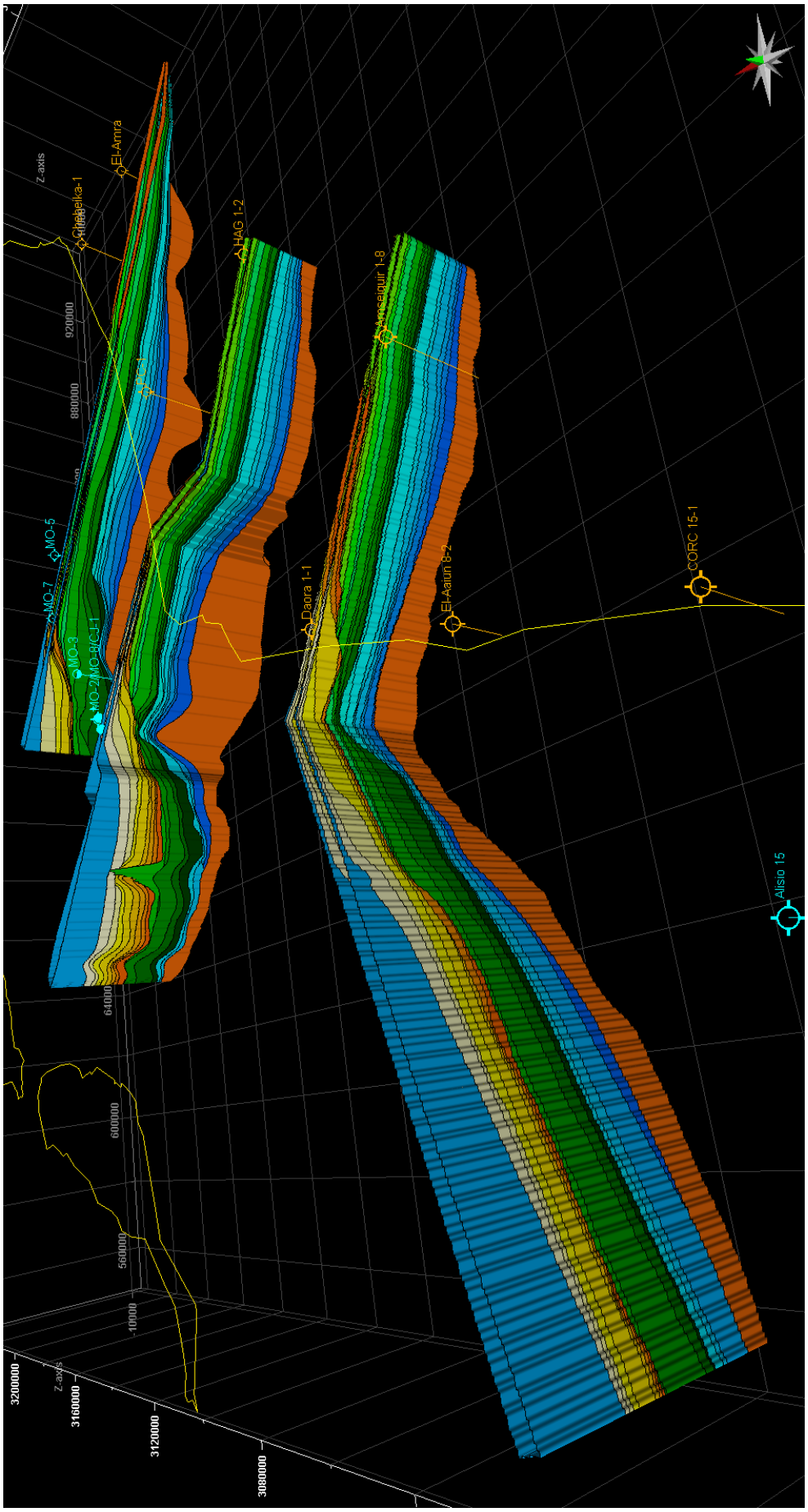
Z-axis
El-Amra
Ghabelka-1
HAG 1-2
Ansequir 1-8
MO-5
MO-7
MO-3
MO-2
MO-8/CJ-1
Dqora 1-1
El-Aalun 8-2
CORC 15-1
Alsio 15
920000
880000
640000
600000
560000
10000
3200000
3160000
3120000
3080000

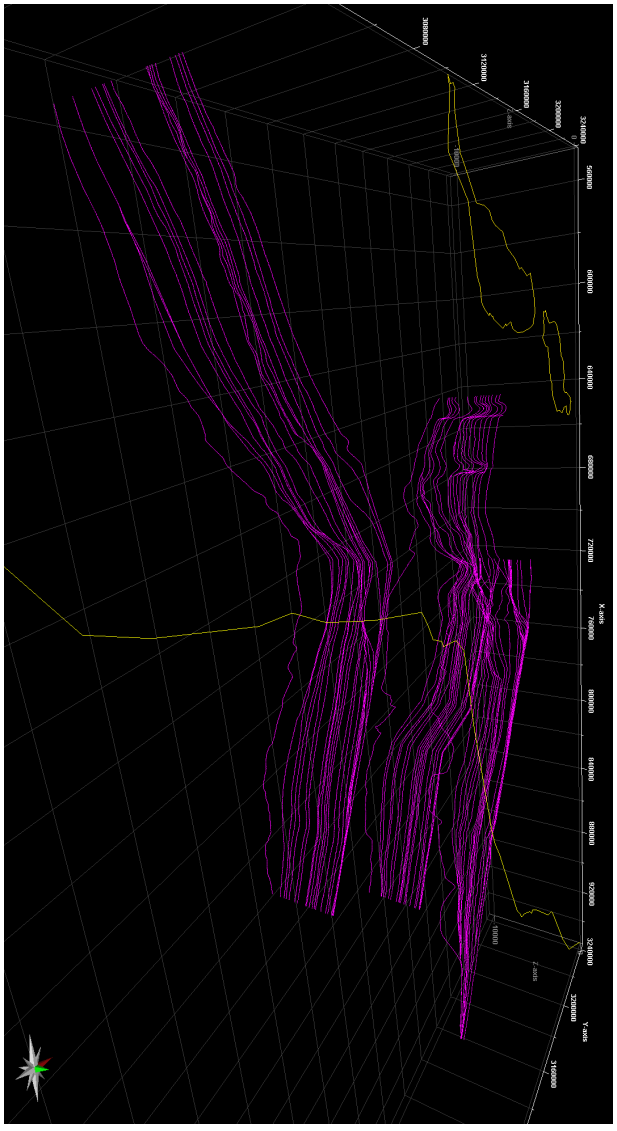

Fig. 35: Synthetic transects. The transects are subdivided into 400 virtual shot points (transect points). Following subsidence analyses was performed on one key point of each transect.

data from industry well reports and published studies. Third order eustatic sea-level fluctuations from Hardenbol et al. (1998) have been recalibrated based on the geologic time scale of Gradstein et al. (2004).

Fourth order sea-level changes (cf. Wenke et al., 2011) are not included as their periods are significantly shorter than durations of subsidence/uplift trends and major structural reconfigurations. In addition, 4th order sea-level changes involve larger error margins in terms of age and amplitude.

Salt kinetics may superimpose thermo-tectonic subsidence/uplift in areas of salt rise. They could not be modelled separately as part of this study. Areas which may have been affected include the shelf break to lower slope area. Modelling results have been scrutinized for possible effects of salt flow and affected areas have been indicated in the figures.

Lithofacies data come from the on- and offshore wells; eleven clastic, nine carbonate and two evaporite lithologies have been distinguished. For compaction algorithms see Bowman and Vail (1999).

Crustal parameters for flexural reverse modelling are: mantle density, effective elastic thickness (Te), taper limits on continental and oceanic crust. Taper limits define the distances from the center of the sediment-water load with of maximum flexural subsidence to locations unaffected by flexural loading (beam length). The left taper limit is defined by the topographic wavelength, the flexural wavelength, respectively. Its proximal end is located at the cratonward basin margin at the point of non-flexural subsidence. The most distal point is located at the shelf break to upper slope area. The shelf break area generally marks the point of maximum flexural subsidence of passive continental margins (Turcotte & Schubert, 2002; Catuneanu, 2004).

The continental taper limit is located at the western margin of the Zag/Tindouf Basin. To the east, the Mesozoic structural development was not significantly affected by the opening and spreading of the Atlantic. The flexural wavelength varies between 275 km (Tan Tan), 325 km (Cap Juby), and 375 km (Laâyoune).

The oceanic taper limit varies between 1,000 km (Tan Tan & Cap Juby) and 1,250 km (Laâyoune), 3-3.5 wavelengths, respectively. There are no numerical models to which extent the development of the Canary Volcanic Islands has affected the Tarfaya-Laâyoune Basins architecture during the last 60 m.y. However, taper limits for the non-volcanic Dakhla Basin south of the study area range between 1,275 km and 1,625 km, or 4-4.5x flexural wavelengths (e.g. Rona, 1970). The fact that taper limits in both basins are comparable indicate that the thermal anomaly of the Canary Islands has not significantly affected the Tarfaya Basin development in its shelf top to basin margin realms. Estimates for the initial crustal thickness have been derived from Hinz et al. (1982), Contrucci et al. (2004) and Klingelhöfer et al. (2009), with 30 km for the northern Tarfaya, 35 km for the Doukkala and 27 km for the Dakhla basins. The effective lithospheric thickness Te depends on the flexural rigidity of the crust D, Young's

Fig. 34 (previous page): Final depth converted stratigraphic frameset at key transect as final preparation step for reverse modeling (Wenke et al. 2012c).

modulus E and Poisson's ratio n (Bowman & Vail, 1999). Flexural models in this study are based on 32 km total crustal thickness resulting in 9.87 km for Te.

3.2.8. Software used

Regional maps have been generated in ESRI ArcGIS®; log digitization has been performed in GraphClick®, Well log interpretation, 1D high resolution sequence stratigraphy, seismic interpretation, facies mapping and time/depth conversion has been worked out in Schlumberger ISI Petrel® (versions 2008-2013); Seismic post-processing, filtering and 2D high resolution sequence stratigraphy including Wheeler transformation has been performed in dGB OpendTect SSIS® versions 4.06-4.6, 2D-flexural reverse modeling in Petrodynamics Phil/Basim® 1.5.

4. Results

4.1. Outcrop studies

Visited outcrop locations relevant for this study are listed as waypoints (WP) with geographic coordinates is given in Wenke et al. (2009). An outcrop map can be found in Appendix 1.

4.1.1. Rheological Basement

The rheological basement was studied in the Anti-Atlas and Bas Draâ region. Well data was available from the wells CHBK-1, D-2-9, EA-1, F-1-3 located in the Tarfaya-Laâyoune Basins, the wells Semara 2-17 & 3-17 located at the very eastern transition between the Tarfaya, the Dhrou/Zag Basin and the wells AZ-1, Foum El-Hassane-1 & Oum Doul-1.
Two units define the „basement" of the Tarfaya Basin, i) the granitic to metamorphic Proterozoic and ii) Paleozoic (meta-) sediments.
The Paleozoic basement is important for two reasons: i) it represents sediment source of the hinterland (Anti-Atlas, Bas-Draâ, WAC) as well as ii) the base of the Late Paleozoic to Holocene basin fill between the proximal basin margin and the S1 anomaly. To the W of the S1 anomaly, it is assumed that the basement consists of oceanic crust.

4.1.1.1. The Proterozoic basement

The oldest rocks in the study area are exposed in the Central and Western Anti-Atlas as well as the Bas Drâa region. Proterozoic intrusions have been visited in the Bas Drâa region, as well as the Ammeln Valley (Tahala granite). The Ifni granites are exposed close to the present day coastline. The youngest Pan-African magmatic rocks are exposed in the Tasrirt dome represented by the Tafraoute (WP 202, Fig. 36) and Tarçouate intrusions.

4.1.1.2. Paleozoic

The Cambrian rift valley, which was mainly studied in its southern extension (WP 4&5), is filled at the base with conglomerates followed by fine to medium clastic sedimentation alternated with carbonate series.

The Lower Ordovician post-rift/sag valley fill, which includes mainly clay and siltstones (WP 2,3,28&39) as well as sandy ramp/platform sediments of Upper Ordovician age (WP 2,5&28) have been studied at the southern flank of the Anti-Atlas between Akka and Assa. Fig. 37 shows the exposed Ordovician succession of Foum El Hassane. The underlying Lower Ordovician sag deposits are separated from the Upper Ordovician ramp deposits by an angular unconformity.
The Silurian, which consists of mainly pelitic series including the post-glacial transgressive hot shales, which are highly prolific source rocks in the North African region (e.g. Lüning et al., 2000), are not exposed in the study area but present in the subsurface (N 28°46.400' W 9°25.420'). Outcrops of Silurian black shales do exist in the Eastern Anti-Atlas outside of the study area (Helg et al., 2004).
The Lower Devonian is dominated by a carbonate platform rich in fossils and is mainly exposed north of Smara (WP 6,29&39). Fig. 38 & 39 show an exposed part of a Lochkhovian Bryozoa-Stromatopora reef including corals, polyps and crinoids. The location is north of Smara at the transition between the Bas Drâa area and the Tarfaya Basin. The Upper Devonian (WP 6,10&40) is dominated by normal faulting and later subsidence. The sediments are dominated by clastic components with alternating sand, silt and shale lithologies. Hot shales of the Kellwasser event may have been deposited during this period. However, their existence could not be proven during the AMP (Sachse, 2011). Especially the southern parts are dipping south in direction of the Zag Basin with angles between 10° and 30°. Fig. 40 shows a transgressive shale-silt-sand alternation at seismic scale of Fammenian age south of Assa.
Following the road to the south in the direction of the Zag basin, a Tournaisian (WP 7,8,9&27) to Viséan (WP 16&17) succession is exposed before the Paleozoic strata is dipping below the Cenozoic of the Zag Basin (Fig. 41). The Tournaisian succession seems to include a highstand to regressive cycles as sandstone thickness increases. However, the sea-level rises during the late Viséan while sediment flux from the hinterland decreases and carbonate sedimentation prevails. Late Carboniferous and Permian deposits are not exposed in the Bas Drâa region but may exist in deeper parts of the Zag Basin.

Fig. 36: Granitic basement of the Tasrirt plateau close to Tafraoute in the Anti-Atlas as a part of Pan-African basement (WP 202). The age of the intrusion is dated 549 (+/- 6) Ma and can be classified as latest Ediacarian/Precambrian (ICS 2012). The granites show typical spheroidal weathering, blue and pink colors are part of the artwork *Les Rochers Bleu* by Jean Vérame. Foto: Anne WENKE (2012)

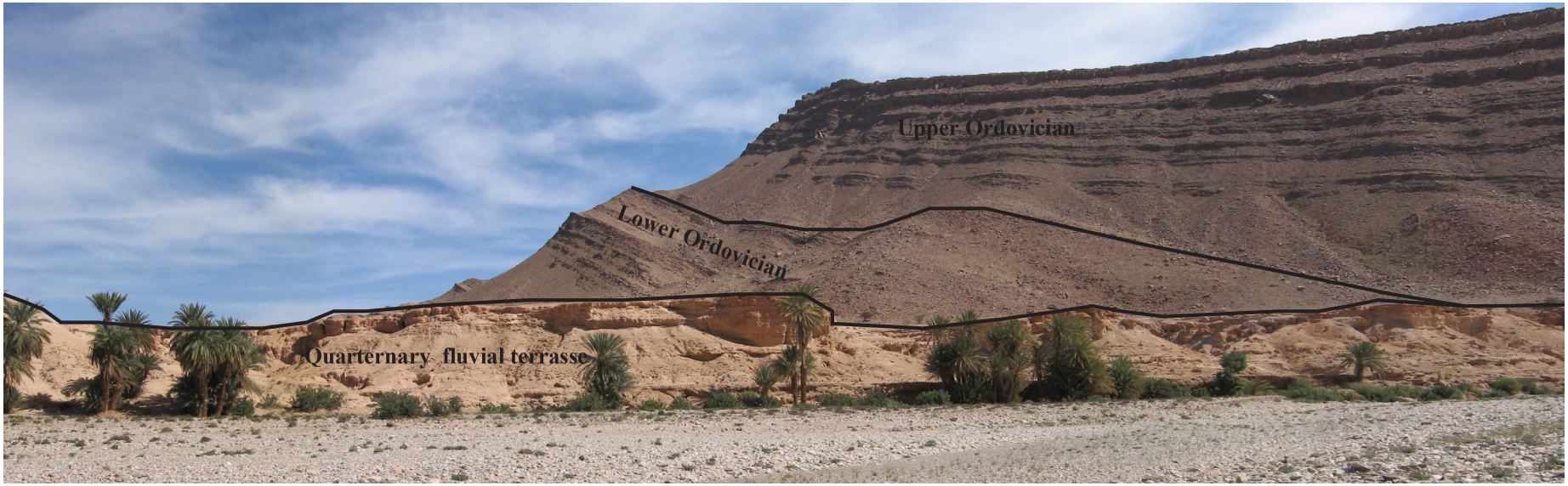

Fig. 37: Ordovician of Foum El Hassane (WP 29; WENKE et al. 2009).

Fig. 38 & 39: Bryozoa-Stromatopora reef of Lower Devonian age including corals, polyps and crinoids (WP 39).

Fig. 40: Famennian silt-sandstone alternation in seismic scale between Assa and Zag (WP 6). Two coarsening upward cycles covered, the transgressive peak is defined by a tempestite. The range in the background is a clastic series of overlying Lower Carboniferous (Tournaisian). Supervisor for scale (Wenke et al. 2009).

4.1.1.3 Relevance

The investigation of the pre-Permian basin fill was not a key part of this study. However, the Precambrian plutonites and metamorphites, as well as the Cambrian to Lower Carboniferous succession form the rheological or seismic basement of the Tarfaya-Laâyoune Basins between the continentward basin margin and the S1 anomaly. The basement in geological interpretations and subsequent geological models, also in this study, is often presented as a uniformal lithological unit. It is actually more complex. In the studied area, the Paleozoic succession includes two potential, even if not verified, source rocks of the Ordovician-Silurian post glacial transgression (OS) and the Devonian Kellwasser (KW) event, as well as potential clastic and carbonatic reservoirs of Viséan age.
It was also noticed that the degree of diagenesis decreases with age. Cambrian sandstones are in general overprinted by low-metamorphic compression and heating while Carboniferous sandstones are mainly silicified but retain the internal texture.
Aside from the negligible hydrocarbon potential of this succession, the thickness variations of the plutonic basement that is overlying the sediments can have a significant impact on the error of estimating a basal heat flow when it comes to basin modelling.

4.1.2 Basin Fill

The Late Permian to Early Jurassic rift section and Jurassic early drift succession are not exposed in the Tarfaya-Laâyoune Basins. Some outcrops of this age were visited in the Western High Atlas (WHA, WP 200).

4.1.2.1 Early Cretaceous Tan Tan Delta

Early Cretaceous Berriasian to Aptian rocks exposed in the Tarfaya-Laâyoune Basins are mainly part of the Tan-Tan Delta of proximal depositional settings. Fig. 42-44 illustrates the contact of Lower Cretaceous Tan Tan micro-conglomerates and the fluvial plain overlying Late Devonian shales („basement“) at Khraybichat, north of Smara (WP 158&159).
Fig. 45 to 48 show the proximal Aptian to Albian succession (WP 152-157). The basal part is dominated by sandstones and conglomerates of the fluvial plain and contain high amounts of cross-stratification (Fig. 45). Progressing to the top of the sequence the succession features a proximal deepening

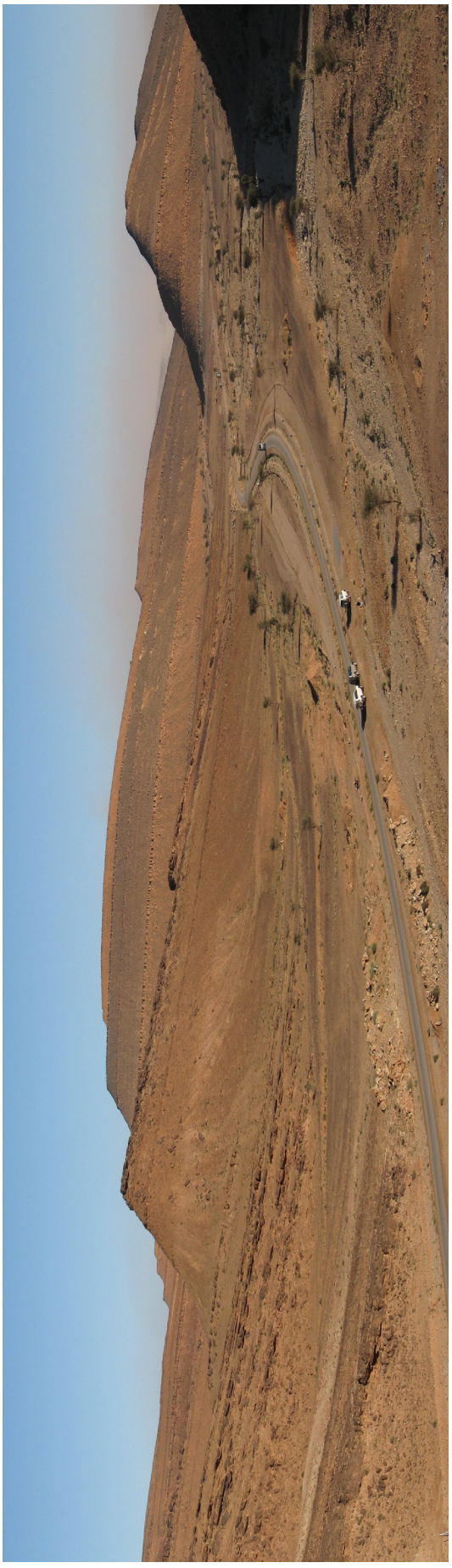

Fig. 41: Lower Viséan clastic ramps of silty to sandy grainsize (WP 8, left and center) covered by Upper Viséan (right of road, WP9) carbonates including Brachiopodes, on top with Rugosa (Wenke et al. 2009).

Fig. 42, 43 & 44: Lower Cretaceous (micro-)conglomerate on Devonian shales (basement, WP 158&159)). top: overview and contact, 40: Devonian shales, 41: Tan Tan microconglomerate of the fluvial plain (Wenke et al. 2009).

Figure: 45: Cross-stratified sands and conglomerates of the fluvial plain of the Aptian Tan Tan delta (Wenke et al. 2009; WP 152).

Figure: 46: Paleosoils of the second unit of the Abteh section (Wenke et al. 2009, WP 153).

Figure: 47: Transition from fluvial to brackish facies (units 2 and 3). The contact may shows the Aptian/Albian boundary. Abdelouahed Lmoubessine for scale (Wenke et al. 2009, WP 155).

Fig. 48: Aptian/Albian proximal section at Abteh at the boundary of the Tarfaya Basin and the Anti-Atlas (WP 152-157). The whole succession can be diversified into for units: i) basal fluvial sandstones, ii) fluvial clay/paleosoils to siltstones with interbedded sandstones, iii) brackish to shallow marine fineclastics (light brown and iv) red conglomerates on top (Wenke et al. 2009, WP 151).

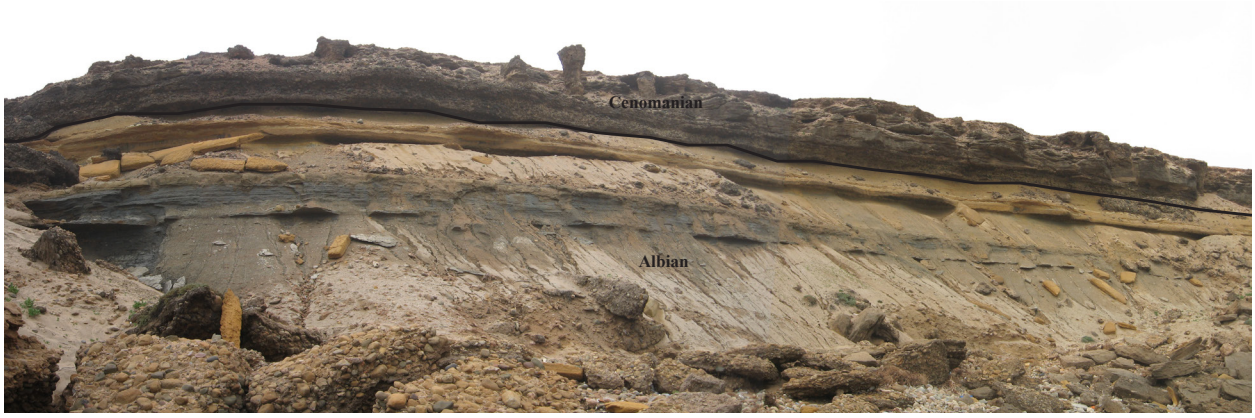

Fig. 49: Albian to Cenomanian succession of Oued Chebeika (WP 164-170). The lower part includes the Calcaire d'Aquidir succession including black shales correlating with the late OAE 1 (c or d) events (Wenke et al. 2009).

Fig. 50: Sampling anoxic clay to siltstones of Albian age at the mouth of Oued Chebeika for organochemical analysis. Victoria Sachse and Abdelouahed Lmoubessine for scale (Wenke et al. 2009, WP 166).

trend of brackish/marine ingression including silty to sandy deposits containing high amounts of less diversified shells that indicate a base level rise. The marine ingression may correlate with the Aptian/Albian boundary. The succession is covered by fluvial conglomerates of unknown age.

4.1.2.2 Late Cretaceous to Early Oligocene flooded shelf

The Albian to Early Oligocene succession is very well exposed in the onshore Tarfaya-Laâyoune Basins in various depositional settings.

The time equivalent of the Albian to Cenomanian Calcaire d'Aquidir Fm was primarily studied at the mouth of Oued Chebeika in an inner to mid-shelf environment and at El Ouatia in a subtidal environment.

The section at Oued Chebeika consists of carbonatic mudstones alternating with silty claystones of dark and light greyish colors at the base with the latter exhibiting bioturbation that represents cycles of anoxic to oxic environmental changes (WP 165-167). High TOC was recognized in the dark shales during the AMP project (Sachse, 2011; Sachse et al., 2011; 2014) and the sediments have been deposited during one of the later OAE 1 events (c or d). This fossil rich carbonate clay siltstone interbedded section represents the Albian and has an exposed thickness of 15m. Above an erosional truncation, coarse grained material of the Lebtaina Fm. overlie the Aptian corresponding to a base level fall during Early Cenomanian (WP169&170). The conglomerate and sand layers, which show trough geometries and internal cross-bedding of different directions, are interbedded with fossil-rich carbonates.

Fig. 49 shows the full outcrop of the Oued Chebeika succession. Fig. 50 shows the exposed inorganic mudstone facies of the Albian.

The section at El Ouatia contains Albian mudstones of a glauconitic facies indicating an open marine environment with water depths in the range of 50-200m (cf. Heling, 1988). It is bounded at the base and top by clastic channels of the lower and upper delta plain. The upper clastics are covered by carbonates and bioclastites (WP 175&176, Fig. 51). Proximal, the Albian succession is marine dominated with some regressive sands

Fig.51: Shallowing upward trend at El Ouatia (WP 171-176). The greenish color of the basal fineclastics indicates a subtidal, reductive environment (glauconites). The central part of this section is represented by organic fineclastics at the base and a red fluvial facies at the top. Above, marine carbonates are following (WENKE et al. 2009).

and conglomerates migrating into the marine system.

The Cenomanian is often represented by delta plain sediments, cross-stratified sandstones with numerous channels that contain significant amounts of low diversified shells that represent a short period of regression in the Late Cretaceous.

The Calcaire d'Aquidir succession (WP 80-88), which is exposed in the Foum Aquidir WSW of Akhfennir in the Puerto Cansado anticline includes black shales at the base (OAE-1c or d) and is covered by high porous limestones referred to as the „calcaire caverneaux" (Fig. 52, WP 97). Fig. 53 shows a piece of the organic rich Albian black shale (WP 94).

The overlying upper Aguidir section of Cenomanian/Turonian age includes a 70m thick transgressive- regressive cycle consisting mostly of limestones alternating with silty clay/mudstones that in turn are covered by fine grained sandstones (Fig. 54).

The Late Cretaceous is represented by the Lebtaina Fm. The coastline retrograded and a coastal facies developed 120km east of the present day coastline or 100km east of Laâyoune. The

Fig. 52: "Carbonates Caverneux" containing cm-dm vugs on top of the Calcaire d'Aquidir Fm. black shales of Foum Aquidir (WP 97, WENKE et al. 2009).

Fig. 53: OM-rich mudstone of the Albian Calcaire d'Aquidir succession (WP 94, WENKE et al. 2009).

Fig. 54: The upper Calcaire d'Aquidir Fm. on top of the Calcaire Caverneaux. The succession describes a transgressive regressive cycle of alternating carbonates and mudstones covered by fine sandstones (WP 80-88, WENKE et al. 2009).

Fig. 55: Upper Cretaceous of Labtaina al Talliya. The whole succession shows a shallowing upward trend from marine clastics of lower delta plain to beach facies (WP 152-157, WENKE et al. 2009).

succession of Labtaina al Talliya is split in a southern shallowing-upward succession from marine sandstones to beach facies (Fig. 51) containing cross stratified sandstones and microconglomerates (Fig. 52) and a northern lagoonal facies mainly consisting of clay to siltstones with interbedded evaporites.

The Turonian marine succession is dramatically exposed at the mouth of Oued Ma Fatma (WP 188-192, Fig. 24). There a basal unit of black shales (WP 188), well known as the Tarfaya hot shale and described in various studies, represents open marine shelf sediments of the Bonarelli Event (OAE-2) (e.g. KOLONIC et al.; 2002; MORT et al., 2008; KUHNT et al., 2009; SACHSE et al., 2011). A 15 to 20 m thick unit of shales in some layers interbedded with silty limestones deve-

Fig. 56: Cross stratified sandstones representing near coast high energy sediments overlain by bioturbatic siltstones (WP 154, WENKE et al. 2009).

Fig. 57: Ball and pillow structures in the Turonian blackshales of Oued Ma Fatma. The whitish color is a weathering effect. The black color of the Tarfaya hot shale can be exposed by simply scrubbing on the surface of the rocks (WP 188).

loped as pillows (balls and pillows structures) alternate with bioclastic mud-/siltsones (Fig. 57). The shales vary between oxic and anoxic conditions which can be identified by a change of the color from dark to light grey.
The Turonian black shales are covered by Senonian mudstones which are heavily weathered and contain a high amount of flint (WP 191).
The whole Coniacian to Maastrichtian of the Tarfaya-Laâyoune Basins in the study area is dominated by the deposition of fine clastic material, often heavily weathered and overprinted

Fig. 58: Santonian outcrop between in the northern Laâyoune Basin between Laâyoune and Smara. As a consequence of a heavy weathering (desert varnish, fracturing) accompanied with silification of the rocks, the original texture of the rocks are hardly to identify (WP 143-146).

Fig. 59: Eocene of Oued Itgui. Post-sedimentary hydrothermal fluids caused the development of geods (WP 100, Wenke et al. 2009).

by silex which makes it difficult to identify the original texture of the sediment. At last, mainly mudstones have been deposited during the Senonian in the Tarfaya-Laâyoune Basins. Fieldstones and rock surfaces are covered by desert varnish (WP 143-146). A Santonian succession including black shales of the OAE-3 event is provided in Fig. 58.

The Paleocene and Eocene remain dominated by the deposition of fine clastic material and contain hot shales of the PETM event. At

Fig. 60: Eocene anoxia/oxia cycles at the coastline north of Lemsid (WP 72-79, Wenke et al. 2009).

Fig. 61: PETM hot shales of the Eocene of Lemsid. The surface of the shales turned pale by weathering. Fresh cuts showed a dark grey to black color with a strong bituminous odor (WP 75, Wenke et al. 2009).

Bou Kraa, hydrothermal fluids triggered the growth of geodes in the shales (Fig. 59, WP 100). The PETM event is widely distributed in the Tarfaya-Laâyoune Basins and well exposed at the coastline near the village of Lemsid. A 40

Fig. 62: Tarfaya Oil Shale Pit. Turonian black shales covered by Miocene fine to coarse sands and Quarternary Hamada. Manuel Sehrt for scale (WP 52, Wenke et al. 2009).

to 50m thick succession of shales representing stacked shallowing upward anoxia/oxia cycles of the PETM event is exposed (Fig. 60, WP 72-79). The thickness of oxic cycles increases upwards and is finally truncated by coarser clastic material. The black shales have a bituminous texture and a strong hc-odor (Fig. 61).
A combination of eustatic sea-level fall and uplift of the Atlasian and Anti-Atlasian domains during Oligocene time resulted in the non-deposition/non-preservation of Oligocene rocks in the area of the field studies.
Miocene and post-Miocene sedimentary rocks are composed of eroded material from the uplifted areas and are mainly consisting of conglomerates (Matmarfag, 50km south of Laâyoune) and sandstones (Tarfaya). At a former oil shale pit run by Shell in the early 1980's Miocene sandstones (Grés de Tarfaya) directly overlie Turonian black shales (WP52, Fig. 62).

4.2. Stratigraphic well overview

The wells drilled in the Tarfaya-Laâyoune Basins have been mainly set on structural highs like fault blocks or anticlines. Their distribution is concentrated at four locations: i) inner shelf, ii) central shelf, iii) outer shelf and iv) continental slope. The wells can be allocated as followed:

- i) CHBK-1, EA-1, F3-1, D-2-9 & LAY-8-1
- ii) IF-1, PC-1, HAG-1-2, AMS-1-8, CORC-23-1 & CORC-23-2
- iii) TTN-1, MO-1 to MO-8, CJ-1, DAO-1-1, LAY-8-2, LAY-8-3, CORC-15-1, 15-A-1
- iv) HM-1, TAR-1, DSDP-369, DSDP-397

Table 3 shows the stratigraphic coverage of the wells drilled in the study area.

4.3. Well data screening on source rock indications and migrated hydrocarbons

The available well, literature and reported data has been screened on stratigraphy, log availability and hc-shows. An overview of the available and screened well data is provided in table format in Table 2.

Regarding source rock indicators the following results can be summarized:

4.3.1. Paleozoic

Weak shows with no further specification are reported for the Cambro-Ordovician of the well D-2-9, a source rock presence is not approved.

4.3.2. Triassic

The Permian to Triassic rift stage occurred under semi-arid to arid conditions. The evaporation rates have been high as the Tarfaya-Laâyoune Basins were located in an equatorial position and a continental climate prevailed. Water filled depressions likely dried quickly in addition to the first connected rift basins which also dried out after marine ingressions. These settings facilitate the development of a carbonate/evaporitic source rock type with local to regional distribution. Indications for the presence of this source rock are reported for the well CHBK-1 (1.5-2.5% TOC, inner shelf) and CJ-1 (0.1-0.63%, outer shelf/slope). Data about source rock quality and kerogen type, e.g. HI, OI, PI, S1 or S2, are not available and can only be assumed. The existence of a subsalt source rock in the Tarfaya-Laâyoune Basin is conceivable, however the presence is not yet proven. Additional information about migrated hydrocarbons is sparse. Traces of gas and bitumen are reported for the well CHBK-1 (ONHYM 2008), a total gas (TG) of 0.3% has been measured in the clastic succession of the Cap Juby well (CJ-1; ONAREP 1985).
However, traces of oil and gas in the Triassic succession, some with test results, are known from the onshore Laâyoune Basin at the southern boundary of the study area (UETAT wells, ONHYM 2008).

4.3.3 Jurassic

Since the Jurassic turnover during the Toarcian is well known as a global anoxic event (e.g. Jenkyns 1988), source rock information of that time interval is required. As the Tarfaya-Laâyoune Basins had a very restrictive character during the initial drift phase and oil was proven in mid-Jurassic carbonates in well MO-8, a Toarcian source rock is most likely. However indications are small with TOC content of Early Jurassic samples measured at 0.1-0.3% in well CJ-1 (outer shelf) up to 1.0% in well PC-1 (inner to mid-shelf). Cornford et al. (2013) investigated

Tab. 3: (Litho-)stratigraphic/formation distribution in the drilled wells of the study area. First order left to right: inner-, mid-, outer shelf and slope. Second order left to right: North to South.

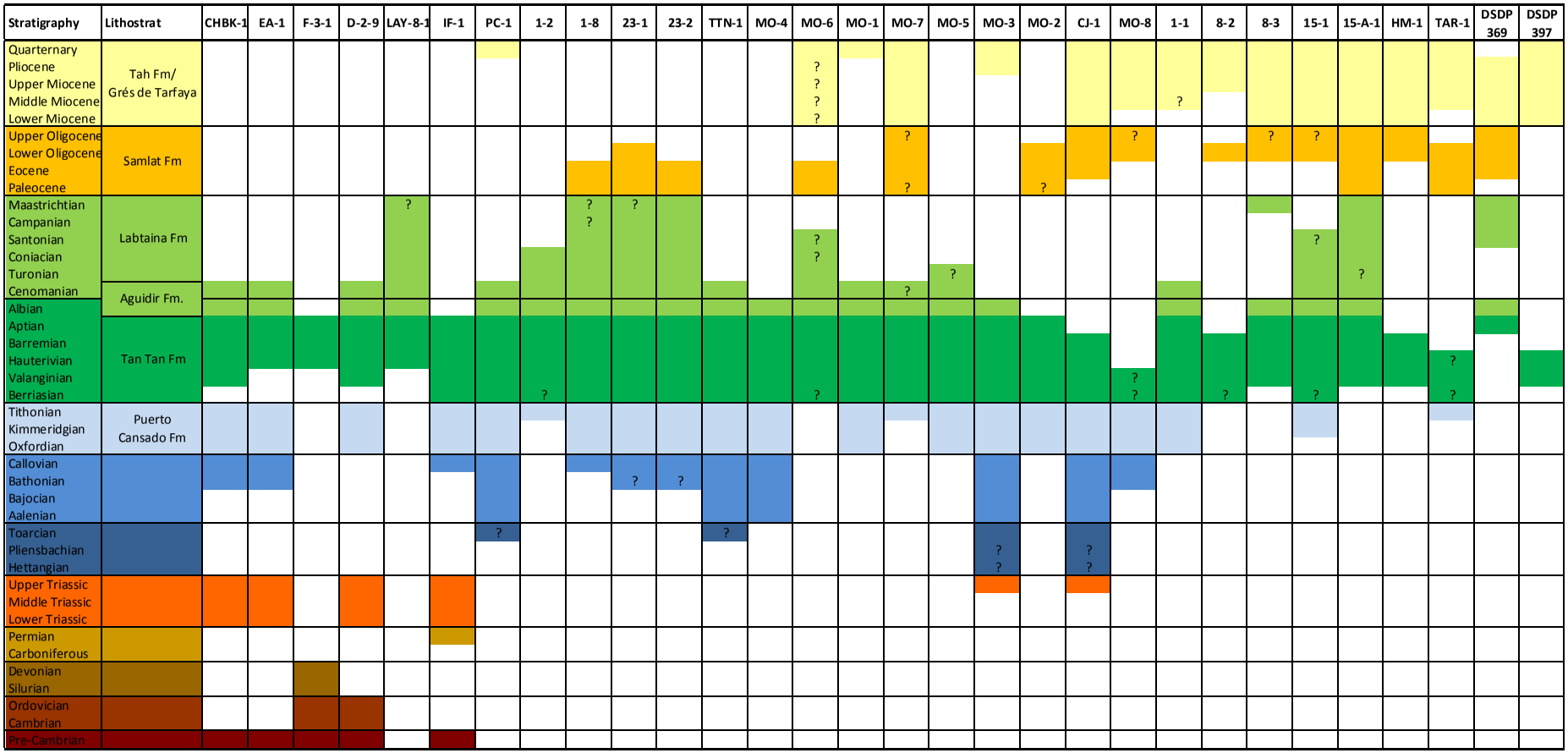

the geochemistry of the Toarcian sequence of Fuerteventura but the results did not show any source rock potential. More promising are the results from DSDP well 547B (slope location) where TOC concentrations of 0.42-8.89% have been measured (Simoneit et al., 1984) and were classified as a Type I kerogen alginite with HI values around 550 mgHC/gCorg suggesting probable deposition in a lacustrine setting during the sag stage. In addition, traces of asphalts in the Toarcian succession are reported from the well MO-3.
TOC values between 1.47% to 2.49% in a potential mid-Jurassic source rock (Callovian or Oxfordian) have been reported for well TTN-1 (outer shelf/slope). A Callovian source rock is proven for the Essaouira Basin and therefore is considered to be part of a proven petroleum system.
A technical discovery in Middle Jurassic tight oolitic carbonates (κ < 1mD) is reported from the well MO-8 with 45 liters of production of 33.8° API oil during a production test. Based on the sequence stratigraphic well correlation performed during this study (chapter 4.6.1) the age of the discovery was assigned to Bathonian age. Oil shows in Oxfordian carbonates are also reported for well MO-3.
Middle Jurassic gas shows are reported from the wells 23-2 and CJ-1, the latter below 0,5%.
The accumulation of organic matter during the development of the late Jurassic (Kimmeridgian) carbonate platforms was low with TOC values ranging from 0.2-0.5% measured from the inner to outer shelf position of wells MO-2,MO-7, CJ-1, MO-4, PC-1 & CHBK-1.
Two oil discoveries are reported for the Late Jurassic succession. MO-2 produced heavy oil of 11.8-12.4° API from a Tithonian reservoir, MO-3 has a non-tested oil column of 30m in Kimmeridgian to Tithonian carbonates. Heavy oil and gas was also recognized in well MO-4, asphalt in well D-2-9.

4.3.4 Cretaceous

4.3.4.1 Early Cretaceous

The Lower Cretaceous is dominated by the progradation and development of the Tan Tan Delta. Although sediment flux was consistently high, with dilution effects causing a decrease in TOC concentrations during that period, some stratigraphic intervals with elevated concentrations of OM have been recognized. Very slightly elevated TOC content with concentrations between 0.25-0.5% has been reported for the Berriasian deep marine fan drilled in well MO-7 indicating a terrestrial run-off (BTR) after the base-level fall at the end of the Jurassic.
Indications for the accumulation of elevated amounts of TOC during the Hauterivian Faraoni event are reported from the wells CJ-1 and MO-7 with concentrations around 0.5% in the outer shelf region and up to 1% in DSDP 397 at the lower slope.
The Barremian to Aptian succession exhibits increased OM accumulations, probably of the Selli and Jacobs (OAE-1a and b) events, in the wells 15-A-1, CJ-1, MO-2, MO-4, MO-7 and PC-1 with values between 0.6 and 1.35% TOC for the inner to outer shelf region and up to 1.75% for the northern Moroccan offshore Mazagan in DSDP 370.
Maximum TOC concentrations of 1% TOC have been reported for well MO-7 in the outer shelf area. Following MO-7 and DSDP 397 analysis, the OM accumulations recognized in the Tan Tan Delta so far are of type III/IV kerogens (terrestrial to dead kerogen) with HI values between 25 (Valanginian) and 200 mgHC/gCorg (Barremian/Aptian).
The source rock potential increases dramatically with the termination of the Tan Tan Delta during the Albian (OAE-1c/d). TOC concentrations between 1% and 3% have been recognized on the shelf in MO-7 with HI values between 180 and 381 which is in the range of type II/III marine to terrestrial kerogen.
Migrated hydrocarbons are accumulated hydrocarbons mainly recognized as gas peaks on the mud log or asphalt in the drilled cuttings. Elevated gas logs in the Tan Tan Fm. have been measured in the wells TAR-1, LAY-8-2 and LAY-8-3 with the presence of asphalt reported from the wells MO-1, MO-3 and in the Hauterivian section of well MO-6.

4.3.4.2 Late Cretaceous

The source rock potential of the Albian and Turonian black shales of the Tarfaya Basin have been widely discussed in literature based on outcrop sample analysis (e.g. Sachse, 2011; Sachse et al., 2011; 2012) with magnific OM-concentrations up to 17%TOC. These very high amounts have not been reported offshore, however, TOC concentrations between 0.8 to 4%TOC were measured on the shelf in various wells (15-A-1, MO-5, MO-6 & MO-7) and up to 6%TOC in the lower slope area (DSDP 369) with HI values around 500-700 mgHC/gCorg (Sachse 2011). The presence of a Santonian/Campanian (OAE-3) source rock has also been described

by Sachse (2011) with TOC values between 1% and 8% of mixed marine-terrestrial type II/III kerogen with HI values between <50 to 700 mgHC/gCorg.
Elevated gas is reported for the wells LAY-8-2, LAY-8-3, EA-1 and 23-1. Asphalt in the Late Cretaceous succession was found in the well 23-1. Oil shows are reported from well 23-1.

4.3.5 Cenozoic

The Cenozoic source rock generation is mainly concentrated on the PETM event which is exposed in the Laâyoune Basin at the localities of Lemsid and Bou Kraa (see chapt. 4.1.2.2). Sachse (2011) reports TOC concentrations between 0.6% and 4.5% of a type II/III source rocks with HI values between 87-700 mgHC/gCorg for the inner to central shelf while TOC concentrations between 0.6-2.9% of an oil-prone source rock are reported for the wells 15-A-1, CJ-1 and MO-6 for the outer shelf regions.
As gas of biogenic origin is very common in the overburden, gas accumulations in the Cenozoic succession were recognized in various wells (CJ-1, 15-1, 23-1, EA-1, LAY-8-2, LAY-8-3) with values up to 5%. Oil shows are reported for the well 23-1 also for the Cenozoic interval.

4.3.6 Summary and uncertainties on source rock assignment

As a consequence of excellent source rock exposure of the Albian to Eocene stratigraphic interval and the confirmation of their existence in the outer shelf by well results, the source rock presence on the shelf is widely proven and their potential and thickness well known.
Indications of potential source rocks of older stratigraphic age deposited during the Faraoni event, Toarcian turnover event or Middle Jurassic events are sparse. Further source rocks, for example those deposited during a Berriasian Terrestrial runoff or during Triassic evaporation are possible, however, there is little exact evidence available of this interval. As a result, a comment on their thickness and real potential cannot be made based on the available data.
For the further study, the blackshales of the following events are classified as proven source rocks of the study area:

- PETM (Paleocene/Eocene)
- OAE-3 (Coniacian-Campanian)
- OAE-2 (Turonian)
- OAE-1d (Albian/Cenomanian)
- OAE-1c (Albian)
- OAE-1b (Aptian)
- OAE-1a (Barremian)
- Faraoni (Hauterivian

Classified as possible/potential source rocks with local distribution are the black shales of the following events:

- BTR (Berriasian)
- OCC (Oxfordian)
- CCC (Callovian)
- Jurassic turnover (Toarcian)
- TR (Triassic)
- Kellwasser (KW)
- OS (Ord.-Sil. extinction)

4.4 Seismic interpretation

4.4.1 Regional mapping

Eight reflectors have been picked basin wide (cf. chapter 3.4.3; fig. 63).
The top seafloor/ground level is defined as the uppermost bright reflector below the seismic transparent water column.
The top Miocene is a bright reflector developed in the outer shelf, slope and basin areas with good well control. It is concordant to the underlying reflectors while the overburden shows onlap against it.
The top Eocene (Early Oligocene or PAU) has more or less the same distribution like the top Miocene, It is a bright reflector defining the top of the Paleogene shelf margin wedge with onlap of the overburden aiaginst the underlying continentward and concordance to the underburden in basinward direction.
The base Cenozoic or IAU is a bright reflector cutting in the outer shelf area the whole Late Cretaceous and up to the half thickness of the Early Cretaceous strata. It is discordant at the base while the overburden shows onlap in the outer shelf to lower slope, and concordant to under and overburden in the middle to inner shelf areas.
The Top Aptian is defined as a bright positive amplitude (hard kick) caused by a sudden lithology contrast on the top of the Tan Tan Delta between the clastic Tan Tan Fm and the carbonate/fine clastic Calcaire d'Aquidir Fm. This reflector is only deve-

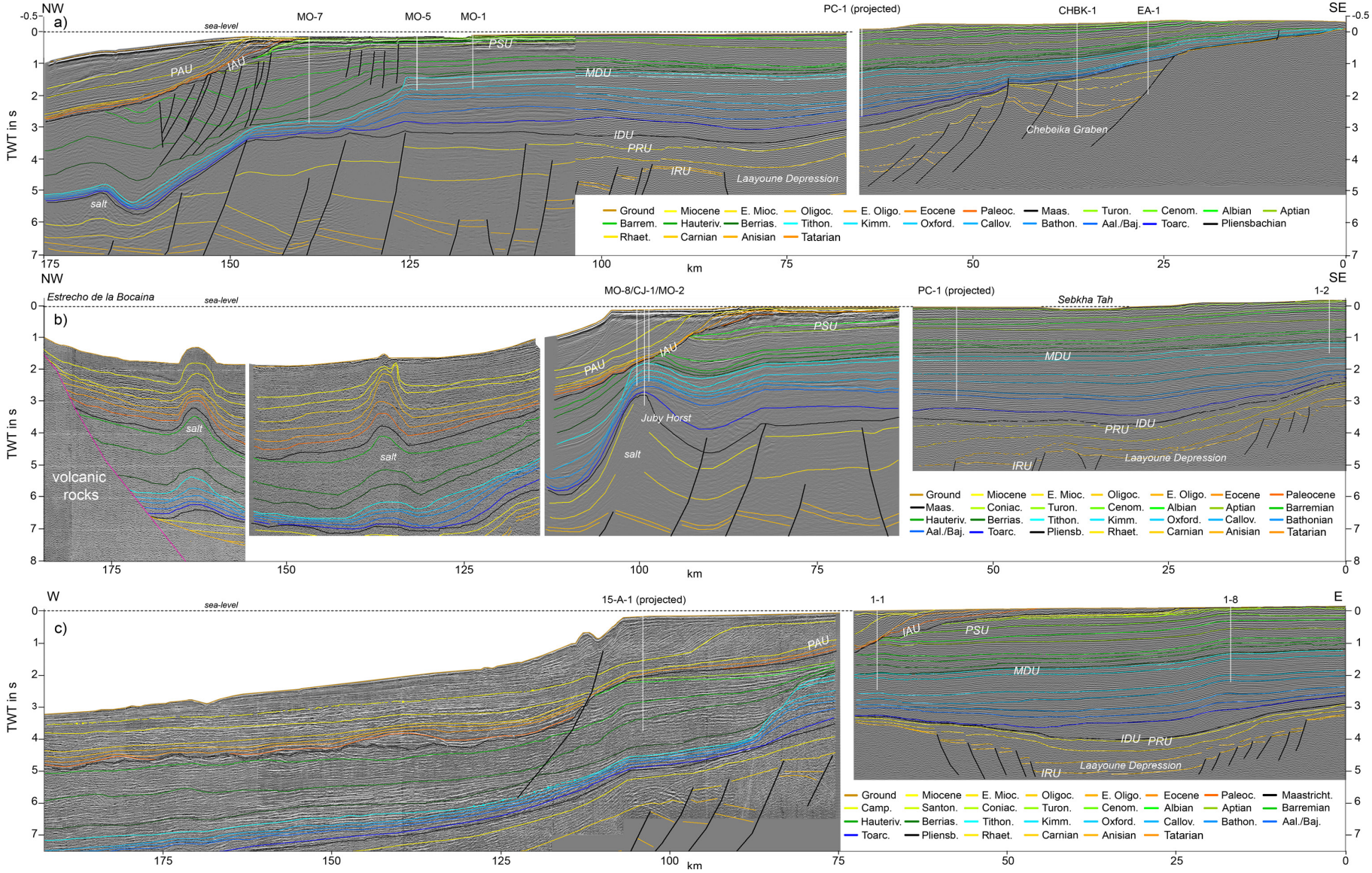

Fig. 63: Interpretation of seismic reflection profiles in the Tarfaya and northern Laâyoune Basins, with a) Tan Tan Delta, b) Cap Juby oil discovery, c) northern Laâyoune basin. Unconformities: i) IRU – Initial Rift Unconformity, ii) PRU – Post Rift Unconformity, iii) IDU – Initial Drift Unconformity, iv) MDU – Mature Drift Unconformity, v) PSU – Peak Spreading Unconformity, vi) IAU – Initial Atlasian Unconformity, vii) Peak Atlasian Unconformity (WENKE et al., subm.).

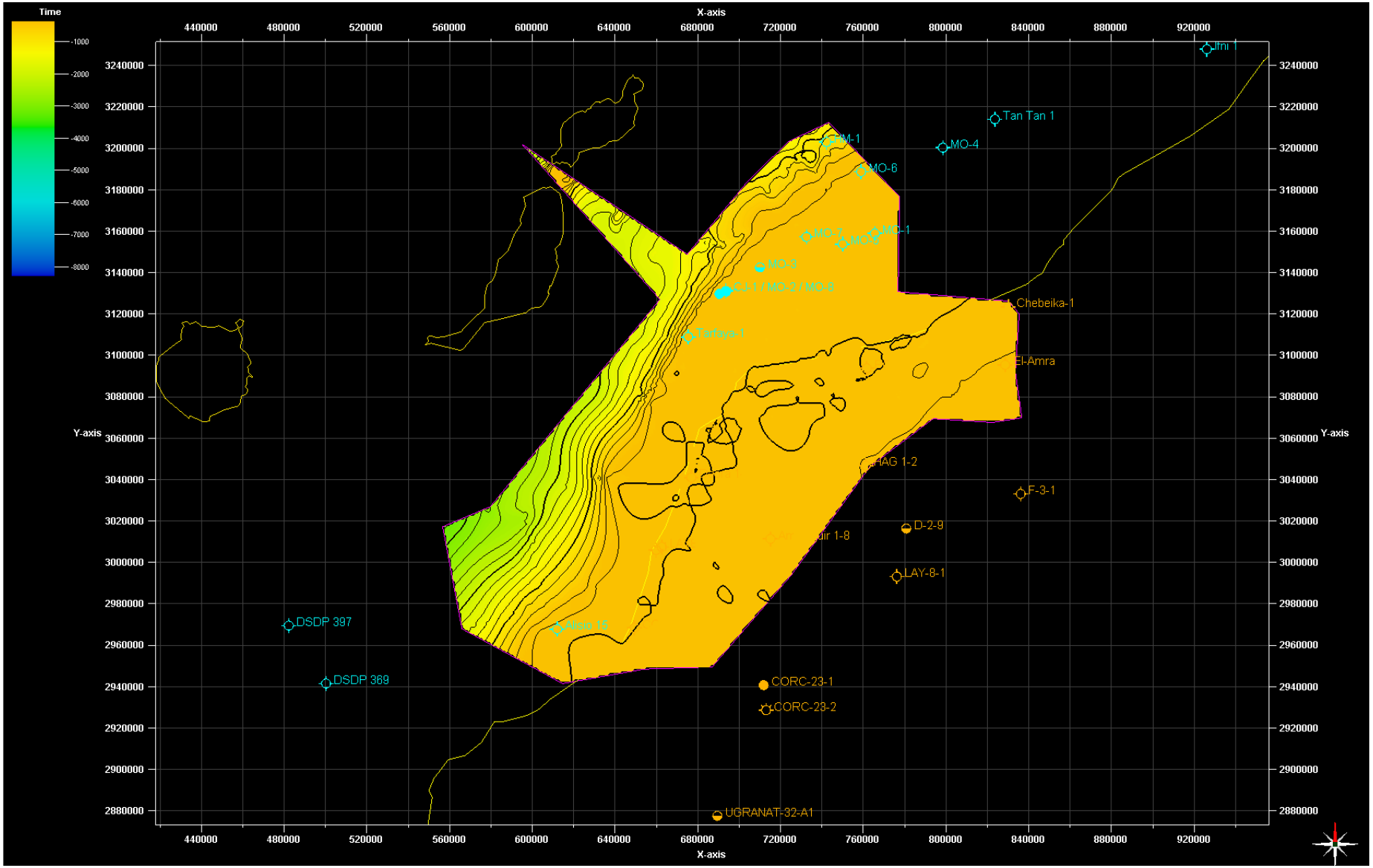

Fig. 64: Surface of the present day seafloor/ground level in TWT [ms] (WENKE & ZÜHLKE, 2011).

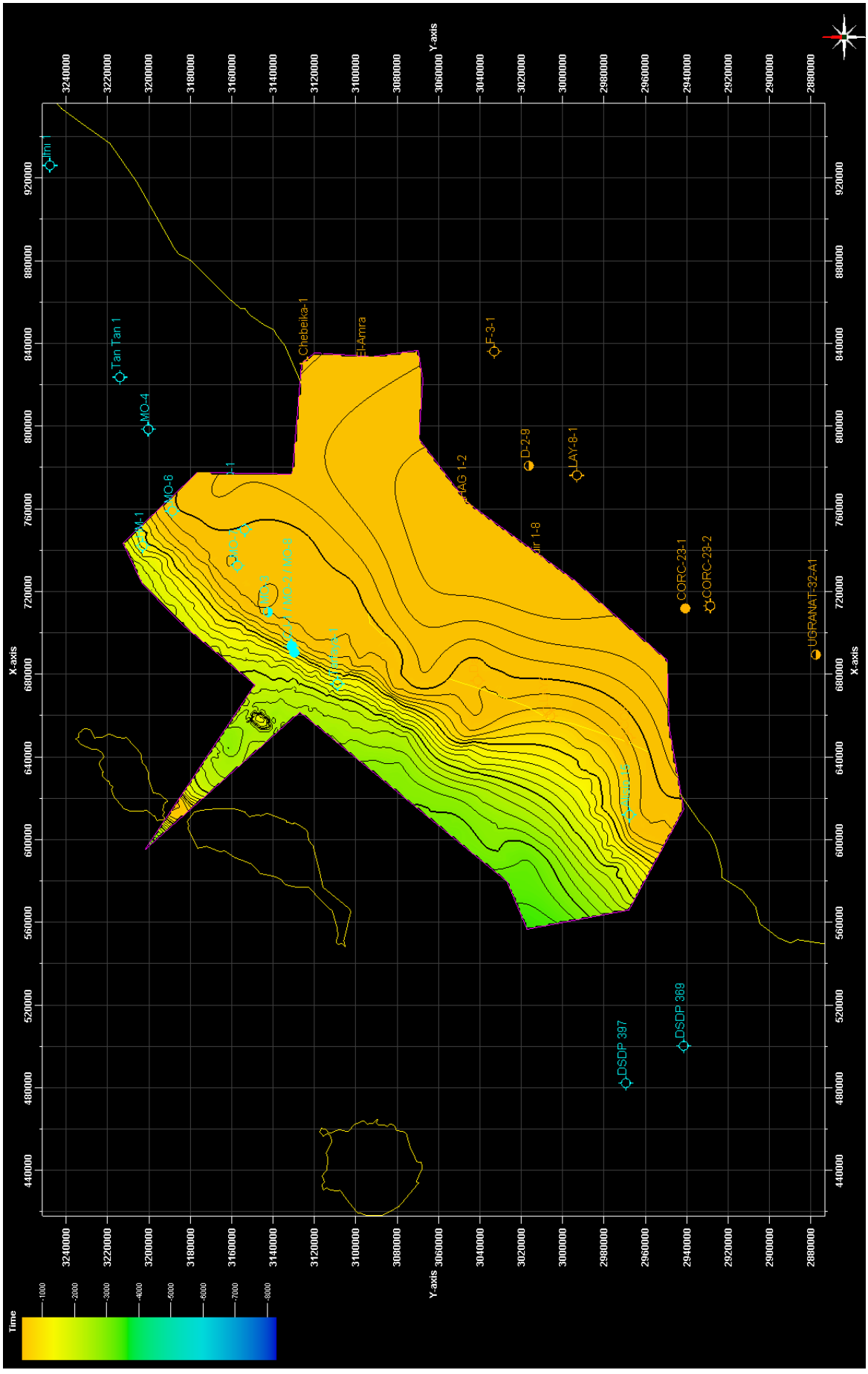

Fig. 65: Surface of top Miocene in TWT [ms] (Wenke & Zühlke, 2011).

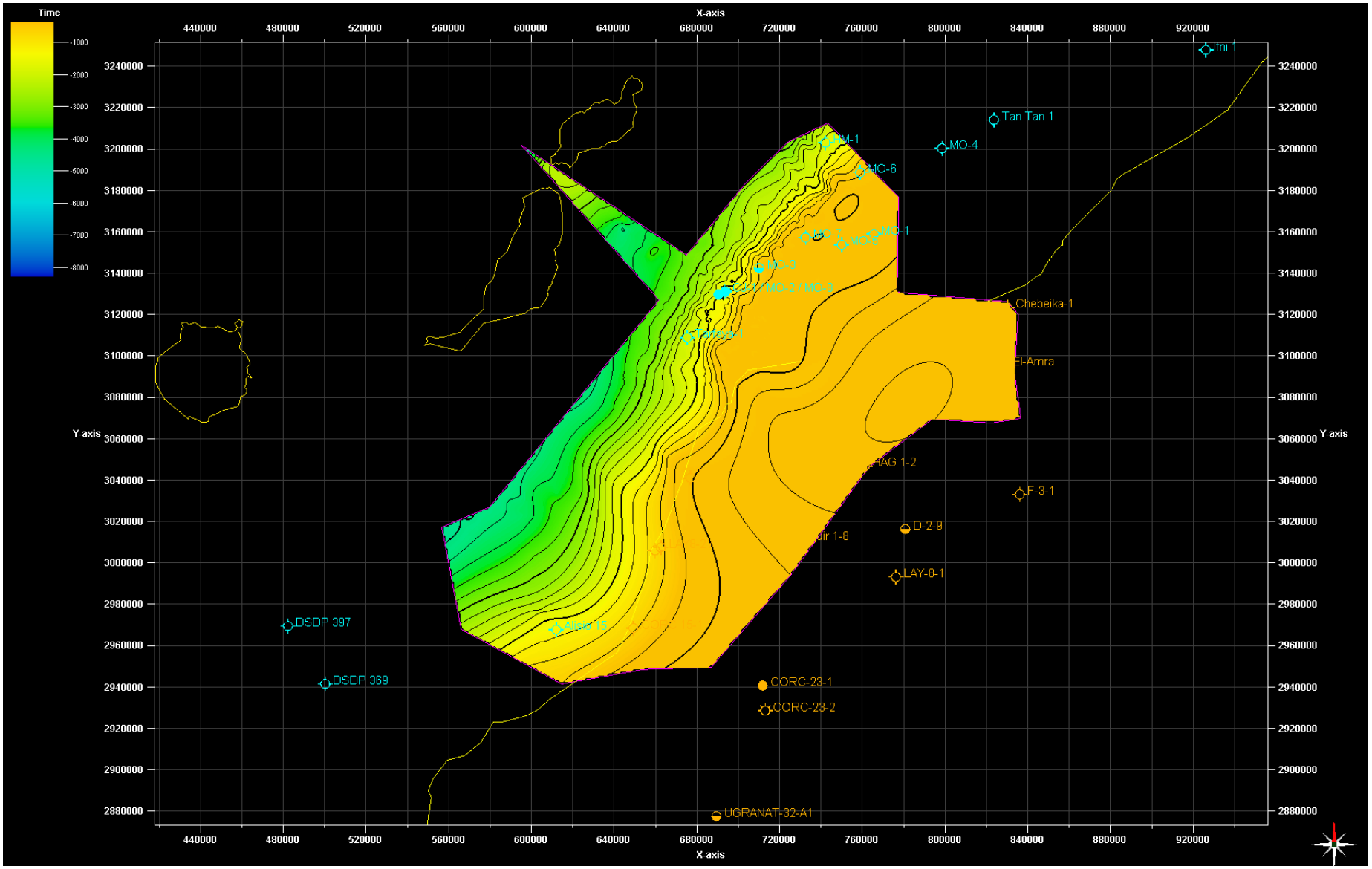

Fig. 66: Surface of top Eocene (Early Oligocene)/the PAU in TWT [ms] (WENKE & ZÜHLKE, 2011).

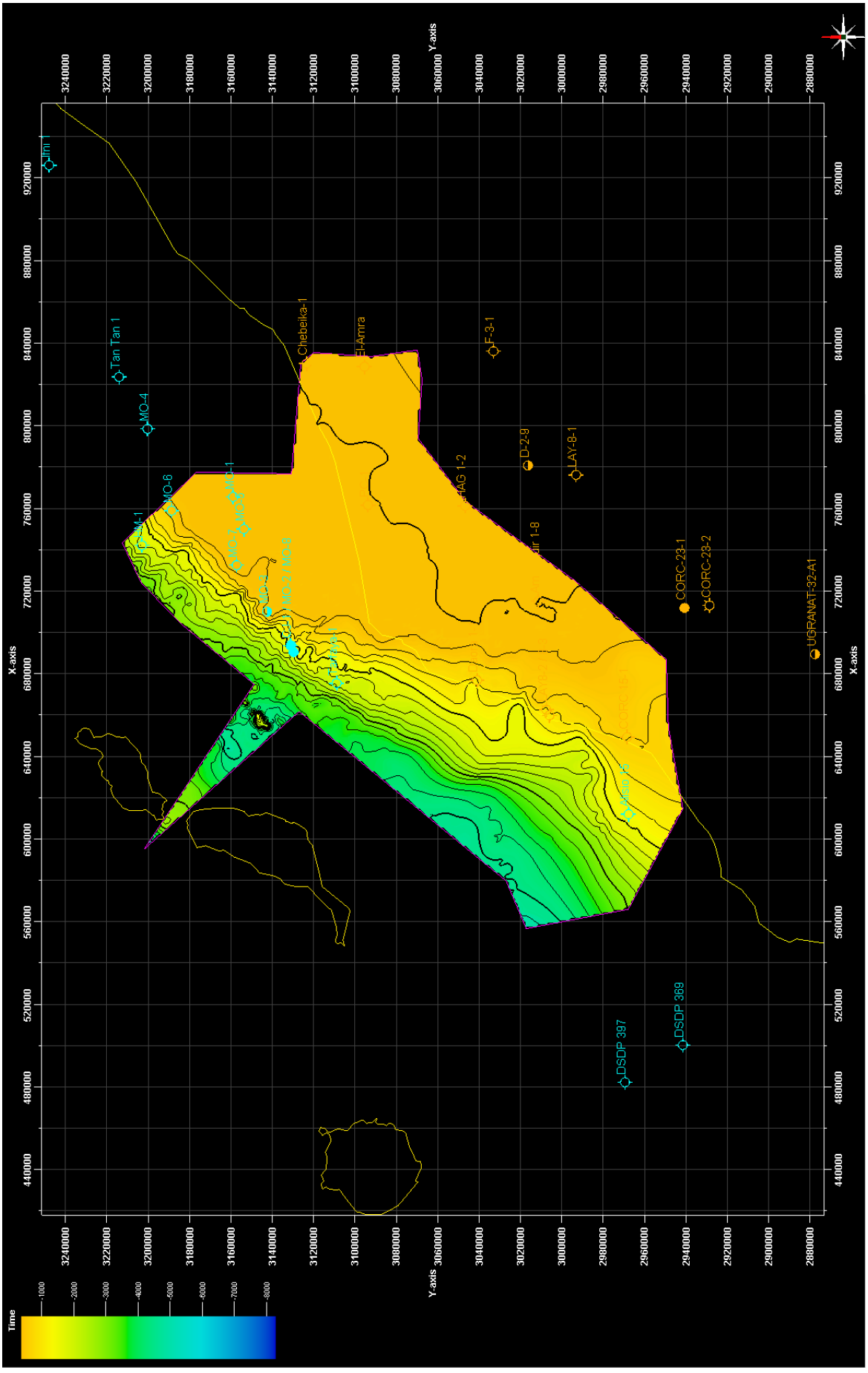

Fig. 67: Surface of base Cenozoic/IAU in TWT [ms] (Wenke & Zühlke, 2011).

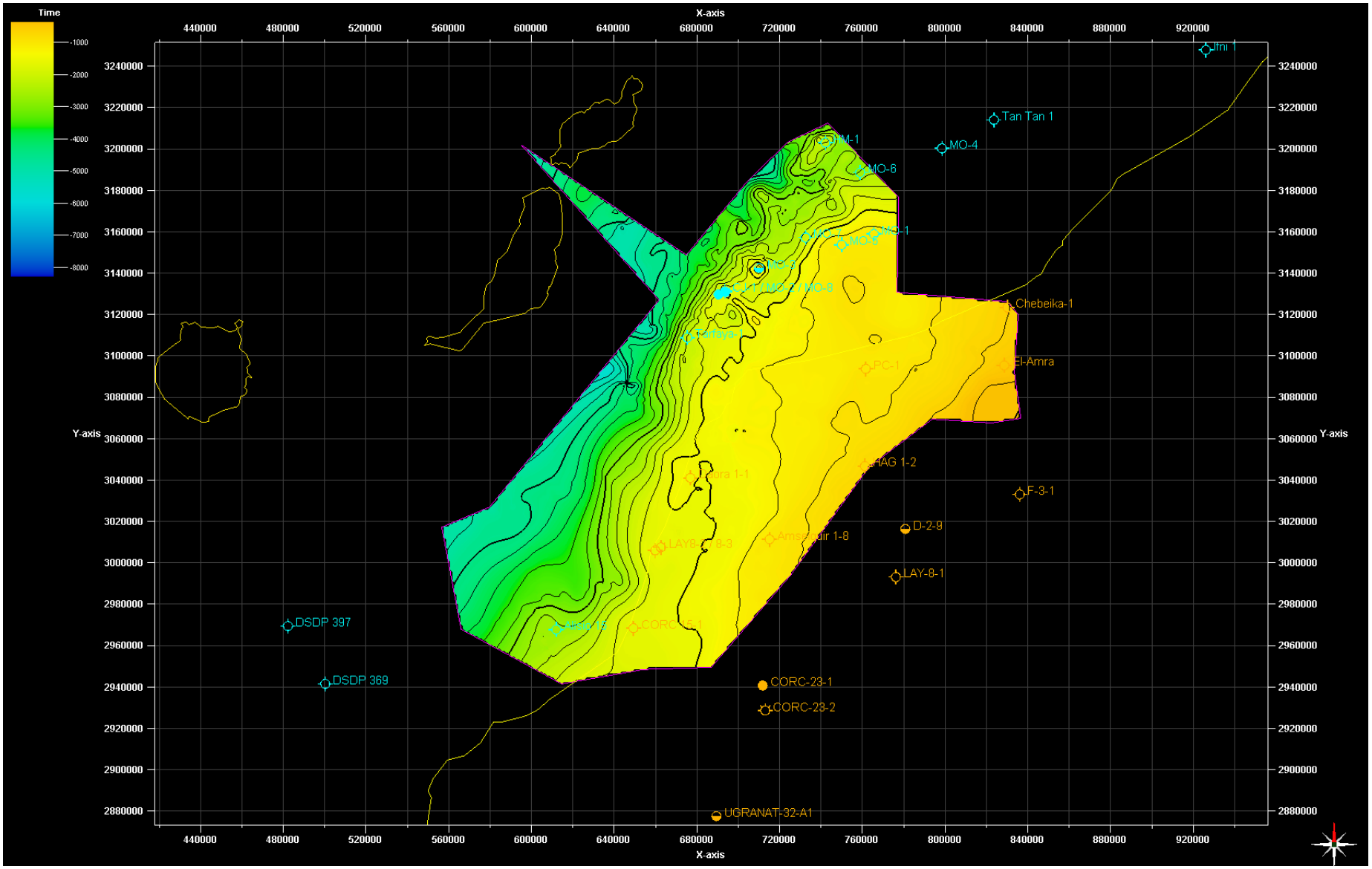

Fig. 68: Surface of top Hauterivian in TWT [ms] (WENKE & ZÜHLKE, 2011).

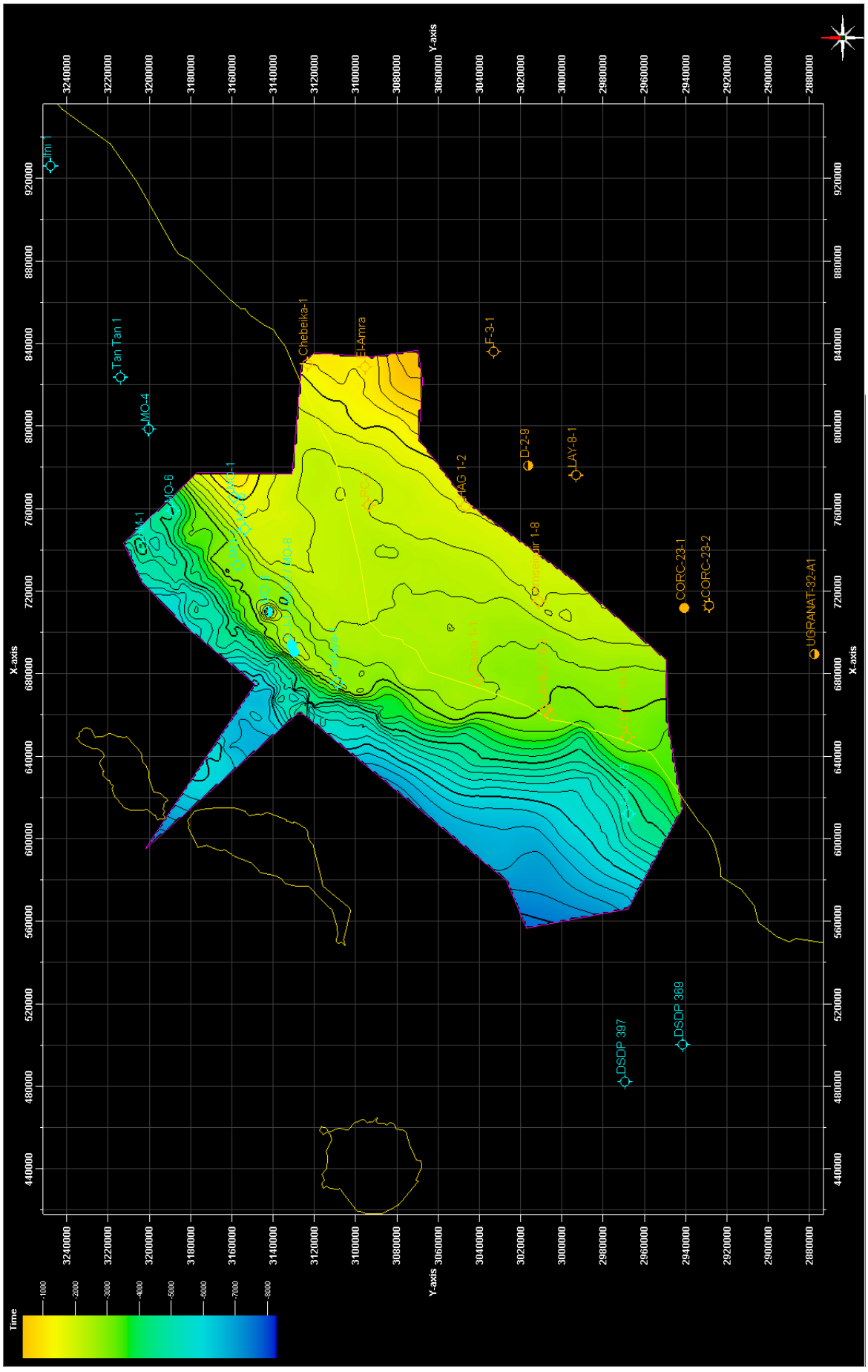

Fig. 69: Surface of top Tithonian/MDU in TWT [ms] (WENKE & ZÜHLKE, 2011).

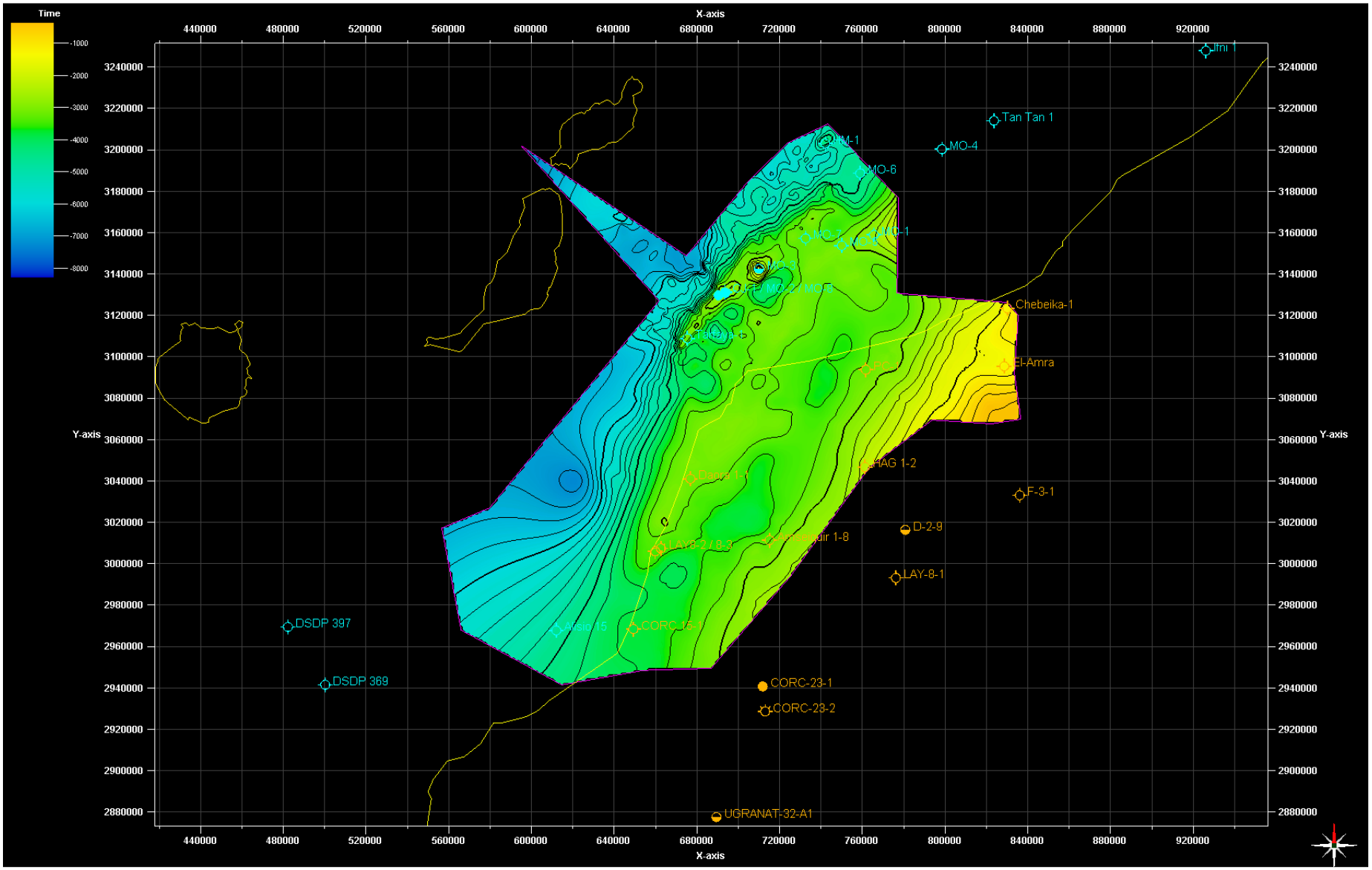

Fig. 70: Top Pliensbachian/IDU in TWT [ms] (Wenke & Zühlke, 2011).

loped on the shelf and is mainly concordant to the under- and overlying strata. However, in some regions, the Albian shows onlap against the Top Aptian. As the top Aptian has a lagoonal trough like shape, the onlap can be developed in the coastal as well as in the basinal direction.
The Top Hauterivian is defined as the reflector at the base of the Barremian progradation which can be recognized by foreset bed reflectors. The Hauterivian is concordant to the under- and overburden on the shelf while the overburden is downlapping onto the top Hauterivian.
The Top Tithonian or MDU is defined as a major regional unconformity. The reflector is very bright on the shelf due to the lithological change from Jurassic carbonates of the Puerto Cansado formation to clastic sediments of the Tan Tan Delta. On the shelf, the reflector is more or less concordant to the underburden while the overburden shows onlap at inner shelf regions, is concordant on the mid shelf and shows downlap at the (Jurassic) outer shelf. The shelf break is very abrupt and describes nearly a right angle cutting all the Tithonian and Kimmeridgian shelf strata before the character of the surface becomes more listric. In the deep offshore, the reflector is developed as a concordant conformity.
The Top Pliensbachian or IDU defines the end of the rift/sag stage. It is discordant to the underburden while the overburden shows onlap at the inner shelf.

4.4.2 3rd order sequence stratigraphic interpretation

Thirty reflectors/formation tops tied to 20 calibration wells have been mapped on the three key areas/transects and provide the stratigraphic and structural framework for mapping the gross depositional environments (GDE), 2D high-resolution sequence stratigraphy, time/depth conversion and 2D flexural reverse modelling.
Seismic reflectors define the top of the basement, four rift basin units and 25 3rd order sequences with an average duration of 7.6 m.y. (min. 2.3, max. 21.1 m.y). Biostratigraphic data have been tied to the geologic time-scale of Gradstein et al. (2004) for absolute ages. The interpretation of 3rd order sequences is based on unconformities, biostratigraphically constrained formation tops and vertical sediment stacking patterns from logs.
The seismic interpretation of the Tan Tan, Cap Juby and Laâyoune transects is given in Fig. 63. The Meso-/Cenozoic basin fill of the Tarfaya Basin has been preserved to the largest extent in the Laâyoune area (Fig. 63c). Because of regional uplift and erosion or non-deposition, no Santonian and Campanian basin fill has remained NW of Tarfaya. No post-Coniacian basin fill is preserved NW of Akhfennir.

4.4.3 Regional surfaces

Based on the regional interpretation described in chapter 4.4.1 seven regional surfaces representing 2nd order sequence boundaries have been generated in time domain (Fig. 64-70): top Quarternary, the PAU, the IAU, the top Hauterivian, the MDU, and the IDU. Stepping back in geological time the following changes in shelf geometry can be recognized: i) a basinward progradation of the shelf break in time, ii) a continuous growth of the shelf with peak extension in Late Cretaceous, and iii) a second order cyclicity of the slope inclination from a flat dipping slope in Early Jurassic to a rimmed shelf edge geometry in Tithonian followed by a flattening during the Cretaceous/Paleogene and final steepening during the Neogene.

4.5 Facies distribution

4.5.1 Late Permian to Early Jurassic rift sedimentation

In the Tarfaya-Laâyoune Basins the Triassic to Liassic basin fill is not exposed. However, it was drilled in the wells CHBK-1, EA-1, MO-3 (300 m of red clastics and salt, located offshore on a salt plume) and CJ-1. Well CJ-1 is located on a tilted rift block informally called the Cap Juby Anticline in the literature (Fig. 63). During the initial rift, rift climax and sag basin stages (Late Permian to Early Pliensbachian) terrigenous (alluvial fan, fluvial) conglomerates to red silt- and sandstones were deposited. Evaporites occur in the Early Norian. Late Norian basaltic extrusives and sills belong to the Central Atlantic Magmatic Province (CAMP). Initial open marine deposition after the rift basin stage took place in the Sinemurian. The proximal part of this early basin is represented by sandstones of an alluvial environment.
The Hettangian to Pliensbachian inner to outer shelf is represented by a hiatus, the IDU.
Potential reservoir facies can be expected in the late rift blocks located at marginal structural highs of the Chebeika Graben, the Laâyoune Depression or the

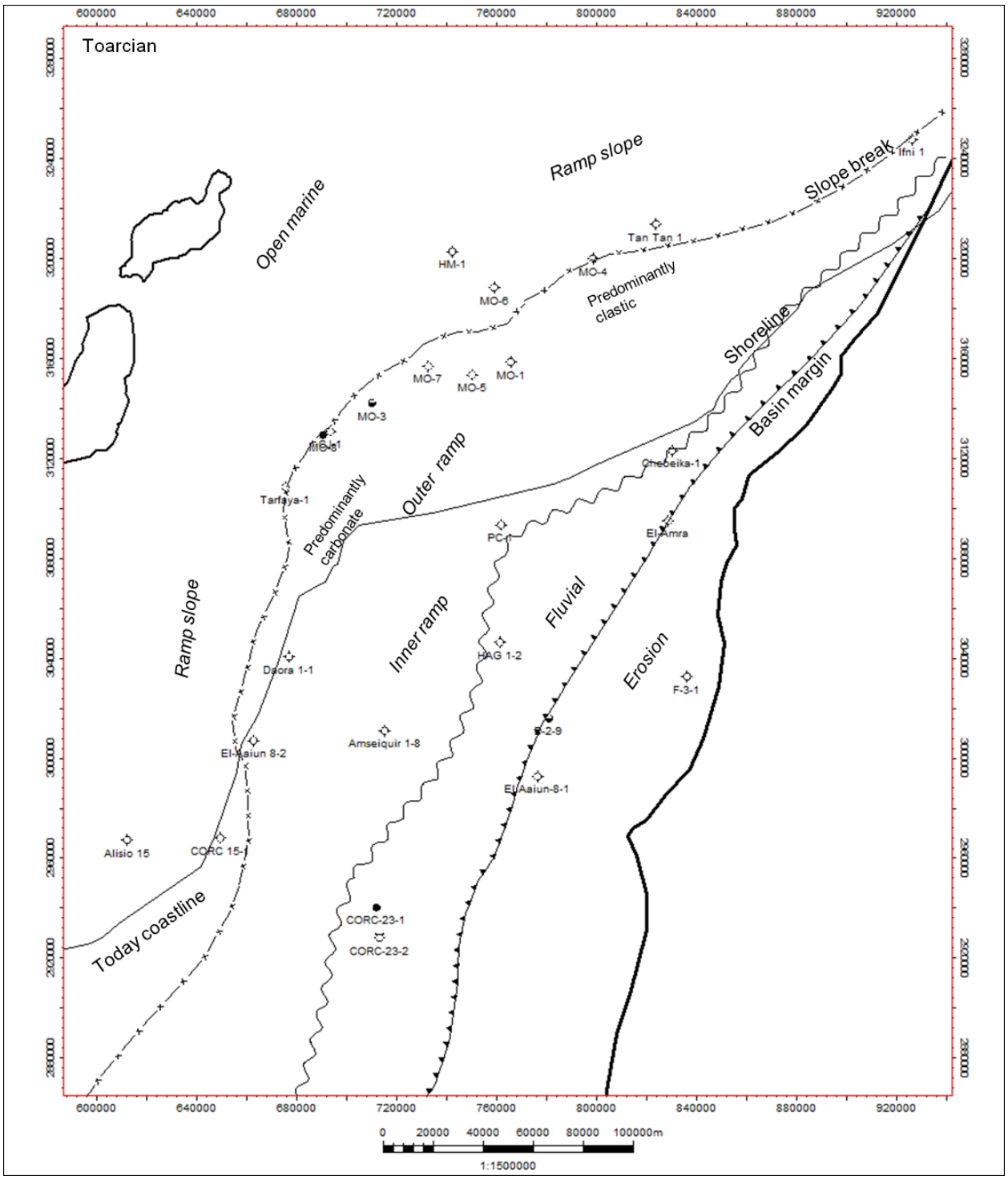

Fig. 71: Toarcian GDE map of the Tarfaya-Laâyoune Basins based on well evaluation and regional seismic interpretation (Wenke & Zühlke, 2011).

Atlantic Basin.
Rift and sag seal facies are represented by salt as well as post rift shales of the sag stage.

4.5.2 Pliensbachian to Toarcian ramps

Early Jurassic sediments were drilled in the wells CJ-1, MO-3, TTN-1 and PC-1. The Pliensbachian to Toarcian Tarfaya-Laâyoune Basins are subdivided into six depositional environments. Erosion prevailed in the area of the wells F-3-1. D-2-9 and LAY-8-1. In the proximal part of the Early Jurassic basins, fluvial sediments represented by red and yellow medium to coarse grained clastic sediments, have been deposited. The inner to outer ramp de-

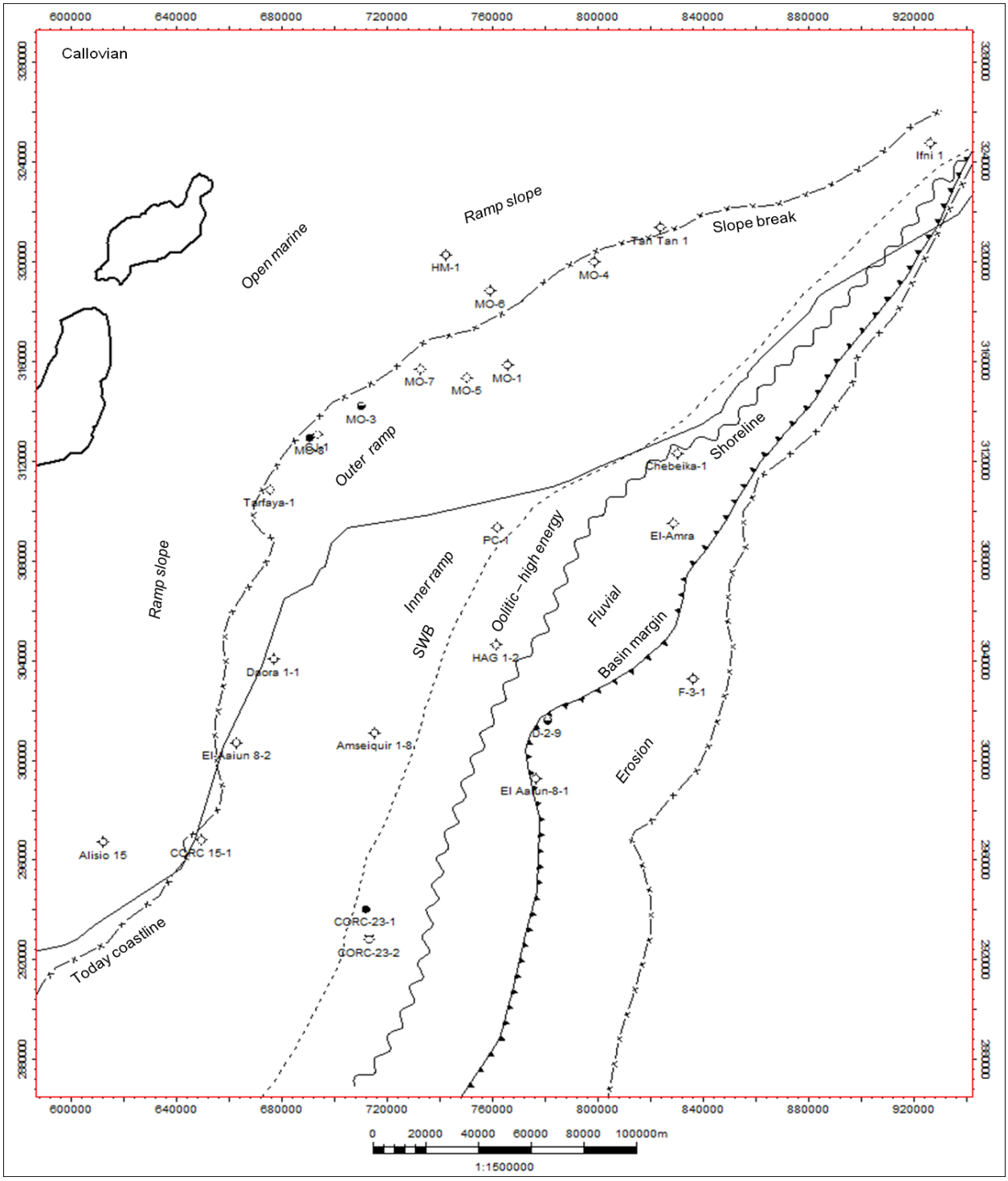

Fig. 72: Callovian GDE map of the Tarfaya-Laâyoune Basins based on well evaluation and regional seismic interpretation (Wenke & Zühlke, 2011).

positional systems are divided into a southern part dominated by marine carbonates of well PC-1, and a northern part dominated by prograding fine to medium sandstones recognized in wells CHBK-1, CJ-1, MO-3, TTN-1. Ramp slope and open marine environments follow in the distal direction. Turbidites are exposed on the Canary Islands (cf. chapter 2). During their progradation, the ramps covered or diluted marine anoxic sediments of the Jurassic Turnover event. Higher accumulations of OM may have prevailed in the basin between the Early Jurassic slope and the Canary Islands. However, their existence is not proven. Fig. 71 shows a GDE map of the area based on two-way-time seismic interpretation and interpolation (Fig. 64) and additional well

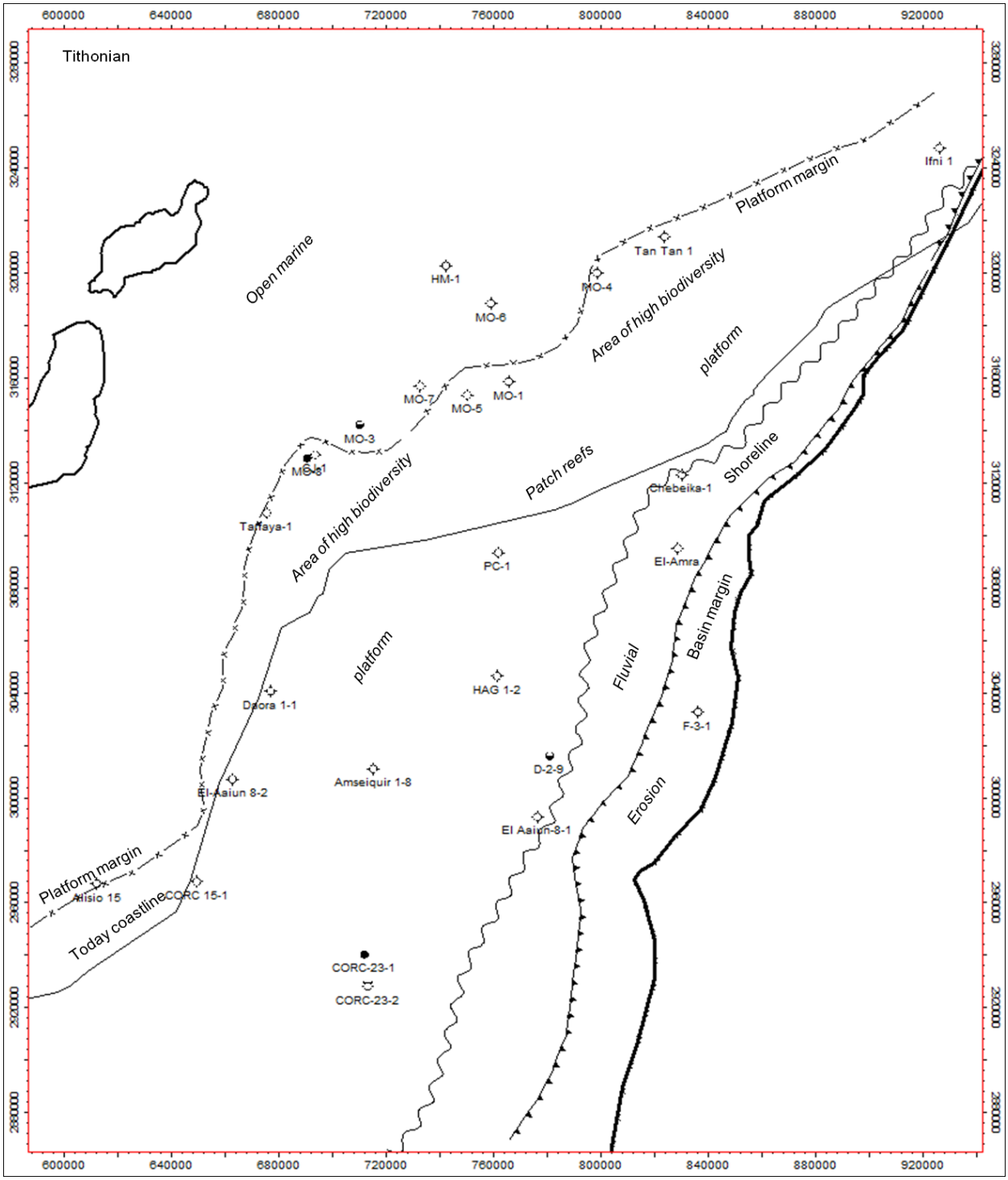

Fig. 73: Tithonian GDE map of the Tarfaya-Laâyoune Basins based on well evaluation and regional seismic interpretation (Wenke & Zühlke, 2011).

data evaluation.

The Toarcian clastic ramp represents a potential hydrocarbon reservoir. In the basinal direction a potential Toarcian source rock may also act as a seal.

4.5.3 Aalenian to Callovian clastic to carbonate ramps

The lower Middle Jurassic (Aalenian/Bajocian) succession was drilled in the wells CJ-1, MO-3, TTN-1 and PC-1, in addition Bathonian to Callovian sediments have been drilled in the wells CHBK-1,

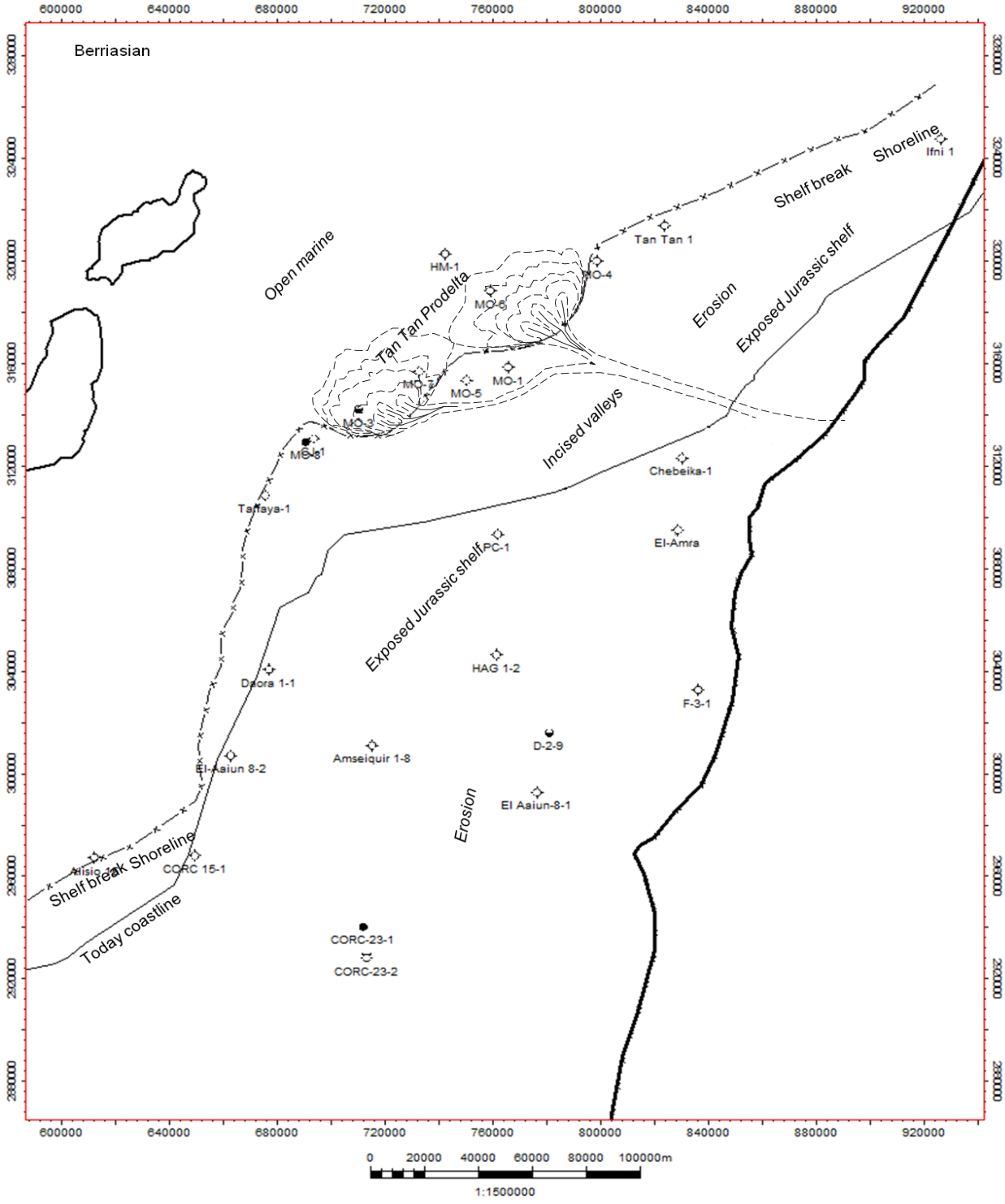

Fig. 74: Berriasian GDE map of the Tarfaya-Laâyoune Basins based on well evaluation and regional seismic interpretation (Wenke & Zühlke, 2011).

EA-1,IFNI-1, AMS-1-8, CORC-23-1 & 23-2, and MO-8. The Bajocian outer ramp includes intertidal platform carbonates. The Middle Jurassic of AMS-1-8 and PC-1 shows considerable clastic input and a more proximal, marine environment.

An increasing relative sea-level rise during the Bathonian results in the development of subtidal inner shelf carbonates to marginal platform deposits.

During the Callovian the proximal basin margin shifted in continentward direction. However, a fluvial environment still dominated the inner shelf area as represented by the wells CHBK-1 and EA-1.

Oolites indicate high energy carbonate sedimentation on the marine inner ramp. Low energy carbonate

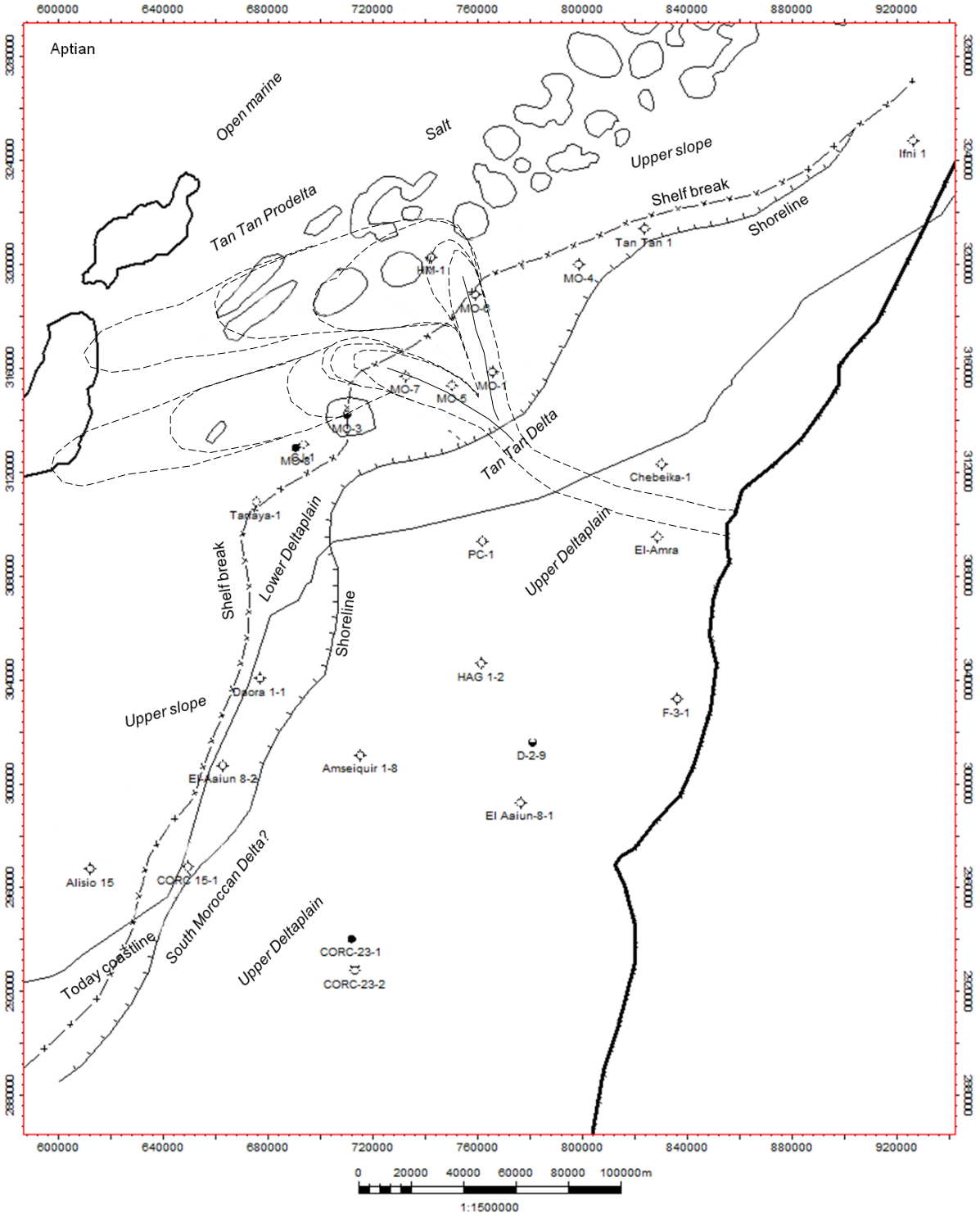

Fig. 75: Aptian GDE map of the Tarfaya-Laâyoune Basins based on well evaluation and regional seismic interpretation (Wenke & Zühlke, 2011).

systems deposited below a storm wave base (SWB) dominate the inner to outer ramp area.

Carbonates, especially where oolites have been deposited, have the highest reservoir potential in the Tarfaya-Laâyoune Basins. The MO-8 light oil discovery is bound with Bathonian oolites with 0.3 barrels of 38.5° API (45 l) oil recovered from this interval. However, reservoir properties can be very poor. Studies from the Canadian conjugate margin also suggest dolomitized shelf carbonates as potential reservoirs (e.g. Eliuk & Wach, 2010) as they were drilled in the CJ-1 well. Mudstone facies deposited during the Callovian transgression has the highest seal potential. A Callovian GDE map is gi-

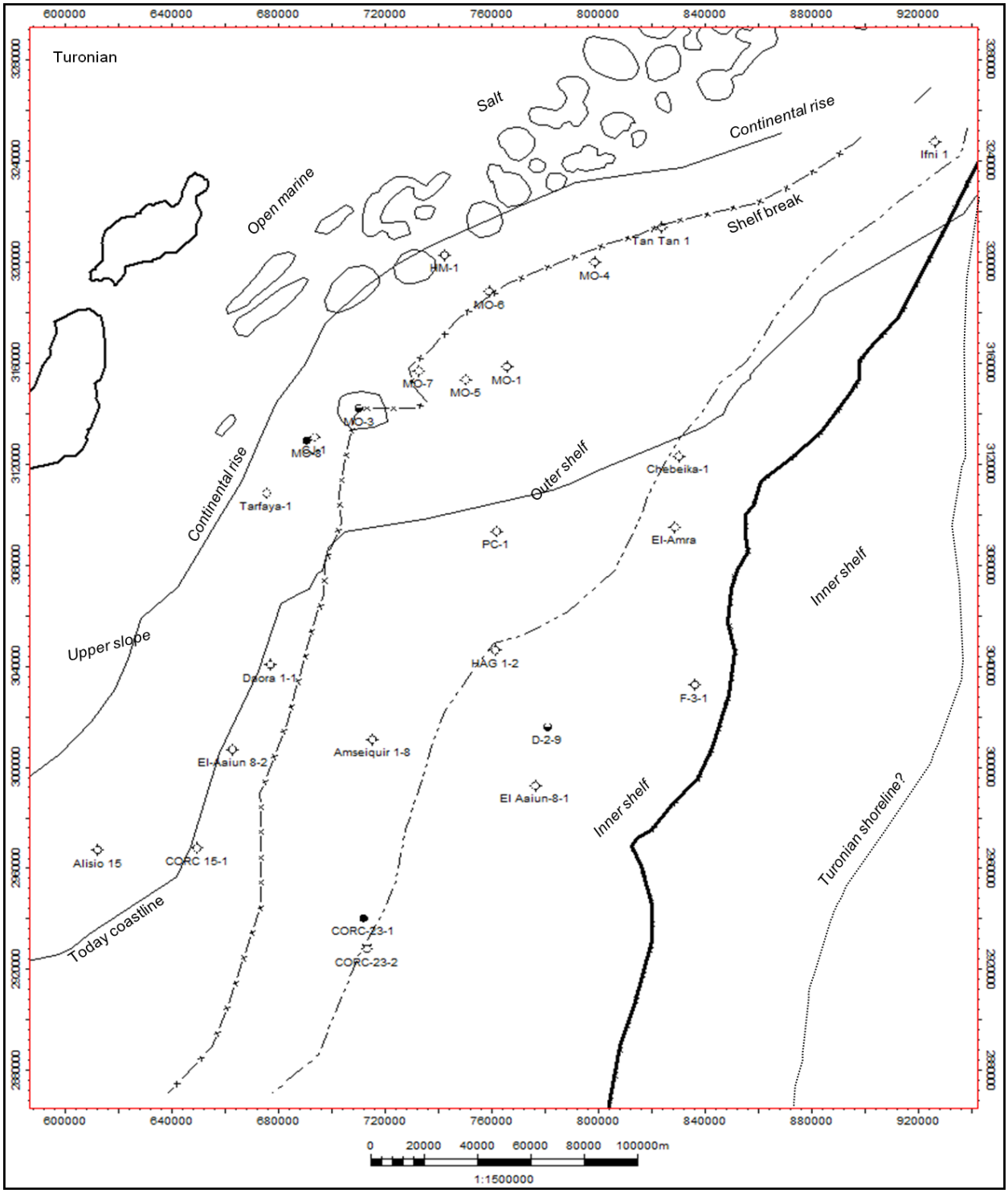

Fig. 76: Turonian GDE map of the Tarfaya-Laâyoune Basins based on well evaluation and regional seismic interpretation (Wenke & Zühlke, 2011).

ven in Fig. 72.

4.5.4 Oxfordian to Tithonian carbonate platforms

The Upper Jurassic is represented by carbonate platforms of the Lower Puerto Cansado Fm. which

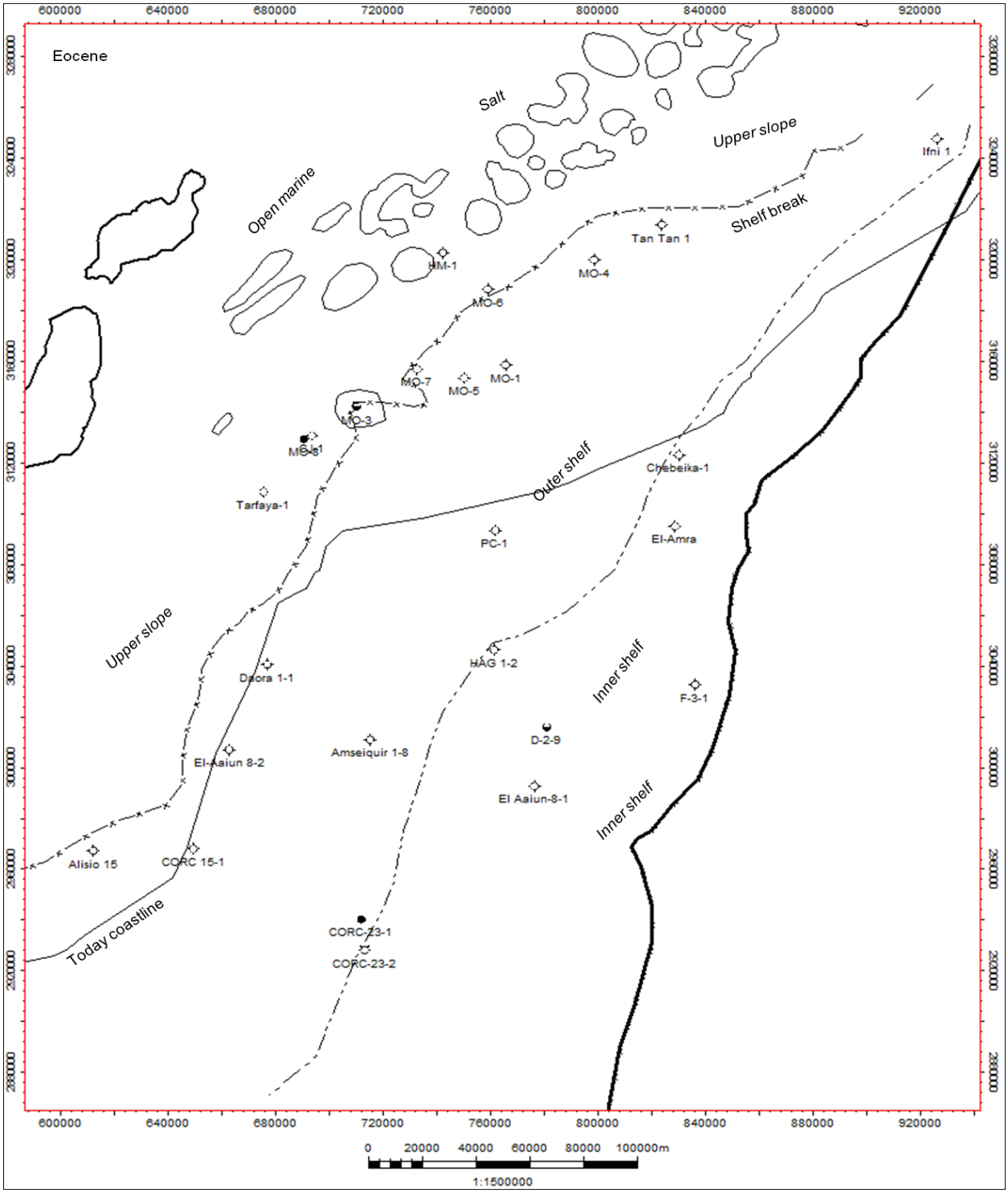

Fig. 77: Eocene GDE map of the Tarfaya-Laâyoune Basins based on well evaluation and regional seismic interpretation (Wenke & Zühlke, 2011).

grades laterally into detrital facies towards the continent and into marly facies towards the basin. It is part of a greater system of Atlantic carbonate platforms extending from Portugal to Guinea-Bissau (Jansa 1981, Hafid et al. 2008). A comparable setting is present at the conjugate margin offshore Canada (Smith et al. 2010).

The Upper Jurassic in this study has been subdivided into three basinwide seismo-stratigraphic units. Oxfordian well tops are available for the wells PC-1 (onshore), CJ-1, MO-3 and MO-8 (both onshore). PC-1 is located on the inner shelf of the Oxfordian carbonate platform with low clastic input; CJ-1 and MO-8 are located at the open marine outer shelf.

Kimmeridgian well tops have been available for the wells CJ-1, Daora 1-1, MO-3, MO-8, PC-1, and TAR-1. Low clastic input occurs in well PC-1.
The Tithonian shelf and reefal margin shows well developed carbonate platform geometries (Fig. 88). MO-7 is drilled into the offcut of the former Jurassic slope, which probably collapsed during the Early Berriasian eustatic lowstand. The Upper Jurassic shows alluvial deposition in wells CHBK-1 and EA-1 while erosion still prevails in well F-3-1.
The marine Tithonian section has well control in AMS 1-8, CHBK-1, CJ-1, CORC 15-1, Daora 1-1, EA-1, HAG 1-2, MO-1, MO-3, MO-5, MO-7, MO-8, PC-1 and TAR-1 and is represented by inner platform carbonates, patch-reef complexes and a fossil rich reefal platform margin, especially the Kimmeridgian to Tithonian reef facies and bioherms that represent the most prolific reservoir facies in the Tarfaya-Laâyoune Basins so far. The MO-2, MO-3 and CJ-1 discoveries are bound to these facies types. Seal facies is represented by post MDU transgressive shales.
A GDE map of Late Tithonian is given in Fig. 73.

4.5.5 The Berriasian to Aptian southern Moroccan delta complexes.

The Early Cretaceous Tan Tan-Delta is exposed onshore in the northeastern part of the study area between Smara and Tan Tan Plage. The upper delta plain is represented by paleosoils and red conglomerates of the fluvial plain north of Smara. The continental onlap of the Tan Tan Delta system against the Anti-Atlas is not exposed in the area visited during the field trip (cf. chapter 4.1.2.1). An upper to lower delta plain section was investigated at the village of Abteh, where distributary channels with micro-conglomerates are intercalated with delta plain siltstones, evaporites and few marginal marine/brackish sandstones with shells.
The most distal outcrops of the Tan Tan Fm. with lower delta plain environments are located at the mouth of Oued Chebeika (Fig. 49). Main lithologies are cross-stratified sandstones and micro-conglomerates.
The Aptian to Albian age lagoonal facies of the Aguidir Fm. are located west of Smara (N 27°01.765, W 12°00.648) where fine-grained clastics and evaporites alternate with carbonates that were deposited in shoreface to backshore depositional environments of the Tan Tan Fm.
The transition from the Early Cretaceous Tan Tan Fm. to the Albian carbonate Aguidir Fm. has been recognized west of Smara (N 26°38.186, W 11°53.204).
1D- and 2D-data analysis indicate an initial delta complex in front of an incised valley that cuts into the Tithonian carbonate platform during the Late Tithonian/Early Berriasian global sea-level fall with the lowest sea-level recorded in the Middle Valanginian. This incised valley was located in a similar position than the recent Oued Chebeika (Fig. 49). The source of the sediments is located in the northeasterly adjacent Anti-Atlas where sediment was supplied by the fluvial system of the Oued Draa. Thermochronological data of the southern Anti-Atlas show a moderate but continuous uplift between 150 to 110 mya (c.f. Sehrt, 2014), when the Tan Tan Delta was active. The strongly increased sediment input in the Early Cretaceous triggered the basinward flow of salt. South of the Tan Tan Delta a diapir intruded at the northern margin of a tilted rift block (line EM 45). A specific structural situation allowed an uplift of an autochthonous salt in the MO-3 area while the rest of the deposited salt was squeezed out in basin direction. Many allochthonous salt diapirs are located between the shelf margin and the Canary Islands.
Berriasian facies associations are given in Fig. 74 and a GDE map for Late Aptian is given in Fig 75.
The distribution of reservoir and seal facies follows sequence stratigraphic cycles with sand being transported and deposited in the Tan Tan Delta Complex mainly during HST or FSST times. A forced regression occurred during the Barremian and features prograding clinoforms becoming well developed on seismic lines during the evolution of a river dominated delta system. During Aptian times the sand contribution was high during base level rise and the Tan Tan Delta developed a wave- to tidal-dominated character with widespread sand distribution.
Seal facies are deposited between the channels as delta front shales or delta swamps and lake fines.

4.5.6 Albian to Campanian

In the late Early Cretaceous the Early Aptian delta is followed by Albian marine pelitic to carbonate shelf sediments. With the onset of a long-term eustatic sea-level rise between the Late Aptian and the Early Turonian, sediment input decreased and shelf retrogradation occurred. Fragmentation of the slope into separate fault blocks from Early Cretaceous salt flow and gravity-induced sliding on the top Jurassic led to the development of a major regional unconfor-

mity referred to hereafter as the IAU. Onshore, the Cenomanian-Turonian Lower Lebtaina Fm. consists of silty clay- to mudstones of an inner shelf environment. Proximal coastal depositional environments crop out in the area between Smara and Bou' Kraa (N 26°40.577, W°12 21.053 and N 26°34.682, W 12°14.696) where inner shelf clay- and siltstones are interbedded with fossiliferous carbonate and sandstone storm deposit layers. Subtidal environments above the SWB received little to moderate sediment input.

Cenomanian to Turonian black shales at the mouth of Oued Ma Fatma (Fig. 24&57) show anoxic/oxic cycles. The basal to middle part of each cycle consists of argillaceous sediments interbedded by carbonatic siltstones. In the middle to upper part of each cycle, anoxic sediments are replaced by chert. Towards the top of the Turonian succession, conglomerates and bioclastic sandstones with distinct cross-bedding indicate a shift to fluvial channels in the Campanian. In the former oil pit operated by Shell near Tarfaya, Turonian black shales are unconformably overlain by Miocene bioturbated shelly sands of a lower delta plain environment (Fig. 62).

The Coniacian to Santonian basin fill is exposed east of Smara (Fig. 58) and Bou' Kraa (N 26°41.163 W 12°24.352) in proximal marine shelf facies and in the area of Akhfennir (Fig. 52-54) in distal facies. On the basin scale, lateral facies changes are gradual and indicate moderate shelf progradation after the Turonian eustatic sea–level highstand with argillites and silty mudstones interbedded with carbonate mudstones slowly transitioning into a silty to fine sandy depositional system. The Campanian Upper Lebtaina Fm. consists of argillites interbedded by shelf carbonate mudstones. Marine platform sediments are also deposited in proximal areas of the TB close to Smara (Fig. 55&56) and show anoxic/oxic cycles in distal areas close to Akhfennir (Fig. 52-54). In the onshore area of the Tan Tan area, the post-Coniacian was eroded whereas south of Laâyoune the Late Cretaceous succession is largely preserved in the subsurface.

Late Cretaceous retrogradation to aggradation terminated in Middle to Late Campanian time. During this period of at least 25 mya, shallow to open marine deposition prevailed across the shelf and pelitic clastic and carbonate sediments were deposited. The flooded Tarfaya shelf and the Gulf of Zag were intermittently divided by a narrow seaway. During long-term low sedimentation rates a minimum of seven oceanic anoxic events was deposited; the Selli event (OAE-1a), the Urbino event (OAE-1b), the Tollebuc events (OAE-1c, Fig. 50), the Breistroffer event (OAE-1d), the Bonarelli event (OAE-2, Fig. 24&57) and the Campanian OAE-3 event. Until today, OAE-3 has been described only for the equatorial Atlantic, southern Caribbean and Western Interior Seaway (WIS). However, sampling and analyses as part of the Atlantic Margin Project did proof the presence of OAE-3 in the TB (Sachse et al. 2014). A Turonian GDE map is given in Fig. 76.

4.5.7 Campanian to Late Oligocene

During the Middle Campanian to Early Oligocene, eustatic sea-level did not fall significantly and most of the shelf region experienced marine conditions with increasing sediment input. A shelf margin wedge started to grow at the shelf margin slowly covering the IAU.

Onshore, Eocene sediments have been studied in the area between Smara, Bou' Kraa and Lemsid. West of Smara (N 26°40.670, W 12°35.356), the Eocene basin fill is represented by argillites and fine sandstones interbedded with normal graded coarse sandstones containing phosphate and chert nodules and geodes (Fig. 59). Argillites include geodes of hydrothermal origin (N 26°39.736, W12°56.323). On a basin-wide scale, anoxic sediments increase in western direction. The Aridal Fm. in the Sebkha Aridal (N 26°16.304, W 13°49.369) includes clays to fine sandstones with plant remains, which are overlain by normally graded conglomerates and sandstones. Close to Lemsid (N 26°36.516, W 13°42.477), a large-scale (40 m thickness) deepening-upward trend is exposed with bituminous siltstones to fine sandstone below and argillites interbedded with silty carbonates above. These shales represent the Paleocene-Eocene Temperature Maximum (PETM) event (Fig. 60).

The Paleocene and Eocene basin reaches maximum thicknesses at the shelf break. In the inner shelf, small thicknesses prevail or the Paleocene did not develop.

The PETM sampled in Lemsid is also described as immature but with high organic content in wells CJ-1 and MO-8.

A GDE map illustrating the Eocene is given in Fig. 77.

4.5.8 Neogene

The Oligocene onshore is exposed only in the very south of the Dakhla Basin. The reason is a combination of a eustatic sea level fall and the uplift of the Western High Atlas. Basin inversion and flexural uplift of the northeastern basin were triggered during the Atlasian orogeny. A new sediment input source was initiated in the Late Oligocene to Early Miocene. Two sediment pathways ran south of the High Atlas along the Oued Souss and the Oued Draa.
In the marine realm, shelf-margin parallel currents transported sediment to the south in the Tarfaya-Dakhla Basin. The development of the Canary Islands led to the development of a channel effect which further increased current velocities.
An interim eustatic sea-level highstand in the Late Miocene triggered shallow marine sedimentation on the inner shelf. Outcrops of the Miocene basin fill exist at the Sebkha Tah. Shelf carbonate mudstones of the Tah Fm. are overlain by marine sandstones of the Izic Fm. (N 27°43.456, W 12°54.151). In the Western Sahara 100 km south of Laâyoune (N 26°25.381, W 13°15.790) the Miocene succession is represented by massive fine-medium sandstone overlain by oncoidal rud- to floatstone.

4.6 High-resolution sequence stratigraphy

4.6.1 1D sequence stratigraphy

4.6.1.1 Tan Tan Transect

The Tan Tan transect is located in the northern part of the study area and covers the wells EA-1, PC-1, MO-5 and MO-7. In order to achieve the best possible biostratigraphic framework, cross-correlations from the surrounding wells CHBK-1, MO-1, MO-6 and HM-1 have been integrated. The corresponding seismic lines are 87-TA-15, 69-EM39 and 83MMO-15. The position of MO-7 is 0.8 km SW, MO-5 is located 8.75 km to the NE of line 83MMO-15 and 4.5 km NW of line 83MMO-10. Well PC-1 was drilled on an anticline further to the south of Tan Tan transect and has no seismic coverage. For this study, it has been projected to line 87-TA-01E and line 87-TA-1W2. Well EA-1 is located north of line 87-TA-15. Seismic coverage is provided by line 87-TA-17-2 where well tops could be traced via 87-TA-16. Fig. 63 shows the projected position of the wells on the seismic transects and Fig. 78 shows the well correlation of this transect.

EA-1 (El Amra-1)

The well EA-1 was drilled in 1961 by SOMIP in the proximal part of the TB close to the Anti-Atlas. It reached a depth of 2574 m below ground and covers the complete Mesozoic succession. Available information is sparse for this study. It comprises a lithostratigraphic chart compiled by ONHYM with 5 units (Precambrian basement, in literature also as Early Paleozoic, Triassic, Upper Jurassic, Lower Cretaceous and Upper Cretaceous.
Sequence stratigraphic well log interpretation is based on an R-log for the units Upper Jurassic, Lower Cretaceous and Upper Cretaceous.
The Triassic succession includes continental deposits with stacked alluvial fans, fluvial channels and alluvial plain sediments. Given the available data resolution a sequence stratigraphic interpretation was not reasonably possible.
The Upper Jurassic and the Lower Cretaceous succession is represented by alluvial deposits without any biostratigraphic information or lithostratigraphic subdivision. However, seismic interpretation, well pattern detection and sequence stratigraphic modelling in this study has allowed a more detailed subdivision to be performed. The Upper Jurassic contains deposits of Bathonian (Bat - Sequences: Bat 3/4), Callovian (Call - Call 4/5), Oxfordian to Kimmeridgian (Ox/Ki - Ox/Ki 4/5) and Tithonian (Ti -Ti 6). Lower Cretaceous (LC) contains Berriasian (Be - Be 4), Valanginian (Va - Va 6), Hauterivian (Ha - Ha 5), Barremian (Barr - Barr 3), Aptian (Ap - Ap 3/5/6), and Albian (Al - Al 4) deposits. The Upper Jurassic succession is represented by two Cenomanian sequences (Ce - Ce 2/3) and consists of shallow marine shales and carbonates with clastic intercalations. All sequences represent regional- relative sea-level highstands or phases of transgression. The well finishes in the sequence Ce 3 at top surface casing.

PC-1 (Puerto Cansado 1)

The well PC-1 was drilled in 1961/62 by SOMIP in a wide anticline close in the shallow offshore between the towns of Tan Tan and Tarfaya. It reached a depth of 4091 m below ground in Lower Jurassic sediments. The Jurassic is a more or less a marine succession with detailed biostratigraphic control.

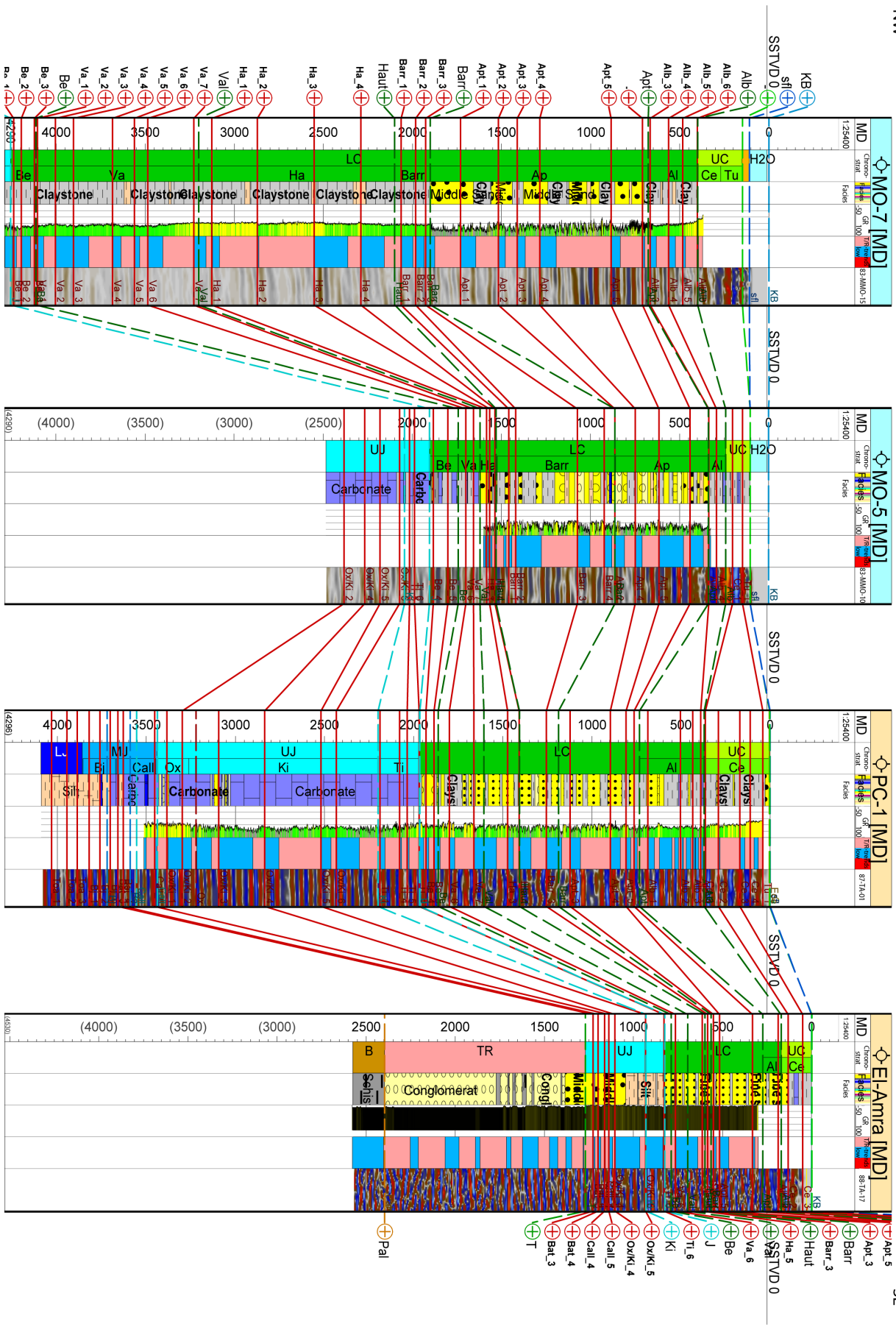

Fig. 78: 4th order sequence stratigraphic well correlation based on GR- and R- logs of the Tan Tan transect including the wells EA-1, PC-1, MO-5 and MO-7 (right to left) (WENKE et al. 2011).

The basal part is assigned to Toarcian (Toa) age based foraminifers (Pseudoclammina Liasica HOTTINGER, Choubert et al. 1966). Vail et al. (1977) and Beicip (1990) proposed that the Toarcian onlaps against the IDU, PRU in more proximal regions and is not drilled onshore.
Sequence stratigraphic log pattern detection on this well has been performed on a γ-ray log. The three basal sequences were assigned to the Lower Jurassic which correlates well with the seismic interpretation (Toa 1-3). The top Toa is placed at a depth of 3855 m. The Middle Jurassic of PC-1 contains seven sequences of Bj to Call age (Bj-3, Bat 1/2/6, Call 3/4), and includes a moderate relative sea-level rise and the transition from clastic to carbonate ramps. The relative sea-level rise continues throughout the Upper Jurassic. At least twelve Upper Jurassic sequences have been defined, of which ten fit with the 2D interpretation (Ox/Ki 1-6, Ti 1/4-6). Some fourth to fifth order sequences may not be recognizable in the Upper Jurassic succession because of the poor γ-ray log response in carbonate rocks.
The Lower Cretaceous in PC-1 is represented by a condensed section of mainly fine clastic sediments with coarse clastic intercalations and includes an upper deltaplain facies of the Lower Cretaceous Tan Tan Delta Complex. Initial Tan Tan delta sediments were deposited on the proximal Jurassic shelf area during the Late Berriasian. The final Tan Tan deposits were sedimented in the late Ap and are followed by marine fine clastics of the Al Aguidir Fm. Fifteen Lower Cretaceous sequences were interpreted by their γ-ray response character (Be 4/5, Va 6/7, Ha 3/4, Barr 3, Ap 3-6, Al 1-4).
The Upper Cretaceous at PC-1 contains five sequences of Cenomanian to Turonian age (Ce 1-4 and Tu 1) and consists of mainly marine fine clastic sediments. Coniacian (Co) to recent age was not drilled in PC-1.

MO-5 (Moroccan Offshore 5)

The well MO-5 was drilled in 1969 by Exxon Morocco close to the Jurassic shelf break and was completed at a depth of 2485 m below sea-level into Lower Oxfordian strata. Well report information is sparse but a detailed biostratigraphic chart for the Beerriasian to Hauterivian interval made by AMOCO (ONAREP, 1985) has been available for this study. 1D-sequence stratigraphic interpretation covers only the Barremian to Aptian succession where a γ-ray log has been available. Upper Jurassic, Berrisian to Haauterivian and Albian to seafloor (sf) sequences in the well correlation panel (Fig. 78) are taken from the 2D-interpretation.
The Upper Jurassic of MO-5 contains six sequences (Ox/Ki 2/4-6, Ti 5/6) of reefal carbonates (bryozoa, corals) with very few fine clastic intercalations that represent flooding surfaces.
Fifteen sequences were identified for the Lower Cretaceous Tan Tan Fm. After a thin basal mid-Be rriasian coarse clastic sequence (Be 4) LC sequences consist of mainly fine clastics (Be 5, Va 6/7, Ha 3) and show a large-scale coarsening upward trend to the Top Aptian (Ha 4, Ha 5, Barr-4, Apt 2/4-6) which is interpreted as the prograding Tan Tan Delta Complex. Albian to Upper Cretaceous marine fine clastics to carbonates are represented by four sequences (Al 3/4, Ce 1 and Tu 1). Coniacian to recent sediments were not drilled in MO-5.

MO-7 (Moroccan Offshore 7)

MO-7 was drilled in 1969/70 at the recent shelf break to a final depth of 4319 m below sea level. It reaches the Portlandian as indicated in the well report (Ti). A reliable stratigraphic subdivision is not possible. Based on seismic interpretation the drilled top of Jurassic may be resedimented Tithonian, residual parts of a former slope (Ti) or Middle Jurassic/ Bathonian (Ba) carbonate ramp deposits.
Sequence stratigraphic log pattern recognition is based on the γ-ray log. MO-7 shows the most complete Lower Cretaceous succession, which was drilled with a thickness of 3800 m. Lower Cretaceous sedimentation started after a major relative sea-level fall at the MDU which is presumed to have triggered the collapse of the existing Jurassic slope (Vail et al. 1977).
Carbonate dissolution by meteoric water may have triggered the collapse of the exposed Jurassic, carbonate shelf-break and slope. Slope tilting and growth faulting by salt withdrawal constitute an additional or alternative mechanism. Marine deposition of the early Berriasian shows a clear lowstand geometry. Middle to Upper Berriasian timelines onlap at a high angle against the collapsed Jurassic shelf in cratonward direction. In addition they show downlap against an unresolved basinal Jurassic succession in ocean-ward direction. Initial Lower Cretaceous

Fig. 79 (next page): 4th order sequence stratigraphic well correlation based on GR- and R- logs of the Cap Juby transect including the wells 1-2, PC-1, CJ-1 and MO-8 (right to left) (Wenke & Zühlke, 2011).

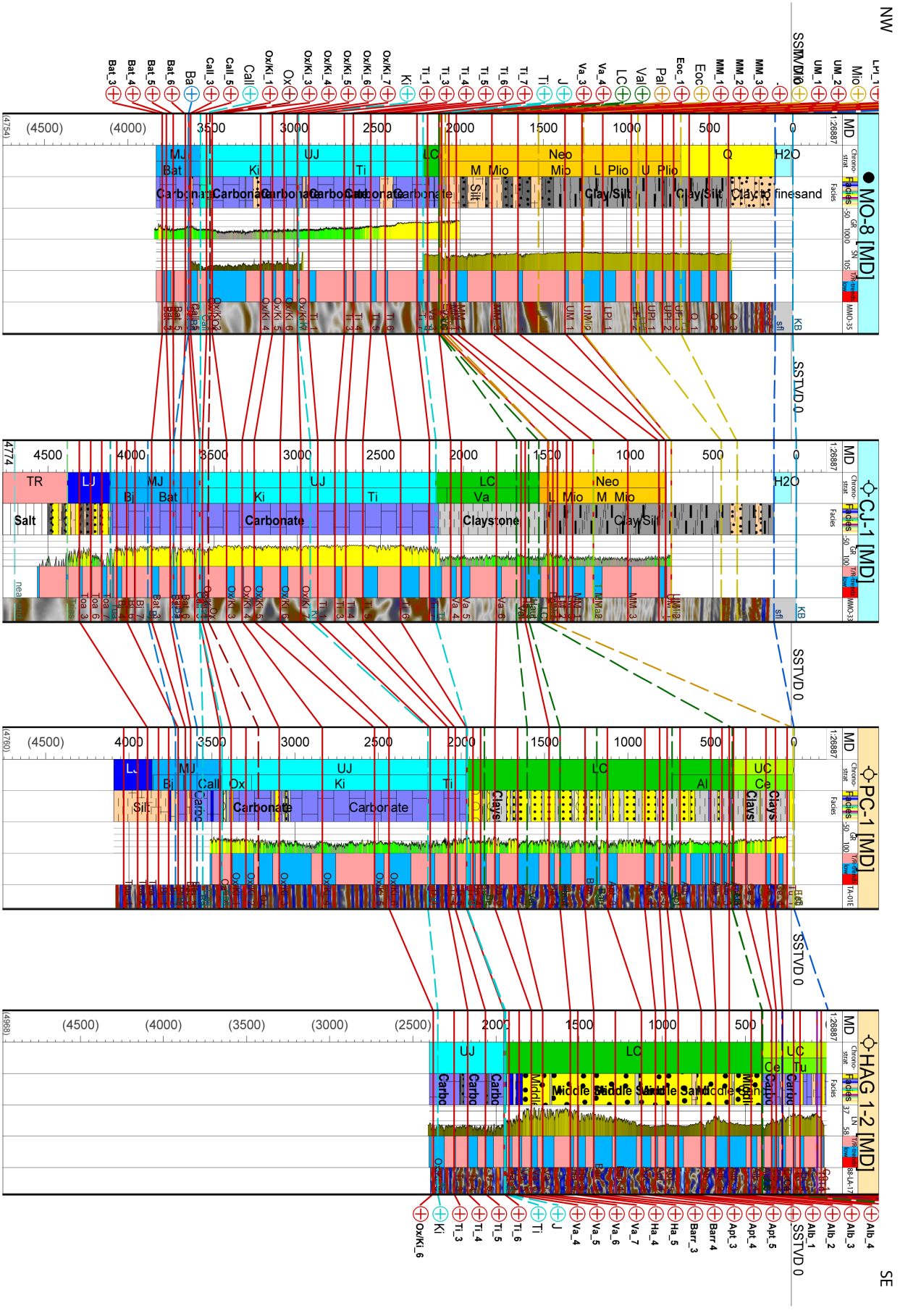
NW
SE
MO-8 [MD]
CJ-1 [MD]
PC-1 [MD]
HAG 1-2 [MD]
SSTVD 0
KB
MD
Chrono-strat
Facies
GR
SN
Carbonate
Claystone
Clay/Silt
Salt
Silt
finesand
H2O

progradation on top of the Jurassic shelf started in the Upper Beriasian (Be 4 and 5) with basal coarse clastics overlain by fine clastic deposits. Delta top sandstones developed on the shelf during Hauterivian (MO-5), the Berriasian, Valanginian, Hauterivian, and Lower Barremian succession in MO-7 consists of fine clastic sediments of a lower delta plain to upper slope environment. The Middle Barremian to Aptian succession contains an average of 60-65% sandstones. With the early Albian the Tan Tan Delta became largely inactive and shallow marine conditions prevailed. The Albian sequences consist of argillaceous to silty mudstones of an outer shelf region. The Lower Cretaceous of MO-7 has been subdivided into twenty-seven sequences.
The Upper Cretaceous succession of MO-7 has a thickness of 250 m and consists of three sequences (Ce 1, Tu 1/2). The uppermost 67 m below seafloor are of Paleocene to Eocene age.

4.6.1.2 Cap Juby transect

The Cap Juby transect is located in the central to southern part of the Tarfaya Basin, trends SE-NW and covers the wells HAG 1-2, PC-1, CJ-1 and MO-8. Biostratigraphic cross-correlation includes the wells MO-2 and TAR-1. The corresponding seismic lines are 88-LA-17, 87-TA-04 and 83-MMO-35/33. The position of MO-8 is close to line 83-MMO-35 and CJ-1 is located on line 83-MMO-33. For the position of PC-1 see Fig. 23. HAG-1-2 is located on line 88-LA-17.
Fig. 63 shows the wells projected to the seismic transect and Fig. 79 the well correlation of the transect.

HAG-1-2 (Hagounia 1-2)

The well HAG-1-2 was drilled 1962 by Union Oil Company of Spain and reached a final depth of 2401 m below surface. Bio- and lithostratigraphic data have been taken from the well report. At least five lithostratigraphic units have been described (Upper Jurassic, Late Cretaceous, Cenomanian, Turonian and Coniacian). Sequence stratigraphic interpretation is based on the R-log.
The Upper Jurassic consists of five sequences (Ox/Ki 6, Ti 3-6) of lagoonal and reefal shelf carbonates. A thin shallow marine to coastal succession in the Lower Cretaceous is overlain by a 1600 m thick Lower Cretaceous succession of continental sandstones. Sixteen sequence boundaries have been identified.
The Upper Cretaceous is represented by shallow marine carbonates with a thickness of 400 m containing seven sequences (Ce 2-4, Tu 2-4 and Co 1).

PC-1

cf 4.6.1.1

CJ-1 (Cap Juby 1)

Well CJ-1 was drilled in 1985 by Mobil and extensive data have been available for this study. It is located offshore at the Upper Jurassic shelf break with a final depth of 4798 m below sea-level and dropped off in the Triassic. Its structural position is on a tilted fault block which includes the MO-2 discovery. The CJ-1 well contains the most complete Jurassic succession of all wells in the Tarfaya Basin. The sequence stratigraphic interpretation is based on the γ-ray log.
Above Triassic sabkha to shallow marine sediments, the Toa is represented by three sequences of a prograding supratidal to outer neritic/open marine carbonate to clastic ramps (Toa 3/6/7). Internal outer shelf to open marine mudstones dominate the following eight sequences of Aalenian (Aa) to Bat time (Aa 1, Bj 4/6/7, Bat 3/4-6). The top of the Middle Jurassic ends with oolitic bar sediments (Call 3). After a short open marine episode in the Oxfordian (Ox/Ki 1), the Kimmeridgian to Tithonian is represented by mainly subtidal to intratidal platform carbonates with eleven sequences (Ox/Ki 3-7, Ti 1/3-7).
Compared to well MO-7, the Lower Cretaceous succession in CJ-1 shows a reduced thickness of 600 m. It contains six sequences of the Valanginian (Va 4-6) and Hauterivian (Ha 2/3). Above the IAU a thin layer of about 50 m represents Paleogene to Oligocene neritic fine clastics with high organic content. The Paleogene of well CJ-1 tends to be oil-prone but is immature.
The Neogene reaches a thickness of about 1400 m and eight sequences could be identified by log pattern recognition (Lower Miocene - LM 1-3, Mid-Miocene - MM 1-4, Upper Miocene - UM 1/2).
Above 700 m depth no log data have been available.

MO-8 (Moroccan Offshore 8)

Well MO-8 was drilled in 1972/1973 by Exxon with a total depth of 3830 m penetrating Bathonian carbonates. It is located on the same fault block than MO-2, MO-3 CJ-1 and TAR-1. Log pattern recogni-

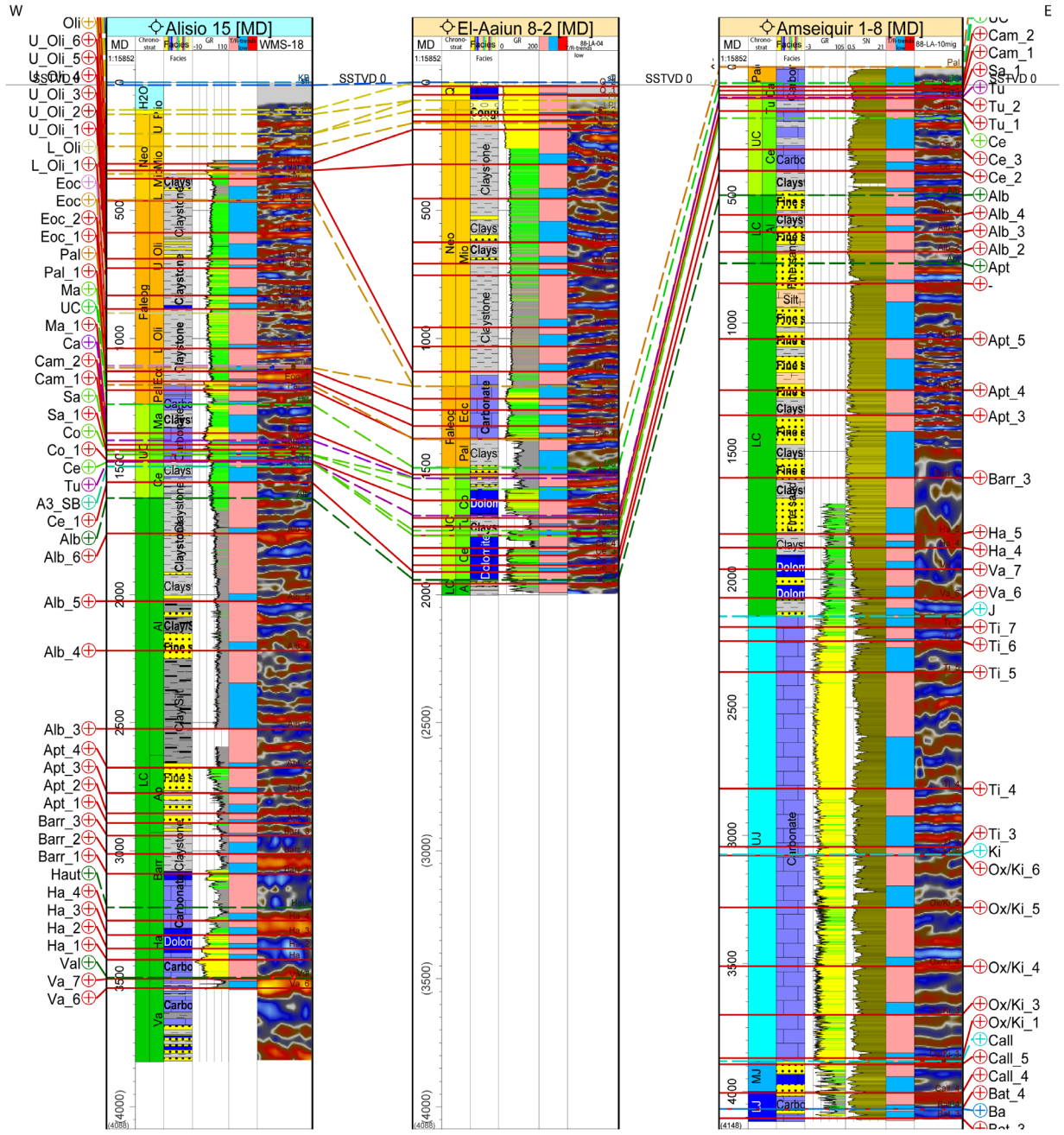

Fig. 80: 4th order sequence stratigraphic well correlation based on GR- and R- logs of the Cap Juby transect including the wells 15-A-1, LAY-8-2, and AMS-1-8 (right to left) (Wenke & Zühlke, 2011).

tion for the Jurassic und Lower Cretaceous succession is based on γ-ray response, for the Cenozoic on R-log response.

Open marine conditions (outer neritic to bathyal) prevail in the Middle Jurassic succession. It has been subdivided into six sequences (Bat 3-6, Call 3/5). A moderate but continuous relative sea-level fall led to shallow marine conditions on the Upper Jurassic carbonate platform. Twelve sequences have been recognized in the Oxfordian to Tithonian interval (Ox/Ki 3-7, Ti 1/3-6).

The Lower Cretaceous reaches a thickness of 100m and consists of upper bathyal carbonates. (Va 3/4). After 6 m of Upper Paleogene outer shelf to open marine silty limestones, fourteen sequences of fine clastics with sandy, salt water bearing sandstones of the Lower Miocene exist (MM 1-4, Um 1/2, LPl 1/2, UPl 1-3, Q 1-3).

4.6.1.3 Laâyoune transect

The Laâyoune transect containing the wells AMS-

1-8, LAY-8-2 and 15-A-1 is located in the southern part of the TB and trends NE to SW. Biostratigraphic cross-correlation includes the wells CORC-15-1 and Daoura 1. Fig. 81 shows the well correlation for the Laâyoune transect.

AMS-1-8 (Amseiquir 1-8)

Well AMS-1-8 was drilled in 1961/62 by Union Oil of Spain to a depth of 4117m below surface. It is located 25 km to the E of the city of Laâyoune. A lithostratigraphic well chart and a biostratigraphic report have been available for this study. Seven lithostratigraphic units are described (Lower - Middle Jurassic, Upper Jurassic, Lower Cretaceous, Cenomanian, Turonian, Senonian, Paleocene). Log pattern recognition is based on a γ-ray log for the Jurassic and lower Lower Cretaceous and on a R-log for the upper Lower Cretaceous to surface.
The 1900 m thick Jurassic succession in well AMS-1-8 is developed as shelf-interior stacked carbonate ramps and platforms. It is questionable whether the well reached Toa sediments or stuck in Aalenian (cf. 4.2.1 PC-1). The basal part of AMS-1-8 is attributed to the Bathonian to Callovian.
Four sequence boundaries have been recognized in the Middle Jurassic (Bat 3/4, Call 4/5) and ten in the Upper Jurassic (Ox/Ki 1/3-6, Ti 3-7).
The basal Lower Cretaceous consists of tidal flat to lagoonal carbonates and fine clastics followed by lagoonal to delta plain deposits of upper Valanginian and Barremian age. After a short shallow marine ingression the Aptian is dominated by fluvial sandstones.
A sea-level rise during the Aptian and lower Upper Cretaceous led to the deposition of mainly open marine outer carbonate platform sediments. Twelve sequence boundaries have been recognized in the Lower Cretaceous (Va 6/7, HA 4/5, Barr 3, Ap 3-6, Al 2-4) and eight in the Upper Cretaceous (Ce 2/3, Tu 1/2, Sa 1, Cam 1/2). The Turonian is overlain by Santonian and Campanian carbonates. The uppermost drilled sediments are of Paleogene age.

LAY-8-2 (Laâyoune / El Aiun 8-2)

LAY-8-2 was drilled in 1972 by ENPASA to a depth of 2003 m. It is located SW of Laâyoune close to the recent shoreline and was drilled through an incised valley with Cenozoic infill.
Available information about this well is ambiguous. The Base Cenozoic has been uniformly defined for a depth of 1393 m. In the well report, the following 610 m are attributed to the Lower Cretaceous. This definition is assumed in Franlab Beicip (1990). ONHYM studies suggest an Upper Cretaceous interval from 1393 to 1942 m underlain by Albian fine clastics. The last definition has been chosen in this study because seismic interpretation cannot provide more detailed information so far. Sequence boundaries are based on γ-ray logs. A single sequence boundary has been attributed to the Lower Cretaceous (AL 6) and nine for the marine to lagoonal Upper Cretaceous (Ce 1-5, Tu 1/2, Co 1 and Ma 1). A 320 m thick succession of Paleocene siltstones and Lower Eocene silicified silty chalks contains four sequences (Pal 1, Eoc 1-3).
Thirteen sequences were identified in the Neogene fine clastic incised channel fill (LM 1-3, MM 1-4, UM 1/2, Lower Pliocene - LPl 1/2, Q1/2).

15-A-1 (Alisio 15-1)

15-A-1 was drilled in 1970 by ENPASA offshore

Tab. 4: ProMAX® and SSIS® filtering and noise reduction parameters. Modified from Wenke et al. (2011).

Filter/Attribute	C83MMO lines	EM & WMS lines	Vibro-lines
Low-cut (8-16 Hz)	-	+	-
Vertical Scaling	$Z^n = 1.1$	-	-
Lateral scaling	Amp*c0 = 4,285.7	Amp*c0 =1,428.5	-
BG fast steering	Step out: 3/3 Filter step out 10/3	Step out: 3/3 Filter step out 10/3	Step out: 3/3 Filter step out 10/3
DSMF	Step out: 6	Step out: 6	Step out: 6
NSMF	-	+	-
Similarity	-	+	-
Average similarity	-	+	-
Conditional DSMF	-	Dipvar < c0 ? NSMF:DSMF	
FFT steering	+	+	+

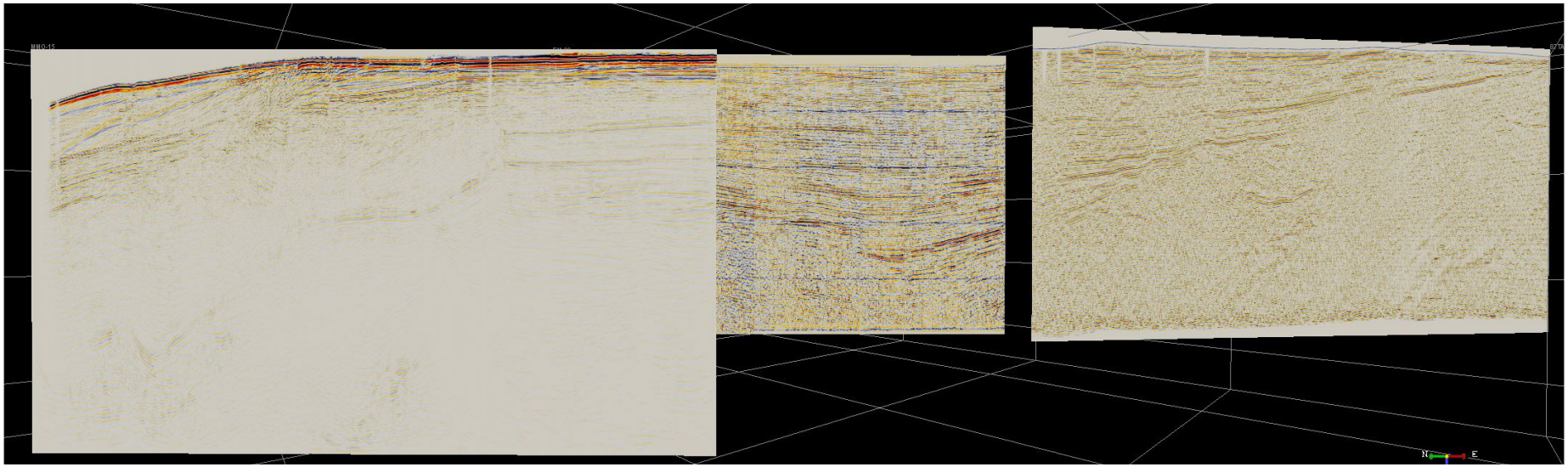

Fig. 81: Pre-recomputed seismic lines of the Tan Tan transect. From left to right: C83MMO-15, EM-39 & 87-TA-15. Note the pale amplitude strengths on line C83MM-MO-15, the paper folds in line EM-39 and the slightly noise reflector pattern of line 87-TA-15.

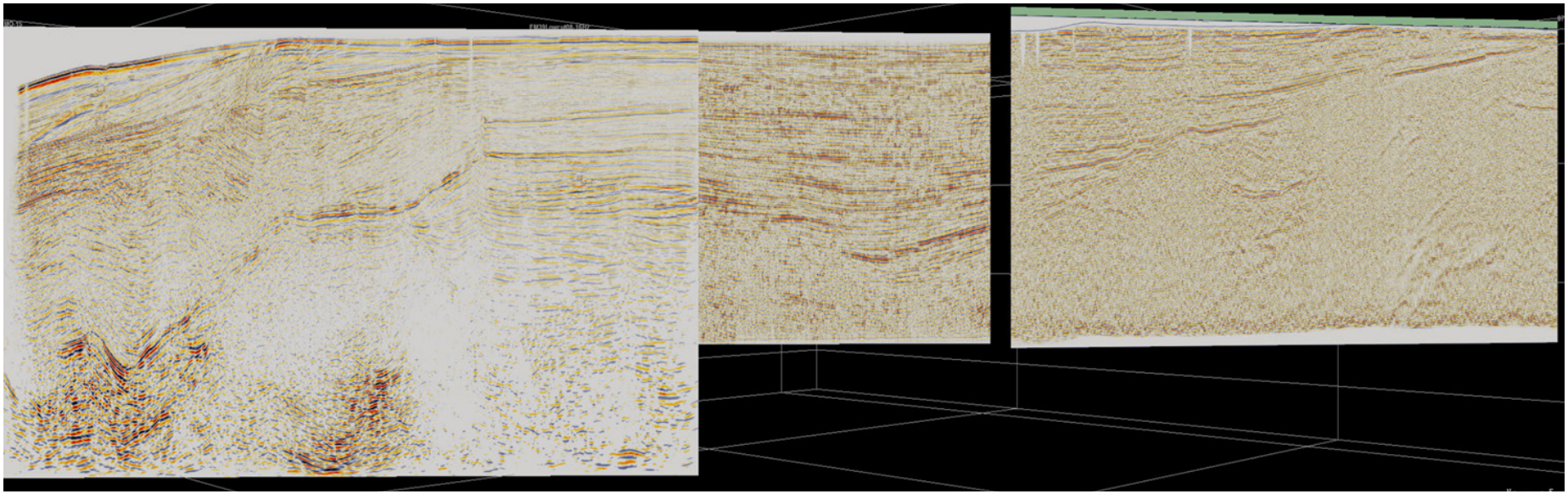

Fig. 82: Tan Tan transect after post-processing (low-cut on line EM.39, central), vertical (Line C83MMO-15, left) and lateral scaling.

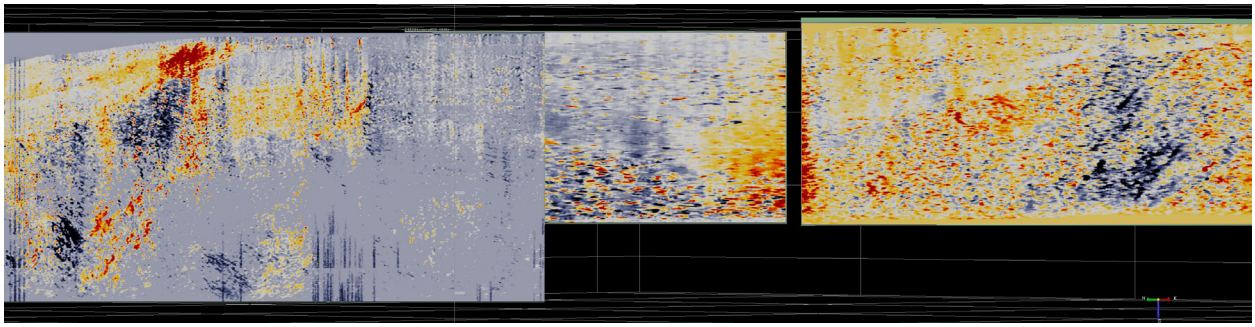

Fig. 83: BG fast steering analysis of the seismic lines of the Tan Tan transect. Red shows positive values, blue negative. The steering results were combined with a DSMF to equalize reflector dip and amplitude strength.

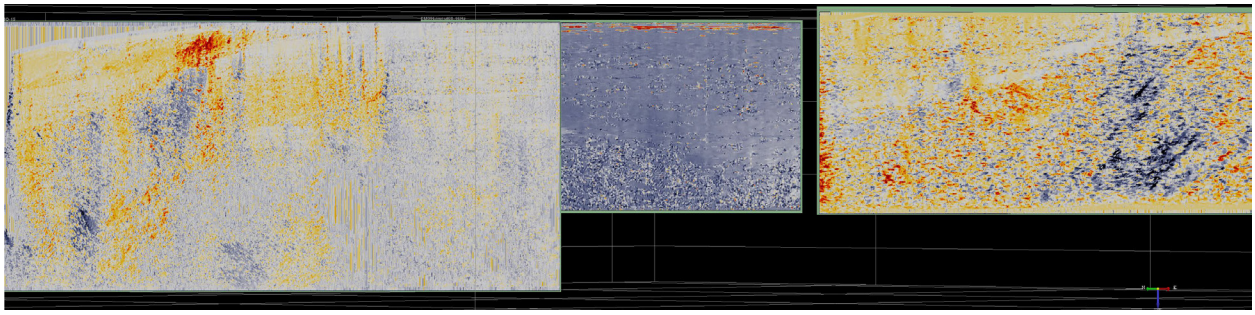

Fig. 84: FFT analysis results of the seismic lines of the Tan Tan transect, color code as above.

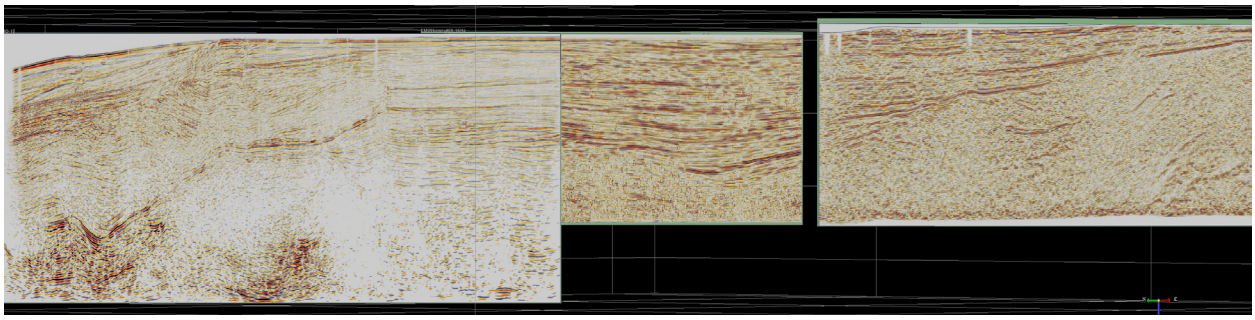

Fig. 85: Lines C83MMO-15 (left), EM-39 (center) and 87-TA-15 (right) after post-processing, scaling and filtering. High resolution sequence stratigraphy was performed based on the seismic transects prepared after this method.

Lemsid to a depth of 3824 m below sea-level and is located south of the Moroccan Atlantic Salt Province. The stratigraphic record for this well is considerably large. Unfortunately, seismic coverage in this study in insufficient.

The sequence stratigraphic interpretation is based on γ-ray response.

In the Lower Cretaceous, a more or less complete succession was drilled from the Valanginian to Albian, starting with basal Valanginian sandstones, followed by open marine carbonates of Hauterivian and early Barremian times. The Upper Barremian to Lower Albian contains more sandstones. They are interpreted as the marginal facies of the Lower Cretaceous Laâyoune Delta Complex. Sand content decreases towards the Al/Ce boundary. At least 17 sequence boundaries have been recognized in the Lower Cretaceous (Va 6/7, Ha 1-4, Barr 1-3, Ap 1-4 and Al 3-6). The Upper Cretaceous of 15-A-1 contains the most complete succession of all wells of the study area. Seven sequences have been recognized in the Upper Cretaceous (Ce 1, Tu 1, Co 1, Sa 1, Campanian - Ca 1/2, Ma 1). They show open marine fine clastic and carbonate deposits.

The 800 m thick Eocene and Oligocene (Oli) succession includes marine fine clastics with carbonate intercalations. Ten sequences have been recognized (Pal 1, Eoc 1/2, Lower Oligocene - LOli 1, Upper Oligocene - UOli 1-6). The Miocene contains 3 sequences (LM 1, UM 1/2).

4.6.2 2D-sequence stratigraphy

4.6.2.1 Post-processing, scaling and filtering

Auto-detection of reflector traces requires a largely

Tab. 5: 3rd order sequences of the Tarfaya-Laâyoune basin fill.

Q: Quarternary:	Geometry: onlap against Pliocene, erosional Deposition: shelf (Hamada), recent shelf margin, slope, basin
PL: Pliocene:	Geometry: toplap against Q, progradational Deposition: shelf, slope & basin,
M3: Upper Miocene	Geometry: in slope areas toplap against PL, onlap against M2, retrogradational Deposition: outer shelf, slope, basin
M2: Mid Miocene	Geometry: toplap against Q, downlap in basin, pivot: retro- to progradational Geometry: shelf, slope, basin (MTC)
M1: Lower Miocene	Geometry: onlap against PE, retrogradational Deposition: slope and basin (MTC)
OL: Oligocene	Geometry: onlap against PE, intra-Oligocene PAU, retrogradational Deposition: lower slope and basin (MTC)
PE: Paleocene to Eocene	Geometry: onlap against IAU, progradational Deposition: shelf (Laâyoune Basin), slope, basin
UC: Upper Cretaceous	Geometry: low-angle toplap against Q, cycle: retro-, aggra-, progradation Deposition: Shelf, slope (eroded) and basin (eroded)
LC4: Albian to L. Cenoman.	Geometry: coastal onlap, basinal downlap, mainly retrogradational Deposition: Shelf, slope, basin, partially eroded at slope and basin, retrograd.
LC3: Aptian	Geometry: coastal onlap, basinal downlap (partially eroded), retrogradational, PSU Deposition: shelf, slope and in basin (partially eroded)
LC2: Hauterive to Barremian	Geometry: clinoforms in outer shelf, MTC, coastal onlap, progradational Deposition: shelf slope and basin (partially eroded)
LC1: Berriasian to Valanginian	Geometry: basal part: marine onlap against UJ, downlap against UJ, concordant on shelf, retrogradational Deposition: shelf, mainly slope, basin
UJ2: Tithonian	Geometry: carbonate platform coastal onlap against UJ1(very proximal), MDU, rimmed shelf edge, aggradational to progradational Deposition: shelf, basin, (slope not preserved)
UJ1: Oxfordian to Kimmeridgian	Geometry: coastal onlap against TR, truncated MDU, retro- to aggradational Deposition: shelf, basin, (slope not preserved)
MJ3: Callovian	Geometry: coastal onlap against TR, downlap, retrogradational Deposition: shelf, slope, basin, pro- to retrogradational
MJ2: Bathonian	Geometry: coastal onlap against TR, progradational Deposition: lower inner to outer shelf, slope, basin
MJ1: Aalenian to Bajocian	Geometry: clinoforms, coastal onlap against TR, progradational Deposition: lower inner to outer shelf, slope, basin
LJ: Sinemurian to Toarcian	Geometry: coastal onlap, clinoforms, progradational Deposition: Central to outer shelf, slope, basin, IDU at base
TR: Permian to Hettangian	Geometry: onlap against structural highs, onlap on normal faults, internal PRU Deposition: fills of shelf halfgrabens, on continental crust in the basin

uniform seismic data set in terms of bandwidth, reflector amplitude, and noise reduction. The Tarfaya-Laâyoune Basins seismic transects represent composites out of five seismic surveys: i) vibro-lines of the CGG Tarfaya survey, inner shelf, acquired in 1987 (Line 87-TA-15, Tan Tan transect; Line 87-TA-04, Cap Juby transect); ii) vibro-lines of the CGG Laâyoune survey, inner shelf, acquired in 1988 (Line 88-LA-17, Cap Juby transect; Line 88-LA-03, Laâyoune transect) iii) marine seismic line, inner to outer shelf, acquired in 1969 (Line EM-39, Tan Tan transect), iv) marine seismic lines, outer shelf to middle slope, acquired in 1983 (Line C83MMO-15, Tan Tan transect, Line C83MMO-35, Cap Juby transect) and v) marine seismic line, outer shelf to basin, acquired in 1977 (Line WMS-5, Laâyoune transect). All lines are not directly connected.

Several post-processing and filtering steps have

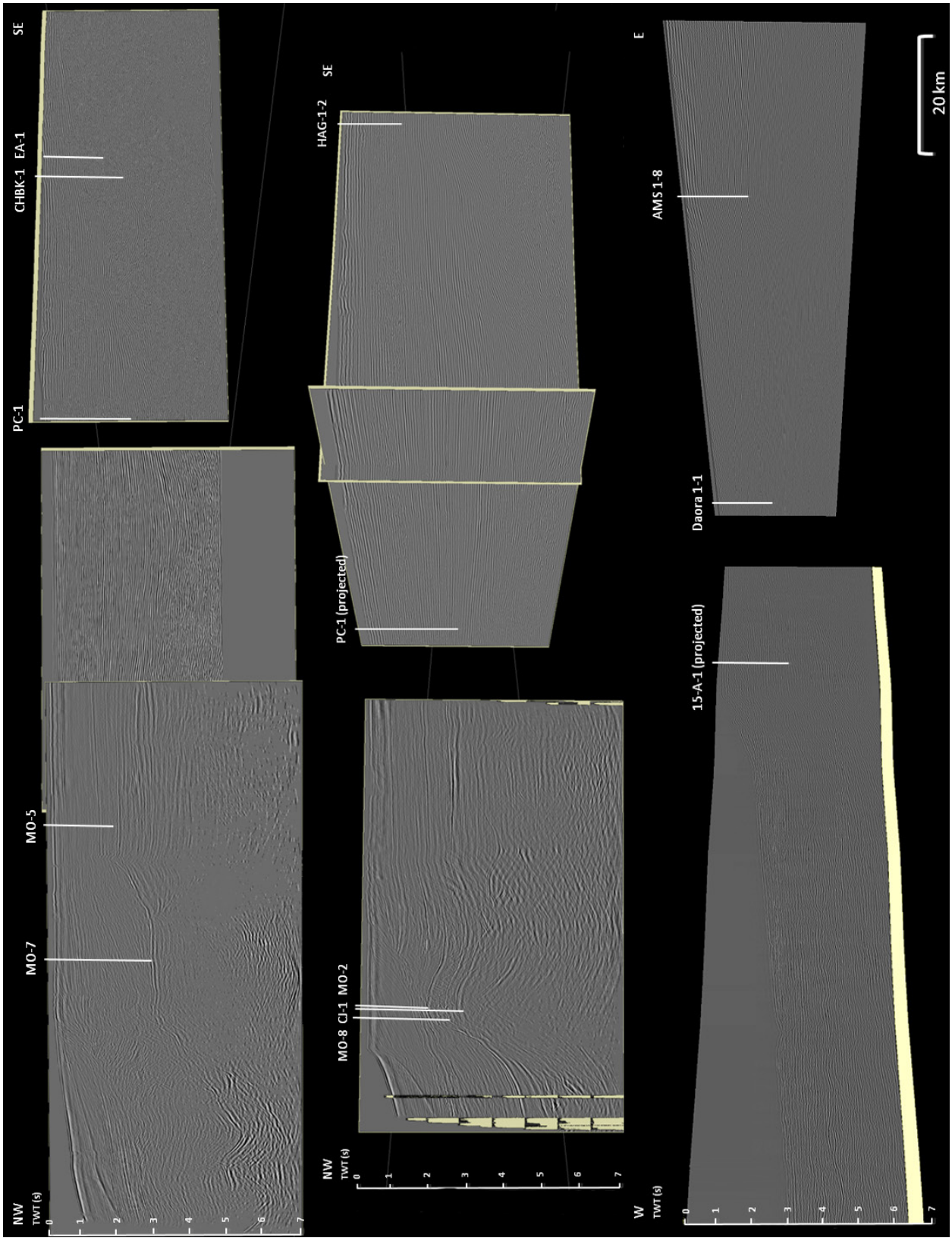

Fig. 86: The Tan Tan (top), the Cap Juby (center) and Laâyoune transect (bottom) after post-processing, scaling and filtering without interpretation.

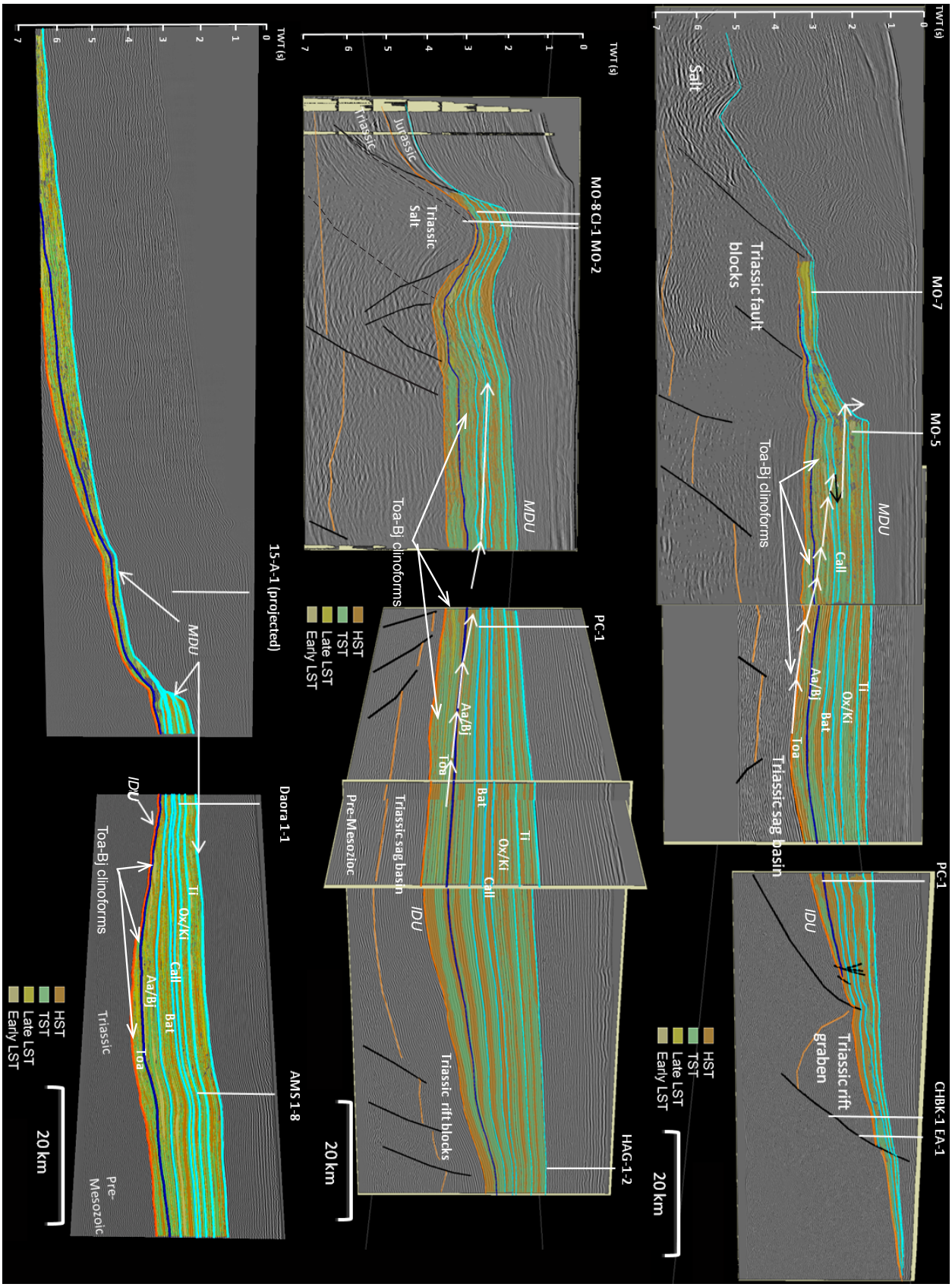

Fig. 87: SSIS ® interpretation of the Jurassic early drift basin fill. From top to bottom: Tan Tan (top), Cap Juby (center) and Laâyoune (bottom) transect. Prograding shelf-break trajectories are colored white, retrograding black. Systems tracts as illustrated (Wenke & Zühlke, 2011).

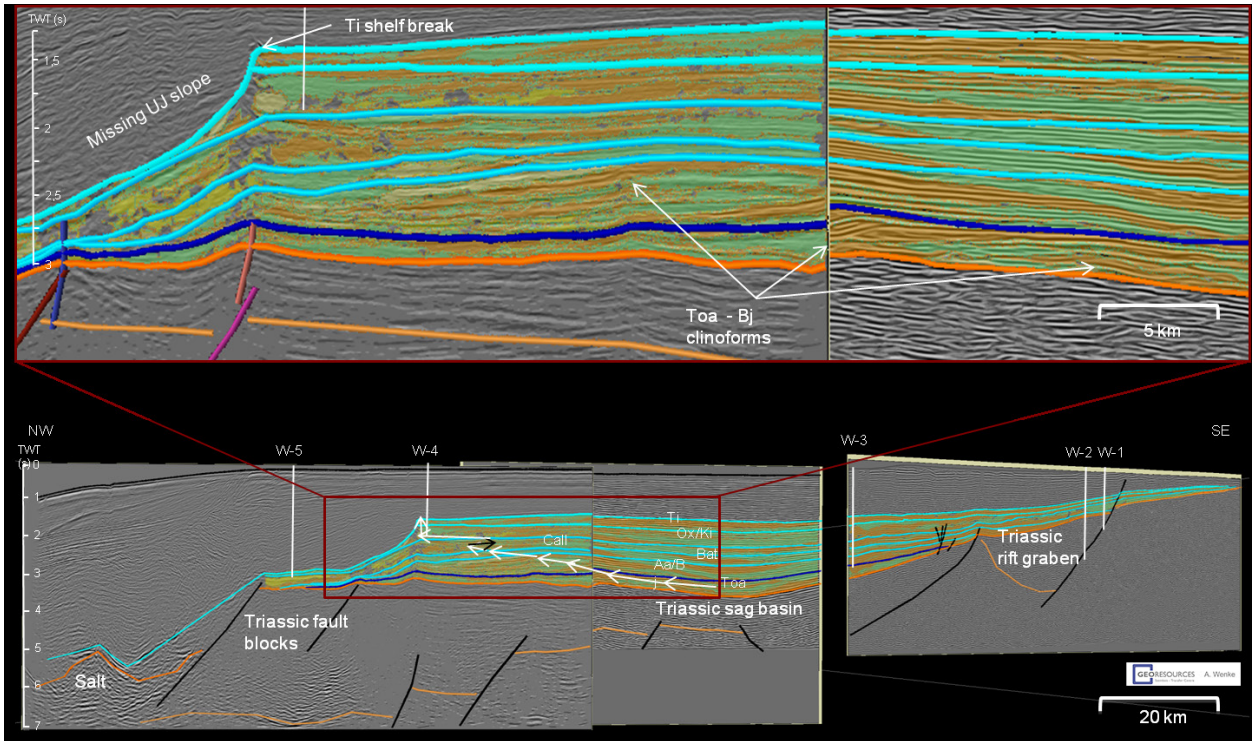

Fig. 88: SSIS® interpretation of the Jurassic succession of the Tan Tan transect (bottom) and zoomed outer shelf region. The clinoforms of the prograding Toarcian to Bajocian ramp are well to identify (Wenke et al. 2010 b).

been tested, the final workflow includes i) low frequency cuts, ii) vertical scaling, iii) lateral scaling, iv) noise filtering. The used post-processing, scaling and filtering parameters are summarized in Tab. 4, the results are exemplarily presented for the Tan Tan transect. Figure 76 shows the Tan Tan transect seismic data before post-processing, scaling and filtering.

A cut of the low frequency bandwidth (8-16 Hz) has been performed on the EM 39 and WMS-5 lines by using a Halliburton Landmark ProMAX® software to pale out damages from data storage (paper folds, Fig. 76). All further scaling and filtering steps have been performed in OpendTect.

A vertical scaling was necessary for line C83M-MO-15 as only the Neogene reflectors had a clear response. A factor of Zn=1.1 was appropriate to strengthen the amplitude gradually in depth.

Lateral scaling was necessary to adjust the different bandwidth between the surveys. The vibro-lines with the clearest response and highest bandwidth (+/-17,000) were chosen as standard, the low bandwidth of EM (+/-12) and MMO lines (+/-4) were broadened (Tab. 4).

The reduced noise and amplitude variations have been filtered by using diverse noise reduction tools available in OpendTect.

A BG (British Gas) steering attribute was applied first as a quick algorithm to analyze the vertical and lateral gradient of the amplitude data. The result of the fast steering analysis is illustrated in Fig. 78. The BG fast steering analysis was combined with a dip steered median filter (DSMF) to equalize amplitude strength and flatten amplitude dip variations (noise reduction). As a consequence of data quality a few interim stages have been applied. A conditional DSMF has been used by integrating the amplitude and waveform similarity before fast steering. In a further step the DSMF was combined with a non-steered median filter (NSMF). The use of the DSMF, the NSMF respectively, then depends on the coherency variations (dip variance).

Finally, a fast Fourier-transformation (FFT) algorithm has been applied to eliminate any residual noise on the seismic lines. The residual noise analysis is given in Fig. 79. The final post-processed, scaled and filtered Tan Tan seismic transect is given in Fig. 80.

4.6.2.2 3rd order sequence stratigraphy

The presented 3rd order sequence stratigraphy developed in this study is in agreement with the studies of Mitchum et al. (1977) and Rad et al. (1982). The results were first presented in Wenke et al. (2009) and Wenke et al. (2010a, b). Indicative reflector

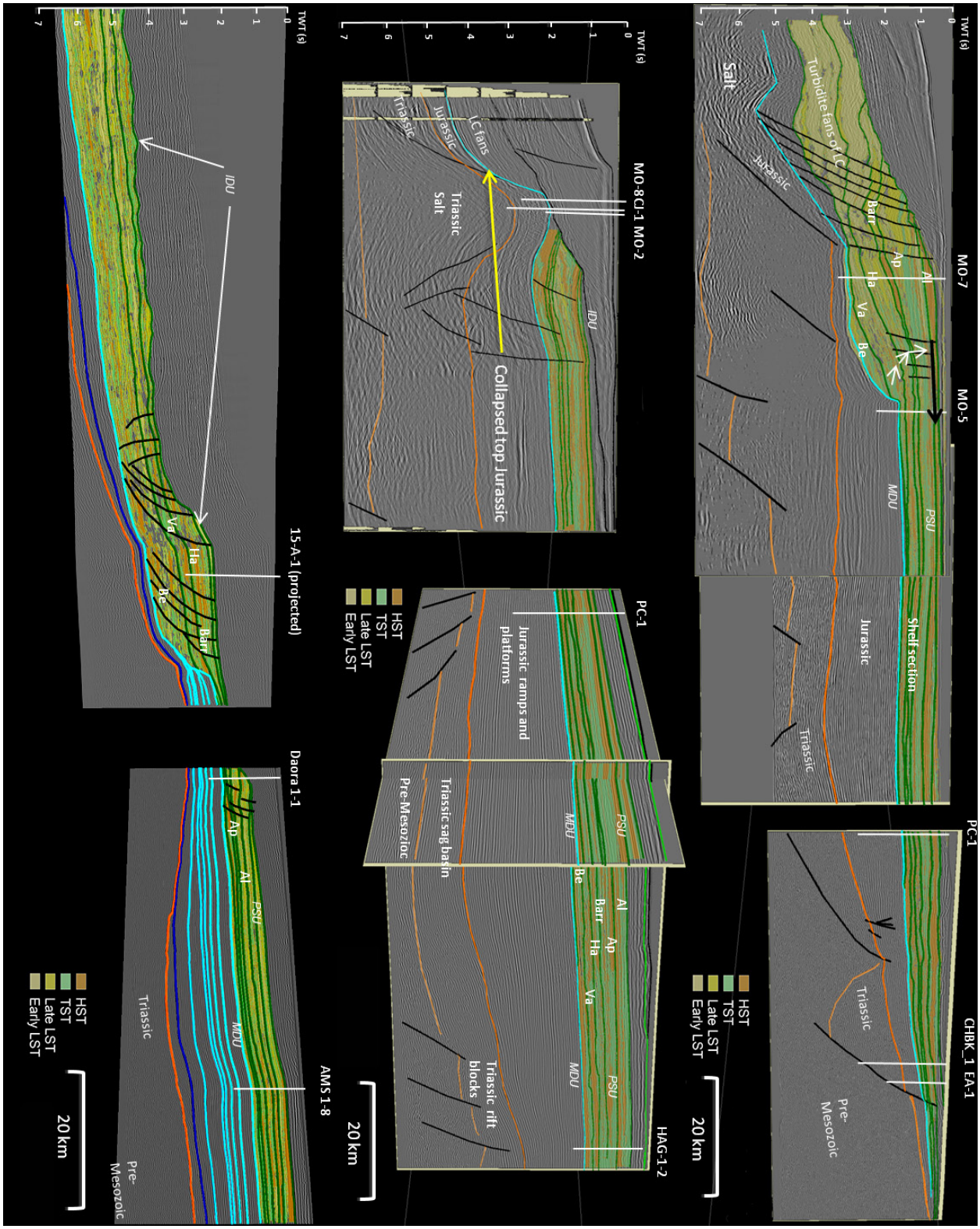

Fig.89 a-c: SSIS® interpretation of the Lower Cretaceous mature drift basin fill. From top to bottom: Tan Tan, Cap Juby and Laâyoune transect. A marine channel has cut the entire Cretaceous shelf and slope down to top Jurassic on the Cap Juby transect (center) (Wenke & Zühlke, 2011).

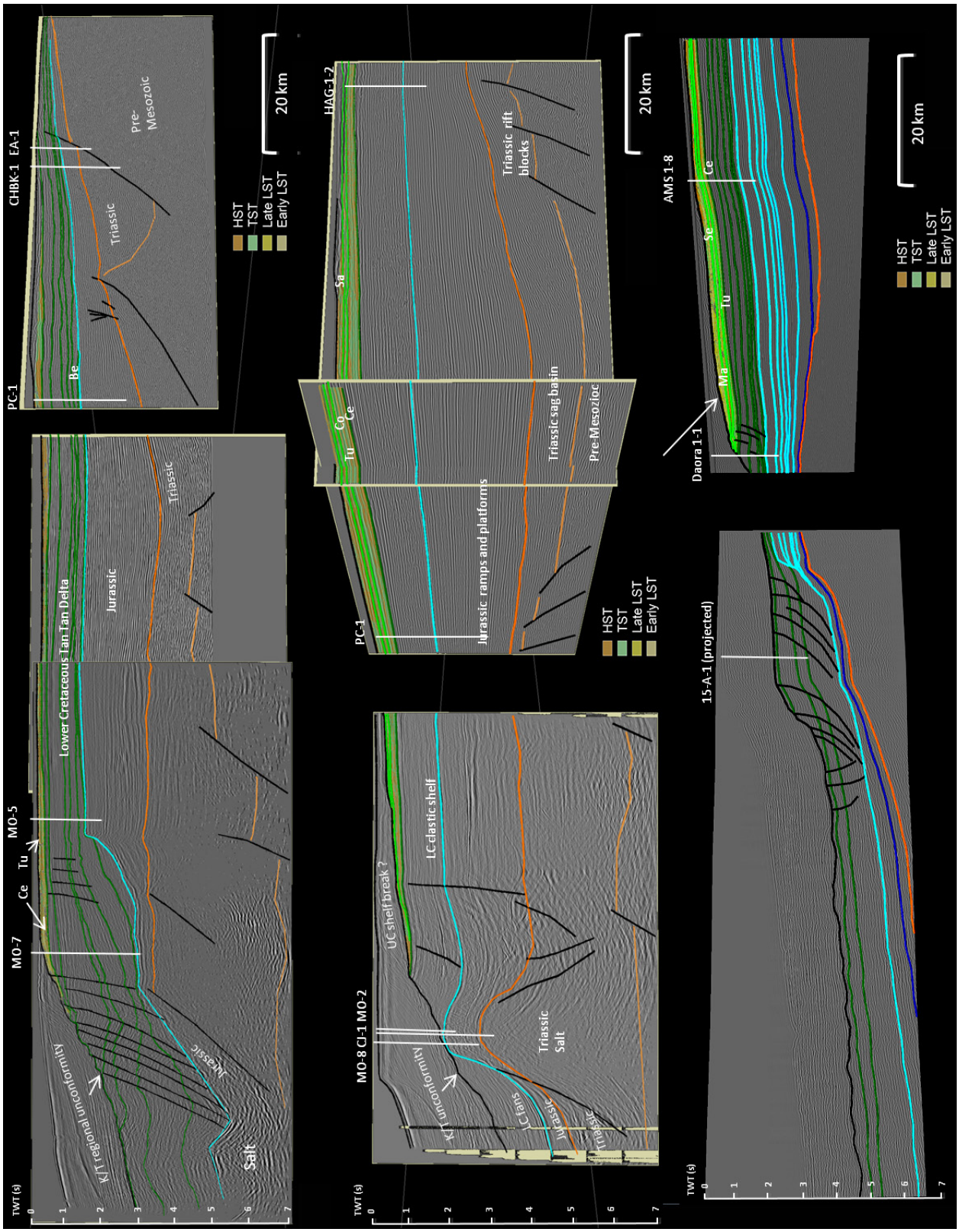

Fig.90 a-c: SSIS® interpretation of the Late Cretaceous mature drift basin fill. From top to bottom: Tan Tan, Cap Juby and Laâyoune transect. A marine channel has cut the entire Cretaceous shelf and slope down to top Jurassic on the Cap Juby transect (center) (Wenke & Zühlke, 2011).

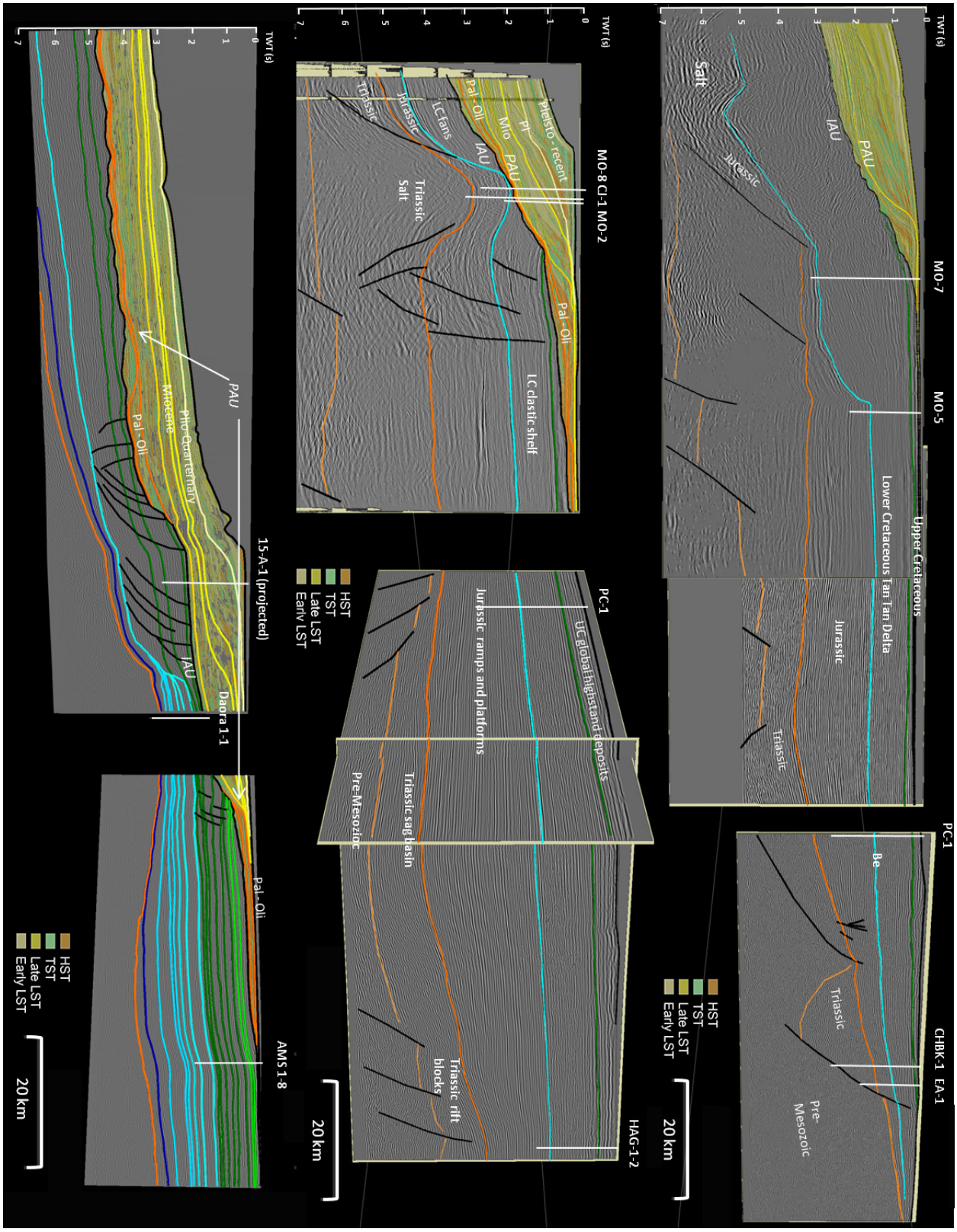

Fig. 91 (above): SSIS® interpretation of the Cenozoic succession. From top to bottom: Tan Tan, Cap Juby and Laâyoune transect. The maximum thickness of the Cenozoic was recognized in the TAR-1 well (Wenke & Zühlke, 2011).

Fig. 92 & 93 (next page): Full SSIS® interpretation of the Tan Tan (top) and Cap Juby (bottom) transects with estimated deposition of OAE. The high prolific source rocks of the Late Cretaceous OAE 1-3 events did not reach high subsidence. Jurassic Turnover, Faraoni event and PETM are distributed in slope and basin areas (Wenke & Zühlke, 2011).

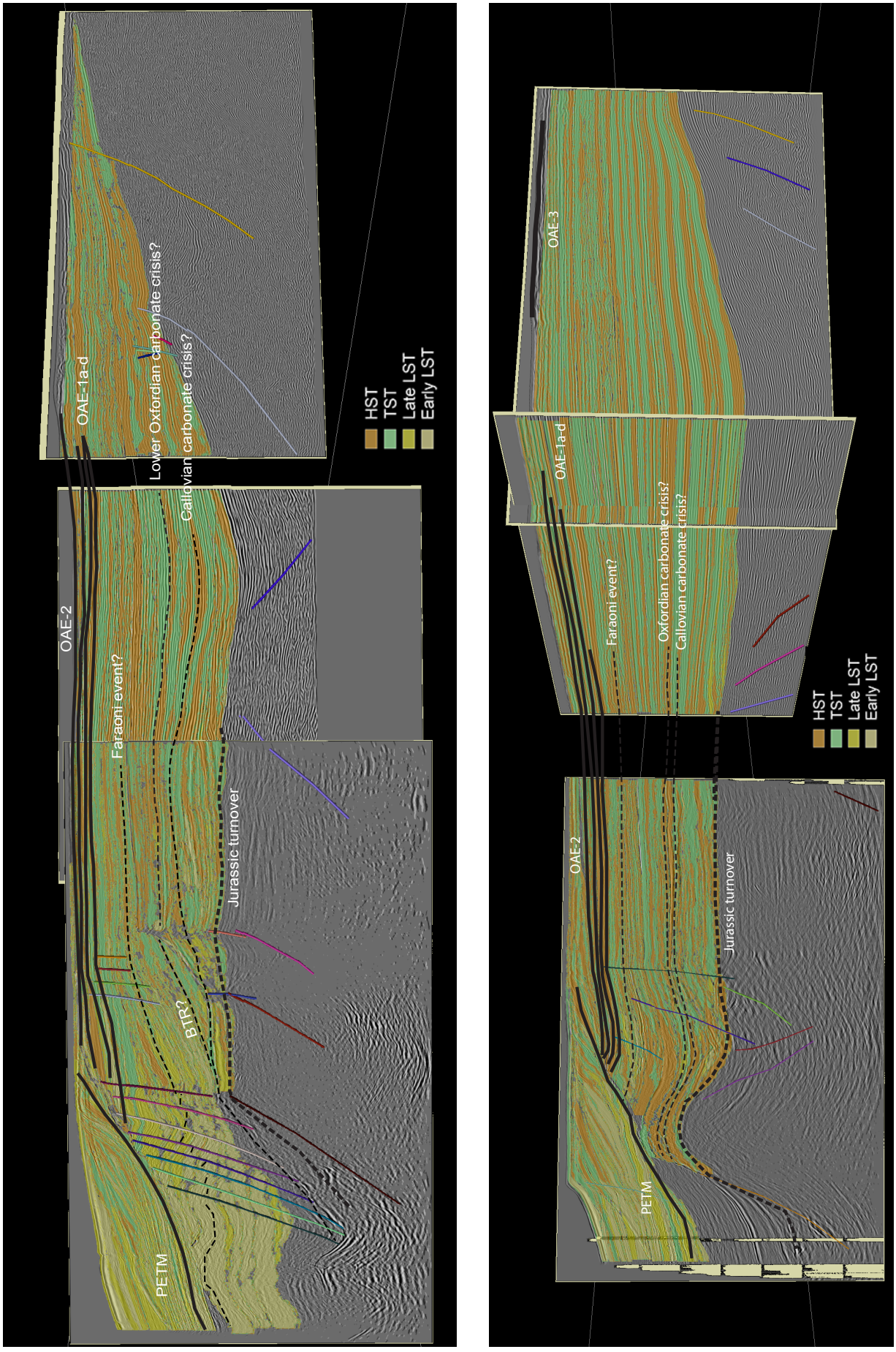
OAE-1a-d
Lower Oxfordian carbonate crisis?
Callovian carbonate crisis?
HST
TST
Late LST
Early LST
OAE-2
Faraoni event?
Jurassic turnover
BTR?
PETM
OAE-3
OAE-1a-d
Faraoni event?
Oxfordian carbonate crisis?
Callovian carbonate crisis?
HST
TST
Late LST
Early LST
OAE-2
Jurassic turnover
PETM


TM
PETM
Jurassic turnover
Lower Oxfordian carbonate crisis ?
Callovian carbonate crisis ?
OAE 2/3
OAE 1a-d

terminations and internal geometries of individual sequences in the Tarfaya Basin are given in Tab. 5. The interpretation following the 3rd order sequence stratigraphic pattern is shown in Fig. 63.

4.6.2.3 High-resolution sequence stratigraphy

Fig. 86 shows the uninterpreted seismic composite sections of the Tan Tan, the Cap Juby and the Laâyoune transects, Fig. 87 the SSIS® interpretation of the Jurassic early drift succession of the three transects and Fig. 88 shows a zoomed outer shelf Jurassic section of the Tan Tan transect.

The general development of the post rift and initial drift depositional pattern starts with coastal onlap of Pliensbachian/Toarcian strata against the Triassic in the central shelf area west of the Chebeika Graben. The onlap is just recognizable on the Tan Tan transect as proximal seismic lines were not available for the Cap Juby and Laâyoune transects. Toarcian reflectors show prograding clinoforms in basinward direction. In the Tan Tan area, the clinoforms are well developed between the central shelf area (approx. 20 km NW of PC-1) and the Jurassic shelf break in the MO-5 area (Fig 87 top).

On the central Cap Juby transect, the proximal onset of the clinoforms is located between the center of the Laâyoune depression and the present day inner to central shelf area (Fig. 87 center). The Bajocian clinoforms show downlap approx. 20 km SE landward of the Cap Juby oil field (MO-2, CJ-1).

To the south, the proximal onset of ramp progradation is located in the area of well AMS 1-8 while the clinoforms terminate at the western flank of the Laâyoune depression. The most distal clinoforms are located in the area of well Daora 1-1 (Fig. 87 bottom).

Seven sequences have been interpreted in the Toarcian (Toa) interval, two of which (Toa 3/4) extend basinward to below the recent shelf break. The progradation of the Toarcian ramp into a restricted basin during the time of a global anoxic event, the Jurassic Turnover (cf. chapters 2.5 & 4.3), may overprint a high amount of primary (bio-)production by sedimentary dilution effects in this part of the basin.

Fig. 94 & 95 (previous page): Full SSIS® interpretation of the proximal (top) and distal (bottom) Laâyoune transect with estimated deposition of Oceanic Anoxic Events (OAE). The high prolific source rocks of the Late Cretaceous OAE 1-3 events did not reach high subsidence. Jurassic Turnover, Faraoni event and PETM are distributed in slope and basin areas (Wenke & Zühlke, 2011).

Aalenian/Bajocian (Aa/Bj) reflector geometries indicate westward progradation of the shelf break of more than 20 km compared to its Toarcian position, in the Cap Juby area up to 35 km. Coastal onlap occurs against the Triassic rift half-graben in the direction of the continent. At least six Aa/Bj sequences have been identified.

The Bathonian sequences, of which four have been identified, show decreasing progradation widths. A small retrogradational event was recognized in the sequence Bat 4.

The Callovian (Ca) sequences Ca 1–5 show predominant shelf aggradation with coastal onlap.

Oxfordian/Kimmeridgian (Ox/Ki) reflectors do not show any specific large-scale progradation geometries. Selected features include i) an upward increasing thickness in the central shelf area, ii) retrogradation in the Kimmeridgian combined with, iii) strong eastward shift of coastal onlap. Because of the limited well (log response in aggrading carbonate systems) and seismic data quality available, only nine sequences could be identified for the Oxfordian/Kimmeridgian.

During the Tithonian the Late Jurassic shelf break features progradation once again (Ti 1–4). The shelf break and slope experienced a large-scale collapse in the Late Tithonian to Early Berriasian. The Top Jurassic reflector represents the MDU.

In total, 35 Jurassic sequences have been identified.

For the slope and basin area, a sequence stratigraphic interpretation was not applicable as a consequence of lacking geometries and well control. However, the whole Jurassic early drift succession is exposed in isolated outcrops on Fuerteventura (cf. chapter 2.5).

In the Tan Tan area, 2/3 of the Jurassic shelf is located offshore and in the Cap Juby area 1/3. In the Laâyoune area, more than 90% of the shelf is located onshore.

After a major base-level fall at the end of the Jurassic, the Early Cretaceous Berriasian to Aptian is dominated by the Tan Tan Delta and the Laâyoune Delta respectively which started to develop in front of the post-collapse slope of the Jurassic continental shelf. The Tan Tan Fm is best represented in the central to northern Tarfaya Basin (Tan Tan transect). The Berriasian delta covers seven reflectors at maximum which show onlap against the Jurassic slope and downlap towards the basin. Berriasian shelf reflector geometries show low-angle progradation on the middle to outer shelf. The Berriasian includes five sequences in the Tan Tan region.

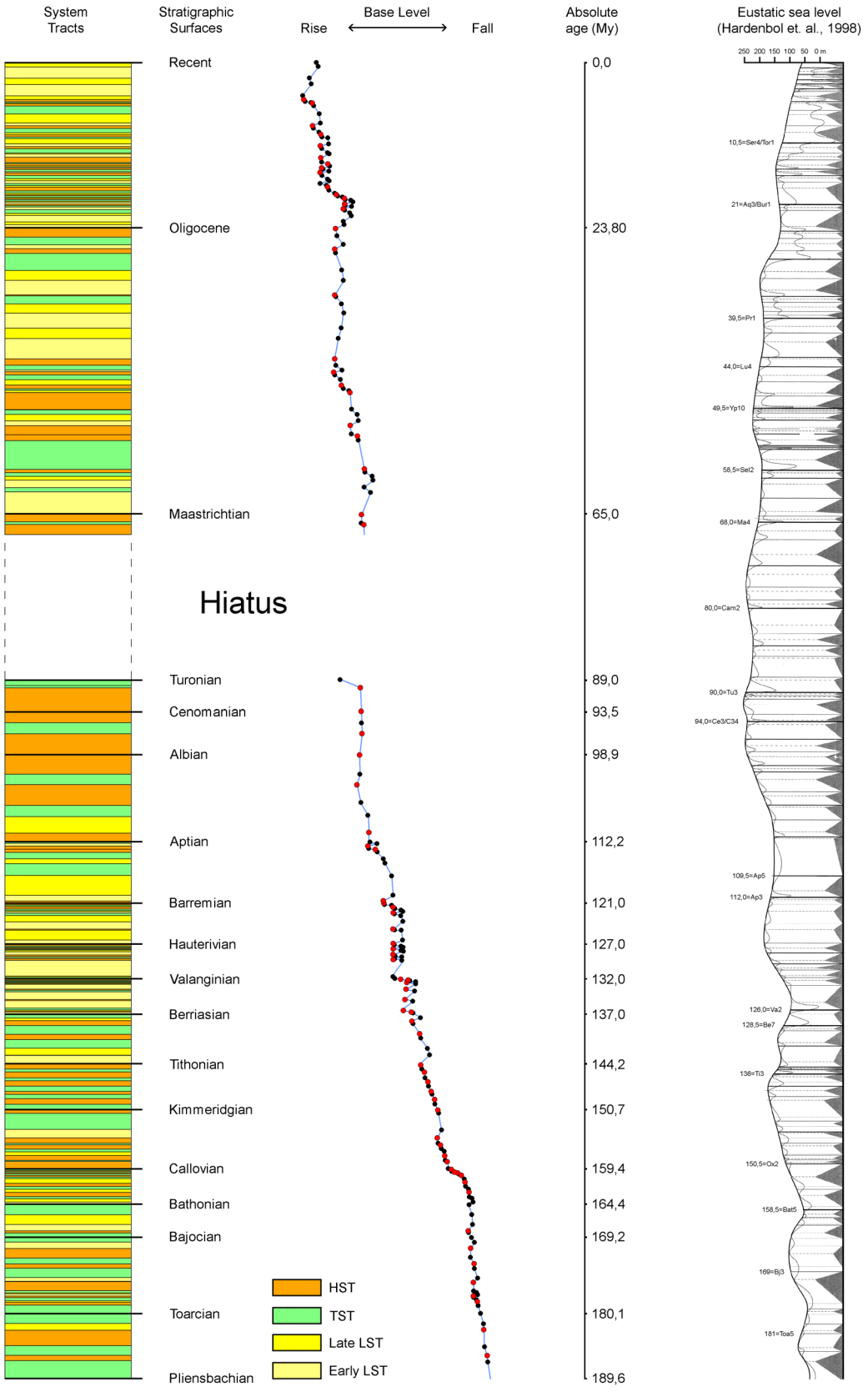

Fig. 96: Tarfaya base level curve for the northern Tarfaya Basin generated during high resolution sequence stratigraphic interpretation of the Tan Tan transect vs. eustatic sea level curve (Hardenbol, 1998). From Wenke et al. (2011).

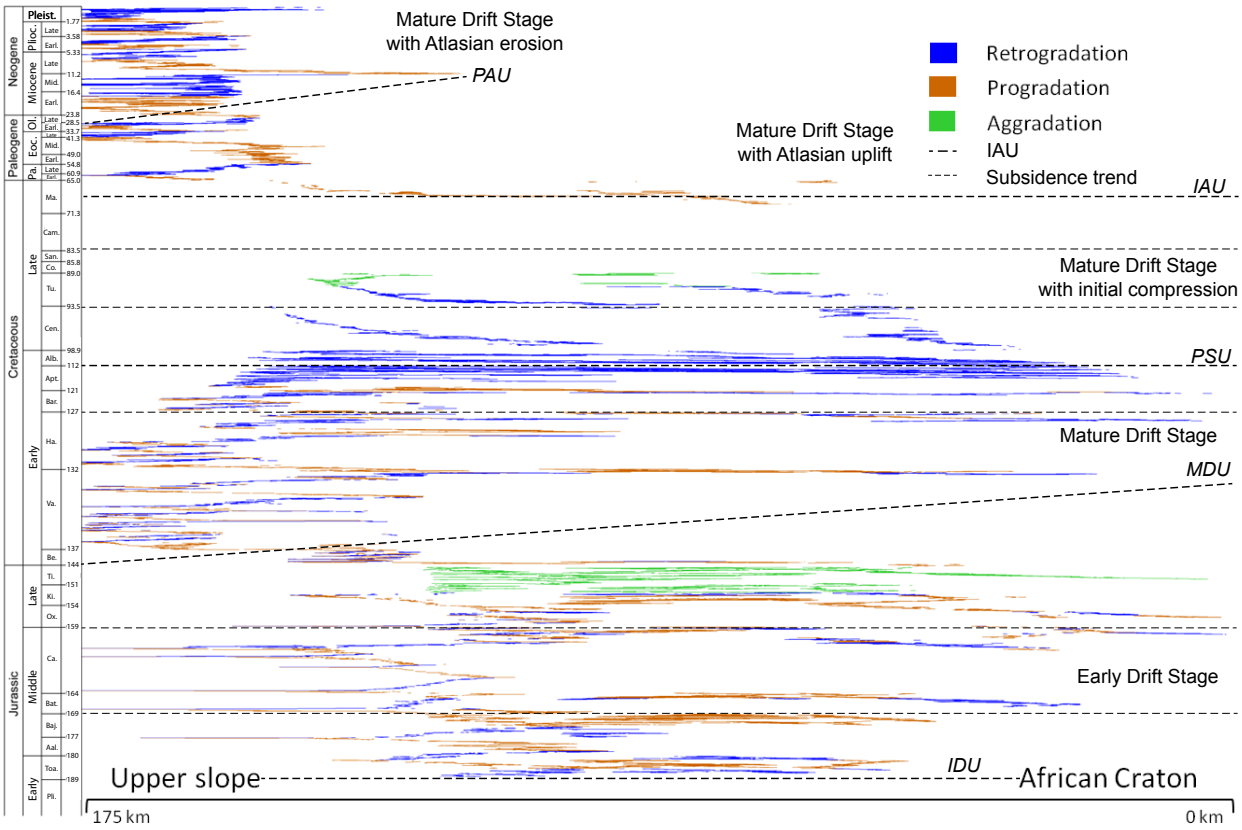

Fig. 97: Chronostratigraphic plot of the Tan Tan tranect with sequence stratigraphic interpretation following Neal & Abreu (2009). From Wenke et al. (2011).

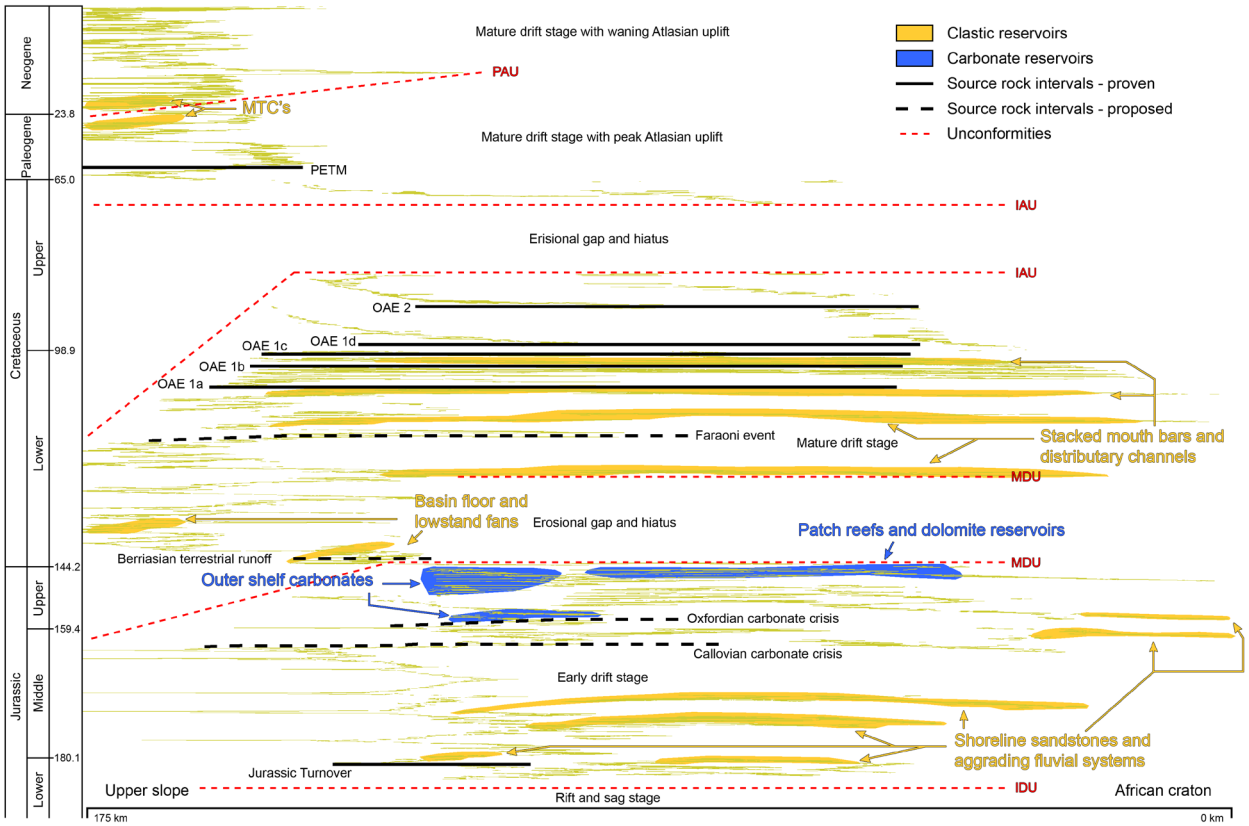

Fig. 98: Chrono-stratigraphic diagram of the Tan Tan transect with highlighted source and reservoir facies distribution (Wenke et al. 2011).

Valanginian to Hauterivian reflectors show delta progradation. Early Valanginian sequences are onlapping against the Jurassic shelf in the Tan Tan area (marine onlap). To the south, most of the distal parts of the Early Cretaceous is eroded and cut by the IAU.
Late Valanginian sequences are concordant to the underlying Jurassic in outer to mid-shelf regions and show onlap against the MDU in inner shelf areas. In general, the Valanginian depositional system shows a major retrogradational trend. In total, seven sequences have been identified in the Valanginian succession.
Progradation as a consequence of high sediment input prevailed during the following Hauterivian (four sequences) and Barremian (five sequences). Stacked deep marine fans were deposited in the deep offshore until the Barremian before the depositional system started to retrograde in the Early Aptian. Overall retrogradation continued until the Campanian. Aptian (Ap) thickness increases below the recent shoreline. Sequences Ap 1–4 are restricted to the outer shelf top. Sequences Ap 3–6 extend to the inner shelf top and show coastal onlap towards the continent. The top of Aptian is defined by the PSU.
Above the PSU the Albian shows further retrogradation and low angle reflectors. Some stratal terminations have been developed in the mid shelf depression. A coastal onlap could not be identified in the southern Tarfaya and northern Laâyoune Basins. Five sequences have been identified.
The Late Cretaceous succession is very reduced in the northern part and proximal areas of the study area but full preserved in the Laâyoune Basin.
In the northern Tarfaya Basin, only the Cenomanian and Turonian intervals, comprising 5-10 reflectors in total without specific geometries, have been deposited or preserved on the inner and middle shelf (Lines 87-TA-15 & EM 39). Five sequences, three Ce and two Tu, have been identified in the Tan Tan region. In the Cap Juby area, nine sequences are preserved including Coniacian sequences.
The Late Cretaceous is fully preserved in the Laâyoune area where 12 sequences have been noticed.
The Late Cretaceous is characterized by a major Cenomanian to Campanian retrogradation including minor progradations during Early Coniacian and Late Santonian, followed by Maastrichtian progradation. The Late Cretaceous high-resolution sequence stratigraphic pattern for all three transects is given in Fig. 90.
The Cenozoic (except a Miocene succession of 10–15 m thickness) has not been deposited on the shelf or has been eroded and exists only west of MO-7. On the western part of Line C83MMO-15, the Cretaceous/Cenozoic boundary is represented by the IAU which cuts down to the Barremian succession at maximum. The Paleogene basin fill is restricted to a long-term shelf margin wedge with 10 sequences in front of the Late Cretaceous margin. In contrast to the Oligocene, shelf downstepping, progradation and bypass sedimentation characterizes the Neogene sequences. The Neogene time interval increases up to 2 s TWT at the northwestern end of Line 83-MMO-15. Fifteen Neogene sequences have been interpreted. Nine additional sequences may have developed in the basinward direction of the key transects. Fig. 91 shows the SSIS® interpretation of the Cenozoic succession of all three key transects and Fig.92 the full drift basin fill SSIS® interpretation.
The development and extent of potential source rocks has been assessed from the stratigraphic position based on well evaluation, screening of OM (OAE correlation) in well data and their high-resolution sequence stratigraphic correlation. The Figs. 87 - 90 show a systems tract interpretation of all three key transects with the position of proven and potential source rocks.

4.6.2.4 Base-level curve

The base-level curve of the Tan Tan transect, resulting from high-resolution sequence stratigraphic interpretation, covers the Toarcian to Holocene (Fig. 96). Base-level is controlled by eustatic sea level, marine erosion depths and total subsidence. Base-level changes in the Tarfaya Basin have been tentatively correlated to eustatic sea level changes as inferred from the sequence stratigraphy of European basins (Hardenbol et al., 1998). Long-term (3rd order) relative base level trends as interpreted in the Tarfaya-Laâyoune Basins are largely comparable to eustatic sea-level changes on the Eurasian plate. Short term (4th order) relative base level changes (shorter than 3–5 Ma) indicate variations in sediment supply.

4.6.2.5 Chronostratigraphic diagrams (Wheeler diagrams)

Chronostratigraphic diagrams have been analyzed for all three transects based on sub-wavelet resolution analysis of seismic reflectors with SSIS®. Diagrams include:

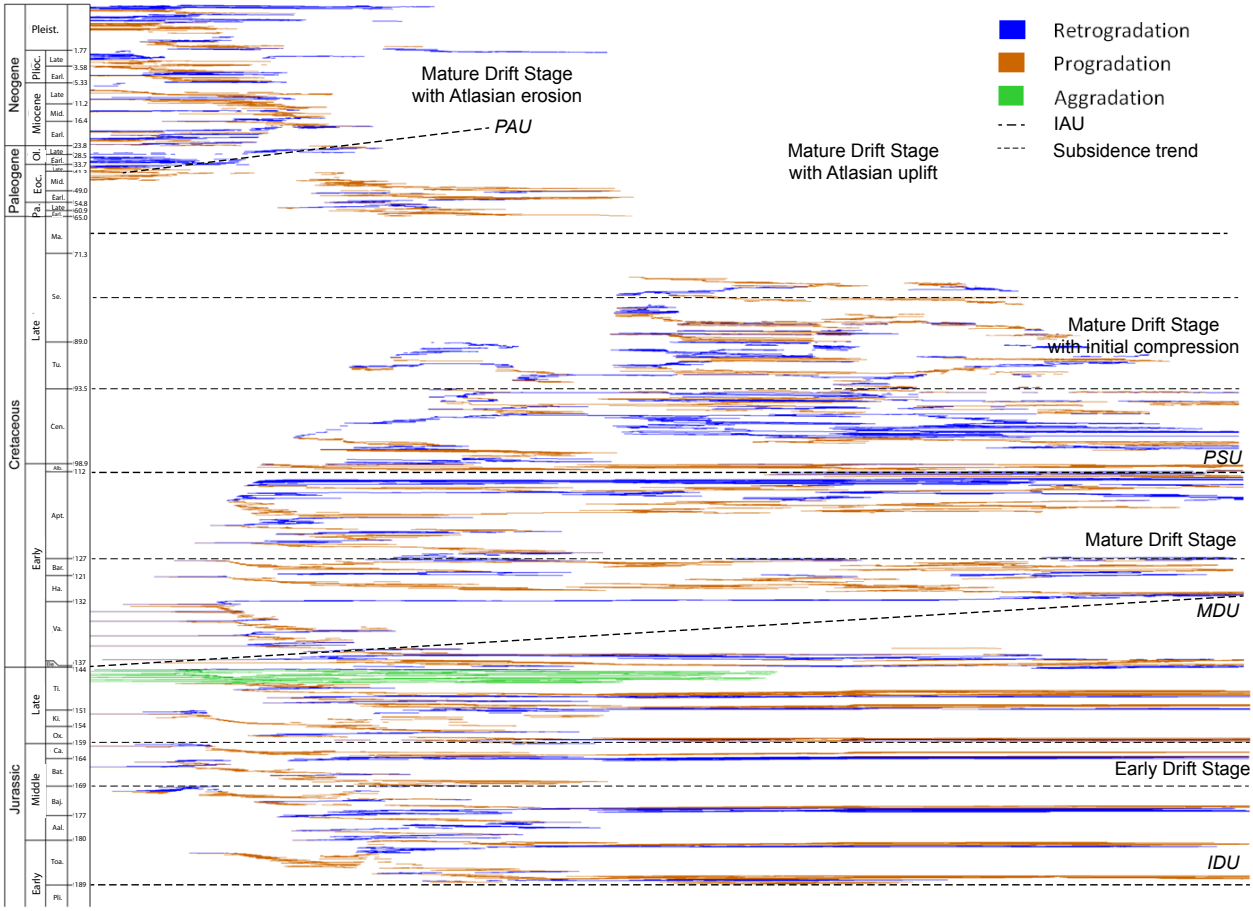

Fig. 99: Chronostratigraphic plot of the Cap Juby transect with sequence stratigraphic interpretation following NEAL & ABREU (2009).

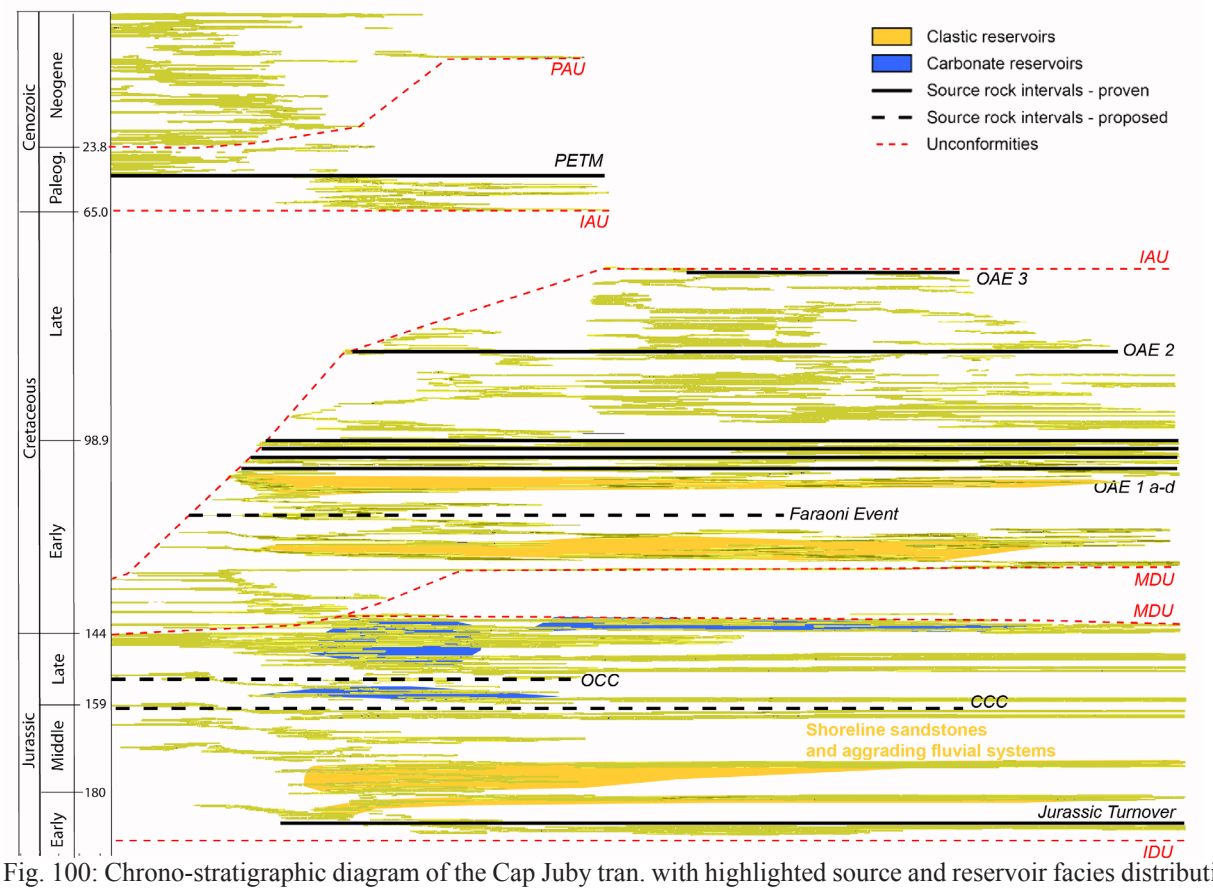

Fig. 100: Chrono-stratigraphic diagram of the Cap Juby tran. with highlighted source and reservoir facies distribution.

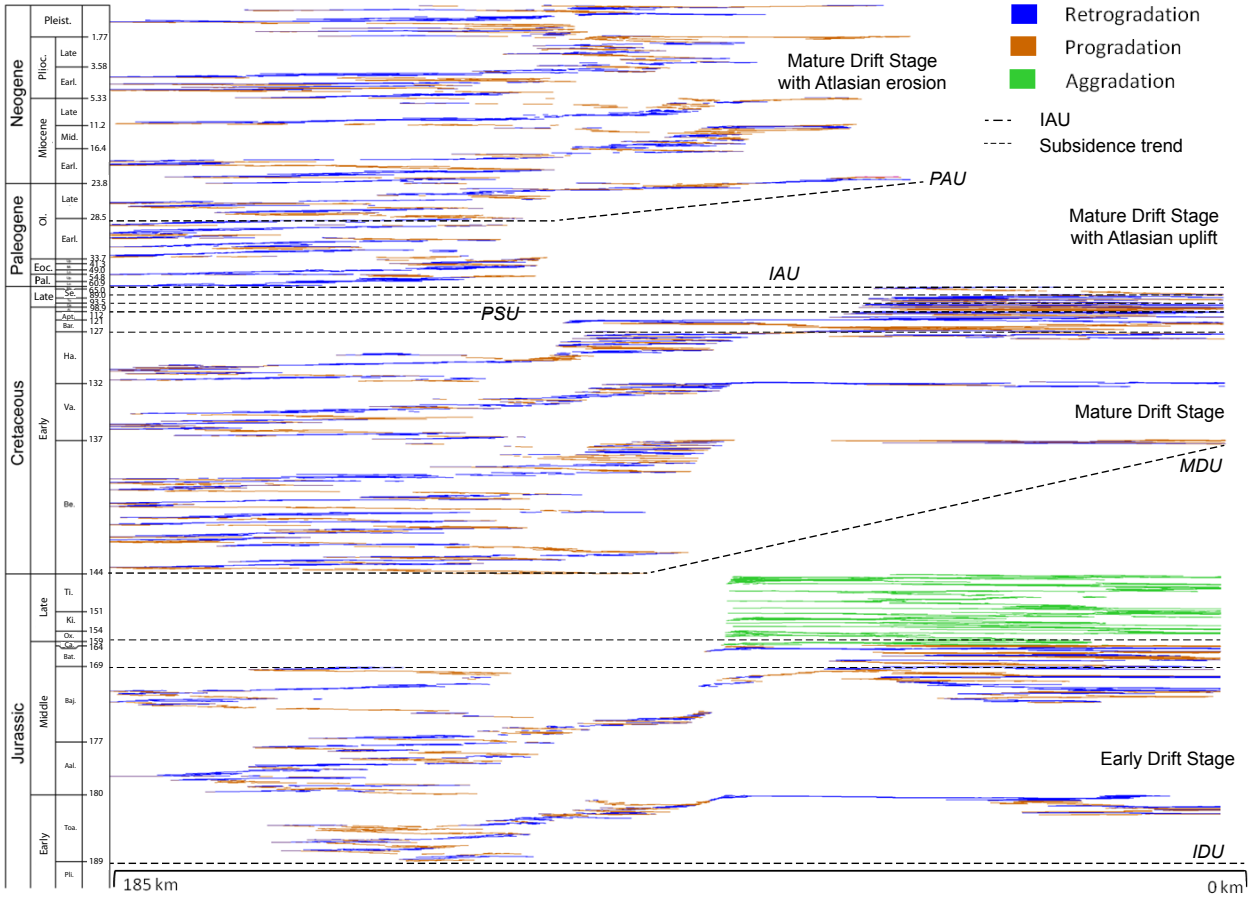

Fig. 101: Chronostratigraphic plot of the Laâyoune transect with sequence stratigraphic interpretation following Neal & Abreu (2009).

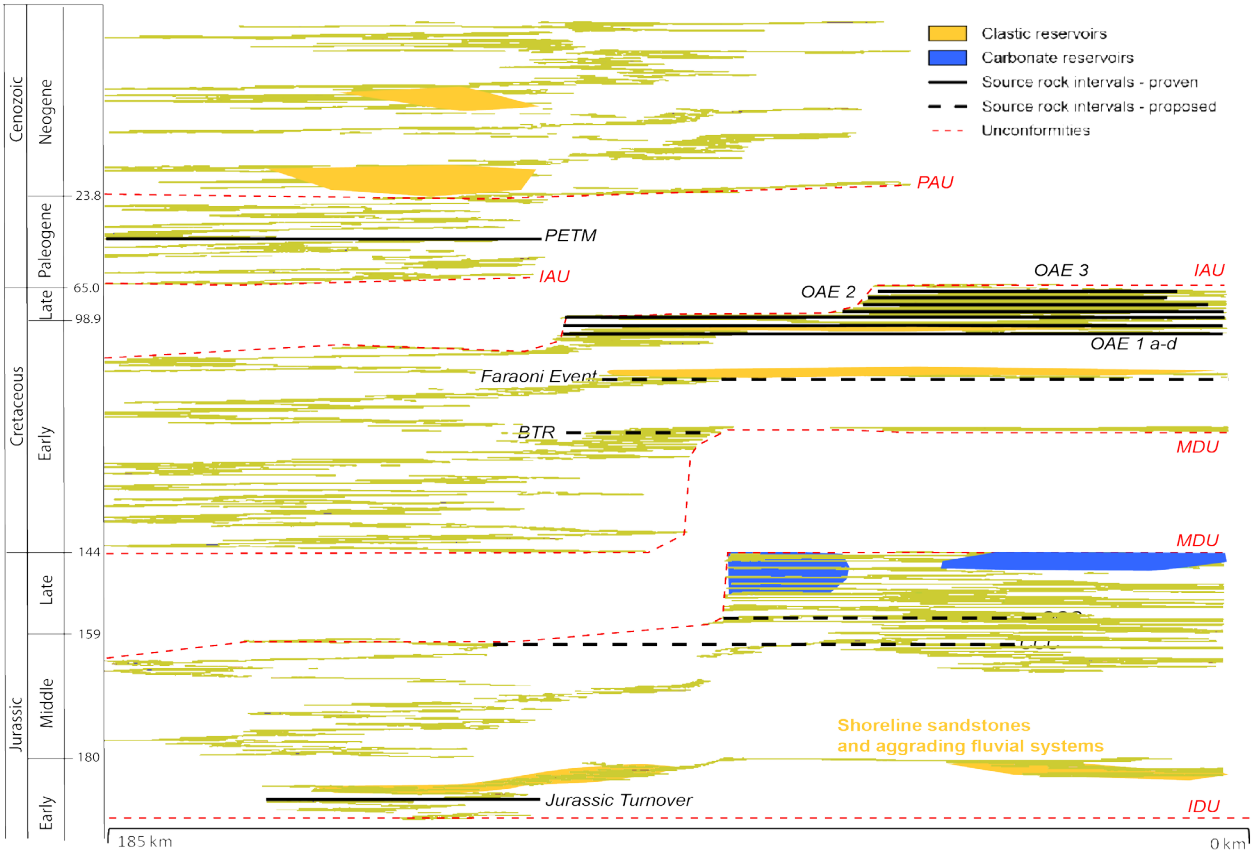

Fig. 102: Chrono-stratigraphic diagram of the Laâyoune tran. with highlighted source and reservoir facies distribution.

i) shelf line pattern, i.e. migration of the depositional systems in time and space, in modification of the concept of Neil and Abreu (2009): progradation (brown), aggradation (green), retrogradation (blue) and non-deposition (white). Shelf trajectories allow for initial prediction for the location and shifts of potential reservoir facies (Fig 97, 99 & 101);
ii) distribution and lateral migration of potential source rocks and reservoirs, e.g. shelf margins and lowstand fans. Chronostratigraphic diagrams provide an initial prediction on the location of the two elements of HC systems (Fig .98, 100 & 102);
iii) areal extent and timing of major unconformities in the basin fill.

Tan Tan transect

The Early Jurassic clastic-carbonate ramp systems show six major progradation/shallowing-upward cycles until the Middle Callovian (Fig. 97&98). Subsequent to three major retrogradation/deepening-upward cycles between the Middle Callovian to Late Kimmeridgian, shelf aggradation prevailed during the Tithonian. Deposition took place in the central and cratonward parts of the continental margin as covered by the Cap Juby transect.
In the Berriasian the delta system deposition was restricted to the lower slope and basin margin of the collapsed Jurassic shelf. Increasing sediment input sustained progradation and aggradation of the Tan Tan Delta until the Late Valanginian to Early Hauterivian.
From Hauterivian to Coniacian times, the continental shelf experienced major retrogradation, triggered by increasing accommodation space. Key driving factors include: i) high subsidence rates (e.g. chapter 4.7) and, ii) a continuous 3rd order eustatic sea-level rise (Fig. 96). In addition, sediment input sharply decreased, so that the Tan Tan Delta became inactive by the Late Aptian to Early Albian. In the Tan Tan area no Late Coniacian to Early Maastrichtian sediments were deposited or have been preserved. Initial deposition after the Late Cretaceous unconformity includes Late Maastrichtian outer shelf deposits.
The Maastrichtian to Eocene is restricted to the NW part of the transect. After a progradation/retrogradation cycle, deposition took place in a very small area at the shelf break. Paleogene sediments may have been deposited on the shelf but is possibly eroded in Late Oligocene. Retrogradation took place in the Mid-Miocene when clastic sediments were deposited on the shelf.
Fig. 98 shows the distribution and stratigraphic position of anoxic events (potential source rocks) and reservoir intervals. Additional potential source rocks in the Middle and Upper Jurassic (Kimmeridge clay analogue) have been described by MacGregor & Moody et al. (1998) and Morabet et al. (1998).
Potential reservoir intervals include: i) Lower to Middle Jurassic: shoreline and shelf-top sandstones, aggrading fluvial systems, ii) Middle Jurassic oolites, iii) Kimmeridgian to Tithonian: reefal shelf margins, carbonate shelf top with karstification, fractured shelf-top dolomites, iv) Berriasian to Middle Valanginian: basin floor and lowstand fans, v) Late Valanginian to Aptian: delta system incl. stacked mouth bars, distributary channel and, vi) Cenozoic: coarse-grained mass transport complexes, associated to the peak Atlasian uplift or the strong Serravalian eustatic sea-level fall.
Major seal formations are i) Lower to Middle Jurassic mudstones, ii) Upper Cretaceous shales and, iii) shales of Lower and Upper Miocene.
Fig. 98 indicates, that the Middle to lowermost Upper Jurassic succession may have allowed HC generation with well-defined migration pathways to Jurassic shelf-top sandstone or carbonate platform reservoirs. Wells MO-2 and CJ-1 have produced/were successfully tested from Upper Jurassic carbonate reservoirs. OAE 1a-d as well as OAE 2 are probably immature (Sachse et al. 2012). Potential Upper Cretaceous reservoirs could not be identified.
Fig. 92 indicates the major unconformities at basin scale. The Toarcian which covers the Triassic/Early Liassic rift phase is separated from the Jurassic early drift stage by a major regional unconformity, the IDU.
The MDU cuts into the Upper Tithonian to Valanginian succession, a regional unconformity, the PSU, separates Tan Tan delta sediments from the Early Cretaceous from Late Cretaceous open marine depositional settings.
The IAU cuts the Middle Hauterivian (basin) to Coniacian (shelf).
Sedimentation recommenced in the Late Maastrichtian. A shelf margin wedge developed in the Paleogene and is bounded at the top by the PAU. Neogene sediments are restricted to the outer shelf/shelf break, slope and deep offshore.

Cap Juby transect

The Toarcian to Middle Callovian clastic-carbonate ramp systems show six major progradation/shallowing-upward cycles until the Middle Callovian (Fig. 94). The three major retrogradation/deepening-upward cycles between the Middle Callovian to Kimmeridgian are less developed than in the Tan Tan area but are still present. Shelf aggradation prevailed also in the Cap Juby area during the Tithonian (incl. Portlandian). Deposition took place in the central and cratonward parts of the continental margin.
Berriasian to Valanginian shows six progradation cycles, in actual fact the tilted block geometry and the deep cutting IAU make a clear interpretation difficult.
From Hauterivian to Coniacian times, the continental shelf experienced major retrogradation, triggered by increasing accommodation space. During Early Hauterivian to Turonian 13 stacked progradation/retrogradation trends show an overall retrogradation. Retrogradation accelerated in the Upper Cretaceous until Middle Senonian.
Maastrichtian to Eocene shelf development is easier to comprehend on the Cap Juby transect. Shelf margin progradation was continuous during that time while coastal onlaps shifted cratonward. A slowly increasing amount of sediment input per time could be an explanation. An interpretation of Neogene depocenter variations is limited.
The transect crosses the Cap Juby oilfield which produced a few days from Upper Jurassic (Tithonian) shelf margin (bioherms) reservoirs. The reservoir formation is located on a structural higher position, the trap is provided by the combination of a tilted/ fault block and upwelling salt. Oil migration probably took place from the SE where the Jurassic experienced deeper burial and is more mature. A number of HC-bearing reservoir formations are conceivable. Potential reservoirs include the Callovian, Kimmeridgian and Tithonian intervals fractured during salt deformation. However, reservoirs may have as well experienced HC leakage because of seal failures. Lower Cretaceous potential reservoir intervals seem to spread over large parts of the shelf. The Cap Juby transect is located between the Tan Tan and the Laâyoune Delta Complexes. Source and reservoir distribution is given in Fig. 100.
Unconformities and subsidence trends largely correspond to the Tan Tan transect. However, the PAU cuts deeper into the Late Cretaceous (Senonian) and partly into the Upper Valanginian.
The early Cenozoic shelf wedge extends over a larger area and shows shallower dips.

Laâyoune transect

The Toarcian to Middle Callovian clastic-carbonate ramp system is more prominent on the Laâyoune transect. Ramp progradation took place in eight steps until Late Bajocian including a major retrogradation in Late Toarcian and Early Bajocian. (Fig. 101). A major retrogradation lasted from Early Bathonian to Oxfordian. Platform aggradation prevailed during the whole Kimmeridgian to Tithonian.
After Early Berriasian deep marine progradation, shelf deposition restarted in the Late Berriasian due to a rising eustatic sea level. Two major progradation cycles are developed for the Early to the Middle Valanginian and the Early Hauterivian. Subsequently, the system is retrograding in two steps until the Early Maastrichtian.
Maastrichtian to Eocene shelf margin progradation took place in seven progradation cycles. During the Neogene deposition took place in the slope and basin areas or on the shelf during eustatic highstands. Highstands are notable for Middle Miocene, Upper Miocene and Upper Pliocene.
The Laâyoune transect is located in the relatively least explored part of the study area. The Upper Jurassic shelf margin is located 10 to 20 km offshore. Upper Jurassic asphalt has been proven onshore for site CORC-15-1. However, the position of Jurassic source rock intervals may be less favorable. More high-quality data for the region would be necessary for a better assessment of the basin fill, subsidence trends and the HC system (Fig. 102).
Unconformities and subsidence trends correspond largely to the Tan Tan transect. However, the PAU cuts deeper into the Late Cretaceous (Senonian) and partly into the Upper Valanginian. The early Cenozoic shelf wedge extends over a larger area and shows shallower dips.

4.7 Time/depth conversion

The velocity cube of Fig. 103 incorporates lateral changes in thickness, lithology and structural dip. Individual seismic reference datums of the available on- and offshore seismic surveys have been unified to one datum.
Low velocity layers with values of 1.400 to 1.500 m/s prevail in the study area (Fig. 103). Significantly higher average velocities at shallow levels of up

to 2.000 m/s in the northeastern onshore (CHBK-1 & EA-1 region) of the study area represent a striking exception. This level of acoustic velocities is usually indicative for burial depths of approx. 1000m. The actual excess velocity implies that a sediment column of 1000m must have been removed by uplift and erosion in the northern onshore area. Wells CHBK-1 and EA-1 are located in the uplifted area with high velocities, while PC-1 is situated in low velocity areas.
Fig. 104 shows the Meso-/Cenozoic basin fill along the three transects in depth domain. The horizon tops ("time lines") have been used for flexural basin modelling (c.f. 4.7).
The maximum modelled thickness for the basin fill varies between 11.4km in the outer Tan Tan region, 11.6km at Cap Juby prospect and 13.4km in the outer Laâyoune area. The maximum sediment thickness is located at the shelf break/upper slope region of the study area. It defines the point of maximum sediment load and separates the continentward from the basinward taper.
The overall sediment thicknesses are very unique on all three analyzed transects. The rift basin fill thickness varies between 1000m in the deep offshore landward of the S1 anomaly and at the Laâyoune Horst, 1500 to 2000m in the Chebeika Graben, 2000 to 3500m in the Laâyoune depression and 4000 to 5500m in the shelf break/upper slope area. The sag interval between rifting and drifting has an additional maximum thickness of 1000m.
The early drift stage basin fill thickness strongly varies in the basin. The maximum proximal thickness of the Jurassic succession has been recognized in the Chebeika Graben with 1300m in well CHBK-1 thinning out (onlap against IDU) in proximal direction. The thickness of the rift succession in proximal wells amount to 480m in D-2-9 and 445m in EA-1.
The Jurassic sediment column has its maximum thickness in the Laâyoune depression, the area of maximum sediment load during the Middle and Late Jurassic, reaching 3250m in the Tan Tan and 3750m in the Laâyoune area. In the Jurassic outer shelf area the Jurassic thickness averages 3000m.
In the deep offshore, the modeled thickness varies between 400m in the Tan Tan area and 1000m in the offshore Laâyoune area. However, Jurassic open marine turbidites are exposed on Fuerteventura with a thickness of 825 m (Steiner et al., 1998).
The Early Cretaceous basin fill has its highest thickness in the slope and basin area reaching 3500m in the Laâyoune and 5000m in the Tan Tan area. However, thickness variations are dependent on sediment flux during time of deposition and Meso- to Ceonozoic salt movements. On the shelf, the Early Cretaceous sedimentary column averages at values between 1000m and 1500m and thins out in landward direction.
Apart from some spots of Cenomanian/Turonian in the deep offshore, Late Cretaceous is just present on the shelf. The most complete succession is preserved in the southern part of the study area and was drilled in the Alisio well (15-A-1). In the north the thickest succession has been recognized in the Puerto Cansado well (PC-1) with a thickness of 350-400m. Late Cretaceous sediment thickness increases to the south and a total thickness of 600m can be recognized in the central shelf area of the Cap Juby transect, 800 m in the Laâyoune central shelf, respectively.
The Cenozoic is mainly deposited and preserved in the shelf break to basin area and reaches a thickness of 2000m at the slope of the Tan Tan transect and 3250 m in the basin between Cap Juby and Fuerteventura.

4.8 2D-flexural reverse modeling

4.8.1 Basin architecture and depositional geometries through time

Fig. 105 & 106 show eleven time slices (corresponding to subsidence trends of 4.8.2) in depth domain for each transect. They show the development of the basin architecture, the shift of depocenters, lateral thickness changes and variations in bathymetry during the basin development. Time slices containing one or more OAEs, e.g. the Toarcian (Jurassic Turnover), potential source rock formations are highlighted. In addition, the approximate positions of the oil and the gas window in time and space are indicated. Temperature data have been taken from Zarhloule et al. (2005) based on present day geothermal gradients. Variations in heat flux were not taken into consideration.

4.8.1.1 Rift and sag stage

The basal IRU (259.3 Ma) marks the onset of rifting with normal faulting and the development of compartmentalized sub-basins (Fig. 98 top row). Subsidence and sediment flux is related to isolated basins (ST1 in Fig. 98, second row).
Strongly increasing and laterally expanding subsi-

dence resulted in the development of three NNE-SSW trending major rift basins separated by two horst structures during the Anisian to Ladinian (Peak rifting: 234.4 -220.7 Ma) of which two will fail during basin development.
The Chebeika Graben with a width of approximately 12 - 15km is located adjacently to the continentward hinge zone. Seismic coverage in this study is restricted to the Tan Tan area, stratigraphic control to the wells CHBK-1 and EA-1 (Fig. 63 & 104).
The Chebeika Horst features an E-W extension of 5 -12km and separates the Chebeika Graben from the Laâyoune Graben (Laâyoune Depression; BEICIP, 1991; EL KHATIB et al. 1995). It extends for 25 – 35km and is bounded to the west by the Juby Horst (Horst du Juby, LE ROY, 1997) with a width of 15 -20 km.
The proto-Atlantic represents the most western (half-)graben extending to the continental-oceanic transitional crust which is defined by the S1 magnetic anomaly. The distance between the eastern Juby Horst and the S1 anomaly is about 75 - 125 km.
The depositional environment and rift to sag basin geometries for the Chebeika Graben can best be described as a lacustrine environment within an asymmetric half-graben (c.f. LIN CHANGSONG et al, 1997 as analogue). Basal through-like reflectors with an increased dip and varying amplitude represent alluvial and subaqueous fan deposits followed by fan braided stream delta deposits and deep lacustrine deposits. The mature rift stage in this proximal area is dominated by prodelta and delta fan deposits while the sag stage is represented by fluvial and alluvial plain sediments (see Interpretation of the Tan Tan transect in Fig. 63).
During the mature rift stage (Figure 105, second row) between the Early Norian and Latest Rhaetian (220.7 – 204.3 Ma) areas of major subsidence extended laterally, but overall subsidence rates and fault-offsets decreased. Marine ingressions are constrained to the Laâyoune Graben and the (proto-) Atlantic Basin, evaporation resulted in the deposition of extensional salt provinces.
The rift stage is followed by the sag stage (Fig. 105 third row) between Middle Hettangian and Middle Pliensbachian (204.3 Ma - 189.6 Ma) age, as represented by the fourth horizon in ST2. Major features in basin architecture include the lack of extensional faulting and the development of two depocenters covering the Chebeika-Laâyoune Grabens and the major rift basin (Fig. 63, 104 & 105). The sag stage is bounded at the base by the PRU (204.3 Ma) which is defined on seismic lines as the first continuous reflector above the rift faults (Fig. 63). The rift and sag basin fill is bounded at the top by the IDU of Mid-Pliensbachian (189.6 Ma) age.

4.8.1.2 Early Drift Stage

The onset of sea-floor spreading in the Central Atlantic and increased flexural subsidence in basinward direction (Fig. 105, third row) led to the development of low-angle (<1°) depositional ramps above the IDU (Fig. 59 & 104). After the progradation of an initial clastic ramp including large scale foresets (Toarcian – Early Bajocian, Fig. 63) clastic input decreased and finally terminated in the Bathonian when stable tectonic conditions prevailed in continental hinterlands (Fig. 105 fourth row).
The Late Jurassic to Early Cretaceous basin fill of the southern Moroccan margin includes one of the largest-scale Jurassic carbonate shelf-to-basin transitions worldwide (see also Todd & Mitchum, 1977) with a rimmed shelf geometrical offset of 1000m in the Tan Tan area (Fig. 104, Fig. 98, fifth row). During the Late Jurassic the depocenter was located in the Laâyoune Depression above the point of maximum crustal thinning during the sag stage (Figs. 59 and 97). The Lower Jurassic shelf width measured 75 – 100 km between the coastal onlap to shelf break and successively increased by continent-ward onlap migration to 140 – 200 km. The MDU (144.2 Ma distal, 144.2 – 127.0 Ma proximal) marks the end of carbonate production on the southern Moroccan margin. It is represented on seismic transects by a high amplitude discontinuous reflector (Fig. 63).

4.8.1.3 Mature drift stage

The Lower Cretaceous Berriasian to Aptian southern Moroccan depositional history (Fig. 105, bottom row) is dominated by terrestrial run off and the development of two delta systems (Tan Tan and Boujdour/Laâyoune Delta Systems) which were active

Fig. 103 (next page): Velocity cube based on 3rd order sequence stratigraphic reflector interpretation. Time/depth conversion is based on VSP data of five wells and synthetic check shots of additional fifteen wells (WENKE et al., subm.).

Fig. 104 (after next page): Depth-converted transects with chronostratigraphic units; a) Tan Tan transect, b) Cap Juby Transect, c) Laâyoune transect. From WENKE et al. (subm.)

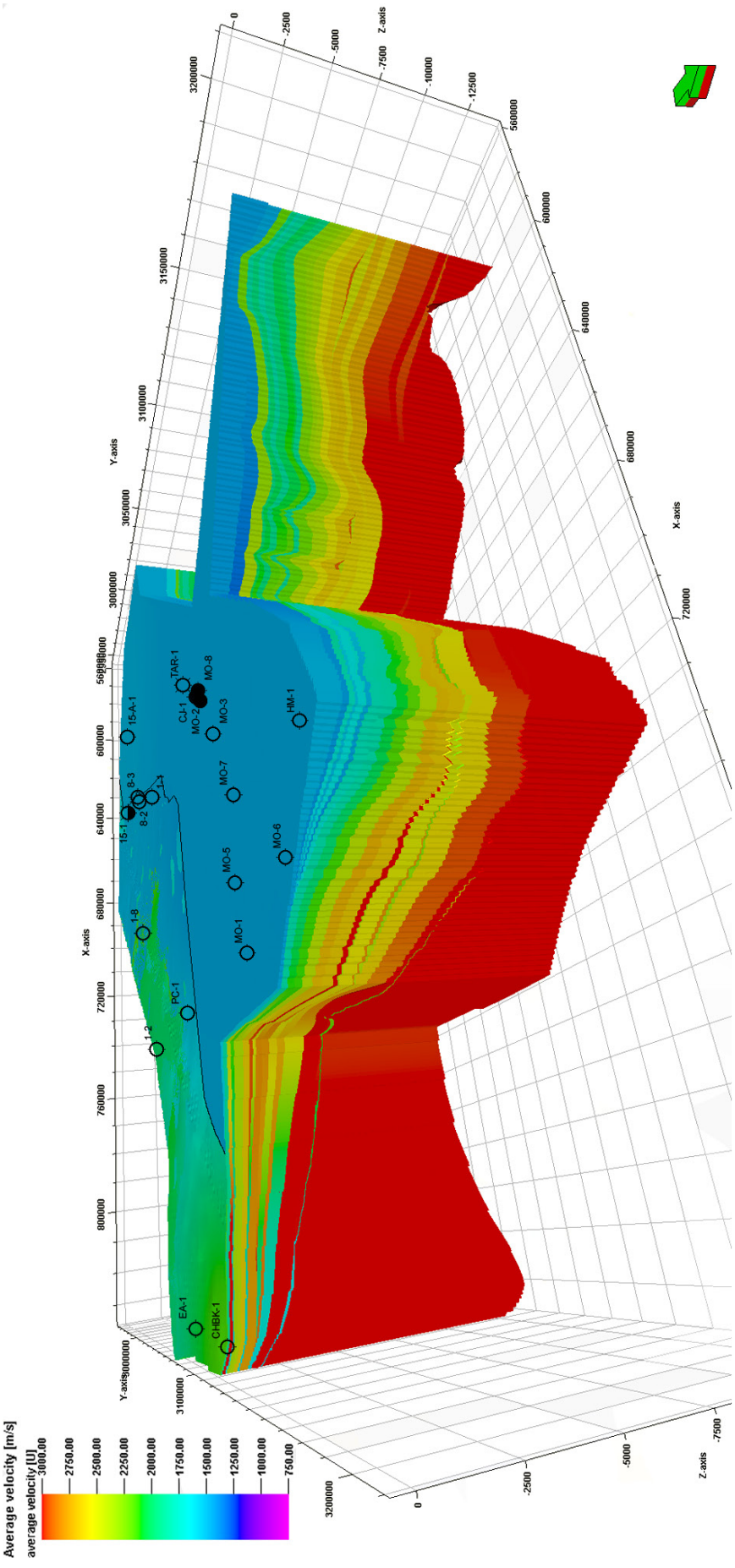
Average velocity [m/s]
average velocity [U]
3000.00
2750.00
2500.00
2250.00
2000.00
1750.00
1500.00
1250.00
1000.00
750.00
X-axis
Y-axis
Z-axis
TAR-1
MO-8
CJ-1
MO-2
MO-3
I5-A-1
HM-1
MO-7
8-3
8-2
15-1
MO-6
MO-5
I-8
MO-1
PC-1
I-2
EA-1
CHBK-1

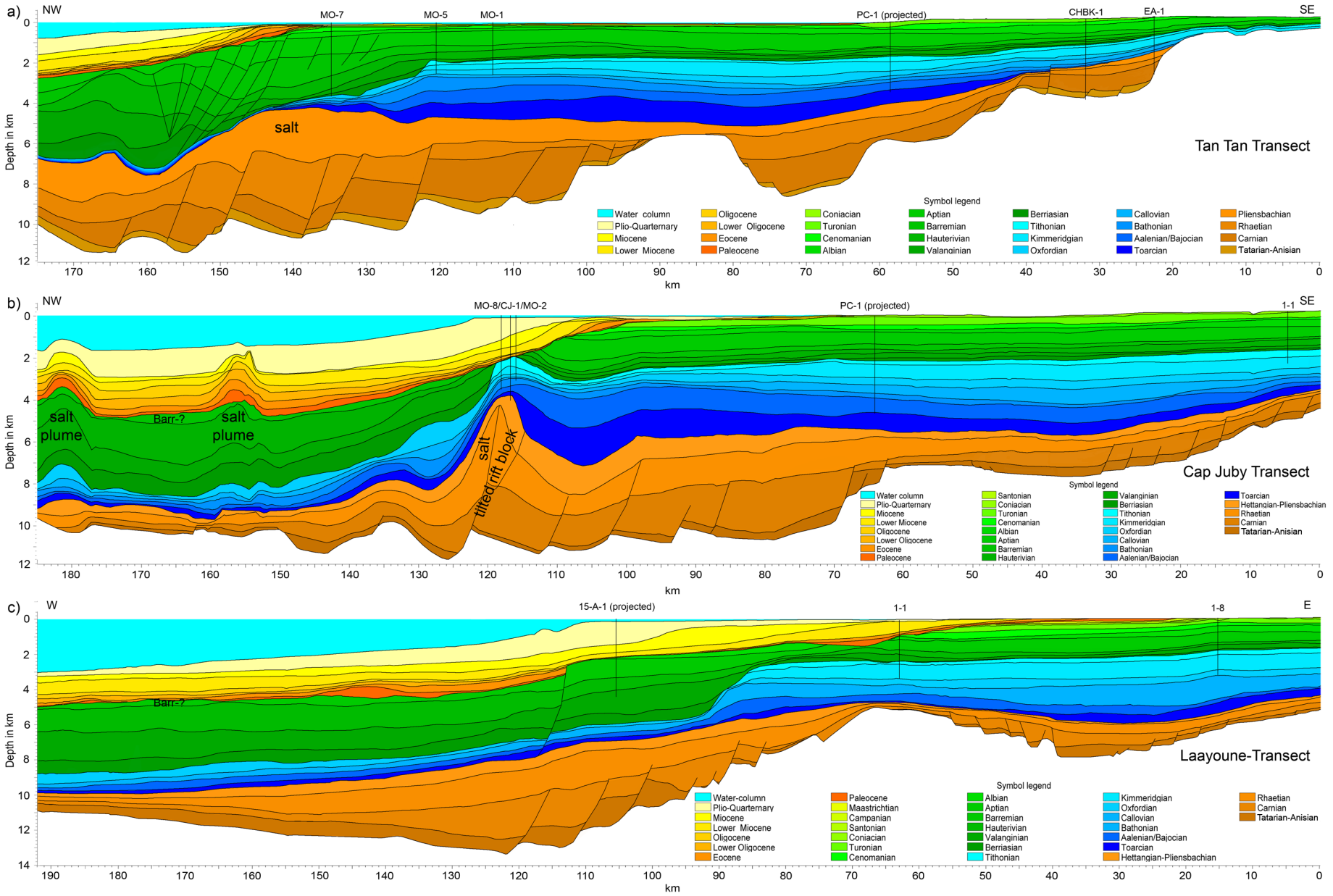
a)
NW
SE
MO-7
MO-5
MO-1
PC-1 (projected)
CHBK-1
EA-1
salt
Depth in km
km
Tan Tan Transect
Symbol legend
Water column
Plio-Quarternary
Miocene
Lower Miocene
Oligocene
Lower Oligocene
Eocene
Paleocene
Coniacian
Turonian
Cenomanian
Albian
Aptian
Barremian
Hauterivian
Valanginian
Berriasian
Tithonian
Kimmeridgian
Oxfordian
Callovian
Bathonian
Aalenian/Bajocian
Toarcian
Pliensbachian
Rhaetian
Carnian
Tatarian-Anisian
b)
NW
SE
MO-8/CJ-1/MO-2
PC-1 (projected)
1-1
salt plume
Barr-?
salt plume
salt
tilted rift block
Depth in km
km
Cap Juby Transect
Symbol legend
Water column
Plio-Quarternary
Miocene
Lower Miocene
Oligocene
Lower Oligocene
Eocene
Paleocene
Santonian
Coniacian
Turonian
Cenomanian
Albian
Aptian
Barremian
Hauterivian
Valanginian
Berriasian
Tithonian
Kimmeridgian
Oxfordian
Callovian
Bathonian
Aalenian/Bajocian
Toarcian
Hettangian-Pliensbachian
Rhaetian
Carnian
Tatarian-Anisian
c)
W
E
15-A-1 (projected)
1-1
1-8
Barr-?
Depth in km
km
Laayoune-Transect
Symbol legend
Water-column
Plio-Quarternary
Miocene
Lower Miocene
Oligocene
Lower Oligocene
Eocene
Paleocene
Maastrichtian
Campanian
Santonian
Coniacian
Turonian
Cenomanian
Albian
Aptian
Barremian
Hauterivian
Valanginian
Berriasian
Tithonian
Kimmeridgian
Oxfordian
Callovian
Bathonian
Aalenian/Bajocian
Toarcian
Hettangian-Pliensbachian
Rhaetian
Carnian
Tatarian-Anisian

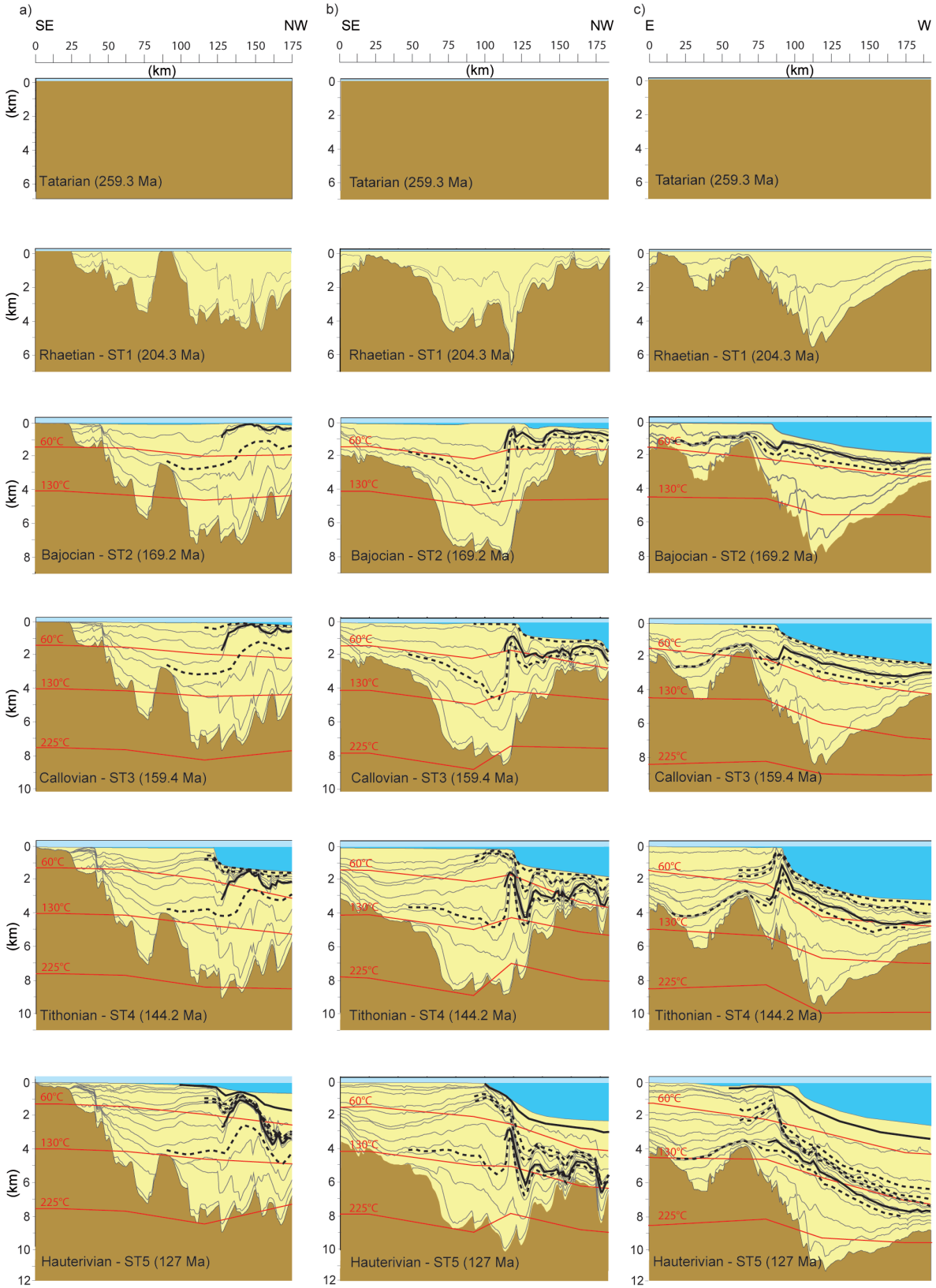

Figures 105 (this page) & 106 (next page): Chronostratigraphic plots of the a) Tan Tan, b) Cap Juby and, c) northern Laâyoune Transects with the basin architecture and paleo-water depths for ten selected time layers. Vertical and horizontal scales are in km. The Tan Tan Transect (a) covers the complete shelf. Deep offshore areas are covered by the Cap Juby and Laâyoune Transects (b, c). Plots illustrate the position of black shale intervals in the basin fill and oil, gas and recombined gas window maturation stages. Late Cretaceous "hot shales" of the OAE 1b – OAE 3 events probably have not yet reached the oil window (Wenke et al., subm.).

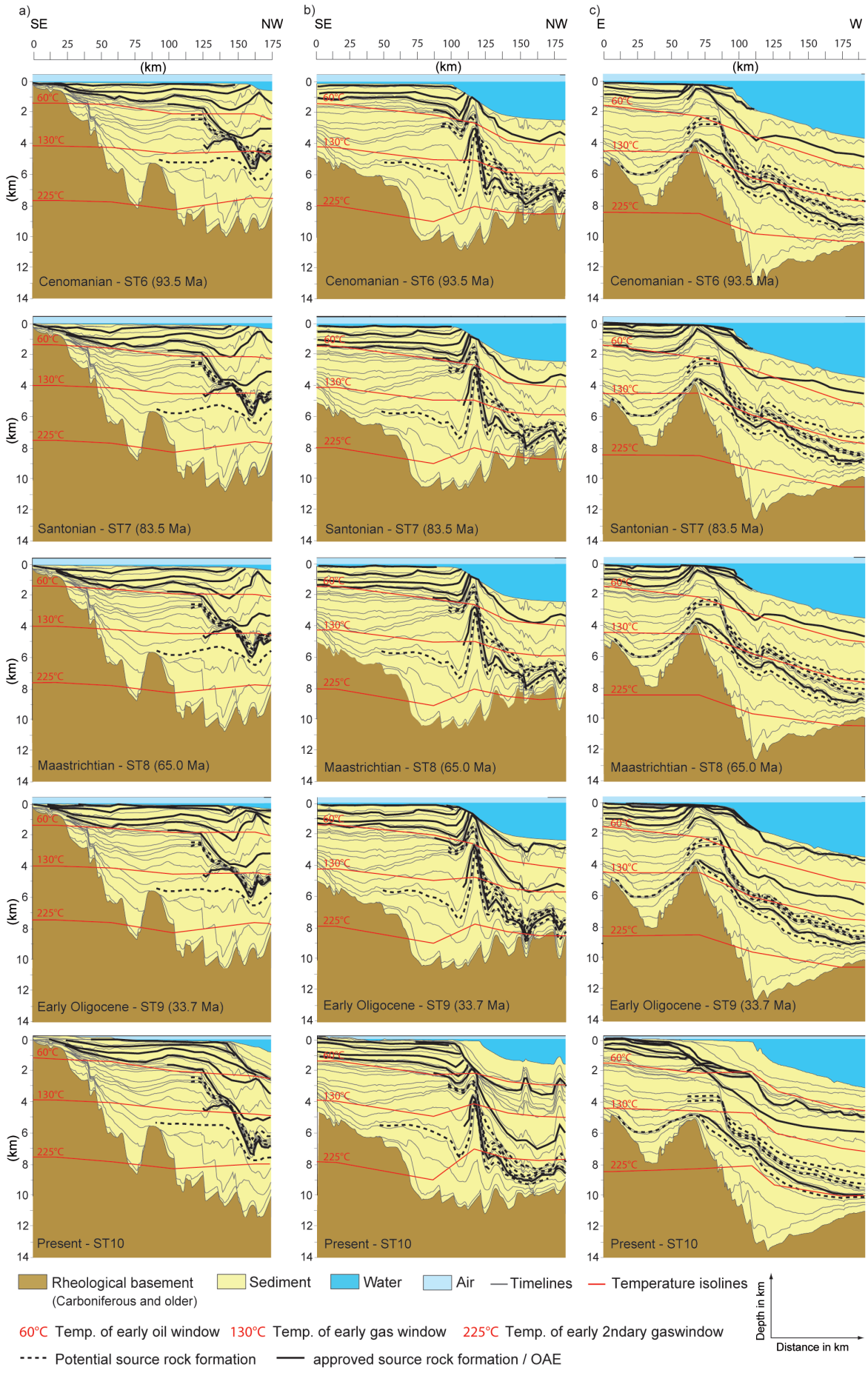
a)
SE
NW
b)
SE
NW
c)
E
W
0 25 50 75 100 125 150 175
(km)
(km)
60°C
130°C
225°C
Cenomanian - ST6 (93.5 Ma)
Santonian - ST7 (83.5 Ma)
Maastrichtian - ST8 (65.0 Ma)
Early Oligocene - ST9 (33.7 Ma)
Present - ST10
Rheological basement
(Carboniferous and older)
Sediment
Water
Air
Timelines
Temperature isolines
60°C Temp. of early oil window
130°C Temp. of early gas window
225°C Temp. of early 2ndary gaswindow
Potential source rock formation
approved source rock formation / OAE
Depth in km
Distance in km

over a period of 32 m.y. Delta development started with a shift of the depocenters from the central Jurassic shelf 20 to 40 km in a basin-ward direction.
Seismic reflectors of the incipient Berriasian to Early Valanginian Tan Tan Delta show onlap and downlap termination against the MDU (Fig. 63, 89a). Sediment input from the continent bypassed the shelf top. Sedimentation on the shelf re-occurred only during the Late Valanginian. Late Valanginian to Aptian shelf sedimentation consists of a condensed section with several hiata and concordant, subhorizontal reflectors. Delta systems showed both basinward and lateral progradation until the Late Barremian. During the Aptian, the Tan Tan Delta experienced retrogradation although sediment input remained high and foresets developed. The deltas became inactive in the Latest Aptian.
The development of the Tan Tan delta (Tan Tan transect in Figs. 63 & 104) had a significant influence on the structural development of the Tarfaya Basin. Increasing sediment load led to the mobilization of late Triassic salt below the Late Jurassic to Early Cretaceous shelf margin. Salt movement triggered (cf. Figs. 63): i) the collapse of the Jurassic slope, ii) the development of prominent growth faults above the collapsed Jurassic slope, iii) a rotation and uplift of Triassic fault blocks in the Juby Horst, and iv) the rise of salt diapirs in the deep offshore area which continues until recent times. These structural features are largely absent in the northern Laâyoune Basin, where no/less Triassic salt was deposited.
The extension of incipient deltas averaged 20 to 25km in basin margin and lower slope areas. In the Late Hauterivian to Aptian, delta sedimentation spread to the shelf top across the entire study area. The proximal Barremian to Aptian succession has not been preserved and the maximum continentward extension of delta plain sediments can only be inferred.
Deltas are bounded at the top by the PSU (112.2 Ma), a major angular and partially erosional unconformity. It shows strong lithologic and impedance contrast with clastic delta deposits below and Albian outer shelf to open marine carbonates above. The PSU is represented by the high-amplitude reflector above the concordant Early Cretaceous succession (Fig. 63).

4.8.1.4 Mature Drift stage with initial Atlasian/Alpine compression

The Post-PSU depositional system is represented by a retrogradational Late Cretaceous (Aptian – Early Maastrichtian) sequence set (Fig. 106, first three rows). The Tarfaya-Laâyoune Basins reached their widest onshore extension at that time. The exact position of the landward boundary is uncertain since the proximal succession was eroded during the Cenozoic. The most complete Late Cretaceous succession is preserved in the Laâyoune Basin. On the shelf, the Late Cretaceous and Early Cretaceous successions are concordant. A major erosional unconformity, the IAU (pre-65.0 Ma), cuts into the Late Cretaceous succession in some slope areas as deep as the Valanginian.

4.8.1.5 Mature Drift stage with Atlasian Compression and initial uplift

Between the Maastrichtian and Late Oligocene a shelf margin wedge developed. Seismic reflectors show high angle dip in the northern Tarfaya and low angle dip in the Laâyoune Basin (Fig. 63a & c). The Maastrichtian to Late Oligocene marked the second major depocenter shift in a basinward direction. Wedge shaped strata show offlap against the IAU (Fig. 63). Onshore, Paleocene and Eocene deposits are exposed in the northern Laâyoune Basin and consist mainly of shales, marls and carbonates. The Paleogene 2D-chronostratigraphic setting is visualized in Fig 106, fourth row.

4.8.1.6 Mature Drift Stage with peak Atlasian uplift and erosion

This basin stage developed above by the PAU (28.5 Ma). Seismic reflectors show onlap against the Paleogene shelf margin wedge (Fig. 63). Except for a thin Miocene succession east of Tarfaya, the Neogene sediments were bypassed and not deposited on the shelf. Even though the sedimentation rate increased during the Neogene, mainly fine clastic sediments have been deposited during the past 28.5m.y. Flexural uplift can be recognized in the proximal Tan Tan area (Fig. 106a, basal row).

4.8.1.7 Subsidence history of potential and proven source rock formations

The subsidence evolution of the potential and proven source rock formations is outlined in Fig. 105 & 106 except for potential Paleozoic events. Following the modelled basin evolution, earliest hc generation in the Tarfaya Basin started between Bajocian

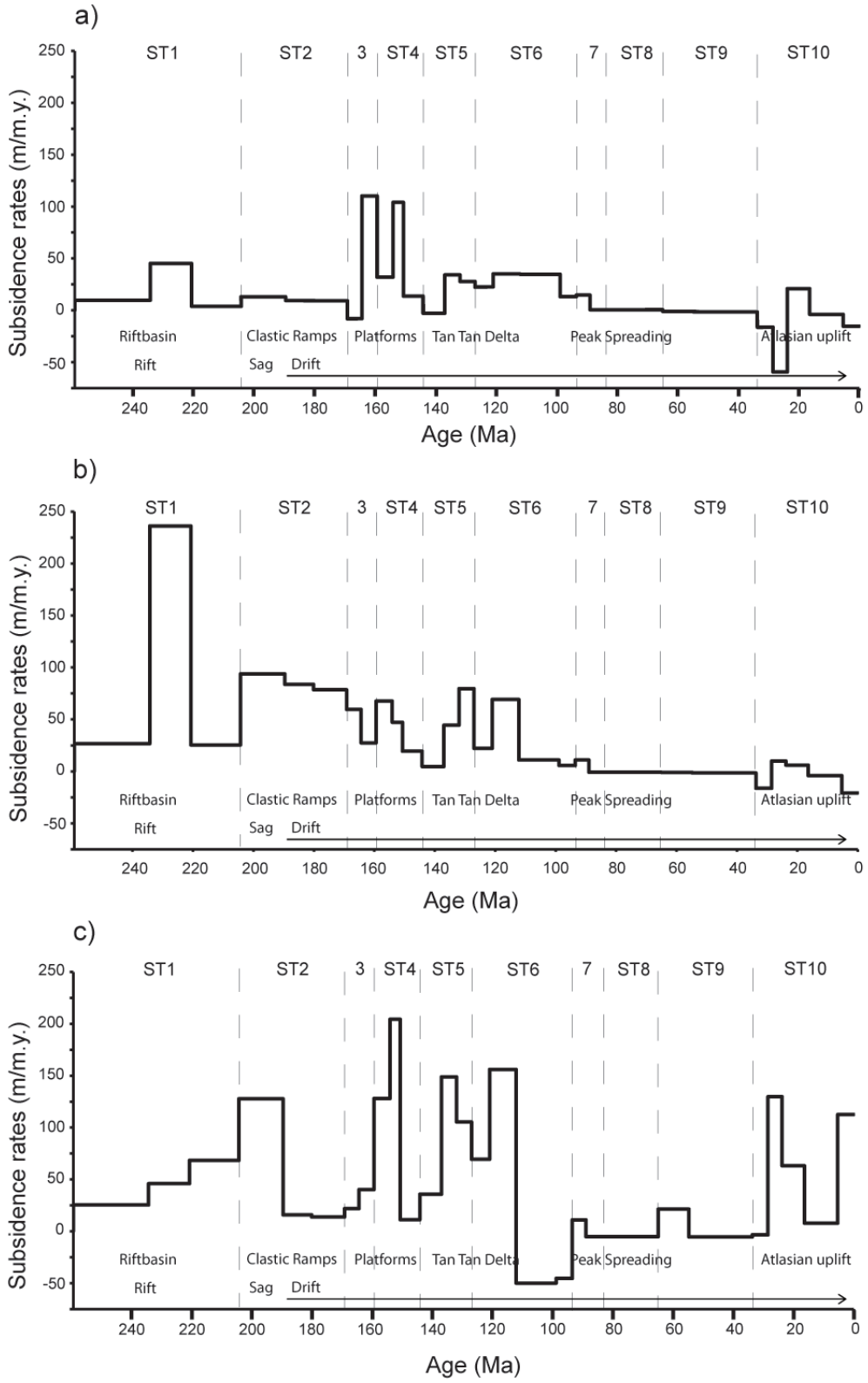

Fig. 107: Late Permian to present day subsidence on the a) inner shelf, b) outer shelf and c) slope areas. Subsidence rates up to 250 m/m.y. occurred in rift grabens (ST1), (b) during the sag stage (early ST2) the peak subsidence was located in outer shelf and slope areas; the progradation of Jurassic ramps was limited to the previous sag basin (ST2), (b) high subsidence occurred across the shelf during the Late Jurassic (ST4); Early Cretaceous delta development showed a gradient from low (<50 m/m.y.) to high (>150 m/m.y.) subsidence in distal direction (ST5, ST6). After a constant subsidence in the Late Cretaceous and Paleogene (ST8 & ST9), Atlasian uplift resulted in uplift onshore (a) and high subsidence offshore (c) during the Neogene (ST10). From Wenke et al. (subm.).

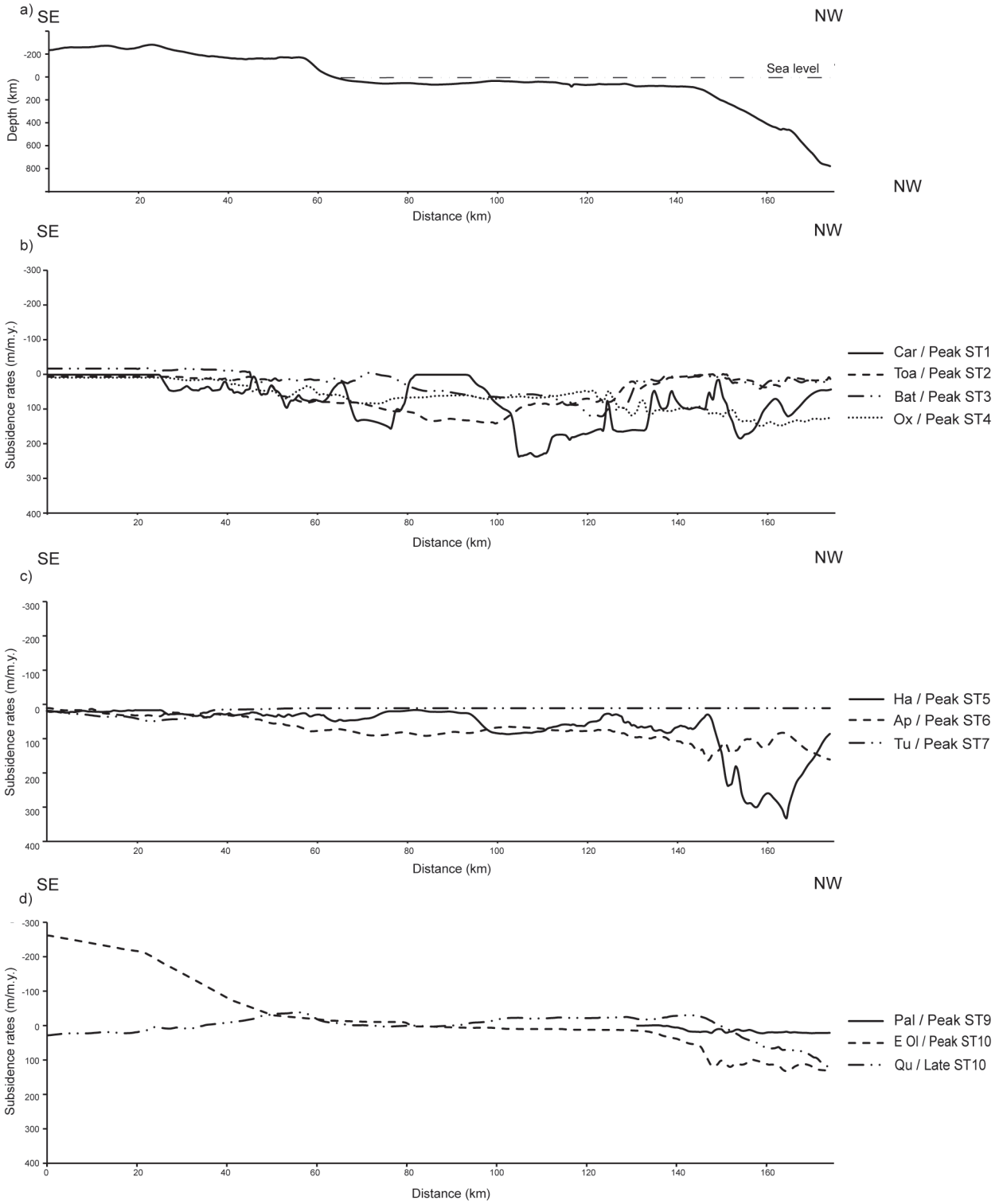

Fig. 108: Present day bathymetric profile (a) and total subsidence along the transect in time. Peak subsidence rates with values >200 m/m.y. occurred during the Carnian (ST1, b) in the Laâyoune graben and in Hauterivian on the Tan Tan delta slope (ST5, c). Onshore uplift of the most proximal shelf during the Early/Late Oligocene (peak ST10) led to widespread continental erosion and high sediment flux resulting in increased total subsidence in the basin (d). From Wenke et al. (subm.).

and Callovian times with the onset of the maturation of Triassic organic rich shales in the outer shelf area. The onset of Jurassic source rock maturation did not start before the Tithonian, expulsion may have started during the Hauterivian in the slope area and may still continue at present. However, figure 106 illustrates that the high oil prone Late Cretaceous source rocks are still immature as they never experienced

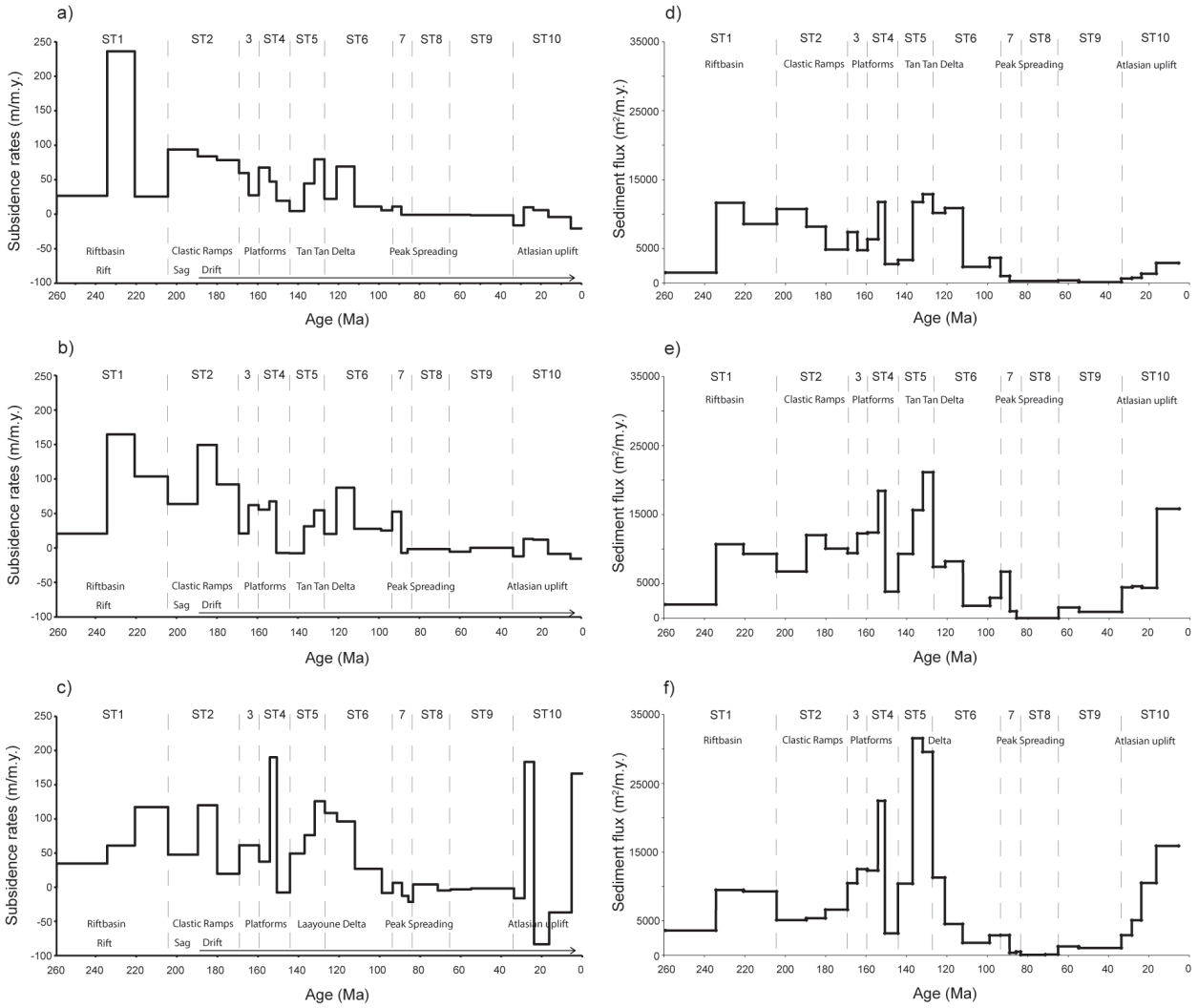

Fig. 109: Permian to present day quantitative subsidence history at the outer shelves of the a) Tan Tan, b) Cap Juby and c) Laâyoune transects vs. sediment flux (d-f respectively). For subsidence -trends see Fig. 100 and the text. Sediment flux in each transect followed the subsidence pattern. Note peak fluxes during the Early Cretaceous delta development (late ST5) and peak Atlasian terrestrial run-off (late ST10). From WENKE et al. (subm.).

sufficient subsidence in the shelf area.
In the deep offshore, Paleocene source rocks may have reached a state of early to mid-maturity however temperature is probably not high enough for hc-expulsion.

4.8.2 Subsidence and sediment flux

The subsidence rates for three locations on the Tan Tan transect are presented in Fig. 107, i) inner shelf (km 44), ii) outer shelf (km 109), and iii) slope (km 172.5). Each trend includes an identical general development pattern i) initially low to zero subsidence or uplift; ii) a gradual increase in subsidence to maximum rates; iii) in most trends, a final moderate decrease in rates occurs.

Rift to mature drift subsidence trends (ST1-ST6) are best developed in the outer shelf areas where erosional/depositional gaps are subordinate. Subsidence trends of the mature drift stages influenced by far-field effects of the alpine collision (ST7 – ST10) are best developed in the slope to basin areas as a consequence of low accommodation space on the shelf. The present day bathymetry of the Tan Tan transect and 2D peak total subsidence rates of each subsidence trend (ST1-ST10) are shown in Fig. 108. During ST1 to ST4 maximum total subsidence occurred in the area of the recent middle shelf. A shift to recent outer shelf to slope areas occurred during Early Cretaceous ST5 –ST7 trends. Uplift of the inner shelf area concurrent to subsidence in basin can be recognized during ST10 indicating a rotation of the left taper. Late Cretaceous (ST8) subsidence ra-

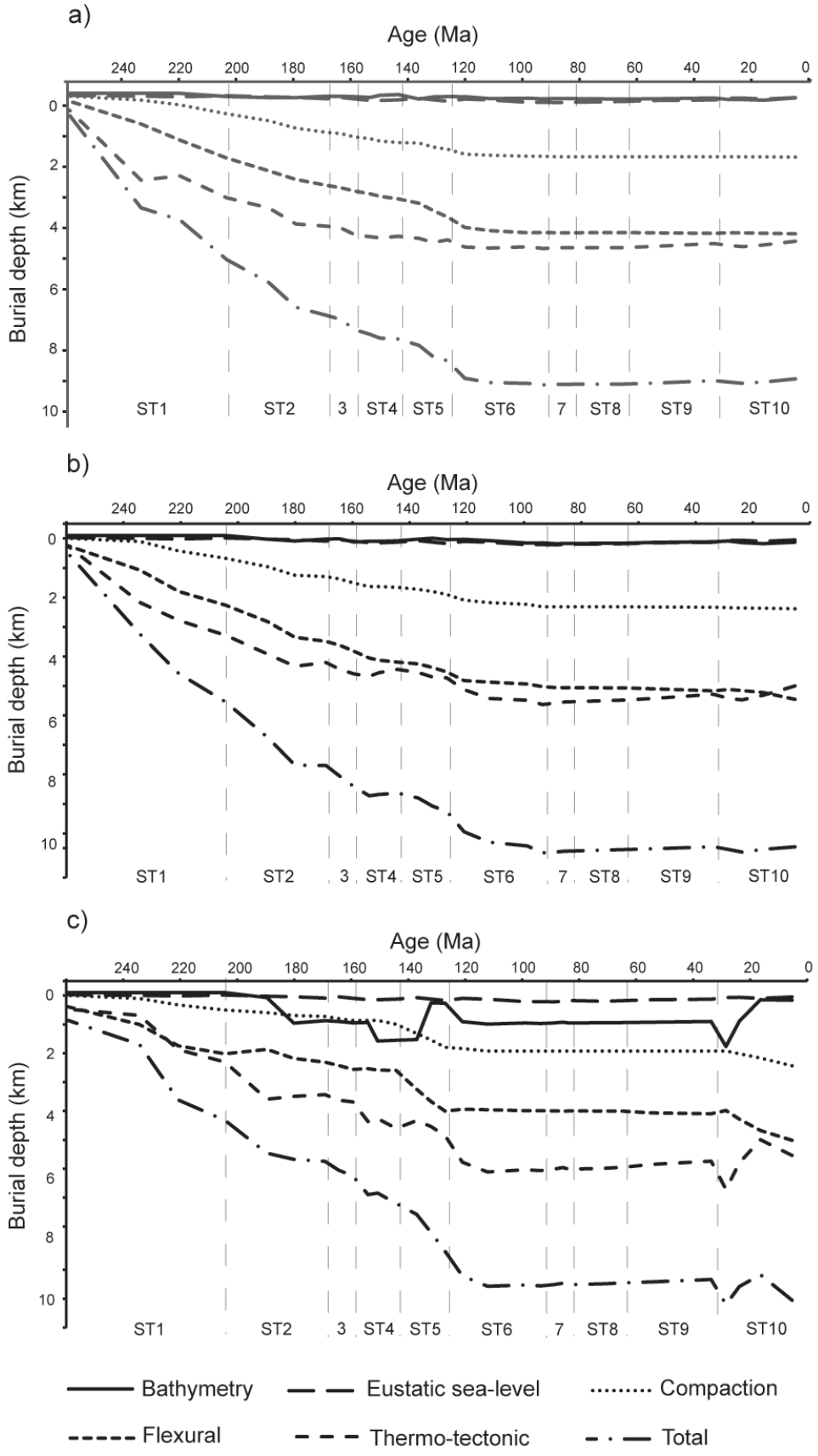

Fig. 110: Geohistory plots of the Tarfaya-Laâyoune Basins (259.3-0 Ma) from flexural basin modeling. The plots show total subsidence, thermo-tectonic subsidence, bathymetry and eustatic sea-level at the outer shelf of the a) Tan Tan, b) Cap Juby and c) Laâyoune transects (Wenke et al., subm.).

tes are not presented due to very low values.
Outer shelf subsidence of the three studied transects and total 2D sediment flux for each transect are given in Fig. 109. The sediment flux pattern fits fairly well with subsidence patterns over basin evolution; peak sediment flux rates occurred during ST4 (carbonate production), late ST5 (Tan Tan Delta) and late ST10 (post Atlasian run off).
Geohistory plots with total subsidence, its genetic components thermo-tectonic, flexural and compaction-induced subsidence, bathymetry and eustatic sea-level changes are given in Fig. 110.

4.8.2.1 Rift stage (ST1)

Inner to outer shelf subsidence in the Tan Tan area during ST1 shows peak rates of 50 m/m.y. in inner shelf and >225 m/m.y. in outer shelf regions (Figs. 100a & b) during the Ladinian to Carnian (234.3 – 220.7 Ma). This peak (>160 m/m.y.) can be recognized on the outer shelf of the Cap Juby area (Fig. 102). Subsidence rates decreased significantly to 25 - 120 m/m.y during the last rift stage of ST1 in the Norian to Rhaetian (220.7 – 204.3 Ma; Fig. 102). However, the present day slope (Tan Tan Transect) to continental rise areas (Laâyoune Transect) show peak subsidence rates between 70 m/m.y. to 120 m/m.y. during the same time (Fig. 107c). These subsidence variations refer to rift grabens and horsts, different positions on rotating growth fault block, or inaccurate biostratigraphic correlation. An opposite thermo-tectonic trend in outer shelf regions of the Laâyoune Transect (Fig. 110) supports the rotating growth fault block explanation.
The rift stage sediment flux pattern does not precisely reflect the outer shelf subsidence pattern in the Tarfaya area (Fig. 109). After a 2D sediment flux of 1,500 m2/m.y. (Tan Tan transect) to 4,000 m^2/m.y. (Laâyoune Transect) during Tatarian to Anisian, sediment input increases up to 7,500 m^2/m.y. (Tan Tan area) to 11,000 m^2/m.y. (Cap Juby area) during Ladinian – Carnian, but did not decrease as much as expected to values around 6,500 m^2/m.y. (Tan Tan transect) to 9,500 (Cap Juby and Laâyoune transects). This means, that the development of accommodation space during the first two rift stages was faster than the filling of the graben structures. Thermo-tectonic subsidence was the main genetic component during rifting triggering the development of fault blocks, normal faults as well as superordinated horst and graben structures.

4.8.2.2 Sag and early drift stage (ST2 –ST4)

During the sag stage (Early Hettangian to Late Pliensbachian; 204.3 – 189.6), total subsidence in the Tan Tan area increased from 25 to 100 m/m.y. in ST1, significantly higher than in the southern Tarfaya and northern Laâyoune Basins (50 - 65 m/m.y., Fig. 109). This difference is also reflected in thermo-tectonic subsidence (decreasing in the Tan Tan area, increasing in the Cap Juby and Laâyoune areas). Sediment flux patterns (Laâyoune: 5,000 m^2/m.y. Tan Tan: 10,000 m^2/m.y.) on all three transects equal the respective subsidence pattern.
Initial sea-floor spreading resulted in an increase of thermo-tectonic subsidence in the Tarfaya Basin (Fig. 9). Outer shelf total subsidence rates reached up to 90 m/m.y. (Tan Tan transect) and 150 m/m.y. (Cap Juby transect) in the Toarcian (189.6 - 180.1 Ma). They decreased until the end of ST2 (169.2, Late Bajocian) to 20 m/m.y. (Laâyoune transect) and to 80 m/m.y. (Cap Juby transect).
Outer shelf subsidence rates showed several peaks in time, in the Laâyoune area during the Bathonian (169.2 – 164.4 Ma) from 20 m/m.y. to 50 m/m.y., in the Cap Juby area during the Callovian (164.4 – 159.4 Ma) from 30 m/m.y. to 60 m/m.y., and in the Tan Tan area during the Oxfordian (159.4 – 154.1 Ma) from 25 to 65 m/m.y. (Fig. 109).
Flexural and compaction-induced subsidence reach higher amounts of total subsidence during this period (Fig. 110). High subsidence rates during the Bathonian do not correlate with high sediment flux (Tan Tan: 7,500 m^2/m.y.; Cap Juby and Laâyoune: 10,000 m^2/m.y.). Accommodation space increased significantly during early to middle ST4 (159.4 – 150.7 Ma, Oxfordian – Kimmeridgian) because of increasing total subsidence and a eustatic sea-level rise. Sediment flux including carbonate production increased as well and filled up to exceeded the rate of accommodation space.
In the latest Kimmeridgian, total subsidence rates decreased significantly across the Tan Tan area (Fig. 108). During the Tithonian (150.7 -144.2) (Fig. 8), outer shelf total subsidence decreased from 60 m/m.y. to 10 m/m.y. (Tan Tan) and 190 m/m.y. to -5 to 10 m/m.y. (Laâyoune, minor uplift). Sediment flux decreased from 12,000 m^2/m.y. (Tan Tan) and 22,000 m^2/m.y. (Laâyoune) to 4,000 - 5,000 m^2/m.y.

4.8.2.3 Mature Drift stage (ST5-early ST6)

Initial Tan Tan and Laâyoune delta settings include marine fans and turbidites in front of the pre-existing Jurassic continental slope. Subsidence was confined to these regions (Fig. 107).
Subsidence rates increased during ST5 on all transects (50 – 125 m/m.y. at the end of ST5; 127.0 Ma; Hauterivian) (Fig. 102). Thermo-tectonic uplift in the Early Cretaceous was exceeded by flexural and compaction-induced subsidence (Fig. 110) caused by high sediment flux. Peak sediment flux in the Tarfaya-Laâyoune Basins is reached in ST5 on all transects with up to 14,000 m^2/m.y. (Tan Tan) and >30,000 m^2/m.y. (Laâyoune) (Fig. 109).
The total subsidence decreases during ST6 from 75 m/m.y. (Tan Tan transect) -100 m/m.y. (Laâyoune transect) to -15 – 5 m/m.y. Sediment flux decreased from 10,000-15,000 m2/m.y. (Laâyoune, Tan Tan) to 2,000 m^2/m.y. – 4,000 m^2/m.y.

4.8.2.4 Mature Drift stage with initial alpine convergence (late ST6 to ST8)

A minor increase in subsidence to 15 m/m.y. (Laâyoune)/ 50 m/m.y. (Tan Tan) took place at the beginning of ST7 (93.5 Ma, Tur.; (Fig. 109). The increase was strongest in slope and basin areas (Fig. 101).
During ST8 (83.5 -65.0 Ma, Coniacian – Maastrichtian) the depocenter shifted to slope and basin areas with no deposition on the shelf and the development of a shelf margin wedge started in Late Maastrichtian. On the shelf, minor total subsidence prevailed during ST8 (<10 m/m.y.) (Fig. 109).

4.8.2.5 Mature Drift Stage with Atlasian Compression and Initial Uplift (ST9)

During ST9, subsidence is restricted to outer shelf, slope and basin areas (Fig. 107). An initial subsidence peak occurs only in the Tan Tan area (Fig. 100). In the Cap Juby and Laâyoune areas, increasing subsidence rates occur only during late ST9 (Fig. 109). Sediment flux remained small throughout ST 9.

4.8.2.6 Mature Drift Stage with Peak Atlasian Uplift and Erosion (ST10)

Increased erosion in the High Atlas range and sediment bypass of the inner shelf resulted in high sedimentation rates in outer shelf areas (Laâyoune region, Fig. 109). Flexural subsidence in slope areas (Tan Tan region, Fig. 107) amounted to 150-200 m/m.y. Sediment flux shows major lateral changes in the study area, 4,000 m2/m.y. in the Tarfaya-Laâyoune Basins and 18,000 m2/m.y. in the Cap Juby area (Fig. 109).

4.9 Summarized basin evolution chart

Table 6a & 6b shows a summarized chart illustrating i) chronostratigraphy, ii) stratigraphic ages, iii) Lithostratigraphy, iv) unconformities, v) formations, vi) onset of source rock maturation, vi) tectonic stages, vii) 3rd order sequence stratigraphic trends, viii) subsidence trends, ix) eustatic sea-level curve, x) Atlantic polarity chronozones, xi) Sea-floor spreading (SFS) half rates and xii) regional tectonic development.
In order to assess the potential influence of changes in sea-floor spreading (SFS) half-rates and resulting intra-plate balance forces ("ridge push", e.g White & McKenzie 1989) on the southern Moroccan continental margin, sea-floor spreading rate changes in the Central Atlantic (Table 1) have been correlated to the subsidence rates in the Tarfaya Basin. SFS half-rates are based on Klitgord and Schouten (1986), Vogt & Tucholke (1986), Olivet (1996), Vogt & Tucholke (2000), and Contrucci et al. (2004).

4.10 Errors and uncertainties

A detailed error calculation under consideration of additional error propagation has not been calculated in this thesis as the sources of errors are numerous.
Modeling does not necessarily produce unique results, but presented results represent the geologically most plausible model with the highest confidence possible based on the available data resolution.
Hence, error source and, if possible, standard deviations are described and calculated in this chapter. However, the sum of all errors will not affect the major results of this study.

4.10.1. Field work

Field work has been performed under guidance and supervision of local geologists from ONHYM with excellent regional geographical and geological knowledge and experience. However, paleontological and/or palynological analysis has not been performed during the AMP except for the Albian to

Table 6a&b: Late Paleogene to recent chrono- and lithostratigraphy for the Tarfaya-Laâyoune Basins and key controls on basin development. Formations after Choubert et al. (1966) and Ranke et al. (1982). The onset of HC generation

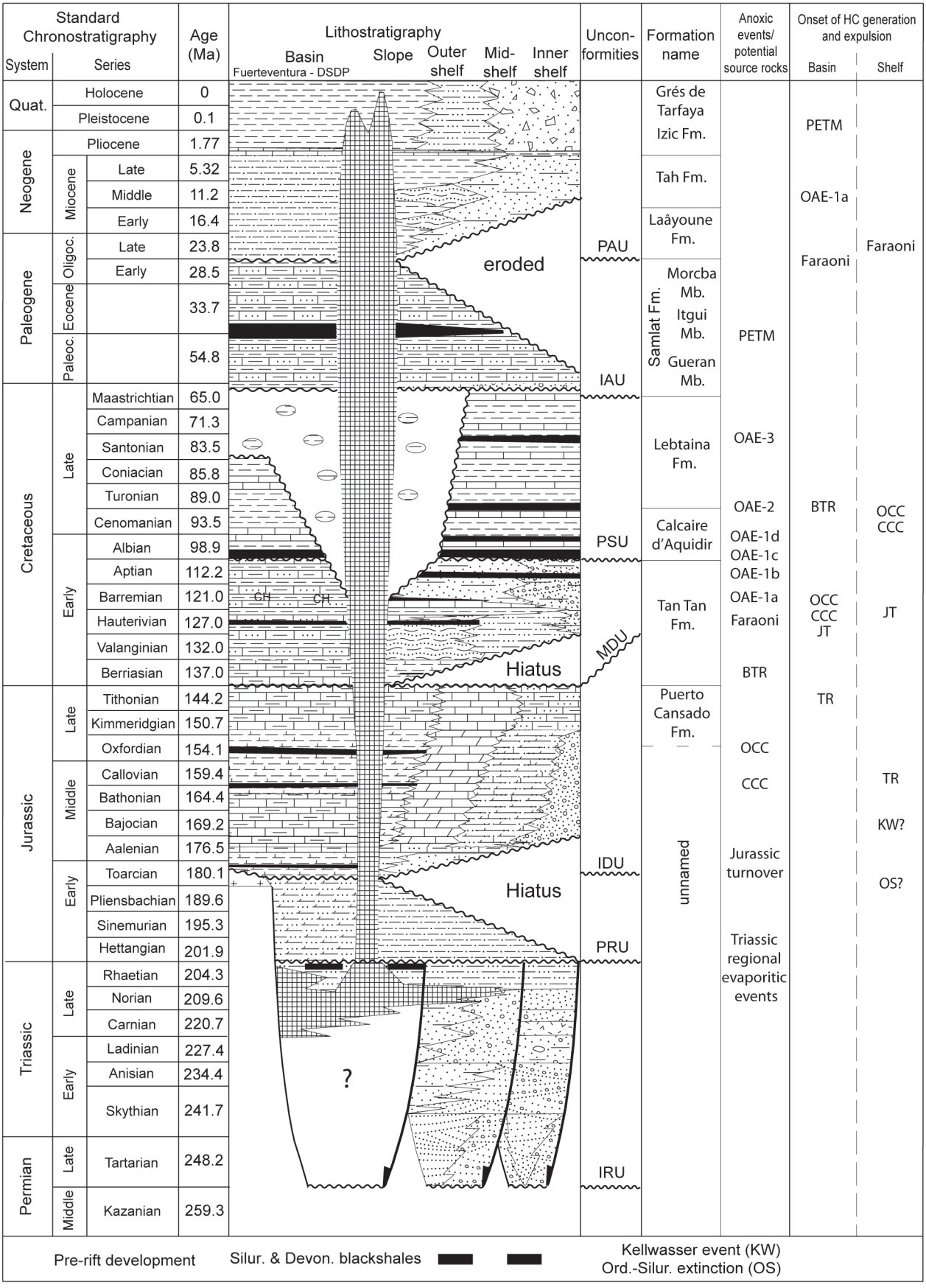

is based on the basin modeling in this study and current geothermal gradients (Zarhloule et al. 2005). Summary of Central Atlantic developments after Zühlke et al. (2004), Contreras et al. (2010) and Heine et al. (2013).

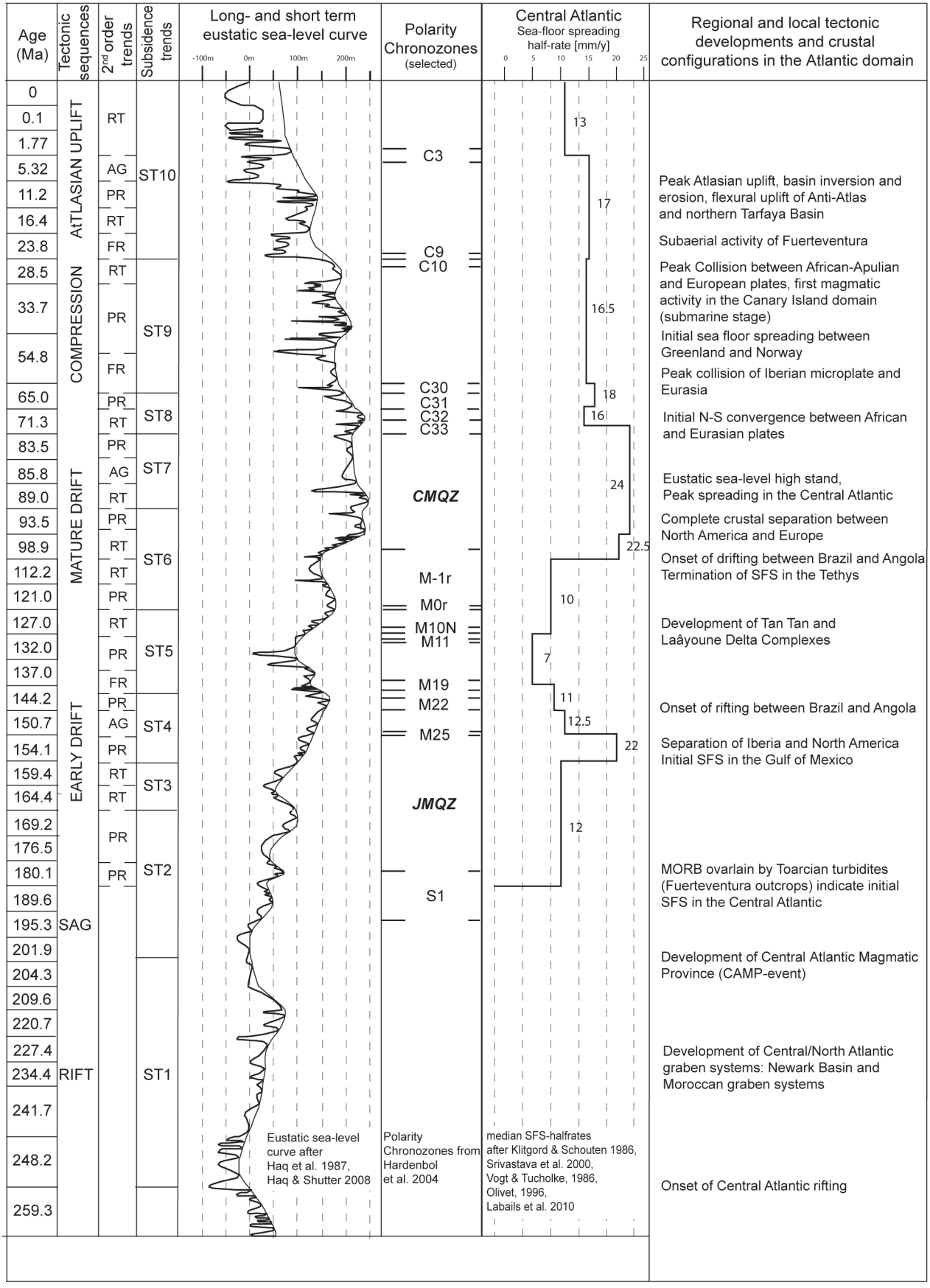

Maastrichtian succession (Aquit, in prep.). The stratigraphic assignment of the collected samples and mapped outcrops is still mainly based on the works of Choubert et al. (1966), Ranke et al. (1982) and El Khatib et al. (1995). As in some areas, field mapping has been used as input data for seismic interpretation, mainly in onshore areas without well control, where an error of one or two phases (10-20m in vertical direction) has to be considered.

4.10.2 Well data

The correct stratigraphic interpretation of well successions is dependent on mainly four factors: i) regional lithostratigraphic zonation, ii) the well site geologist during well campaigns, iii) well logging and iv) biostratigraphy.
As the regional lithostratigraphic frameset is, as a consequence of underexploration, limited, its resolution in depth is not much supporting for mud interpretation. Is the post Aptian succession subdivided into seven formations (Grés de Tarfaya, Izic, Tah, Laâyoune, Samlat, Lebtaina & Calcaire d'Aquidir formations), so is the pre-Albian subdivided into two formations (Tan Tan & Puerto Cansado formations) of Early Cretaceous and Late Jurassic. Mid & Early Jurassic as well as Triassic has not been described in more detail so far. The pre-Albian is the succession with the most prolific source rock formations and reservoirs.
Well site geologists mainly recognized changes from carbonates to clastics as a lithostratigraphic boundary between Calcaire d'Aquidir and Tan Tan formation or from clastics to carbonates at the boundary Tan Tan/Puerto Cansado formations and from grey to red at the IDU which is in general described as Early Jurassic to Triassic. Inconsistencies have been recognized during well evaluation for the definition of the top Lower Cretaceous which was sometimes Aptian and sometimes Albian in age. However, as the Tan Tan Delta became inactive in Late Aptian, the Top Lower Cretaceous was often assigned wrong as it should be the top Tan Tan formation. It has to be considered that lithostratigraphic changes do not always correlate with timelines as facies changes evolve through time.
Inaccurate chronostratigraphic assignments have also be recognized at the Pliensbachian/Toarcian boundary where marine drift clastics overlie „Triassic" rift red beds of Sinemurian/Pliensbachian.
In addition, it has also be considered that every well site geologist has their own interpretation technique and may set well tops different to that of their colleagues.
These „errors" are punctual and cannot be quantified. To eliminate these errors a consistent stratigraphy has been developed for this study mainly based on sequence stratigraphy and biostratigraphy if available. However, sharp boundaries are not often described.
Well log data was available as paper prints and was digitized during this study and are considered accurate enough for inclusion. Differences between depth values recorded during drilling versus depth values recorded during loggingare in general considered neglible (0-10m).
Well log interpretation regarding their sequence stratigraphic log patterns is in general reliable for clastic successions of 3rd and 4th order. Diagenetic overprint of grain sizes should affect lower orders of higher resolution (5th and 6th order pattern detection).

4.10.3 Seismic data

A significant amount of errors can add up during seismic acquisition, processing, and time/depth conversion of which a seismic interpreter and geomodeler has no control. In general marine seismic is more accurate than onshore seismic as the airgun is the more constant energy source while the receiver pattern is constant during one survey and the sea has no relief.
Onshore, geophone pattern and shotpoints often show higher offsets as planned with geographic coordinates needing to be determined for every receiver station, shot point and CMP.
The static data as well as the LWL have to be integrated properly. A poor knowledge of the LWL zone can result in several hundred of meters misinterpretation even though the layer is only a few meters thick.
In addition, technology developed and data quality has become more accurate through time. This was noticed during the setup of the project as older lines had to be stretched and shifted at cross-points such that reflector pattern became more or less traceable over different seismic surveys and data qualities. A quantification of these errors and uncertainties is not possible as the input/seismic raw data was not available.
The uncertainty during horizon interpretation increases with depth especially when data quality decreases. In particular the pre-drift basin fill was often

poorly represented on the seismic dataset.
The error of the time/depth conversion of the seismic dataset, which is based on 1D check shot data, has a standard deviation (SD) of 2.5 to 5% (c.f. Carter & Hyatt, 1990).
For lateral correlation between the well points this deviation can increase in the vertical plane below the well also. The petrography, the grade of compaction as well as the water content of the strata can vary significantly. It is assumed that the SD increases to 10-15% for the slope and basin area as well as the basin fill below 5000m depth.
The high resolution sequence stratigraphy performed in sub-seismic resolution is highly dependent on trace automatic determination.

4.10.4 Flexural reverse modeling

Since the software used is not able to model crustal stretching, the highest error in the modelled part results from an underestimated compaction of the rift basin fill, as well as lateral variations in expansion.

5. Synthesis & conclusions

5.1. Basin development

The Tarfaya-Laâyoune Basins represent a classic passive continental margin (e.g. Einsele, 2000). Following Duval et al. (1998), the basin evolution took place during the current encroachment cycle (Fig. 111), a 1st order sequence defined by the initial break-up of Pangaea and ending with the final fusion of „Pangaea Ultima“ (Scotese, 2006; Williams & Nield, 2007) in approx. 150 to 250 m.y.

Seismic images illustrate that this 1st order sequence is bound at the base with a bright reflector above a chaotic reflector pattern, the IRU, and the present day first break at the sea-floor. These two reflectors bound the whole basin fill which was developed during the continental encroachment cycle. Its geometry (idealized) follows the shape of an upsidedown scalene triangle with the short side represented by the left/continentward taper, the medium side represented by the right/basinward taper and the long side the sea-floor/land surface. The contact of the two short sides is the position of the the maximum sediment load.

Compared with marginal seas like the Norwegian Sea, where three rift phases stretched the rift and sag stage covering of >200 m.y., the Tarfaya-Laâyoune Basins 1st order sequence is developed with a clear amplitude.

The post-IRU evolution of the basin architecture is mainly controlled by six tectonic sequences/tectonic stages or 2nd order sequence stratigraphic cycles (e.g. Myers & Milton, 1996; Fig. 112) with a duration of approximately 50 m.y. The six sequences contain ten subsidence trends: i) rift & sag (duration: 69.7 m.y.; ST1 and early ST2), ii) early drift (duration: 45.4 m.y., late ST2-ST4), (iii) mature drift (duration: 32.0 m.y., ST5-ST6), iv) mature drift with initial Alpine convergence (duration: 47.2 m.y., ST7-ST8), v) mature drift with initial Atlasian compression and uplift (duration: 36.5 m.y., ST9) and vi) mature drift with peak Atlasian uplift and erosion (duration up to now. 28.5 m.y., ST10). The first three tectonic sequences are part of the transgressive phase of the current continental encroachment cycle, the fourth marks a turning point while the last two are part of

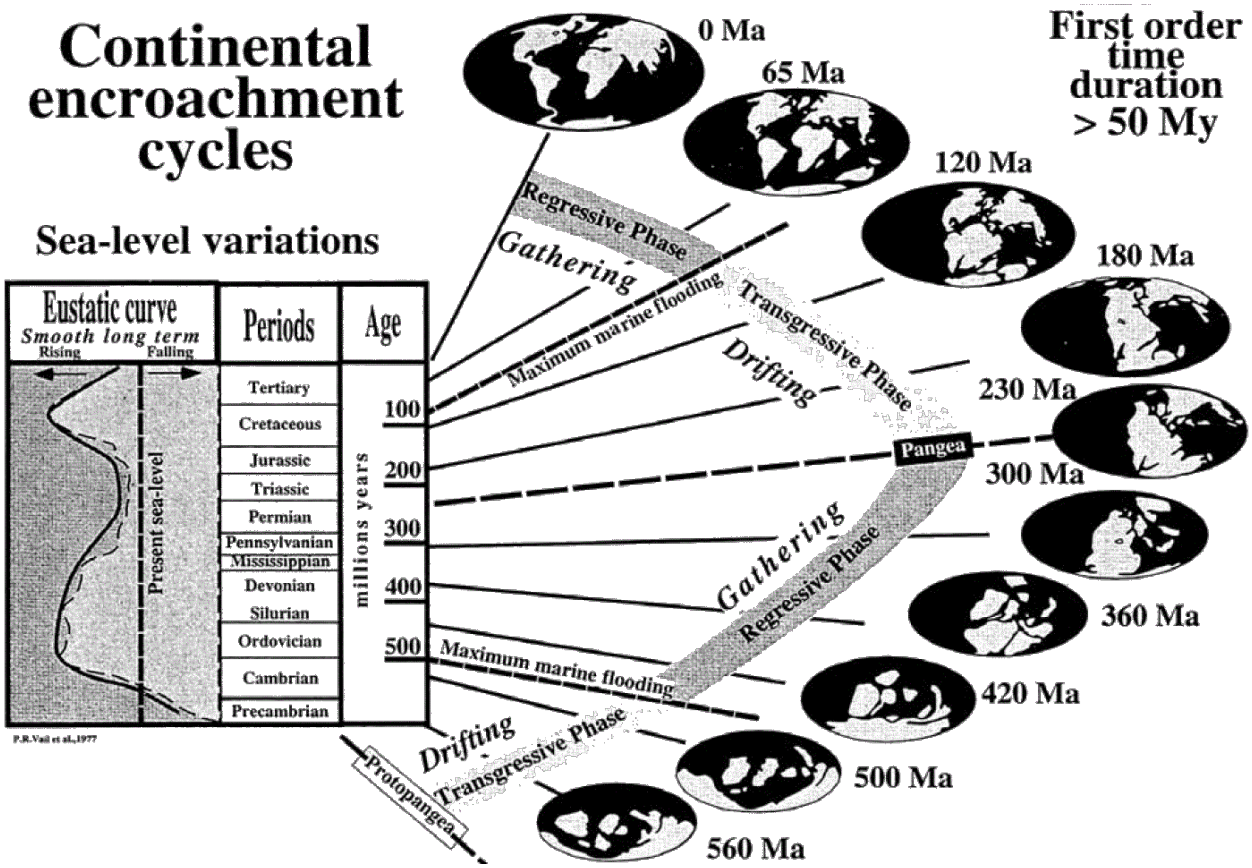

Fig. 111: Two Phanerozoic encroachment cycles/1st order sequences associated with the break-up and gathering of supercontinents (Duval. et al. 1998).

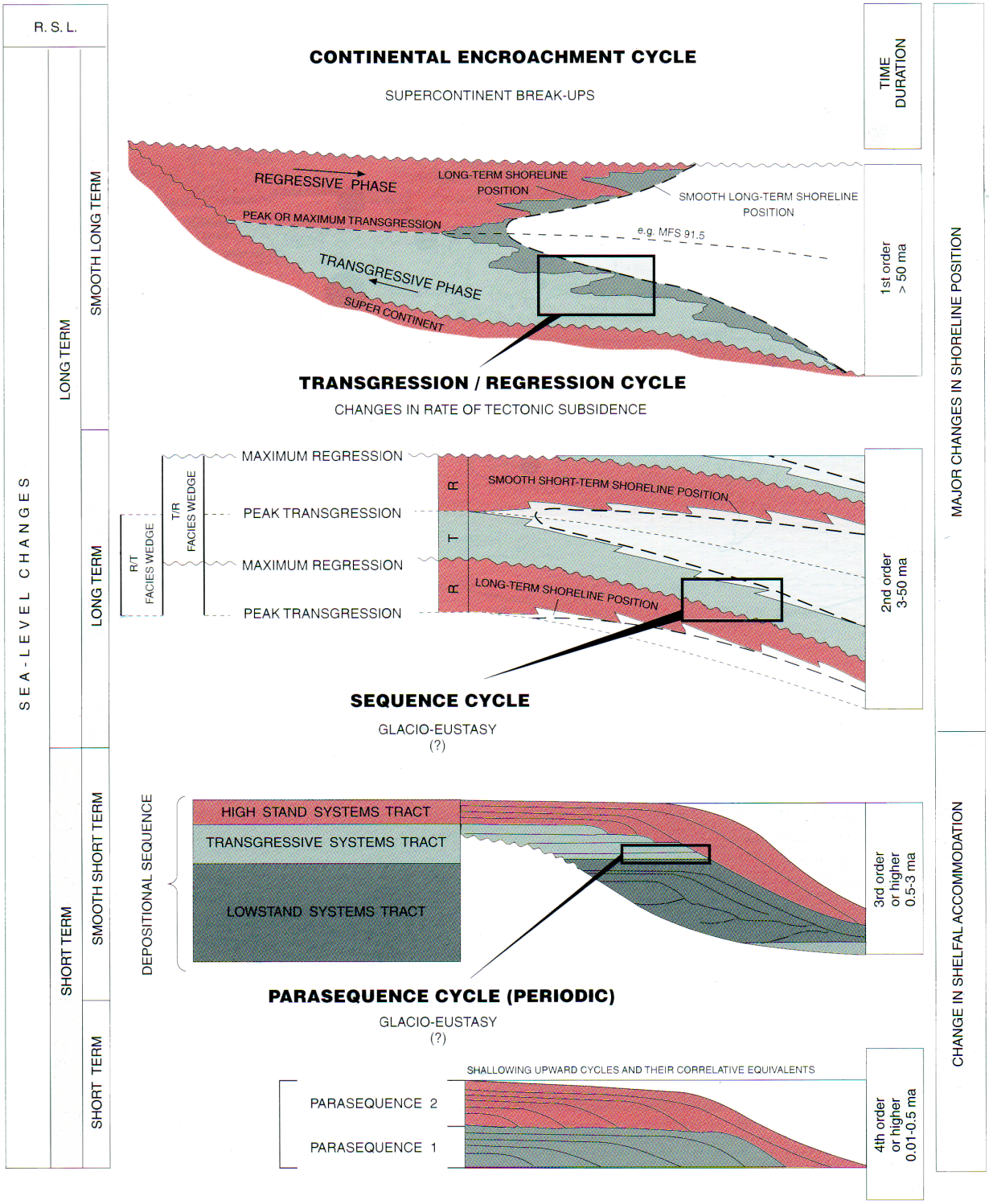

Fig. 112: Hierarchy of stratigraphic cycles (from Myers & Milton, 1996; after Duval et al., 1992).

the regressive phase.
The boundaries of these 2nd order sequences are cleary defined by unconformities which mark major changes in basin architecture.

5.1.1 Second order sequences

5.1.1.1 Rift and sag stage

The first tectonic sequence includes the period from onset of rifting to the end of the sag phase (259.3 - 189.6 Ma).

The IRU is the base of the rift and sag basin fill which is mainly bound to the three Triassic grabens of the study area. It defines the onset of the transgressive phase of the Atlantic super cycle. Subsidence was very rapid with peak values >225 m/m.y. (Fig. 107) in central graben areas, supporting the assumption that the highest subsidence rates during basin evolution are bound to the rift stage (e.g. Einsele, 2000; Veselovský, 2004). The erosion of elevated graben shoulders resulted in 2D peak sediment flux rates up to 11,000 m^2/m.y. (Fig. 109)
The PRU and the IDU represent a transitional period from rift to drift - the sag phase. During this period the majority of rift faults became inactive. At the end of the sag stage, the basin geometry is dominated by a ramp with an inclination <1° terminating very abruptly at a proto-shelf edge. In the NW-W direction of the ramp break the main rift basin or proto-Atlantic is situated.
The terrace-like proto-shelf (Fig. 7) includes the two failed rift halfgrabens Chebeika Graben and Laâyoune Depression (approximated ß-factors around 1.05 to 1.1) which by end of the sag stage are completely filled up with sediments.
The proto-Atlantic includes a amount of tilted fault blocks covered by evaporites from early episodes of marine ingressions.

5.1.1.2 Early drift stage

The second tectonic sequence which is marked by the onset of sea-floor spreading and oceanic crust production, includes the early drift phase (189.6/184.1 - 144.2 Ma) defined by decreasing but still dominant thermo-tectonic subsidence (Fig. 110). Peak subsidence rates reach values above 150 m/m.y. (Fig. 109). To compensate this rapid subsidence during a period of low clastic sediment input, a high carbonate production fills up the generated accomodation space with flux rates of about 10.-12.000 m^2/m.y. (Fig. 109).
Minor amounts of sediment were transported during the flow of MTCs to the young oceanic basin. This second tectonic sequence is a continuation of the superimposed transgressive phase and correlates with continuously increasing SFS-half rates (Tab. 6).

5.1.1.3 Mature drift stage

The third tectonic sequence shows a contradictory development compared to the cratonic supercycle. The exposition of the Jurassic shelf and the subsequent development of large-scale delta systems on top of the MDU describe a major regression during a time of global divergence. This regression correlates with a significant reduction of SFS-half rates and the break-up of the South Atlantic.
During this tectonic sequence, the depocenter shifts basinward from the top of the Jurassic shelf, where the lower deltaplains develop as condensed sections into the adjacent proximal basin, and turbidite flow into distal areas. There, peak subsidence rates of 125 m/m.y. can be reached while the sediment flux reaches the highest amounts during basin development in all three analyzed areas with values up to >30.000 m^2/m.y. (Fig. 109). Total subsidence is mainly flexural and compaction induced which reflects progressive drifting.

5.1.4 Mature drift stage with initial Atlasian conversion

During the early fourth tectonic sequence, sediment supply from the hinterland was significantly reduced while open marine conditions prevailed on the entire shelf during that mid stage. The deposition of shales and carbonates is more or less equally distributed over the entire basin. The SFS-halfrates in the Central Atlantic reach a record high during the Late Cretaceous correlating with the early drift phase in the South Atlantic. Subsidence rates as well as sediment flux are negligible.
A reduction of the SFS-halfrates during the Santonian to Maastrichtian marks the turning point from superimposed transgression to regression and the onset of Alpine convergence.

5.1.1.5 Mature drift stage with initial Atlasian compression and uplift

During the fifth tectonic stage, the depocenter shifts further in basinward direction and a shelf wedge develops on top of the upper Cretaceous slope.
The major subsidence trend shows an onset of basin inversion and the genetic components reflect contradictory trends. While flexural and the compaction induced subsidence remains positive, the thermo-tectonic component indicates uplift (Fig. 110).

5.1.1.6 Mature drift stage with peak Atlasian uplift and erosion

During the sixth stage, proximal areas of the Tarfaya-Laâyoune Basins undergo flexural uplift control-

led by Atlasian uplift. Depending on the position on the shelf, subsidence rates can be positive (basin) or negative (inner shelf, Fig. 107). Major erosion in the High Atlas and the Anti-Atlas significantly increase the amount of sediment flux into the basin concurrent to negative shelf subsidence. This caused the additional shift of the depocenter into the open basin bypassing the entire shelf.

5.1.2 Third order trends

Regional 3rd order sequences and the basin architecture in three areas highlight common features and lateral heterogeneities in the basin development and subsidence history of the Tarfaya and northern Laâyoune Basins. At large scale, basin development and depositional architecture are comparable within the study area. They show many similarities to the northern Agadir Basin (Zühlke et al., 2004) and the northern Moroccan continental margin segments (Le Roy, 1997; Hafid, 2000a). This coherency indicates that far-field plate-tectonic reconfigurations in the Atlantic (and at a later stage the Western Tethys and Alpine plate convergence/collision) exerted key controls on the basin development along the Morrocan margin.
Regional differences in basin development between the Tarfaya Basin and the northern Laâyoune Basin are driven by: i) the flow of Triassic salt, triggered by the rapid increase in burial depth since the Early Cretaceous (Tarfaya Basin); ii) flexural uplift of the lower slope area caused by volcanism of the Canary Island since the Late Paleogene (Tarfaya Basin) and iii) flexural uplift of the inner shelf with its highest rates in the northeastern part of the Tan Tan region caused by Atlasian uplift and Anti-Atlasian southward escape tectonics since the Neogene (e.g. Zouhri et al. 2008).

5.2 Basin fill and subsidence development during superimposed transgression

5.2.1 Rift & sag

After the subduction of the Rheic Ocean and the collision of Gondwana and Laurussia during the Carboniferous, the resulting Western and Central Variscan-Allegheny Mountain Range became the area of initial Central Atlantic rifting. The period of rifting is associated with i) the erosion and isostatic equalisation of the Appalachian-Anti-Atlasian Orogeny, ii) the northernward drift of Gondwana, and iii) a counter-clockwise rotation of Pangaea itself during the Early Permian to Early Jurassic (Blakey, 2008). This rotation, in combination with indenter effects and escape tectonics as well as lithospheric overthickening in the orogenic belt, resulted in uplift and extension of the axial parts of the Variscan belt (Ziegler & Cloetingh 2004; Veevers 2004). Furthermore, collisional stresses exerted on a craton may cause far-field tensional or transtensional reactivation of pre-existing fracture systems and thus the development of rifts and pull-apart-basins (Ziegler & Cloetingh, 2004).
The separation and breakup of large landmasses like Gondwana and Laurussia are not concentrated along a single lineament. Rather, up to 25 graben systems were active on both sides of the Atlantic during early rifting (Le Roy & Piqué, 2001; Letourneau & Olsen, 2003). Le Roy & Piqué (2001) and Gouiza (2010) suggested that during early rift, the three N-S-oriented (half-) graben systems of the Tarfaya-Laâyoune Basins developed by fault-controlled extension. Graben development ceased first in the Chebeika Graben and later also in the Laâyoune Depression. Despite relatively little bio- and lithostratigraphic information available for the Late Permian to Early Triassic basin fill the following results from this study support the model of Le Roy & Piqué (2001) for the rift development of the Tarfaya-Laâyoune Basins: the basement geometry, the reflector pattern of the graben fill, the distribution of rift salt in the study area and the subsidence patterns. Thermo-tectonic subsidence was the main genetic subsidence component during rifting with brittle extension (ST1, Fig. 110). Peak subsidence at inner to outer shelf regions took place during mid ST1 (Ladinian – Carnian). Peak subsidence in present day slope and basin areas was related to the final rift stage in late ST1 (Norian – Rhaetian) or the following sag stage in early ST2 (Hettangian – Pliensbachian). The rift stage (Fig. 109) shows low sediment flux in early ST1, high flux during mid ST1 and a moderate decrease during late ST1. In general, the brittle extension of the lithosphere during the rift phase led to a rise of the asthenosphere and an increased heat flow rate (Frisch et al. 2011). By the end of rifting, thinned crust, in combination with widespread extensional fault zones and thick damage zones, allowed basaltic mantle magma to intrude into the upper crust and finally extrude.
This widespread basaltic intrusive and effusive magmatism (CAMP, Central Atlantic Magmatic

Province, Hames et al. 2003) has a Latest Triassic age (Cirilli et al., 2009) of 200 Ma (Knight et al., 2004) to 201 Ma (Marzoli et al., 1999) and occurred approximately concurrent to the development of the PRU (Rhaetian-Hettangian, 204.3 – 201.9 Ma). The CAMP volcanic rocks represent the transition from fault-related rifting to a post-rift but pre-drift sag stage.

With the termination of extensional faulting by the end of ST1 and ongoing crustal extension caused by thermal re-equilibration between the asthenosphere and the lithosphere during the sag stage (early ST2), flexural subsidence took over as the main genetic component of total subsidence, as indicated in the outer shelf areas (Fig. 110). With initial sea-floor spreading, three terraces subdivide the Tarfaya-Laâyoune Basins: i) the area continentward of the hinge zone, ii) the eastern sag basin covering the Chebeika and Laâyoune depression, and iii) the proto-Atlantic basin. Main areas of subsidence are located in the Laâyoune Depression and the proto-Atlantic while structural highs like the Chebeika and Juby Horsts show minor subsidence and thermo-tectonic uplift.

5.2.2 Early drift

With the onset of sea-floor spreading during mid ST2 (Pliensbachian/Toarcian), thermo-tectonic subsidence was still the dominant genetic component of total subsidence (Fig. 110). Incipient ridge-push forcing may have caused an increase of flexural subsidence in outer shelf to basin regions, but thermal cooling was the main driving force of accommodation space generation in the outer shelf and basin area. Thermal cooling and erosion of elevated graben shoulders during the rift stage (cf. Frisch et al. 2011 for mechanism) had largely levelled the rift topography. The accommodation space generated during the early drift phase was filled by a clastic to carbonate ramp consisting of 13 sequences. With the end of ST2 (Bajocian) sediment input was significantly decreased (Wenke et al. 2011).

Carbonate production could not compensate for the generated accommodation space by thermo-tectonic subsidence during ST3 (Bathonian-Callovian). As a consequence, the depositional system retrograded during the Callovian (Fig. 98). Even if log pattern interpretation is challenging in carbonate systems, nine 3rd order sequences have been identified.

Thermo-tectonic subsidence decreased during ST3 (169.2 to 159.4 Ma) with the increasing distance between the Central Atlantic spreading axis and the adjacent continental margin. A major reason for increasing burial during the Middle and Late Jurassic was the steady eustatic sea-level rise which allowed high carbonate production until the Late Kimmeridgian / Early Tithonian (ST3 – Mid ST4).

Accommodation space generated by flexural and compaction-induced subsidence during ST4 was first filled by prograding carbonate ramps containing three sequences followed by seven aggrading sequences building up a carbonate platform where carbonate production kept pace with the generation of accommodation space. During this time, ridge push forces remained unaltered given the constant spreading rate of 19 mm/y (Klitgord & Schouten, 1986; Srivastava et al., 2000; Vogt & Tucholke, 1986).

When clastic input was at its minimum during the early drift stage, a positive feedback process between carbonate production and flexural/total subsidence took place (Fig. 110). Any accommodation space created was filled and partly exceeded by carbonate production.

Up to this point in basin development, the depositional system shows a continuous superimposed transgressive trend from the onset of rifting at ST1 to the build-up of carbonate platforms in ST4. The top of ST4 represents a major flooding surface.

5.2.3 Mature drift to maximum flooding

The MDU marks a significant change in the Tarfaya-Laâyoune Basin development, which was controlled by the following developments: i) the onset of crustal separation between Africa and South America (Blakey, 2008), ii) a climate change from arid to humid conditions in the western Tethys and Central Atlantic areas (Bádenas et al., 2001; Bover-Arnal & Strasser, 2013), and iii) the major global eustatic sea-level fall in the Latest Jurassic/Early Cretaceous (Hardenbol et al., 1998).

The time delayed rifting in the South Atlantic may have had a negative impact on the Central Atlantic spreading velocity. A reduction of sea-floor spreading half-rates from approx. 19 to 7 mm/y (Klitgord & Schouten, 1986; Srivastava et al., 2000; Vogt & Tucholke, 1986) was related to the build-up of intraplate tensional stresses during the break-up of Gondwana (Guiraud et al., 1992) and resulted in reduced thermo-tectonic subsidence to minor uplift in ST5. Thermo-chronological models for the Western Anti-Atlas domain indicate its exhu-

mation during the Early Cretaceous. Additionally, a Proterozoic source area was uplifted, either in the Eastern Anti-Atlas and/or the Reguibat/West African Craton (Sehrt, 2014; Bertotti & Gouiza, 2012; Frizon de Lamotte et al., 2009). Uplift was not restricted to the Moroccan margin, but occurred on all continental margins of the Central Atlantic (e.g. Miller & Duddy, 1989; Bertotti & Gouiza, 2012). This setting induced the highest sediment flux during the development of the Moroccan margin (ST5) as it included the early to peak development of the South West Moroccan Tan Tan and Laâyoune deltas. The reduced ridge-push in combination with thermal uplift in the South Atlantic significantly influenced the uplift in the hinterland, the erosion of uplifted material and its deposition in the basin. As the sediment flux was higher than the amount of generated accomodation space the development of the Early Cretaceous delta systems induces a major shift of the depositional systems in basinward direction.
The end of ST5 marks the end of the „short" regressive interim of 17.2 m.y.
The two-fold increase in spreading half-rates in the Central Atlantic from 5 mm/y to 10 mm/y (Klitgord & Schouten, 1986; Srivastava et al., 2000; Vogt & Tucholke, 1986) correlates with a transition from rifting to sagging in the South Atlantic domain (Contreras et al., 2010) and led to an increase of (thermo)-tectonic subsidence in the Mesozoic Tarfaya-Laâyoune Basins (Early ST6) as well. According to Gouiza (2010), the amount of thermo-tectonic subsidence was not enhanced by mantle lithosphere thinning but instead superimposed by regional salt flow in response to the high sediment loads of the Tan Tan and Laâyoune deltas. In any case, the impact of far-field developments is presumably high.
However, with the increase of Central Atlantic SFS-halfrates in combination with drift and thermal cooling in the South Atlantic (e.g. Contreras, 2011), the sediment supply as well as subsidence was reduced drastically.
The final separation of South America and Africa and the onset of sea-floor spreading in the South Atlantic correlate with the Cretaceous Magnetic Quiet Zone (CMQZ) of the Central Atlantic. The CMQZ does not allow the accurate calculation of sea-floor spreading rates. Nevertheless, Late Albian half-rates are assumed to be 20 – 25 mm/y (Klitgord & Schouten, 1986; Srivastava et al., 2000; Vogt & Tucholke; 1986, Olivet, 1996). Starved sediment input, maximum drift velocities of the African plate, the increased distance between continental margin and sea-floor spreading axes as well as a eustatic sea-level rise led to very static conditions in the Tarfaya-Laâyoune Basins. Subsidence rates were low during the Late Cretaceous (Late ST6 to ST8) and no significant amounts of sediment have been deposited. Thermo-tectonic uplift at the beginning of ST7 (Fig. 110) was related to the onset of African-Eurasian convergence and initial Atlasian doming.
Only during the Cenomanian a eustatic sea level fall (Cenomanian regression at sequence boundary Ce3, Kuhnt et al., 2009, see also Fig. 49) triggered a small increase in sediment flux and subordinate peaks in flexural and compaction-induced subsidence. Comparable data exist for the adjacent Agadir Basin (Zühlke et al., 2004).
During early ST6 (Aptian) the Moroccan deltas were still active but the depositional systems retrograded. In Aptian times a period of widespread shelf flooding started introducing the final part of the transgressive trend of the current continental encroachment cycle which continued during ST7 and most of ST8. ST8 represents the 1st order maximum flooding surface of this cycle, the Santonian of the the turning point from continental transgression to regression in the Central Atlantic.

5.3 Basin fill and subsidence development during superimposed regression

5.3.1 Mature drift concurrent to Alpine collision

The development of the IAU and the subsequent development of a shelf margin wedge during ST9 correlates with several plate tectonic events: i) a rapid reduction of convergence between Africa and Europe between 67 - 55 Ma (Dewey et al., 1989; Rosenbaum et al., 2002), ii) a decrease in sea-floor spreading half-rates from 24 to 16 mm/y (Klitgord & Schouten, 1986; Srivastava et al., 2000; Vogt & Tucholke, 1986), and iii) an onset of subduction in the eastern Mediterranean – Zagros – Himalaya belt (Agard et al.; 2005). At the end of ST 7, deposition on the southern Moroccan shelf had largely ceased and basin inversion started (Fig. 108). This change follows a global change from 200 m.y. of transgression to the long term regression phase of the current continental encroachment cycle (cf. Fig. 111).
The changes in subsidence and sediment flux from ST8 to ST9 are subordinate. In the Paleogene, compaction- induced and flexural subsidence were

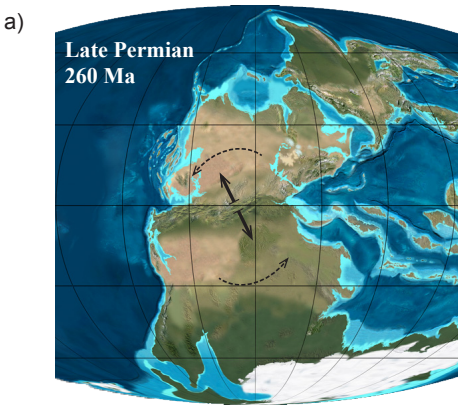

Global: Sinistral rotation of Pangaea, onset of superordinated transgression (Fig. 111)
Atlantic: Onset of rift in the Central Atlantic
Regional: Crustal thinning, development of graben structures, 2nd order transgression
Shelf-subsidence: very high; > 200 m/m.y. in graben areas
Genetic components: tectonic >>> flexural >> compaction
Sediment flux: average; > 10.000 m²/m.y.

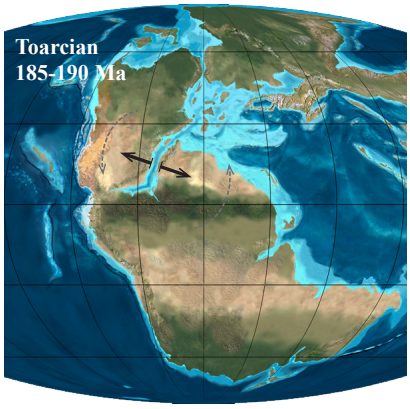

Global: Break-up of Pangaea, superordinated transgression
Atlantic: Onset of drift in the Central Atlantic
Regional: Ridge push main controlling factor on subsidence, 2nd order transgression
Shelf-subsidence: high; > 100 m/m.y.
Genetic components: tectonic ~ flexural > compaction
Sediment flux: average; 7. - 12.000 m²/m.y.

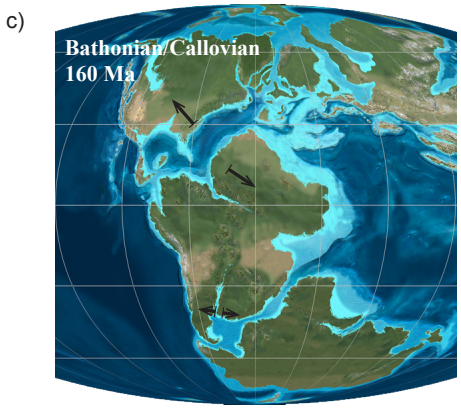

Global: Break-up of Gondwana, superordinated transgression
Atlantic: Initial rifting in the southernmost Atlantic
Regional: Early drift peak spreading rates, era of Jurassic platforms, 2nd order trans.
Shelf-subsidence: high; > 75 m/m.y.
Genetic components: tectonic < flexural ~ compaction
Sediment flux: average; 8. - 13.000 m²/m.y. (carbonate production)

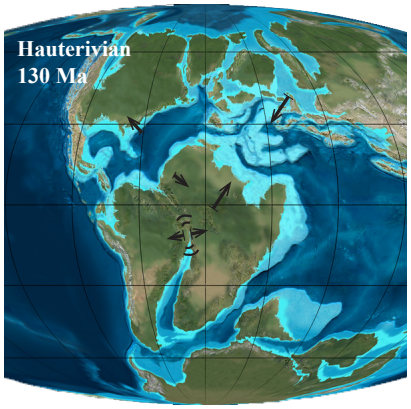

Global: Onset of Tethyan convergence, superordinated transgression
Atlantic: Initial rifting between Brazil and Central West Africa, low SFS-rates
Regional: Decrease of SFS-halfrates, era of deltas, 2nd order regression
Shelf-subsidence: high; > 80 m/m.y.
Genetic components: tectonic << flexural > compaction
Sediment flux: high; 15. - 30.000 m²/m.y.

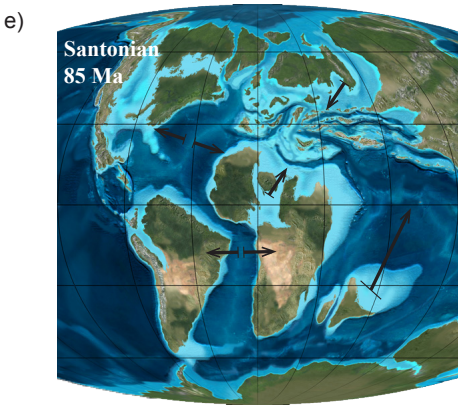

Global: Subduction in Tethyan domain, onset of superordinated regression
Atlantic: Peak spreading rates in the Central Atlantic
Regional: Largest shelf extension, era of Cretaceous black shales, 2nd order trans.
Shelf-subsidence: very low; > 0 - 5 m/m.y.
Genetic components: tectonic < flexural ~ compaction
Sediment flux: low; 0. - 2.500 m²/m.y.

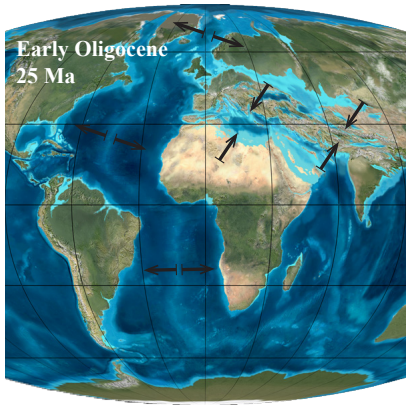

Global: Peak alpine collision, superordinated regression
Atlantic: Maximum extension of the Atlantic spreading ridge
Regional: Peak Atlasian uplift and erosion, 2nd order regression
Shelf-subsidence: inverse; > -5 - -50 m/m.y.
Genetic components: tectonic >> flexural ~ compaction
Sediment flux: average; 10.000 m²/m.y.

Figure: 113: Late Paleozoic and Cenozoic plate motions and the Tarfaya-Laâyoune Basin development i a) the rotation of Pangaea led to rifting and break-up (260 Ma); b) sea-floor spreading and incipient ridge-push resulted in high shelf subsidence (190 Ma); c) increasing spreading half-rates keeps subsidence on high level, accommodation space filled with carbonates (160 Ma); d) decreasing ridge push and an uplift of the Moroccan hinterland resulted in increasing erosion, sediment flux and high flexural and compaction induced subsidence (130 Ma); e) separation of South America and Africa, end of sea-floor spreading in the Tethys Ocean correlate with peak spreading in the Central Atlantic (85 Ma); f) the peak of alpine collision and the Atlasian uplift, decrease of Central Atlantic divergence, and high sedimentation rates (30 Ma). Paleoglobes after Blakey (2003; 2008).

strongly reduced in the basin. Uplift affected the shelf top. According to unpublished industry data, incised valleys bypassed micro-conglomerates and siltstones to the shelf margin and slope.
During ST10 (Neogene), African-Eurasian collision controlled uplift and basin inversion of the Moroccan margin, possibly also the rise of the Canary Islands (Carracedo et al., 1998). Inner shelf reflectors terminate against the terrain surface (Fig. 63) and higher interval velocities at the terrain surface of the inner to central shelf area of the Tarfaya Basin in front of the Anti-Atlas (Fig. 103) indicate massive erosion of Late Cretaceous and Paleogene on the shelf. The uplift of the Canary Islands modified the Tarfaya Basin geometry significantly compared to the adjacent Agadir (Gouiza, 2010) and Laâyoune Basins (Figs. 63 & 104). During ST10, sediment was provided mainly from the High Atlas and Anti Atlasian domain (Sehrt, 2014).
Fig. 113 shows an illustration of global plate motions during important steps of Tarfaya-Laâyoune Basins development.

5.4 Resulting hc-play scenarios

Based on the performed basin analysis in this study, the following play scenarios exist:

- Triassic/Early Jurassic subsalt
- Triassic fault bocks
- Toarcian ramps
- Bathonian oolites
- Jurassic midshelf dolomites
- Tithonian carbonate platforms
- Early Cretaceous deltaic plays
- Late Cretaceous deep offshore
- Late Cretaceous unconventionals
- Cenozoic deep offshore

In the Triassic/Early Jurassic, two play scenarios are possible; the first one is a sub salt-play. It assumes with high likelihood that clastic reservoirs or, like in Brazil, lacustrine carbonates of the rift phase are widely covered by salt of the sag stage. In addition, a source rock of Triassic/Early Jurassic age has to be matured and located in a position from which migration is possible.
The only indication for such a source rock offshore Morocco has been found in well DSDP 547B in 3,000 m waterdepth in front of the Mazagan segment (Winterer & Hinz, 1981; Hinz et al. 1982). For this well a kerogen I source rock of Early Jurassic (Pliensbachian) age has been described. In the sedimentary and biostratigraphic description for this potential „hot shale“ the depositional environment is suggested to be open marine. However, this OM-rich sample from the northern part of the Moroccan passive margin is the only indication for a source rock in the rift and sag stage. Moreover Silurian or Devonian source rocks located in the Paleozoic might source this sub salt scenario.
Regarding the distribution of the salt seal, the play is bound to the outer shelf and slope area. In deep offshore the base of the salt is too deep to be drilled. Anyway, the sub salt play is still very speculative.
Potential plays related to Triassic fault blocks might be present at both flanks of the Juby Horst (Fig. 63 and 104 Cap Juby transect). In addition to the above mentioned source rocks, migration from a potential Toarcian source rock might be possible too, depending on its relative position to the fault blocks. However, even if this source rock is often described in literature, it is still unproven in the region.
Triassic shales of a fluvial plain or Early Jurassic mudstons may represent the top seal in these structural traps. This play has an interesting position in the southern Tarfaya and in the Laâyoune Basins as the distal fault blocks of the Laâyoune Depression can be drilled from an onshore location (Fig. 63 & 104, Laâyoune transect).
A Toarcian play is bound to sands in the foresets of the Toarcian clastic ramp on the central to outer shelf. Regarding their geometry and position on the shelf, the chance of 4-way closures being present is likely. For this setting, all source rocks described above are potential candidates for hc-origin. However, Toarcian sands were just drilled only once in the CJ-1 well with no hc-shows in this interval.
Based on the backstripping results presented in this study, hc-maturation may have started in Late Jurassic and expulsion during the earliest Early to Late Cretaceous.
A Jurassic outer shelf play was proven in the well MO-8, where light oil of 33.8° API was produced from a more or less tight oolitic carbonate with permabilities below 1 mD. For this scenario, a lower to mid-Jurassic source rock is suggested. The seal is represented by Callovian mudstones. Even if the reservoir properties at well position are very poor, this proven play is one of the most promising in the region.
The presence of dolomitic reservoirs in the Late Jurassic midshelf was first suggested by Smith et al. (2010) for the Nova Scotian Abenaki Group. Shelf

Tab. 6: Evaluation of the petroleum plays of the Tarfaya-Laâyoune Basins.

Play	Source Rock	Quality	Maturity	proven	Indications	Reservoir	Tested	Seal	Risk	Confidence
Triassic subsalt	Paleozoic shales Triassic lacustrine Triassic evaporitic	?	shelf-basin: late oil mature, slope: overmature shelf: mid-late oil mature on shelf, slope-basin: gas mature	no	no Kerogen II/III OM, TOC -0.65%, HI>300 in DSDP 546 & 547, CJ-1	stacked fluvial channel sytems	no	Salt	high risk on SR presence, migration, reservoir presence	low
Triassic fault bocks	Paleozoic shales Triassic lacustrine Triassic evaporitic Toarcian turnover	? ? Most likely kerogentype- II	shelf: late oil mature, slope: overmature shelf: mid-late oil mature on shelf, slope-basin: gas mature shelf: mid-oil to lateoil mature, slope-basin: oil-gas mature		no Kerogen II/III OM, TOC -0.65%, HI>300 in DSDP 546 & 547, CJ-1 very poor indication in CJ-1	alluvial to fluvial plain sands in tilted fault blocks	no	shales from sag stage, early drift mudstones	high risk on SR presence, migration, reservoir & seal presence	low
Toarcian ramps	Toarcian turnover	? Most likely kerogentype- II	shelf: mid-oil to lateoil mature, slope-basin: oil-gas mature		very poor indication in CJ-1	shoreline sandstones and aggrading fluvial systems	no	mudstones	high risk on SR presence, migration, reservoir properties	low
Bathonian oolites	Triassic lacustrine Triassic evaporitic Toarcian turnover	? ? ? Most likely kerogentype- II	shelf: mid-oil to lateoil mature, slope-basin: oil-gas mature shelf: mid-oil to lateoil mature, slope-basin: oil-gas mature	no	Kerogen II/III OM, TOC 0.5%, HI>300 in DSDP 546 & 547 very poor indication in CJ-1	outer shelf high energy carbonates (oolites)	yes	mudstones	risk on reservoir propeties, proven play	high
Jurassic midshelf dolomites	Toarcian turnover Callovian	? Most likely kerogentype- II	shelf: mid-oil slope-basin: oil-gas mature		very poor indication in CJ-1	dolomite reservoirs	no	Early Tan Tan shales	high risk on migration, reservoir properties	low
Tithonian carbonate platforms	Toarcian turnover Callovian	? Most likely kerogentype- II	shelf: mid-oil slope-basin: oil-gas mature		very poor indication in CJ-1	outer shelf carbonates and patch reefs	yes	Early Tan Tan shales	high risk on seal capacity, secondry processes	high
Early Cretaceous deltaic plays	BTR Faraoni event	type III type III (Type II subtype)	slope & basin: mid oil to late oil slope & basin: mid oil to late oil		poor in MO wells poor to fair in MO wells	basin floor and lowstand fans basin floor and lowstand fans, stacked mouth bars and distributary channels	no	lateral facies changes	high risk on SR presence, maturation, migration, reservoir properties high risk on SR presence, maturation, migration, seal	very low low - medium
Late Cretaceous deep offshore	OAE-1 (Albian) OAE-2 (Cenomanian) OAE-2 (Turonian) OAE-3 (Coniacian) OAE-3 (Santonian) OAE-3 (Campanian)	k-type II/III; TOC: -3%; HI: 150-400 k-type I/II; TOC: -16.8%; HI: -780 k-type I/II; TOC: -8.5%; HI: -600 k-type II; TOC: -7.0%; HI: -740 k-type I/II; TOC: -5.6%; HI: -700 k-type I/II; TOC: -4.5%; HI: -650	early to late oil mature immature to mid oil mature	yes (outer shelf and onshore)	proven (Ellouz etal, 1998; Sachse et al., 2011; Sachse et al., 2014)	Late Cretaceous turbidites & MTCs	no	Late Cretaceous shales, salt	risk on maturity, migration, reservoir presence	low
Late Cretaceous unconventionals	OAE-1 (Albian) OAE-2 (Cenomanian) OAE-2 (Turonian) OAE-3 (Coniacian) OAE-3 (Santonian) OAE-3 (Campanian)	k-type II/III; TOC: -3%; HI: 150-400 k-type I/II; TOC: -16.8%; HI: -780 k-type I/II; TOC: -8.5%; HI: -600 k-type II; TOC: -7.0%; HI: -740 k-type I/II; TOC: -5.6%; HI: -700 k-type I/II; TOC: -4.5%; HI: -650	early to late oil mature immature to mid oil mature	yes (onshore)	proven (Ellouz etal, 1998; Sachse et al., 2011; Sachse et al., 2014)	source rock	yes	Late Cretaceous shales	risk on maturity and expulsion, reservoir presence	medium- high
Cenozoic deep offshore	OAE-1-3 PETM	s.a. k-type II/III; TOC: -3%; HI: 150-450	immature to mid oil mature	yes (outer shelf and onshore)	proven (Guerra et al.; 1995; Sachse et al., 2011)	MTCs	no	Miocene shales, salt	risk on maturity and expulsion, reservoir presence	low - medium

dolomites may have elevated permeabilities. The top seal for this play is most likely represented by Late Jurassic mudstones or Early Cretaceous shales and may have been charged by Jurassic or Triassic source rocks.
The Kimmeridgian/Tithonian outer shelf play bound to karstified patched reefs and grainstones was proven in the wells MO-2 and CJ-1. Both wells discovered heavy oil of 12-13° API. The source rock is most likely of Lower or Middle Jurassic age (Toarcian/Callovian). The seal is represented by Early Cretaceous shales. However, the residual of heavy oil with no gas cap indicates a high risk on a functioning seal as well as biodegradation in the reservoir. As the wells MO-2 and CJ-1 were drilled into the same structure, this play is very promising. Regarding the timing of the proven Jurassic plays, the onset of source rock maturation is most likely Early Cretaceous. Expulsion and charge may have taken place during Late Cretaceous or Paleogene.
Younger conventional play scenarios are very unlikely in the shelf region. Cretaceous and Cenozoic plays are bound to the slope and deep basin area. There, Barremian foresets as well as Aptian sands represent especially interesting reservoirs; particularly the salt related fault blocks in the Tarfaya Basin west of MO-7 represent interesting unproven drillsites. There sands could be charged from Jurassic source rocks by hc-migration through faults as well as by lateral migration from Early Cretaceous events (Faraoni). Seals are represented by interbedded shaly layers of Early Cretaceous age or Cenozoic shales.
In the deep offshore Oligocene and Miocene MTCs may represent potential reservoirs. They can be identified on seismic data, however, they are not proven in wells so far. Oligocene and Miocene shales could represent top seals, in lateral direction, salt plumes might be effective seal facies.
Even if the Late Cretaceous hot shales are well known from outcrops of the onshore Tarfaya and Laâyoune area, their distribution in the deep offshore is not fully understood. In addition, hc expulsion is questionable and very dependent on the heatflow in the salt basin. In this study, Late Cretaceous source rocks as well as sediments of the Paleogene PETM have just reached early mid oil maturation window, but not expulsion.
Onshore the Late Cretaceous and PETM blackshales have a high unconventional potential as they are located just a few tens to hundreds of meters below surface. Tab. 6 shows an evaluation and risk assessment of the potential petroleum play scenarios in the Tarfaya-Laâyoune Basin.

5.5 Conclusions

Integrated basin analysis of the Tarfaya and northern Laâyoune Basins is based on well, outcrop and 2D-seismic data included i) seismic interpretation & facies mapping, ii) 1D- and 2D- high resolution sequence stratigraphy, iii) time/depth conversion and vi) flexural reverse basin modeling. It provided a plausible qualitative and quantitative reconstruction of the basin architecture through time, both the tectonic evolution as well as the sediment flux and subsidence development.
Above all, the Tarfaya-Laâyoune Basins development is controlled by the highest order cycle of global plate tectonics. The basin evolution is bound to the last cycle starting with the onset of rift at 259.3 Ma, which can be subdivided into two phases, i) a trangressive phase and ii) the regressive phase. During the first phase, subsidence continuously generated accomodation space with a decreasing rate during basin maturation. Uplift or basin inversion started with the onset of superimposed regression in Late Cretaceous (Fig. 110) and in the end of the cycle, geohistory plots will probably follow a u-shape. Second order sequence boundaries are the most obvious changes in basin evolution which can be recognized on seismic and well data by major unconformities and sudden lithological changes. As they correlate with changes in SFS-halfrates, far-field tectonic changes are identified as the main driving force on 2nd order sequence stratigraphy. During superimposed transgression, each sequence is characterized by an overall lithological fining upward trend:

- Rift & sag: conglomerates to alluvial plain fines
- Early drift: clastic ramps to carbonate platforms
- Mature drift and compression: delta sand to shale

The Lower Cretacous deltas represent an exception as the third tectonic sequence starts with a coarsening upward (Berriasian to Barremian) continuing with constant sand supply until the Late Aptian.
However, the development of the Lower Cretaceous delta systems are controlled by the break-up in the South Atlantic which is a divergent process, thus „transgressive“. The main driving force of uplift and erosion of the West African margins is the thermal uplift in the South Atlantic. First order cycles con-

trol long term development of depositional systems like i) continental-clastic during rift, ii) marine-carbonatic during early drift, iii) deltaic-clastic during mature drift, iv) carbonatic-clastic during final transgressive drift, v) fine clastic during drift with early compression and uplift and vi) fine to medium clastic during peak alpine collision.

Third order sequences follow mainly eustatic long- and short term sea-level as well as climatic changes. Eustatic sea-level changes are the second major controlling factor on the development of source rock deposition as nearly every source rock was deposited during periods of long-term eustatic sea-level rise (Tab. 6).

Fourth order changes are may driven by Milankovich cycles and are important when it comes to the understanding of facies distribution on the shelf and in the basin (cf. Fig. 97-102).

The ten identified subsidence trends are directly coupled to crustal stretching trends and SFS-halfrates. ST1 covers the whole rift stage, ST2 the sag and earliest (clastic) drift. ST3 is characterized by constant SFS-halfrates while ST4 experiences a bow-trend of first increasing and finally decreasing spreading-halfrates. ST5 shows the opposite bow trend, while ST6 correlates with a significant increase. The trends ST7-ST10 are mainly correlate with a continuously decrease of the SFS-halfrates and show initial basin inversion.

The factors controlling the basin evolution have been identified in a global as well as regional context. From a hc-exploration point of view, facies analysis allowed to determine the spacial and temporal distribution of source, reservoir and seal formations.

So far, the deposition of potential source rocks took mainly place during the transgressive phase of the 1st order cycle. Twelve global or regional anoxic events have been deposited during this phase, one, the PETM event during the regression. Every third 3rd order transgression includes a potential source rock, while the distribution of reservoir formations is more complex. Seal facies is deposited during most 3rd order transgression.

Based on the results, the components of possible petroleum systems have been identified and potential hydrocarbon play scenarios been developed, ranked and risk assessed. Eleven possible play scenarios have been described. Three scenarios (two Jurassic conventional and one Late Cretaceous unconventional) have been classified as proven - two as likely (Early Cretaceous delta plays and Cenozoic deep water). All other scenarios are high risk or very unlikely. The Tarfaya-Laâyoune Basin is still underexplored however, and new wells will increase the probability for some of the plays or may identify new ones.

References

Abou Ali, N., Chellai, N.H. & Nahim, M. (2004) Anatomie d'une marge passive hybride. Marge Ifni/Tan Tan (Sud du Maroc) au Mésozoique: Apports des données géophysiques. *Estudios Geol.*, **60**, pp. 111-121.

Abou Ali, N., Hafid, M., Chellai, E.H., Nahim, M. & Zizi, M. (2005) Structure de socle, sismostratigraphie et heritage structural au cours du rifting au niveau de la marge d'Ifni/Tan Tan (Maroc sud-occidental). *C. R. Geosci.*, **337**, pp. 1267-1276.

Agard, P., Omrani, J., Jolivet, L., and Mouthereau, F. **(**2005) Convergence history across Zagros (Iran): Constraints from collisional and earlier deformation. *Int. J. Earth Sci.*, **94**, p. 401–419.

Ali, S. (2012): Cretaceous to Quarternary Siliciclastic Sediments of the Tarfaya Basin, Marginal Atlantic, SW Morocco: Petrography, Geochemistry, Provenance, Climate and Weathering. PhD-Thesis, Christian-Albrechts-University (CAU) of Kiel, 145 p.

Arthur, M.A. (1979): Origin of Upper Cretaceous Multicolored Claystones of the Western Atlantic. *Reports of the Deep Sea Drilling Project*, **43**(11), 801-821, doi:10.2973/dsdp.proc.43.111.1979, publication date: May 2007.

Allen, P.A. & Allen, J.R. (2005) Basin Analysis - Principles & Applications. 2nd edition, Blackwell Science Ltd., 549 p.

Allen, P.A. & Allen, J.R. (2013) Basin Analysis - Principles & Applications. 3rd edition, Blackwell Science Ltd., 642 p.

Aquit, M. (in prep.) Depositional and Sea-level history and paleoenvironmental evolution. PhD-Thesis, Christian-Albrechts-University (CAU) of Kiel.

AUXINI (1969) Correlación estratigráfica de los sondeos perforados en el Sahara español. *Inst. Geol. Min., Bol. Geol. Minero*, **80**, pp. 235-251.

Bádenas, B., & Aurell, M. (2001) Kimmeridgian paleogeography and basin evolution of northeastern Iberia. *Palaeogeogr., Palaeoclimatol., Palaeoeco.*, **168**, pp. 291–310.

Bahlburg, H. & Breitkreuz, C. (1998): Grundlagen der Geologie. Enke-Verlag, 328 p.

Beicip (1990) Étude geólogique et géophysique des permis Tarfaya Laâyoune, vol. 1&2. Unpublished Report, ONAREP #31478, 69 p., 52 fig. and 10 tab.

Bertotti, G. & Gouiza, M. (2012): Post-rift vertical movements and horizontal deformations in the eastern margin of the Central Atlantic: Middle Jurassic to Early Cretaceous evolution of Morocco. *Int. J. Earth Sci. (Geol. Rundsch.)*, **101**(8), pp. 2151-2166.

Bertram, G.T., & Milton, N.J. (1996) Seismic Stratigraphy. *In:* Emery, D. & Myers, K.: *Sequence Stratigraphy*, Wiley, pp. 43-60.

Bjørlykke, K. (2010): Petroleum Geoscience - From Sedimentary Environments to Rock Physics, Springer-Verlag Berlin Heidelberg, 508p.

Blakey, R.C. (2003) Carboniferous-Permian paleogeography of the assembly of Pangaea. *In:* Wong, Th.E.: *Proceedings of the XVth International Congress on Carboniferous and Permian Stratigraphy*, Utrecht, the Netherlands, 10.-16. August 2003, pp. 443-456.

Blakey, R.C. (2008) Gondwana paleogeography from assembly to breakup - A 500 m.y. odyssey. *In:* Fielding, C.R., Frank, T.D., & Isbell, J.L., eds., Resolving the Late Paleozoic Age in Time and Space, *Geol. S. Am. S.*, **441**, pp. 1-28.

Bott, M.H.P. (1992) Passive margins and their subsidence. *J. Geol. Soc.,* **149**, pp. 805-812.

Bover-Arnal, T. & Strasser, A. (2013) Relative sea-level change, climate, and sequence boundaries: insights from the Kimmeridgian to Berriasian platform carbonates of Mount Salève (E France). *Int. J. of Earth Sci*, **102**, pp. 493-515.

Bowman, S.A. & Vail, P.R. (1999) Interpreting the stratigraphy of the Baltimore Canyon section offshore New Yersey with PHIL, a stratigraphic simulator, *in:* Harbaugh, J.W., Watney, W.L., Rankey, E.C., Singlerland, R., Goldstein, R.H. and Franseen, E.K.: Numerical Experiments in Stratigraphy: Re-

cent Advances in Stratigraphic and Sedimentologic Computer Simulations. *SEPM Spec. Publ.*, **62**, pp. 117-138.

Brown, R. H. (1980). Triassic rocks of the Argana Valley, southern Morocco, their regional structural implications. *AAPG Bull.*, **64**(7), pp. 988–1003.

Bullard, E.C. (1950) The transfer of heat from the core of the Earth. *Mon. Not. R. Astron. Soc.,* **6**, pp. 36-41.

Carracedo, J.C., Day, S. Guillou, H., Rodriguez Badiola, E., Canas, J.A. & Pérez Torrado, F.J. (1998) Hotspot volcanism close to a passive continental margin: the Canary Islands. *Geol. Mag.*, **135**(5), pp. 591-604.

Carter, M.D. &G. Hyatt (1990) A comparison of depth conversion methods in the Gulf of Mexico: *Proceedings* 60th Annual International Meeting, SEG, pp. 1253-1255.

Catuneanu, O. (2006) Principles of Sequence Stratigraphy, 1st edition, Elsevier, 375 p.

Catuneanu, O., Abreu, V., Bhattacharya, J.P., Blum, M.D., Dalrymple, R.W., Eriksson, P.G., Fielding, C.R., Fisher, W.L., Galloway, W.E., Gibling, M.R., Giles, K.A., Holbrook, J.M., Jordan, R., Kendall, C.G.St.C., Macurda, B., Martinsen, O.J., Miall, A.D., Neal, J.E., Nummedal, D., Pomar, L., Posamentier, H.W., Pratt, B.R., Sarg, J.F., Shanley, K.W., Steel, R.J., Strasser, A., Tucker, M.E., Winker, C. (2009) Towards the standardization of sequence stratigraphy. Earth-Sci. Rev., **92,** pp. 1–33

Catuneanu, O., Bhattacharya, J.P., Blum, M.D., Dalrymple, R.W., Eriksson, P.G., Fielding, C.R., Fisher, W.L., Galloway, W.E., Gianolla, P., Gibling, M.R., Giles, K.A., Holbrook, J.M., Jordan, R., Kendall, C.G.St.C., Macurda, B., Martinsen, O.J., Miall, A.D., Nummedal, D., Posamentier, H.W., Pratt, B.R., Shanley, K.W., Steel, R.J., Strasser, A., Tucker, M.E. (2010) Sequence stratigraphy: common ground after three decades of development. *First Break,* **28**, pp. 21–34.

Catuneanu, O., Galloway, W.E., Kendall, C.G.St.C., Miall, A.D., Posamentier, H.W., Strasser, A., & Tucker, M.E. (2011) Sequence Stratigraphy: Methodology and Nomenclature. *Newsl. Stratigr.*, **44**(3), pp. 173–245.

Chlingarian & Vorabutr (1981) Drilling and Drilling Fluids. Elsevier, 767 p.

Choubert, G., Faure-Muret, Hottinger, L. A., Viotti, C., & Lecointre G. (1966) Le Bassin Côtier de Tarfaya (Maroc méridional), Tome I: Stratigraphie. Notes et Memoires du Service Géologique, Maroc, **175**, Editions du Service Géologique du Maroc, Rabat, 319 p.

Cirilli, S., Marzoli, A., Tanner, L., Bertrand, H., Buratti, N., Jourdan, F., Bellieni, G., Kontak, D. & Renne, P.R. (2009) Latest Triassic onset of the Central Atlantic Magmatic Province (CAMP) volcanism in the Fundy Basin (Nova Scotia): New stratigraphic constraints**.** *Earth Sci, Rev.,* **286**(3-4), pp. 514-525.

Cornford, C. (2013) The Mesozoic Sequence of Fuerteventura (Canary Islands) - a window on the petroleum potential of the ‚deep-basin' southern Moroccan Atlantic margin. *Proceedings*, Oil&Gas Marrakesh Conference & Exhibition, p. 45.

Contreras, J., Zühlke, R., Bowman, S. & Bechstädt, T. (2010) Seismic stratigraphy and subsidence analysis of the southern Brazilian margin (Campos, Santos and Pelotas basins). *Mar. Pet. Geol*., **27**, 1952-1980.

Contreras, J. (2011) Seismo-stratigraphy and numerical basin modelling of the southern Brazilian continental margin. PhD-Thesis of the Institute of Earth Sciences, Heidelberg University, 146 p.

Contrucci, I., Klingelhöfer, F., Perrot, J., Bartolomé, R., Gutscher, M.-A., Sahabi, M:, Malod, J. & Rehault, J.-P. (2004) The crustal structure of the NW Moroccan continental margin from wide-angle and reflection seismic data. *Geophys. J. Int.*, **159**, pp. 117-128.

Cordsen, A., Galbraith, M., & Peirce, J. (2000) Planning land 3-D seismic surveys. *GDS*, **9**, Soc. Expl. Geophys., 204p.

Czuba, W., Grad, M., Mjelde, R., Guterch, A., Libak, A., Krüger, F., Murai, Y. Schweitzer, J. & the IPY Project Group (2011) Continent-ocean transition across a transtensional margin segment: off Bear Island, Barents Sea. *Geophys. J. Int.*, **184** (2), pp. 541-554.

Davison, I. (2005) Central Atlantic margin basins of North West Africa: Geology and hydrocarbon potential (Morocco to Guinea). *J. Afr. Earth. Sci.,* **43**, 254-274.

Davison, I. & Dailly, P. (2010): Salt tectonics in the Cap Boujdour Area, Aaiun Basin, NW Africa. *Mar. Pet. Geol.*, **27**, 435-441.

de Bruin, G, Ligtenberg, H., Hemstra, N. &Tingdahl, K. (2006), Synchronized sequence stratigraphic interpretation in the structural and chronstratigraphic (Wheeler transformed) domain, extended abstract, EAGE Research Workshop 2006, Grenoble.

de Bruin, G., Hemstra, N. & Pouwel, A. (2007) Stratigraphic Surfaces in the Depositional and Chronostratigraphic (Wheeler-transformed) Domain, *TLE,* **26**, pp. 883-888.

de Groot, P. & de Bruin, G, 2006, OpendTect SSIS - Sequence Stratigraphic Interpretation System, *Drilling and Exploration World*, **15**, pp. 31-34.

Destombes J., Hollard H., & Willefert S. (1985) Lower Palaeozoic rocks of Morocco. *In:* Holland C.H. (Ed.) *Lower Palaeozoic Rocks of North-Western and West-Central Africa*. John Wiley, Chichester, pp. 91–336.

Dewey, J.F., Helman, M.L., Turco, E., Hutron, D.H.W. & Knott, S.D. (1989) Kinematics of Western Mediterranean. *In:* Coward, M.P., Detrich, D., & Park, R.G.; Alpine Tectonics. *Geol. Soc. Spec. Publ.,* **45,** pp. 265-283.

Dézes, P., Schmid, S.M. & Ziegler, P.A. (2004) Evolution of the European Cenozoic Rift System: interaction of the Alpine and Pyrenean orogens with their foreland lithosphere. *Tectonophysics*, *389*, pp. 1-33.

Dragoset, B. (2005) A historical reflection on reflections. *TLE*, 24, pp. 46-71.

Duval, B.-C., Cramez, C. & Vail, P.R. (1998) Stratigraphic cycles and major marine source rocks. In: Mesozoic and Cenozoic sequence stratigraphy of European basins. *In:* De Graciansky, P.C., Hardenbol, J., Thierry, J. & Vail, P.R.), Mesozoic and Cenozoic Sequence Stratigraphy of European Basins, *SEPM Spec Publ.*, **60**, pp. 43-52.

Einsele, G. (1992) Sedimentary Basins. Evolution, Facies, and Sediment Budget. Springer Verlag Berlin, Heidelberg, New York, London, Paris, Tokyo, Hong Kong, 628 p.

Einsele, G. (2000) Sedimentary Basins. Evolution, Facies, and Sediment Budget. 2nd edition, Springer Verlag Berlin, Heidelberg, New York, 792 p.

Eliouk, L. & Wach, G., (2010) Regional Setting of the Late Jurassic Deep Panuke Field, offshore Nova Scotia, Canada II: Part 1 - Distant and fractal analogues and possible process controls for a thick carbonate platform flanked by a large delta. *Proceedings,* 2nd Central & North Atlantic Conjugate Margins Conference, Lisbon, pp. 107-110.

Ellouz, N., Müller, C. & Faure, J.-L. (1998) Datations et Etude Geochémique des Forages BTS 1 et MO-7 du Bassin de Tarfaya – Maroc. Unpublished report of ifp, EAP & ONAREP, ONAREP #41016, 83 p.

Ellouz, N., Patriat, M., Gaulier, J.-M., Bouatmani, R. & Sabounji, S. (2003) From rifting to Alpine inversion: Mesozoic and Cenozoic subsidence history of some Moroccan basins. *Sediment. Geol.*, **156**, pp. 185-212.

El Khatib, J., Ruellan, É., El Foughali, A. & El Morabet, A.'M. (1995) Évolution de la marge atlantique sud marocaine: bassin de Tarfaya-Laâyoune. *C.R. Acad. Sci. Paris*, **320**(IIa), pp. 117-124.

El Mostaine, M. (1991) Évaluation du Potentiel Pétrolier du Bassin de Tarfaya-Laâyoune onshore. ONAREP internal report #31526, 92 p.

Embry, A. F. & Johannessen, E. P. (1992) T–R sequence stratigraphy, facies analysis and reservoir distribution in the upper most Triassic–Lower Jurassic succession, Western Sverdrup Basin, Arctic Canada. *In:* Vorren,T. O., Bergsager, E., Dahl-Stamnes, O. A., Holter, E., Johansen, B., Lie, E. and Lund, T. B.: Arctic Geology and Petroleum Potential, *NPF. Sp. Publ.*, **2**, pp. 121–146.

Emmerich, A., Tscherny, R., Bechstädt, T., Büker, C., Glasmacher, U.A., Littke, R. & Zühlke, R., 2008. Numerical simulation of the syn- to post-depositional history of a prograding carbonate platform: the Rosengarten, Middle Triassic, Dolomites, Italy. *In*: *Boer, P., Postma, G., Van der Zwan, K., Burgess, P.*

& Kukla, *P.*: Analogue and Numerical Modelling of Sedimentary Systems: From Understanding to Prediction. *IAS Spec Publ.*, **40**, 1-36.

energy tomorrow (2014): Seismic Surveys: Why and How are Seismic Survey's Done?, online publication: http://energytomorrow.org/energy-101/offshore-drilling/seismic-surveys-why-and-how.

Éspitalie, J., Laport, L.J., Madec, M., Marquis, F., Leplat, P., Paulet, J., & Boutefeu, A. (1977) Methode rapide de caracterisation des roches mères, de leur potential petrolier et de leur dagré d'evolution. *Rev. Inst. Franc. Pétrole*, **31**, pp. 32-42.

Frisch, W., Meschede, M. & Blakey, R. (2011) Plate Tectonics: Continental Drift and Mountain Building. Springer, Heidelberg, 212 p.

Frizon de Lamotte, D., Leturmy, P., Missenard, Y., Khomsi, S., Ruiz, G., Saddiqi O., Guillocheau, F., & Michard, A. (2009) Mesozoic and Cenozoic vertical movements in the Atlas system (Algeria, Morocco, Tunisia) : An overview, *Tectonophysics*, **475**, pp. 9-28.

Galloway, W.E. (1989) Genetic stratigraphic sequences in basin analysis; I, Architecture and genesis of flooding-surface bounded depositional units. *AAPG Bull.*, **73**(2), pp. 125-142.

Gasquet, D., Ennih, N., Liégois, J.-P., Soulaimani, A., & Michard, A. (2008) The Pan-African Belt. *In:* Michard, A., Saddiqi, O., Chalouan, A., & Frizon De Lamotte, D.: *Continental Evolution: The Geology of Morocco.* 1st edn, pp. 33-64, Springer Verlag, Berlin Heidelberg.

Geoffroy, L. (2005) Volcanic passive margins. C. R. Geosci., **337**, 1395-1408.

Giraud, R., Binks, R.M., Fairhead, J.D., & Wilson, M. (1992) Chronology and geodynamic setting of Cretaceous-Cenozoic rifting in West & Central Africa. *Tectonophysics*, **213**, pp. 227-234.

Goetz, J. F., Dupal, L., and Bowler, J. (1979) An investigation into discrepancies between sonic log and seismic check-shot velocities. *APEAJ*, **19**(1), pp. 131-141.

Gohl K. & Haywood, A. (2009) IPY Project PLATES & GATES: Plate tectonics and polar gateways in the Erath system - tectonic control on long-term climate evolution. Environ. Geol., **56**, pp. 1249-1250.

Gouiza, M. (2011) Mesozoic Source-to-Sink Systems in NW Africa: Geology of vertical movements during the birth and growth of the Moroccan rifted margin. Unpublished Doctoral Thesis, Vrije Universiteit Amsterdam, 170 p.

Gradstein, F., Ogg, J. & Smith, A. (2004) A Geologic Time Scale. Cambridge University Press, 589 p.

Guerra, R.T., Stapleton, R.P., Abbott, W.H., Root, S.A. & Gerhard, J.E. (1985) Biostratigraphy, Ecology and Organic Geochemistry of the Mobil Cap Juby #1 Well, (Offshore) Morocco. Unpublished ONAREP internal report #40825, 48 p.

Hafid, M. (2000a) Triassic-early Liassic extensional systems and their Tertiary inversion, Essaouira Basin (Morocco). *Mar. Pet. Geol.*, **17**, pp. 409-429.

Hafid, M., Aït Salem, A. & Bally, A.W. (2000b) The western termination of the Jibelet-High Atlas system (Offshore Essaouira Basin, Morocco). *Mar. Pet. Geol.*, **17**, pp. 431-443.

Hafid, M., Tari, G., Bouhadioui, D., El Moussaid, I., Echarfaoui, H., AÏt Salem, A., Nahim, M & Dakki, M. (2008) Atlantic Basins. *In:* Michard, A., Saddiqi, O., Chalouan, A., & Frizon De Lamotte, D.: Continental Evolution: The Geology of Morocco. 1st edn, pp. 303-329, Springer Verlag, Berlin Heidelberg.

Haq, B.U., Hardenbol, J., and Vail, P.R. (1987) Chronology of fluctuating sea levels since the Triassic (250 million years ago to present). *Science*, **235**, pp. 1156–1167**.**

Haq, B.U. & S.R. Shutter (2008) A chronology of Paleozoic sea-level changes. *Science*, **322**, pp. 64-68.

Hames, W.E., McHone, J.G., Renne, P.R., Ruppel, C. (2003), The Central AtlanticMagmatic Province: Insights from Fragments of Pangea. *Am. Geophys. Union Geophys. Monograph,* **136**. 267 p.

Hardenbol, J., Thierry, J., Farley, M.B., Jacquin, T., De Graciansky, P.-C. & Vail, P.R. (1998) Mesozoic and Cenozoic Sequence Chronostratigraphic Frame-

work of European Basins. *In:* De Graciansky, P.-C., Hardenbol, J. & Vail, P.R., Mesozoic and Cenozoic Sequence Stratigraphy of European Basins, *SEPM Spec. Publ.*, **60**, pp. 3-13.

Heine, C., Zoethout, J., & Müller, R.D. (2013) Kinematics of the South Atlantic rift. *Solid Earth,* **4**, pp. 215-253.

Heise, B. & Stattegger, K. (unpubl.) Source-to-sink analysis (paleobiology and sedimentology), on- and offshore Tarfaya basin, Morocco (Meso-/Cenozoic), unpublished AMP-report, 7 p.

Helg, U., Burkhard, M., Caritg, S., & Robert-Charrues, C. (2004) Folding and inversion tectonics in the Anti-Atlas of Morocco, *Tectonics,* **23**(4), TC4006, doi:10.1029/2003TC001576.

Heling, D. (1988) Ton- und Siltsteine. *In:* Füchtbauer, H.: Sediment-Petrologie Teil II - *Sedimente und Sedimentgesteine.* 4th edition, Schweizerbart, pp. 185-231.

Heyman, M.A.W. (1989) Tectonic and Depositional History of the Moroccan Continental Margin. *AAPG Mem.*, **46**, pp. 323-340.

Hinz, K., Dostmann, H. & Fritsch, J. (1982): The Continental Margin of Morocco: Seismic Sequences, Structural Elements and Geological Development. *In*: vin Rad, U., Hinz, K., Sarntheim, M & Seibold, E.: *Geology of the Northwest African Continental Margin*, Springer-Verlag, Berlin Heidelberg New York, pp. 34-60.

Hobson, G.D. & Tiratsoo, E.N. (1981) Introduction to Petroleum Geology, Scientific Press, 352 p.

Horn, M.K. (2014) Giant Oil and Gas Fields of the World (compiled by M.K. Horn). GIS publication as free download, AAPG datapages, http://www.datapages.com/associatedwebsites/gisopenfiles/horngiantfields.aspx (date: 14th of July, 2014).

Hunt, D. & Tucker, M.E. (1992) Stranded parasequences and the forced regressive wedge systems tract: deposition during base-level fall. *Sedimentary Geology*, **81**, pp. 1-9.

Hunt, D. & Tucker, M.E. (1995), Stranded parasequences and the forced regressive wedge systems tract: deposition during base-level fall-reply. *Sedimentary Geology*, **95**, pp. 147-160.

Hutton, A., Bharati, S. & Robl, T. (1994) Chemical and Petrographic Classification of Kerogen/Macerals, *Energy Fuels,* **8**(6), pp. 1478-1488.

Jansa, L.F. & Wiedmann, J. (1982) Mesozoic-Cenozoic development of teh eastern North American and Northwest Afriacan continental margins: a comparison. In: von Rad, U., Hinz, K., Sarntheim, M & Seibold, E.: Geology of the Northwest African Continental Margin; pp. 215-269, Springer-Verlag, Berlin Heidelberg New York.

Jabour, H., Morabet, A.M. & Bouchta, R. (2000) Hydrocarbon systems of Morocco. *In:* Crasquin-Soleau, S. & Barrier, É.: Peri-Tethys Memoir 5: new data on Peri-Tethyan sedimentary basins, *Mém. Mus. natn. Hist. nat.,* **182**, pp. 143-158.

Jenkyns, H. C. (1988) The early Toarcian (Jurassic) anoxic event: Stratigraphic, sedimentary and geochemical evidence. Am. J. Sci., **288**, pp. 101-151.

Jenkyns, H.C., Jones, C.E., Gröcke, D.R., Hesselbo, S.P. & Parkinson, D.N. (2002) Chemostratigraphy of the Jurassic System: applications, limitations and implications for palaeoceanography. *J. Geol. Soc. London*, **159**, pp. 351-378.

Kendall, C.G.St.C. & Tucker, M.E. (2010) The Depositional Sequence. In: SEPM: *Stratigraphic framework and sedimentary systems*, online publication. SEPM Stratigraphy Web: http://www.sepmstrata.org/page.aspx?pageid=410.

Klemme, H.D. & Ulmishek, G.F. (1991) Effective petroleum source rocks of the world; stratigraphic distribution and controlling depositional factors. AAPG Bull., **75**, pp. 1809-1851.

Klingelhöfer, F., Labails, C., Cosquer, E:, Rouzo, S., Géli, L., Aslanian, D., Olivet, J.-L., Sahabi, M., Nouzé, H. & Unternehr, P. (2009) Crustal structure of the SW-Moroccan margin from wide-angle and reflection seismic data (the DAKHLA experiment) Part A: Wide-angle seismic models. Tectonophysics, **468** (1-4), pp. 63-82.

Klitgord, K.D. & Schouten, H. (1986) Plate kinematics of the central Atlantic. *The Geology of North Ameri-*

ca, vol. **M**. The Western North Atlantic Region, pp. 351-378, The Geological Society of America.

Klitgord, K.D., Hutchinson, D.R. & Schouten, H. (1988) U.S. Atlantic continental margin; Structural and tectonic framework. *The Geology of North America*, vol. **I-2**. The Atlantic Continental Margin: U.S., pp. 19-56, The Geological Society of America.

Knight, K.B., Nomade, S., Renne, P.R., Marzoli, A., Betrand, H. & Youbi, N. (2004) The Central Atlantic Magmatic Province at the Triassic-Jurassic boundary: paleomagnetic and 40Ar/30Ar evidence from Morocco for brief, episodic volcanism. *Earth Planet. Sci. Lett.*, **228**, pp. 143-160.

Kolonic, S., Sinninghe Damsté, J.S., Böttcher, M.E., Kuypers, M.M.M., Kuhnt, W., Beckmann, B., Scheeder, G. & Wagner, T. (2002) Geochemical characterization of Cenomanian/Turonian black shales from the Tarfaya Basin (SW Morocco): Relationships between palaeoenvironmental conditions and early sulphurization of sedimentary organic matter. *J. Pet. Geol.*, **25**(3), pp. 325-350.

Kuhnt, W., Holbourn, A., Gale, A., Chellai, E.A. & Kennedy, J. (2009) Cenomanian sequence stratigraphy and sea-level fluctuations in the Tarfaya Basin (SW Morocco). *Geol. Soc. Am. Bull.*, **121** (11-12), pp. 1695-1710.

Kusznir, N.J. & Karner, G.D. (2007) Continental lithospheric thinning and breakup in response to upwelling divergent mantle fl ow: application to the Woodlark, Newfoundland and Iberia margins. *In:* Karner, G.D., Manatschal, G. and Pinheiro, L.M.: Imaging, Mapping and Modelling Continental Lithosphere Extension and Breakup. *Geol. Soc. Spec. Pub.,* **282**, 389-419.

Labails, C., Olivet, J.-L., Aslanian, D. & Roest, W. (2010): An alternative early opening scenario for the Central Atlantic Ocean. *Earth Planet. Sc. Lett.*, **297**(3-4), pp. 355-368.

Lancelot, Y. & Winterer, E.L. (1980) Evolution of the Moroccan Oceanic Basin and Adjacent Continental Margin – a Synthesis. *Reports of the Deep Sea Drilling Project*, **50**(42), 801-821, doi:10.2973/dsdp.proc.50.1980, publication date: May 2007.

Lee, C., Nott, J., Parrish, A., & Keller, F. B. (2004) Seismic expression of the Tertiary mass transport complexes, deepwater Tarfaya-Agadir Basin, offshore Morocco: *OTC Contribution* **#16741**, 18 p.

Le Pichon, X. & Fox, P.J. (1971) Marginal offsets, fracture zones, and the early opening of the North Atlantic. *J. Geophys. Res,* **76**(26), pp. 6294-6308.

Le Roy, P. (1997) Les basin Ouest-marocains; Leur formation et leur évolution dans le cadre de l'ouverture et du développement de l'Atlantique central (Marge afriquaine). Unpublished Doctoral Thesis, Université de Bretagne Occidental, Brest, 328 p.

Le Roy, P., Guillocheau, F., Piqué, A. & Morabet, A.M. (1998) Subsidence of the Atlantic Moroccan margin during the Mesozoic. *Can. J. Earth Sci.*, **35** (4), pp. 476-493.

Le Roy, P. & Piqué, A. (2001) Triassic-Liassic Western Moroccan synrift basins in relation to the Central Atlantic opening. *Mar. Geol.*, **172**, pp. 359-381.

Letourneau, P.M. & Olsen, P.E. (2003) Tectonics, Structure, and Volcanism. *In:* Letourneau, P.M. & Olsen, P.E, *The Great Rift Valleys of Pangea in Eastern North America,* **I**, 214 p.

Ligtenberg, H., G. de Bruin, N. Hemstra and C. Geel (20069 Sequence Stratigraphic Interpretation in the Wheeler Transformed (Flattened) Seismic Domain, *Proceedings*, extended abstract, 68th EAGE C&E, Vienna

Lin Changsong, Li Sitian, Wan Yongxian, Ren Jangye & Zhang Yanmei (1997) Depositional systems, sequence stratigraphy and basin filling evolution of Erlian fault lacustrine basin, Northeast China. *Proceedings, 30th Int#l Geol. Congr.*, **8**, pp. 163-175.

Lüning. S., Craig, J., Loydell, D.K., Štorch, P. & Fitches, B (2000) Lower Silurian 'hot shales' in North Africa and Arabia: regional distribution and depositional model. *Earth Sci. Rev.*, **49**, pp. 121-200.

Maillard, A., Malod, J., Thiébot, E., Klingelhöfer, F. & Réhaut, J.P. (2006) Imaging a lithospheric detachement at the continental-ocean crustal transition off Morocco. *Earth Plant. Sci. Lett.*, **241**, pp. 686-698.

Mann, P., Gahagan, L., & Gordon, M. (2001) Tectonic Setting of the World's Giant Oil Fields. World Oil, **222** (10), pp. 78-79.

Marzoli, A., Renne, P.R., Piccirillo, E.M., Ernesto, M., Bellieni, G., & De Min, A. (1999). Extensive 200 million-year-old continental flood basalts of the central Atlantic magmatic province. *Science,* **284** (5414), pp. 616–618.

MacGregor, D.S. & Moody, T.J. (1998) Mesozoic and Cenozoic petroleum systems of North Africa. *In:* MacGregor, D.S., Moody, T.J. & Clark-Lowes, D.D.: Petroleum Geology of North Africa. *Geol. Soc. Spec. Publ.* **132**, pp. 283-296

McKenzie, D. (1978) Some remarks on the development of sedimentary basins. *Earth Planet. Sc. Lett.,* **40**, pp. 25-32.

Meunier, J. (2011) Seismic Acquisition from Yester

day to Tomorrow. *EAGE SEG Distinguished Instructor Series*, **14**, 236 p.

Michard, A., Hoepffner, C., Soulaimani, A. & Baidder, L. (2008) The Variscan Belt. *In:* Michard, A., Saddiqi, O., Chalouan, A., & Frizon De Lamotte, D.: *Continental Evolution: The Geology of Morocco.* 1st edn, pp. 65-132, Springer Verlag, Berlin Heidelberg.

Miller, D.S. & Duddy, I.R. (1989). Early Cretaceous Uplift and Erosion of the Northern Appalachian Basin, New York, based on Apatite Fission Track Analysis. *Earth Planet. Sci. Lett.*, **93**, pp. 35-49.

Mitchum, R.M. Vail, P.R., Todd. R.G. & Sangree, J.B. (1976) Regional seismic interpretations using sequences and eustatic cycles. *AAPG Bull.*, **60**, p. 669

Morabet, A.M., Bouchta, R., & Jabour, H. (1998) An overview of the petroleum systems of Morocco . *In:* MacGregor, D.S., Moody, T.J. & Clark-Lowes, D.D.: Petroleum Geology of North Africa. *Geol. Soc. Spec. Publ.* **132**, pp. 283-296

Mort, H.P., Adatte, T., Keller, G., Bartels, D., Föllmi, K.B. Steinmann, P., Berner, Z. & Chellai, E.H. (2008) Organic carbon deposition and phosphorus accumulation during Oceanic Anoxic Event 2 in Tarfaya, Morocco. *Cretaceous Res.*, **29**(5-6), pp. 1008-1023.

Moucha, R., Forte, A.M., Mitrovica, J.X., Rowley, D.B., & Quéré, S. (2008) Dynamic Topography and Long-Term Sea-Level Variations: There May Be No Such Thing as a Stable Continental Platform. *Earth Planet. Sc. Letters*, **271**, pp. 101-108, 2008.

Müller, R.D., Sdrolias, C., Gaina, C., & Roest, W.R. (2008): Age, spreading rates and spreading symmetry of the world's ocean crust. Geochem. Geophys. Geosyst., **9**(4), Q04006, doi:10.1029/2007GC001743, 19 p.

Myers, K.J. & Milton, N.J. (1996) Concepts and Principles of Sequence Stratigraphy. *In:* Emery, D. & Myers, K.: *Seq. Strat.*, Wiley, pp. 11-41.

Nedimović, M.R. (2000) Seismic reflection imaging in crystalline terrains, Ph.D. thesis, University of Toronto, Canada, 185 p.

Nadin, P.A. and Kusznir N.J. (1995) Paleocene uplift and Eocene subsidence in the northern North Sea Basin from 2D forward and reverse stratigraphic modeling. *J. Geol. Soc London*, **152**, pp. 833-848.

Nadin, P.A. & Kusznir N.J. (1996) Forward and reverse stratigraphic modeling of Cretaceous-Tertiary poststrift subsidence and Paleogene uplift in the Outer Moray Firth Basin, central North Sea, *in*: Knox, R.W.O'B., Corfield, R.M. & Dunay, R.E., Correlation of the Early Paleogene in Northwest Europe. *Geol. Soc. Spec. Publ.*, **101**, pp. 43-62.

Neal, J. & V. Abreu (2009): Sequence stratigraphy hierarchy and the accommodation succession method, *Geology*, **37**, p. 779-782.

Olivet, J.-L. (1996) La cinématique de la plaque Iberique. *Bulletin des Centres de Rechérches Èxploration–Production Elf Aquitaine*, **20**(1), 131–195.

Olsen, P.E. (1997) Stratigraphic record of the Early Mesozoic breakup of Pangea in the Laurasia/Gondwana rift system. *Annu. Rev. Earth Plant. Sci.*, **25**, 337-401.

ONAREP (1985) Composite log of well Cap Juby. Unpublished well chart.

ONAREP (2003) Opportunities for Hydrocarbon Exploration and Production in Morocco. Publ. Brochure.

ONHYM (2008) A collection of stratigraphic charts from 38 wells of southern Morocco. Unpublished stratigraphic well charts, 39 p.

Oyarzun, R., Doblas, M., López-Ruiz, J. & Cebriá, J. M. (1997). Opening of the central Atlantic and asymmetric mantle upwelling phenomena: implications for long-lived magmatism in western North Africa and Europe. *Geology,* **25**, 727–730

Posamentier, H.W., Jervey, M.T. & Vail, P.R. **(**1988) Eustatic controls on clastic deposition. I. Conceptual framework. *In:* Wilgus, C.K., Hastings, B.S., Kendall, C.G.St.C., Posamentier, H.W., Ross, C.A., Van Wagoner, J.C.: Sea Level Changes—An Integrated Approach, *SEPM Spec. Publ.,* **42**, pp. 110–124.

Posamentier, H.W. & Vail, P.R. (1988) Eustatic controls on clastic deposition. II. Sequence and systems tract models. *In:* Wilgus, C.K., Hastings, B.S., Kendall, C.G.St.C., Posamentier, H.W., Ross, C.A., Van Wagoner, J.C.: Sea Level Changes—An Integrated Approach, *SEPM Spec. Publ.,* **42**, pp. 125–154.

Purser, B.H, & Bosence, D.W.J. (1998) Sedimentation and Tectonics of Rift Basins: Red Sea–Gulf of Aden. Chapman & Hall, London, 663 p.

Querol, R. (1966) Regional Geology of the Spanish Sahara. In: *Sedimentary basins of the African coasts, pt. 1, Atlantic Coast*, Paris, pp. 27-40.

Ranke, U., von Rad, U. & Wissmann, G. (1982) Stratigraphy, Facies and Tectonic Development of the On- and Offshore Aaiun-Tarfaya Basin – A Review. *In:* von Rad, U., Hinz, K., Sarntheim, M & Seibold, E.: Geology of the Northwest African Continental Margin; pp. 86-105, Springer-Verlag, Berlin Heidelberg New York.

Ratschiller, L.K. (1970) Lithostratigraphy of the Northern Spanish Sahara. *Mem. Museo Tridentino Sci. Nat.*, **18**, pp. 9-84.

Reading, H.G. (1998) Sedimentary Environments: Processes, Facies and Stratigraphy. Reprinted 3rd edition, Blackwell, 688 p.

Reich, M.: Hunting Underground – A high-tech search for oil, gas and geothermal energy, Verlag addbooks, 160 p.

Roberts, A.M., Yielding G., Kusznir, N.J., Walker, I.M. & Dorn-Lopez, D. (1995) Quantitative analysis of Triassic extension in the northern Viking Graben. *J. Geol. Soc London*, **152**, pp. 15-26.

Roberts, A.M., Lundin, E.R. & Kusznir, N.J. (1997) Subsidence of the Vøring Basin and the influence of the Atlantic continental margin, *in:* Roberts, A.M. & Kusznir, N.J.: Tectonic, Magm. and Depositional Processes at Passive Continental Margins. *Geol. Soc. Spec. Publ.*, **154**, pp. 551-557.

Roberts, A.M., Kusznir, N.J., Yielding, G. &Styles, P. (1998) 2D flexural backstripping of extensional basins: the need for a sideways glance. *Petr. Geosci.*, **4**, 327-338.

Robertson, A.F.H., Searle, M.P., & Ries, A.C. (1990) The Geology and Tectonics of the Oman Region. *Geol. Soc. Spec. Publ.*, **49**, 845 p.

Roden, R. (2005) The evolution of the interpreter‘s toolkit - past, present, and future. *TLE*, 24, pp. 72-78.

Roeser, H.A. (1982) Magnetic Anomalies in the Magnetic Quiet Zone off Morocco. *In:* von Rad, U., Hinz, K., Sarntheim, M & Seibold, E.: Geology of the Northwest African Continental Margin; pp. 61-68, Springer-Verlag, Berlin Heidelberg New York.

Rothe, P. (1968) Mesozoische-Flyschablagerungen auf der Kanareninsel Fuerteventura. *Geol. Rundsch. (Int. J. Earth Sci)* **58**(1), pp. 314-332.

Rona, P.A. (1970) Comparison of Continental Margins of Eastern North America at Cape Hatteras and Northwestern Africa at Cape Blanc. *AAPG Bull.,* **54**(1), 129-157.

Rosenbaum, G., Lister, G.S. & Duboz, C. (2002) Reconstruction of the tectonic evolution of the western Mediterranean since the Oligocene. *In:* Rosenbaum, G. and Lister, G. S. Reconstruction of the evolution of the Alpine-Himalayan Orogen. *Journal of the Virtual Explorer*, **8**, pp. 107 - 130.

Rybarczyk, G. (2012) personal communication during the processing of the 3D-survey ÜWG Groß-Gerau, February 2012.

Saadi, M., Hital, E.A., BensaÏd, M., Boudda, A. & Dahmani, M. (1985) Carte Géologique du Maroc. *Éditions du Service Géologique du Maroc – Notes et Mémoires*, **260**.

Sachse, V.F. (2011) Petroleum source rocks of western and central Africa: the examples of the marine Tarfaya Basin, Morocco and the continental Congo Basin, Democratic Republic of Congo, PhD-Thesis, Rheinisch-Westfälische Technische Hochschule (RWTH) Aachen, 172p.

Sachse, V.F., Littke. R., Heim, S., Kluth, O., Schober, J., Boutib, L., Jabour, H., Persson, F. & Sindern, S. (2011) Petroleum source rocks of the Tarfaya Basin and adjacent areas, Morocco. *Org. Geochem.*, **42**, pp. 209-227.

Sachse, V.F., Heim, H., Jabour, H., Kluth, O., Schümann, T., Aquit, M., & Littke, R. (2014) Organic geochemical characterization of Santonian to Early Campanian organic matter-rich marls (Sondage No 1 cores) as related to OAE3 from the Tarfaya Basin, Morocco. *Mar. Petr. Geol.*, **56**, 290-304.

Sahabi, M., Aslanian, D. & Olvet, J.-L. (2004) Un nouveau point de départ pour l'histoire de l'Atlantique central. *C. R. Geosci.*, **336**, pp. 1041-1052.

Schott, R.A. (2007) Remote Sensing - The Image Chain Approach, 2nd edition, Oxford University Press, 666 p.

Schowengerdt, R.A. (2007) Remote Sensing. 3rd edition, Elsevier, 515 p.

Scotese, C.R. (2006) PALEOMAP Paleogeographic Atlas, online publication of the University of Texas, Department of Geology, http://www.scotese.com.

Scrutton, R.A. (1982): Passive continental margins: a review of observations and mechanisms. *In:* Scrutton, R.A.: *Dynamics of passive margins*. *AGU Geodynamic Series*, **6**, pp. 5-11.

Sehrt, M. (2014): Variscan to Neogene long-term landscape evolution at the Moroccan passive continental margin (Tarfaya Basin and western Anti-Atlas), PhD-Thesis, Ruprecht-Karls-University, Heidelberg, 174 p.

Shaw, D.T. & Roberts, J.D.M. (2009) An Independent Assessment of Wessex Exploration plc., unpublished report, 34 p.

Smith, B.M., Kidston, A.G., Brown, D.E. & Altheim, B. (2010) The Jurassic Carbonate Reef Trend Offshore Nova Scotia. *Proceedings*, 2nd Central & North Atlantic Conjugate Margins Conference, Lisbon, 29. September - 01. October 2010, pp. 266-269.

Stampfli, G.M. & Merchant, R.H. (1997) Geodynamic evolution of the Tethyan margins of the western Alps. *In:* Pfiffner, O.A., Lehner, P., Heitzmann, P., Mueller, St., & Steck. A.. *Deep structure of the Swiss Alps: results of NRP 20*, pp. 223-239.

Seibold, E. (1982) The northwest African continental margin - an introduction. *In:* von Rad, U., Hinz, K., Sarntheim, M & Seibold, E.: Geology of the Northwest African Continental Margin; pp. 3-20, Springer-Verlag, Berlin Heidelberg New York.

Simoneit, B.R.T., Vuchev, V.T. & Grimalt, J.O. (1984) Organic Matter along the Sedimentary Sequences of the Noroccan Continental Margin, Leg 79, Sites 545 and 547. *DSDP Initial Reports*, **79**(33), pp. 807-824.

Smith, B.M., Kidston, A.G., Brown, D.E. and Altheim, B. (2010) The Jurassic Reef Carbonate Trend Offshore Nova Scotia. *Proceedings*, 2nd Central & North Atlantic Conjugate Margins Conference, Lisbon, 29. September - 01. October 2010, pp. 266-269.

Srivastava, S. P., Sibuet, J.-C., Cande, S., Roest, W. R., & Reid, I. D. (2000). Magnetic evidence for slow sea floor spreading during the formation of the Newfoundland and Iberian margin. *Earth Planet. Sci. Lett.*, **182**, pp. 61–76.

State of California (2013) OIl, Gas & Geothermal - Picture of a drill rig. online publication of the Department of Conservation. http://www.conservation.ca.gov/dog/picture_a_well/Pages/qh_drill_rig.aspx.

Steiner, C., Hobson, A., Favre, P., Stampfli, G.M. & Hernandez, J. (1998) Mesozoic sequence of Fuerteventura (Canary Islands): Witness of Early Jurassic sea-floor spreading in the Central Atlantic. *Geol. Soc. Am. Bull.*, **110**(10), pp. 1304-1317.

Tari, G., Molnar, J. & Ashton, P. (2003) Examples of salt tectonics from West Africa: a comparative ap-

proach. *In*: Arthur, T.J., Macgregor, D.S. & Cameron, N.R.: *Petroleum Geology of Africa: New Themes and Developing Technologies*, *Geol. Soc. Spec. Publ.*, **207**, pp. 85-104.

Tari, G., Jabour, H., Molnar, J., Valasek, D. & Zizi, M. (2012): Deep-water Exploration in Atlantic Morocco: Where Are the Reservoirs? *In*: Dengliang, G.: *Tectonics and Sedimentation: Implications for Petroleum Systems*, *AAPG Mem.*, **100**, pp. 337-355.

The Yoeck Project (2002) Carls Spitzweg: Der Geologe. aus: *10.000 Meisterwerke der Malerei*, DVD-ROM, ISBN 3936122202.

Theys, P. (1999) Log Data Acquisition and Quality Control. Edition Technip, Paris, 455 p.

Tissot, R.P. & Welte, D.H. (1984) Petroleum Formation and Occurance. 2nd Ed. Springer Berlin, Heidelberg, New York, 699 p.

Todd, R.G. & Mitchum jr, R.M. (1977) Seismic Stratigraphy and Global Changes of Sea Level, Part 8: Identification of Upper Triassic, Jurassic and Lower Cretaceous Seismic Sequences in Gulf of Mexico and Offshore West Africa. *In:* Vail, P.R., Mitchum jr., R.M., Todd, R.G., Widmier, J.M., Thompson III, S., Sangree, J.B., Bubb, J.N. & Hatlelid, W.G.: Seismic Stratigraphy and Global Changes of Sea Level. *In:* PAYTON, C.E. Seismic Stratigraphy – applications to hydrocarbon exploration, *AAPG Mem.*, 26, pp. 145-163.

Tourani, A., Lund, J. J., Benaouiss, N., & Gaupp, R. (2000). Stratigraphy of Triassic syn-rift deposition in western Morocco. *In:* Bachmann, G. H. & Lerche, I. (Eds.), Epicontinental Triassic, *ZPL GEO PAL,* **9/10,** pp. 1193–1215.

Tucker, M.E. (2003) Sedimentary Rocks in the Field. Wiley and Sons, 234 p.

Turcotte, D.L. & Schubert, G. (2002) Geodynamics, 2nd ed., Cambridge University Press, 719 p.

Tyson, R.V. (2005) Productivity versus preservation controversy: cause, flaws and resolution. In: Harris, N.B. The Deposition of Organic Carbon-Rich Sediments, Geol. Soc. Spec. Publ., **82**, pp. 17-34.

Uchupi, E., Emery, K.O., Bowin, C.O. & Phillip, J.D. (1976) The continental margin off Western Africa: Senegal to Portugal. *AAPG Bull.*, **60**(5), 809-878.

Vail, P.R. & Sangree, J.B. (1971) Time stratigraphy from seismic data. *AAPG Bull.*, **55**, pp. 367-368

Vail, P.R. (1975) Eustatic cycles from seismic data for global stratigraphic analysis. *AAPG Bull.*, **59**, pp. 2198-2199

Vail, P.R., Mitchum jr., R.M., Todd, R.G., Widmier, J.M., Thompson III, S., Sangree, J.B., Bubb, J.N. & Hatlelid, W.G. (1977) Seismic Stratigraphy and Global Changes of Sea Level. In: Payton, C.E.: Seismic Stratigraphy – applications to hydrocarbon exploration, AAPG Mem., 26, pp. 49-212.

van Wagoner, J.C., Posamentier, H.W., Mitchum, R.M., Vail, P.R., Sarg, J.F., Loutit, T.S., Hardenbol, J. **(**1988) An overview of sequence stratigraphy and key definitions. *In*: Wilgus, C.K., Hastings, B.S., Kendall, C.G.St.C., Posamentier, H.W., Ross, C.A., Van Wagoner, J.C.: Sea Level Changes - An Integrated Approach. *SEPM Spec. Publ.*, **42**, pp. 39–45.

Van Wagoner, J. C., Mitchum Jr., R. M., Campion, K. M. & Rahmanian, V. D. (1990) Siliciclastic sequence stratigraphy in well logs, core, and outcrops: concepts for high-resolution correlation of time and facies. *AAPG Methods in Exploration Series***, 7**, 55 p.

Veeken, P.C.H., (2008): Seismic Stratigraphy, Basin Analysis and Reservoir Characterisation. Ed.: Helbig, K. & Treitel, S. *HGE*, **37**, 509 p.

Veevers, J.J (2004) Gondwanaland from 650-500 Ma assembly through 320 Ma merger in Pangaea to 185-100 Ma breakup; supercontinental tectonics via stratigraphy and radiometric dating. *Earth Sci. Rev.,* **68**, pp. 1-132.

Veselovský, Z. (2004) Integrated numerical modelling of a polyhistory basin, Southern Cantabrian Basin (Palaeozoic, NW-Spain), PhD-Thesis of the Geological-Paleontological Institute, Heidelberg University, 225 p.

Veselovský, Z., Bechstädt, T. & Zühlke, R. (2008) Structural, reverse-basin and forward stratigraphic modelling of the Southern Cantabrian Basin, NW

Spain. *In*: Boer, P., Postma, G., Van der Zwan, K., Burgess, P. & Kukla, P.: Analogue and Numerical Modelling of Sedimentary Systems: From Understanding to Prediction. *IAS Spec Publ.*, **40**, pp. 65-96.

Vining, B.A. & Pickering, S.C. (2010) Petroleum Geology: From Mature Basins to New Frontiers; *Proceedings* of the 7th Petroleum Geology Conference, Geol. Soc., 715 p..

Vogt, P. R., & Tucholke, B. E. (1986) The western North Atlantic Region, *The geology of North America,* **M,** Geological Society of America, 696p.

von Rad, U., Hinz, K., Sarntheim, M. & Seibold, E. (1982) Geology of the Northwest African Continentak Margin, 474 p.

von Rad, U. & Arthur, M.A. (1979) Geodynamic, sedimentary and vulcanic evolution of the Cap Bojador contnental margin (NW Africa). *In:* Talwani M., Deep drilling results in the Atlantic Ocean: continental margin and palaeoenvironment. *Amer. Geophys. Union*, **3**, pp. 187-203.

Walther, J. (1893/94) Einleitung in die Geologie als historische Wissenschaft. Beobachtungen über die Bildung der Gesteine und ihrer organischen Einschlüsse. I. Theil: Bionomie des Meeres, II. Theil: Die Lebensweise der Meeresthiere, III. Theil: Lithogenesis der Gegenwart. Gustav Fischer, Jena, 1055 p.

Watts, A.B. & Ryan, W.B.F. (1976) Flexure of the lithosphere and continental margin basins. *Tectonophysics*, **36**(1-3), pp. 25-44

Watts, A.B. & Burov, E.B. (2003) Lithospheric strength and its relationship to the elastic and seismogenic layer thickness. *Earth Planet. Sci. Lett.*, **213**, 113-131.

Weber G. & Green J. (1981) Guide to oil shale. National Conference of State Legislatures. Washington D.C. USA, p. 21

Wegener, A. (1915) Die Entstehung der Kontinente und Ozeane. 1. Auflage, Vieweg & Sohn, Braunschweig, 94 p.

Wegener, A. (1929) Die Entstehung der Kontinente und Ozeane. 4. Aufl., Vieweg & Sohn, Br.schwg., 231 p.

Wenke, A(nne) (2012) Les Rochers Bleu. Photographic panorama. Personal communication

Wenke, A.(A.O.), Dedera, S., Zühlke, R., Kluth, O. and Schober, J. (2009a) Mesozoic to Cenozoic evolution of the Tarfaya Basin, Morocco - an integrated approach, *Abstracts and Field Guide*, 6th Annual Conference of SEPM-CES - Sediment 2009, Kraków, June 2009, p. 46.

Wenke, A.(A.O.), Sachse, V.R., Sehrt, M., Dedera, S., & Zühlke, R. (2009b) Atlantic Margin Project, Morocco: Report of the first field reconnaissance. Unpublished report, 32 p.

Wenke, A.(A.O.), Zühlke, R., Boutib, L., Jabour, H., Kluth, O. & Schober, J. (2010a) Meso- to Cenozoic Sequence Stratigraphy of the Tarfaya Basin, Morocco; *Proceedings*, 72nd EAGE Conference and Exhibition 2010, Barcelona, 14.-17. June 2010, paper J011.

Wenke, A.(A.O.), Zühlke, R., Boutib, L., Jabour, H., Kluth, O. & Schober, J., Sequence stratigraphy and evolution of the Tarfaya Basin, Morocco; *Proceedings*, 2nd Central & North Atlantic Conjugate Margins Conference, Lisbon, 29. September - 01. October 2010, pp. 289-293.

Wenke, A.(A.O.), & Zühlke, R. (2011) Atlantic Margin Project – Sequence Stratigraphy and Basin Development of the Tarfaya Basin. Unpublished Report, 144 p., Steinbeis-Transfer Center GeoResources, Heidelberg

Wenke, A.(A.O.), Zühlke, R., Jabour, H. & Kluth, O. (2011) High-resolution seq. stratigraphy in basin reconnaissance: example from the Tarfaya Basin, Morocco. *First Break*, **29**(11), pp. 85-96.

Wenke, A.(A.O.),, Lorson, C., Zühlke, R., & Bissmann, S. (2012a) Geological Setting at the Eastern Cebtral Upper Rhine Valley - a view into the „Heidelberger Loch“. *Proceedings*, DGMK/ÖGEW-Frühjahrstagung, 19. & 20.04 2012, Celle, pp. 85-92.

Wenke,, A.(A.O.), Bissmann, S., Lorson, C., & Loske, B. (2012b) Tiefe Geothermie in Groß-Gerau - Interpretation 3D-seismischer Daten im Raum Groß-Gerau/Trebur. unpublished report, GeoThermal Engineering/DMT, 68 p.

Wenke, A.(A.O.), Zühlke, R., Jabour, H., Kluth, O. & Schümann, T. (2012c) Quantitative Tarfaya Basin Development, Morocco. Abstract & presentation held at the AAPG 2012 Annual Convention & Exhibition, Long Beach, California, April, 22-25, *AAPG Search & Discovery*, article#10420, http://www.searchanddiscovery.com/documents/2012/10420wenke/ndx_wenke.pdf.

Wenke, A.A.O., Zühlke, R. Jabour, H., & Kluth, O. (subm.) Quantitative subsidence analysis and sediment flux history of the Tarfaya-Laâyoune Basins, North West African passive continental margin, submitted to *Basin Research*

Whaley, J. (2012) Morocco - High Expectations. *GeoExPro*, **9**(2), pp. 60-64.

Williams, C. & Nield, T. (2007) Pangaea, the comeback. *New Sci.*, **2626**, pp. 36-40.

Wilson, R.C.L., Whitmarsh, R.B., Taylor, B., & Froitzheim, N. (2001) Non-volcanic rifting of continental margins; a comparison of evidence from land and sea. *Geol. Soc. Spec. Publ.*, **187**, 576 p.

Winterer, E.L. & Hinz, K. (1981) The Evolution of the Mazagan Continental Margin: A Synthesis of Geophysical and Geological Data with Results of Drilling during Deep Sea Drilling Project Leg 79. *Reports of the Deep Sea Drilling Project*, **79**(38), 893-919, doi:10.2973/dsdp.proc.79.138.1984. publication date: May 2007.

Zarhloule, Y., Bouri, S., Lahrach, A., Boughriba, M., El Mandour, A. & Ben Dhia, H. (2005): Hydrostratigraphical Study, Geochemistry of Thermal Springs, Shallow and Deep Geothermal Exploration in Morocco, *Proceedings* of the World Geothermal Congress, Antalya, Turkey, 24th - 29th of April 2005, 13 p.

Ziegler, P.A. & Cloetingh, S. (2004) Dynamic processes controlling evolution of rifted basins. *Earth Sci. Rev.,* **64**, pp. 1–50.

Zöllner, H. & Schikowsky, P. (2003) The influence of near-seafloor low velocity layers on shallow marine seismic measurements. *Proceedings*, EAGE Geophysics of the 21st Century - The Leap into the Future. extended abstract.

Zouhri, S. Kchikach, A. Saddiqi, O., El HaÏmer, F.Z., Baidder, L. & Michard, A (2008): The Cretaceous-Tertiary Plateaus. *In:* Michard, A., Saddiqi, O., Chalouan, A., & Frizon De Lamotte, D.: Continental Evolution: The Geology of Morocco. 1st edn, pp. 331-358, Springer Verlag, Berlin Heidelberg.

Zühlke, R., Bouaouda, M., Ouajhain, B., Bechstädt, T. & Leinfelder, R. (2004): Quantitative Meso-/Cenozoic development of the eastern Central Atlantic continental shelf, western High Atlas, Morocco. *Mar. Pet. Geol.*, **21**, 225-276.

Appendix

Appendix 1
Map of sampling points. Background: Geological map of Morocco (*Saadi *et al., 1986)
from Wenke et al. (2009)

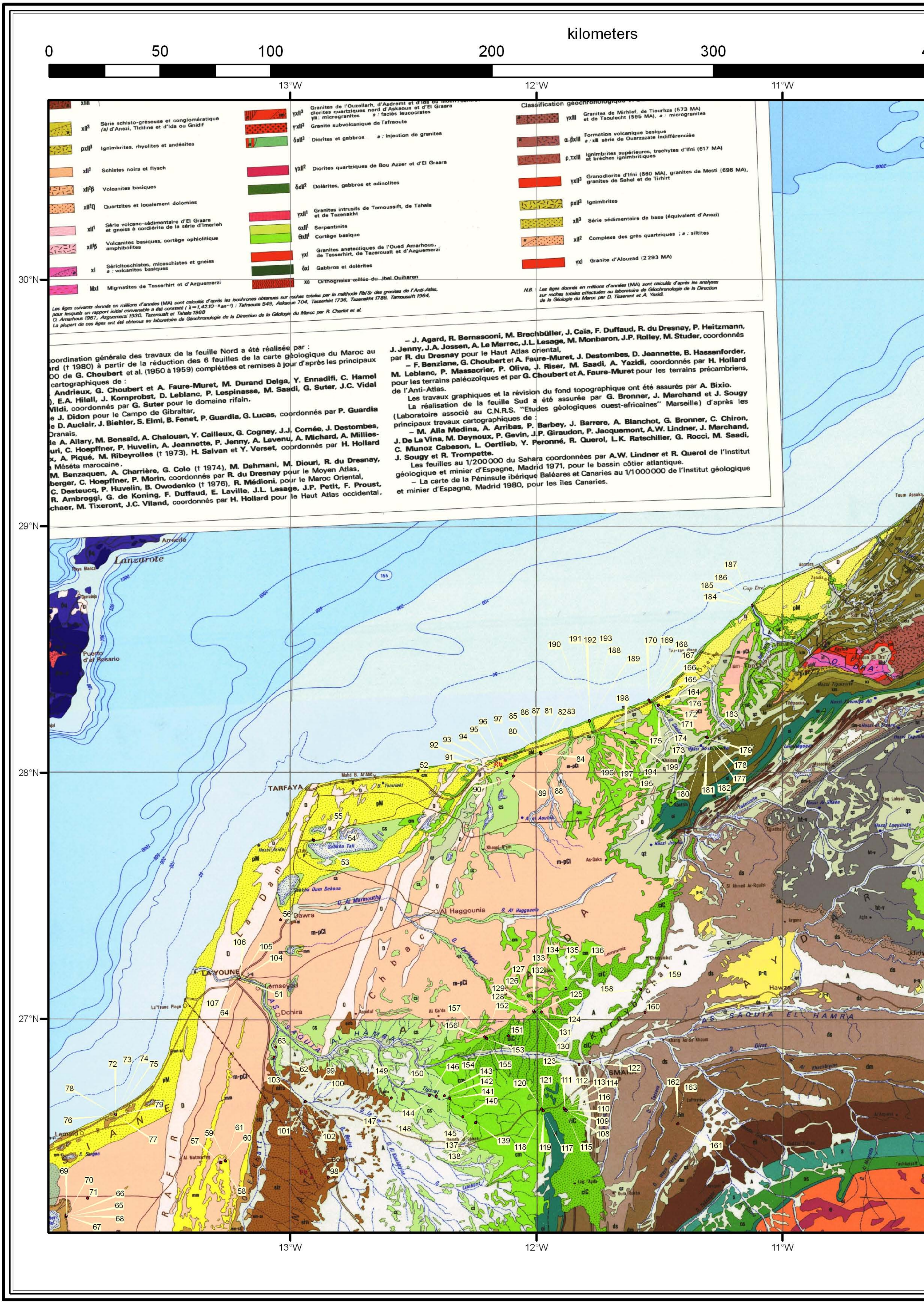

kilometers
0
50
100
200
300
13°W
12°W
11°W
30°N
29°N
28°N
27°N
Série schisto-gréseuse et conglomératique (a) d'Anezi, Tidiline et d'Ida ou Gnidif
Ignimbrites, rhyolites et andésites
Schistes noirs et flysch
Volcanites basiques
Quartzites et localement dolomies
Série volcano-sédimentaire d'El Graara et gneiss à cordiérite de la série d'Imerleh
Volcanites basiques, cortège ophiolitique amphibolites
Séricitoschistes, micaschistes et gneiss
Migmatites de Tasserhirt et d'Azguemerzi
Granite subvolcanique de Tefraoute
Diorites et gabbros
Diorites quartziques de Bou Azzer et d'El Graara
Dolérites, gabbros et adinolites
Granites intrusifs de Tamoussift, de Tahala et de Tazenakht
Serpentinite
Cortège basique
Granites anatectiques de l'Oued Amarhous, de Tasserhirt, de Tazeroualt et d'Azguemerzi
Gabbros et dolérites
Orthogneiss œillés du Jbel Ouiharen
Granites de Mirhlef, de Tiourhza (573 MA) et de Taoulecht (595 MA)
Formation volcanique basique
Ignimbrites supérieures, trachytes d'Ifni (617 MA) et brèches ignimbritiques
Granodiorite d'Ifni (660 MA), granites de Mesti (698 MA), granites de Sahel et de Tirhirt
Ignimbrites
Série sédimentaire de base (équivalent d'Anezi)
Complexe des grès quartziques
Granite d'Alouzad (2293 MA)
coordination générale des travaux de la feuille Nord a été réalisée par :
rd († 1980) à partir de la réduction des 6 feuilles de la carte géologique du Maroc au
00 de G. Choubert et al. (1950 à 1959) complétées et remises à jour d'après les principaux
cartographiques de :
– J. Agard, R. Bernasconi, M. Brechbüller, J. Caïa, F. Duffaud, R. du Dresnay, P. Heitzmann,
J. Jenny, J.A. Jossen, A. Le Marrec, J.L. Lesage, M. Monbaron, J.P. Rolley, M. Studer, coordonnés
par R. du Dresnay pour le Haut Atlas oriental,
Les travaux graphiques et la révision du fond topographique ont été assurés par A. Bixio.
La réalisation de la feuille Sud a été assurée par G. Bronner, J. Marchand et J. Sougy
– M. Alia Medina, A. Arribas, P. Barbey, J. Barrere, A. Blanchot, G. Bronner, C. Chiron,
Les feuilles au 1/200 000 du Sahara coordonnées par A.W. Lindner et R. Querol de l'Institut
géologique et minier d'Espagne, Madrid 1971, pour le bassin côtier atlantique.
– La carte de la Péninsule ibérique Baléares et Canaries au 1/1 000 000 de l'Institut géologique
et minier d'Espagne, Madrid 1980, pour les îles Canaries.
Lanzarote
Arrecife
Puerto del Rosario
Cap Dra
TARFAYA
Sebkha Tah
Al Haggounia
LA'YOUNE
Dchira
Lemseyed
SMARA
Hawza
AS SAQUIA EL HAMRA

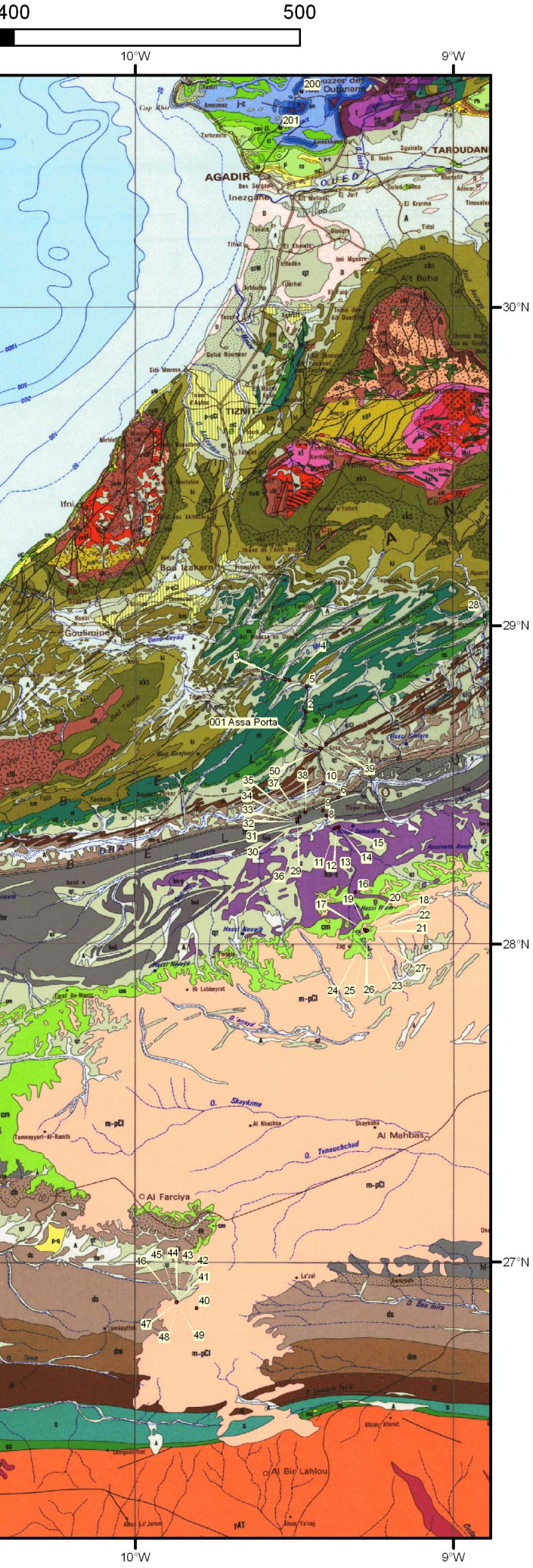

Atlantic Margin Project
First Fieldtrip
March 2009
Waypoints

N
W E
S

1:2.000.000

Appendix 1I
Table of 2D seismic dataset used in this study

Line-name	Survey name	Year of acquisition	Domain	Type	Zmin	Zmax	length (km)
83MMO-01	ONHYM_83MMO	1983	Time	2D	-6996	0	37
83MMO-10	ONHYM_83MMO	1983	Time	2D	-6996	0	121
83MMO-15	ONHYM_83MMO	1983	Time	2D	-6996	0	75
83MMO-30	ONHYM_83MMO	1983	Time	2D	-6996	0	62.5
83MMO-33	ONHYM_83MMO	1983	Time	2D	-6996	0	47.5
83MMO-35	ONHYM_83MMO	1983	Time	2D	-6996	0	55
E98MA03-06	E98MA	1998	Time	2D	-8000	0	61
E98MA03-14	E98MA	1998	Time	2D	-8000	0	98
E98MA03-29	E98MA	1998	Time	2D	-8000	0	140
EM-11	EM	1969	Time	2D	-7880	120	64.5
EM-26	EM	1969	Time	2D	-8000	0	33
EM-31_2	EM	1969	Time	2D	-4990	10	54
EM-31_3	EM	1969	Time	2D	-4970	30	47.5
EM-39	EM	1969	Time	2D	-4965	35	51
EM-45_1	EM	1969	Time	2D	-8000	0	27
EM-45_2	EM	1969	Time	2D	-8000	0	46.5
EM-45_3	EM	1969	Time	2D	-8000	0	75
EM-49	EM	1969	Time	2D	-8000	0	57.5
EM-55	EM	1969	Time	2D	-8000	0	30
EM-85_S	EM	1969	Time	2D	-8000	0	26
EM-86-2-2	EM	1969	Time	2D	-5996	0	39
EM-119	EM	1969	Time	2D	-3950	50	61.5
EM-129	EM	1969	Time	2D	-6000	0	36.5
EM-260	EM	1969	Time	2D	-8161	35	64.5
EM-264	EM	1969	Time	2D	-8196	0	37
EM-272	EM	1969	Time	2D	-8196	0	22.5
IF-91-115	IF-91	1991	Time	2D	-6996	0	17.5
IF-91-123	IF-91	1991	Time	2D	-6996	0	47.75
IF-91-139	IF-91	1991	Time	2D	-6996	0	62.75
IF-91-154	IF-91	1991	Time	2D	-6996	0	14.5
IF-91-160	IF-91	1991	Time	2D	-6996	0	127.5
IF-91-163	IF-91	1991	Time	2D	-6996	0	113
ROCM99-04	ROCM99	1999	Time	2D	-6996	0	41.75
ROCM99-06	ROCM99	1999	Time	2D	-6996	0	32.5
ROCM_99_18	ROCM99	1999	Time	2D	-6996	0	27
88-LA-01	88-LA	1988	Time	2D	-5046	250	51.75
88_LA_02	88-LA	1988	Time	2D	-5046	150	43
88-LA-03	88-LA	1988	Time	2D	-5146	150	42.75
88-LA-04	88-LA	1988	Time	2D	-5146	150	77.75
88-LA-05	88-LA	1988	Time	2D	-5141	155	65.5
88-LA-06	88-LA	1988	Time	2D	-5146	150	101
88-LA-07	88-LA	1988	Time	2D	-5142	154	58.5
88-LA-08	88-LA	1988	Time	2D	-5046	250	97
88-LA-10	88-LA	1988	Time	2D	-5046	250	90
88-LA-11	88-LA	1988	Time	2D	-5146	150	21.5
88_LA_12	88-LA	1988	Time	2D	-5046	250	158.5
88-LA-13	88-LA	1988	Time	2D	-5021	275	55.75
88-LA-15	88-LA	1988	Time	2D	-5021	275	21.5
88-LA-17	88-LA	1988	Time	2D	-5016	280	43.5
87-TA-01W	87-TA	1987	Time	2D	-5021	175	38.5
87-TA-01E	87-TA	1987	Time	2D	-5021	175	84
87-TA-01W2	87-TA	1987	Time	2D	-5021	175	43.75
87-TA-02	87-TA	1987	Time	2D	-5021	175	35
87-TA-03W	87-TA	1987	Time	2D	-5021	175	68.5
87-TA-04	87-TA	1987	Time	2D	-5021	175	31.25
87-TA-05W	87-TA	1987	Time	2D	-5021	175	53
87-TA-06	87-TA	1987	Time	2D	-5021	175	31
87-TA-07W	87-TA	1987	Time	2D	-5021	175	59.5
87-TA-09	87-TA	1987	Time	2D	-5021	175	40.5
87-TA-10	87-TA	1987	Time	2D	-5021	175	20.25
87_TA_13	87-TA	1987	Time	2D	-5011	385	61.75
87_TA_15	87-TA	1987	Time	2D	-5006	390	65.25
87_TA_19	87-TA	1987	Time	2D	-4996	400	17.5
88-TA-16	88-TA	1988	Time	2D	-5021	375	66.5
88-TA-17-1	88-TA	1988	Time	2D	-5021	375	22.75
88-TA-17-2	88-TA	1988	Time	2D	-4946	450	21.75
WMS-5	WMS	n.k.	Time	2D	-7500	0	113
WMS-18	WMS	n.k.	Time	2D	-7500	0	93
wms_9b	WMS	n.k.	Time	2D	-7400	0	83
fred	Fred	n.k.	Time	2D	-8100	-100	45.5
sem	SEM	n.k.	Time	2D	-10100	-100	65.5
Total							4043

Appendix 1II
Table of available and generated check shot data for this study

MD	TWT	Ave. vel.	Int. vel.	MD	TWT	Ave. vel.	Int. vel.
Ifni-1				MO-1			
0	0		2370.55	9.8	0		1288.57
213.35	180	2096.22	3585.71	100	140	1288.57	3084.5
243.83	197	2224.75	4063.8	1916	1317.5	2893.66	
274.31	212	2354.87	3585.71				
304.79	229	2446.25	3208.26	MO-5			
335.26	248	2504.63	2770.77	9.2	0		1321.38
365.74	270	2526.31	3585.71	105	145	1321.38	2900.16
396.22	287	2589.06	3386.5	1906	1387	2735.11	
426.7	305	2636.13	3585.71				
457.18	322	2686.26	3585.71	CORC 15-1			
487.66	339	2731.36	3386.5	0	-13.53	2000	2656.51
518.13	357	2764.4	3386.5	795	585	2671.69	2575
548.61	375	2794.26	2770.77	1310	985	2632.43	3307.02
579.09	397	2792.96	5541.55	3195	2125	2994.32	
609.57	408	2867.06	4354.07				
640.05	422	2916.39	5079.75	HAG 1-2			
670.53	434	2976.21	5079.75	0	-209.48	2142.45	2547.01
701.01	446	3032.81	4689	68.68	-155.55	2002.19	2212.22
731.48	459	3079.71	3809.81	278	33.69	3181.95	2918.02
761.96	475	3104.31	4063.8	398.66	116.39	2994.42	3157.37
792.44	490	3133.68	2770.77	1942	1094	3140.04	
822.92	512	3118.09	6773				
853.4	521	3181.22	3585.71	CHBK-1			
883.88	538	3194	3585.71	0	-65	2153.85	2897.06
914.36	555	3206	3585.71	197	71	3577.46	3194.24
944.83	572	3217.29	3585.71	1307	766	3229.77	4444.44
975.31	589	3227.92	3809.81	1875	1021.6	3533.67	4461.26
1005.79	605	3243.31	4354.07	2600	1346.62	3757.56	4453.84
1036.27	619	3268.43	4063.8	4170	2051.63	3996.82	
1066.75	634	3287.25	4354.07				
1097.23	648	3310.3	4354.07	TAR-1			
1127.7	662	3332.37	4063.8	10	0		1142.86
1158.18	677	3348.58	4063.8	106	168	1142.86	2345.34
1188.66	692	3364.08	4689	2011	1792.5	2232.64	7485.71
1219.14	705	3388.51	4063.8	2469.5	1915	2568.67	1826.35
1249.62	720	3402.58	4354.07	2622	2082	2509.13	5600
1280.1	734	3420.73	4354.07	2650	2092	2523.9	
1310.58	748	3438.2	3809.81				
1341.05	764	3445.98	5079.75	AMS 1-8			
1371.53	776	3471.25	4063.8	0	-65	2153.85	2105.26
1402.01	791	3482.48	4354.07	500	410	2097.56	3174.6
1432.49	805	3497.64	4063.8	1000	725	2565.52	2105.26
1462.97	820	3508	4689	1500	1200	2383.33	10526.32
1493.45	833	3526.43	4354.07	2000	1295	2980.69	4761.9
1523.93	847	3540.11	4063.8	2500	1505	3229.24	5000
1554.4	862	3549.22	4354.07	3000	1705	3436.95	4878.05
1584.88	876	3562.08	4354.07	3500	1910	3591.62	
1615.36	890	3574.54	4689				
1645.84	903	3590.59	5079.75	CJ-1			
1676.32	915	3610.12	5079.75	0	0		1973.68
1706.8	927	3629.14	5541.55	750	760	1895	2450.33
1737.28	938	3651.57	5079.75	1485.1	1360	2140	2829.55
1767.75	950	3669.61	5541.55	2107.6	1800	2308.56	5318.95
1798.23	961	3691.03	5079.75	3525.1	2333	2996.31	4044.19
1828.71	973	3708.16	5079.75	4065	2600	3103.92	6933.33
1859.19	985	3724.87	5541.55	4325	2675	3211.29	
1889.67	996	3744.94	5079.75				
1920.15	1008	3760.83	5079.75				
1950.62	1020	3776.34	5265.42				
1971.69	1028	3787.93					

MD	TWT	Ave. vel.	Int. vel.
Daora 1-1			
0	-6.2	6451.61	2145
500	460	2086.96	2500
1000	860	2279.07	2166.67
1091	944	2269.07	4247.79
1331	1057	2480.61	2747.97
1500	1180	2508.47	3448.28
2000	1470	2693.88	3448.28
2500	1760	2818.18	1918.7
2618	1883	2759.43	1575.22
2707	1996	2692.38	-36625
3000	1980	3010.1	5555.56
3500	2160	3222.22	
EA 1			
0	-250.83	1993.38	1990.38
171.67	-78.33	2000	1855.62
273.72	31.66	1498.42	1497.98
564.62	420.05	1498.01	1498.11
598.29	465	1498.02	1498.01
696.17	595.68	1498.02	1497.84
788.25	718.63	1497.99	1541.2
825	766.32	1500.68	1623.41
929.97	895.64	1518.4	1623.52
1270	1314.52	1551.9	1623.5
2396	2701.65	1588.66	
HM-1			
11.3	0		1522.14
522.74	672	1522.14	1887.35
964.38	1140	1672.07	2122.04
1193.56	1356	1743.75	2250.51
1416.36	1554	1808.31	2104.52
1504.75	1638	1823.5	2680.29
1595.88	1706	1857.66	2702.99
2971.7	2724	2173.57	3155.33
3303.01	2934	2243.84	
MO-2			
9.8	0		1556.92
111	130	1556.92	3028.85
426	338	2462.72	2075.68
618	523	2325.81	2248.85
862	740	2303.24	2503.31
1240	1042	2361.23	2607.14
1386	1154	2385.1	2742.86
1434	1189	2395.63	2532.26
1905	1561	2428.19	2959.35
2087	1684	2466.98	
MO-6			
9.5	0		1175
108.2	168	1175	1947.66
382.82	450	1659.2	2314.19
581.84	622	1840.32	2229.76
947.52	950	1974.78	3396.78
1633.67	1354	2399.07	3744.98
2468.8	1800	2732.56	4164.01
3651.38	2368	3075.91	

MD	TWT	Ave. vel.	Int. vel.
LAY 8-2			
0	-25	800	2170.21
69.87	39.39	3039.86	3038.36
108.29	64.68	3039.27	3039.78
158.34	97.61	3039.44	3039.6
1186.5	774.12	3039.58	3030.3
1187	774.45	3039.58	3039.52
1392.73	909.82	3039.57	3130.03
1504.3	981.11	3046.14	3142.86
1504.41	981.18	3046.15	3130.23
1544.79	1006.98	3048.3	3230.77
1545	1007.11	3048.33	3129.39
1587.81	1034.47	3050.47	3130.76
1691	1100.39	3055.28	3129.97
1750	1138.09	3057.75	3130.35
1942	1260.76	3064.82	
MO-3			
9.1	0		1321.88
114.85	160	1309.88	3407.6
285.23	260	2116.69	3901.23
412.02	325	2473.6	2061.77
819.22	720	2247.67	2854.65
1021.9	862	2347.66	5392.31
1092	888	2436.8	6597.68
1633.01	1052	3085.46	4594.44
1757.06	1106	3159.13	4105.29
1826.85	1140	3187.35	4281.67
2186.51	1308	3327.91	
MO-7			
10	0		1362.11
100.58	133	1362.11	2272.88
167.63	192	1641.98	1871.58
380.99	420	1766.62	2236.55
691.87	698	1953.78	3371.75
1770.83	1338	2632.03	3217.22
1886.65	1410	2661.91	3579.91
4263.71	2738	3107.17	4183.64
4309.73	2760	3115.75	
15-A-1			
0	0		1815.13
108	119	1647.06	1577.53
459	564	1592.2	1890.49
1115	1258	1756.76	2392.86
1182	1314	1783.87	2792.45
1256	1367	1822.97	2611.11
1397	1475	1880.68	2750
1441	1507	1899.14	2363.64
1454	1518	1902.5	2666.67
1482	1539	1912.93	2769.23
1500	1552	1920.1	2536.08
1623	1649	1956.34	3183.92
2930	2470	2364.37	4262.77
3222	2607	2464.14	5200
3495	2712	2570.06	

MD	TWT	Ave. vel.	Int. vel.
PC-1			
0	-25	1280	1276.87
1.96	-21.93	1280.44	1281.69
3.78	-19.09	1280.25	2802.51
369.9	242.19	2922.5	2013.66
732.64	602.47	2379.01	3321.03
1186.26	875.65	2672.89	3320.87
1406.45	1008.26	2758.12	3320.92
1605.29	1128.01	2817.87	3321.08
1861.86	1282.52	2878.49	3321.3
1965.85	1345.14	2899.1	3320.81
2200	1486.16	2939.12	3320.97
3220.07	2100.48	3050.8	3321.14
3554.06	2301.61	3074.42	3320.13
3590.1	2323.32	3076.72	3320.89
3719.1	2401.01	3084.62	
MO-8			
0	0		1512.69
298	394	1464.47	1973.68
448	546	1606.23	2557.38
760	790	1900	2471.26
975	964	2003.11	1500
981	972	1998.97	2573.03
1210	1150	2087.83	2357.14
1243	1178	2094.23	2333.33
1348	1268	2111.2	1212.64
1453.5	1442	2002.77	10638.89
1645	1478	2213.13	3294.87
1773.5	1556	2267.35	3050
1834.5	1596	2286.97	3156.25
1885	1628	2304.05	3441.18
2002	1696	2349.65	3625
2118	1760	2396.02	4272.73
2212	1804	2441.8	2882.35
2261	1838	2449.95	3928.57
2316	1866	2472.13	5500
2459	1918	2554.22	5666.67
2612	1972	2639.45	5545.45
2734	2016	2702.88	6100
2795	2036	2736.25	5450
2849.5	2056	2762.65	6083.33
2886	2068	2781.91	3736.84
2957	2106	2799.15	7409.09
3038.5	2128	2846.8	6354.17
3191	2176	2924.17	5066.67
3343	2236	2981.66	6244.9
3496	2285	3051.64	3932.2
3612	2344	3073.81	

Appendix IV
Phil input (Reverse modeling)
i) Eustatic Sea-level
ii) Lithologies, initial porosity and compaction rates considered for reverse basin modeling (from Contreras, 2011)

```
Eustatic Sea-level
col.1: Ma
col.2: depthbelowsealevel (m)
SL
M
0        0
5.32     50
16.4     100
23.8     65
28.5     70
33.7     130
54.8     150
65       180
71.3     200
83.5     175
85.8     200
89       220
93.5     210
98.9     215
112.2    130
121      100
127      175
132      125
137      75
144.2    125
150.7    150
154.1    145
159.4    95
164.4    45
169.2    90
180.1    45
189.6    25
204.3    -15
220.7    -5
234.3    -20
259.3    -25
5000     -25
9999
```

Lithology	Density [kg/m^3]	Initial porosity [φ_0]	Compact. rate [r_0]
Coarse sand to cobbles	2650	0.40	0.0001
Quartz silt size	2650	0.30	0.0010
Quartz silt/clay	2650	0.45	0.0030
Quartz sand/clay	2650	0.40	0.0020
Interbedded quartz/silt	2650	0.50	0.0005
Interbedded silt/clay	2750	0.50	0.0020
Marine mud	2750	0.50	0.0030
Clay	2750	0.50	0.0030
Silt/coal	2450	0.60	0.0080
Clay/coal	2300	0.85	0.0090
Coal	2000	0.92	0.0100
Cemented carbonate	2800	0.45	0.0001
Carbonate fine grainstone	2800	0.60	0.0010
Carbonate coarse grainstone	2800	0.70	0.0005
Carbonate boundstone	2800	0.60	0.0020
Micrite	2800	0.70	0.0040
Algal laminates	2800	0.60	0.0005
Dolomite	2900	0.40	0.0001
Gypsum	2330	0.10	0.00001
Evaporites	2150	(?) 0.05	0.00001

Appendix V
Phil output (Reverse modeling)
Sediment flux rates

Tan Tan		Cap Juby		Laâyoune	
Ma	m^2/m.y.	Ma	m^2/m.y.	Ma	m^2/m.y.
0	2912.89	0	15840.7	0	15913.5
16.4	1378.51	16.4	4397.78	16.4	10529.4
23.8	779.084	23.8	4607.83	23.8	5093.11
28.5	661.19	28.5	4474.11	28.5	2919.16
33.7	151.857	33.7	916.207	33.7	1062.97
54.8	390.931	54.8	1533.88	54.8	1291.44
65	319.304	65	4.75142	65	131.607
Hiatus		Hiatus		71.3	65.4996
				83.5	528.704
		85.8	998.644	85.8	352.561
89	1038.56	89	6742.34	89	2934.95
93.5	3675.52	93.5	2955.9	93.5	2900.79
98.9	2350.58	98.9	1790.08	98.9	1811.88
112.2	10892.6	112.2	8225.81	112.2	4554.53
121	10187.2	121	7427.5	121	11307.1
127	12900.6	127	21136.8	127	29570.1
132	11761.9	132	15662.2	132	31558.1
137	3347.71	137	9312.57	137	10415.1
144.2	2764.57	144.2	3843.54	144.2	3194.59
150.7	11755.4	150.7	18433.4	150.7	22466.4
154.1	6368.26	154.1	12410.4	154.1	12331.2
159.4	4783.86	159.4	12274.8	159.4	12535.4
164.4	7397.85	164.4	9419.79	164.4	10478.5
169.2	4869.36	169.2	10088.6	169.2	6629.34
180.1	8184.85	180.1	12032.6	180.1	5393.02
189.6	10760.5	189.6	6761.51	189.6	5124.05
204.3	8584.53	204.3	9308.67	204.3	9292.89
220.7	11636.2	220.7	10701.3	220.7	9505.32
234.3	1527.86	234.3	1977.3	234.3	3615.58
259.3	-5.33E+07	259.3	-6.85E+07	259.3	-7.38E+07
259.301	-5.33E+07	259.301	-6.85E+07	259.301	-7.38E+07
9999.99999	-5.33E+07	9999.99999	-6.85E+07	9999.99999	-7.38E+07

Appendix VI
Phil output (Reverse modeling)
Subsidence rates and basin architecture (graphic output)
for numerical output catalogue (350 p.) contact author

Tan Tan transect, present day to Late Permian age in ka, V.E.: vertical exaggeration

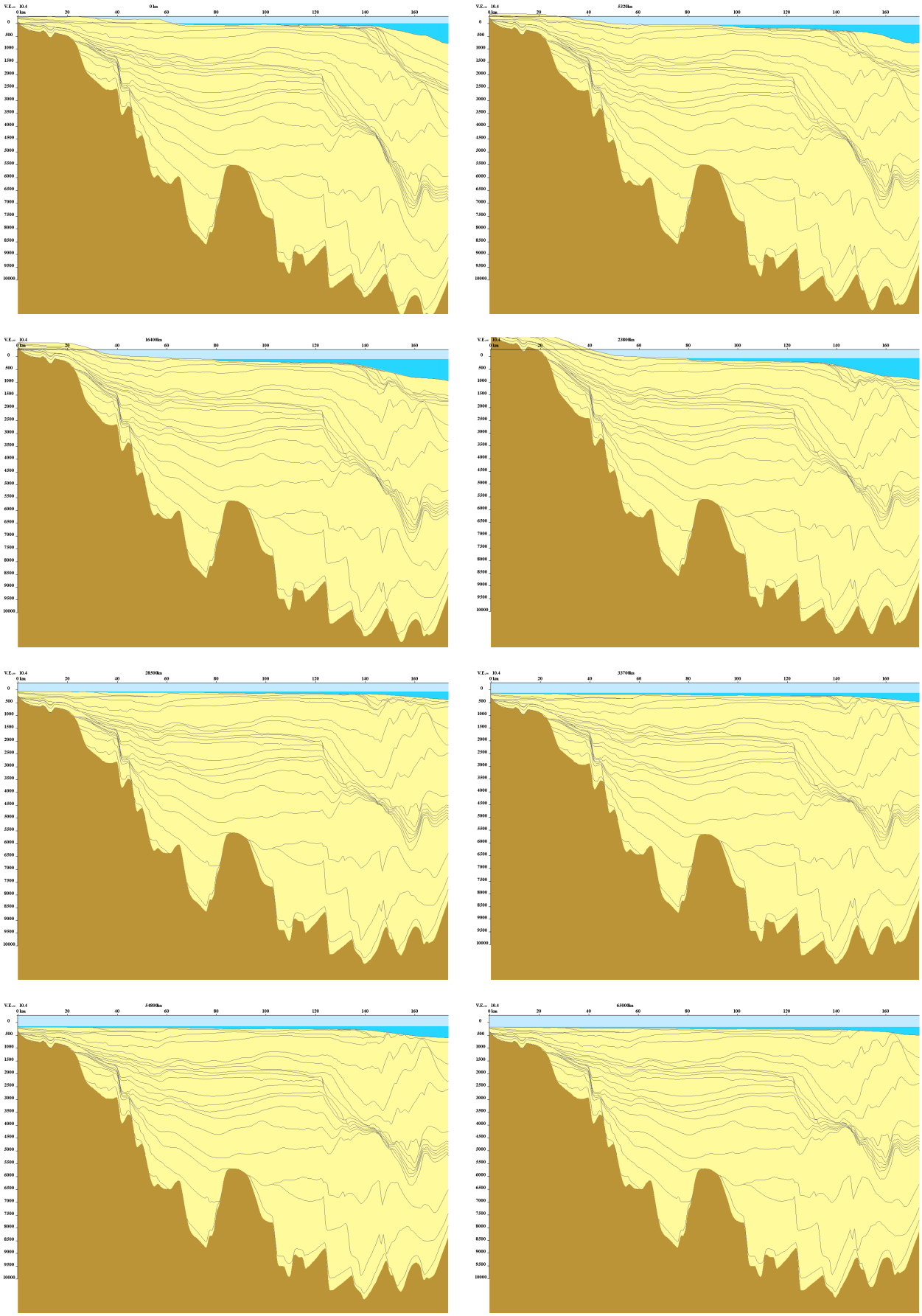

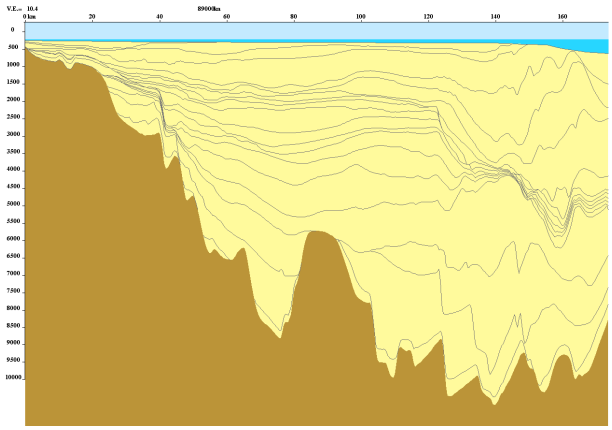

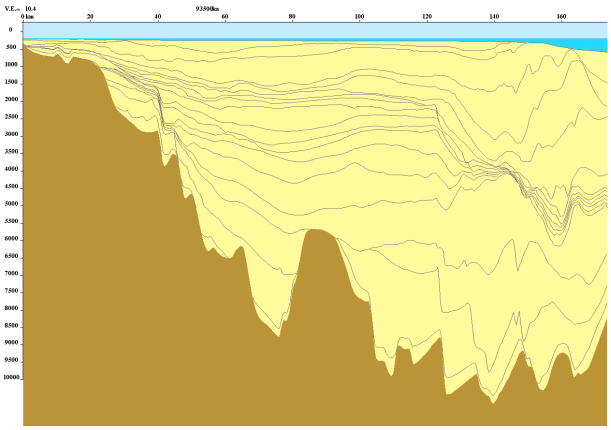

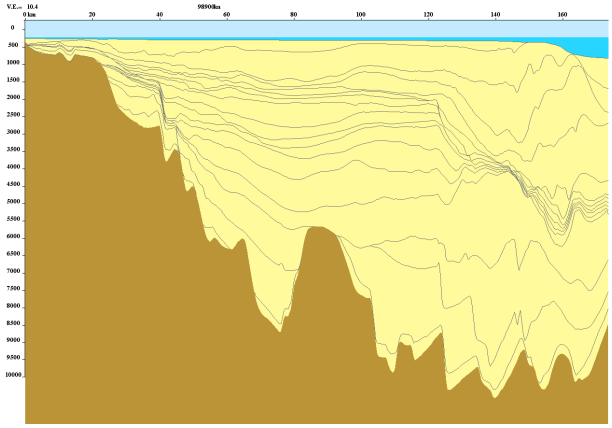

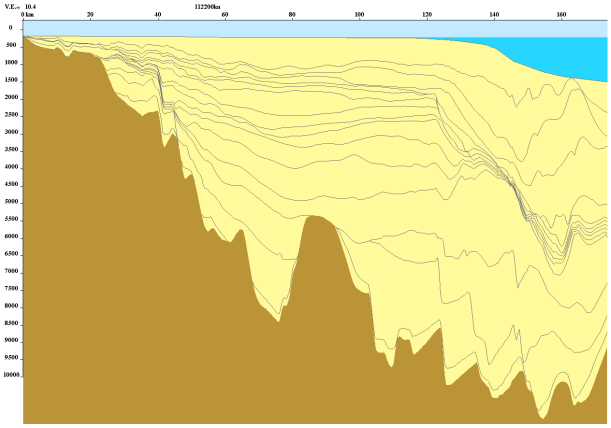

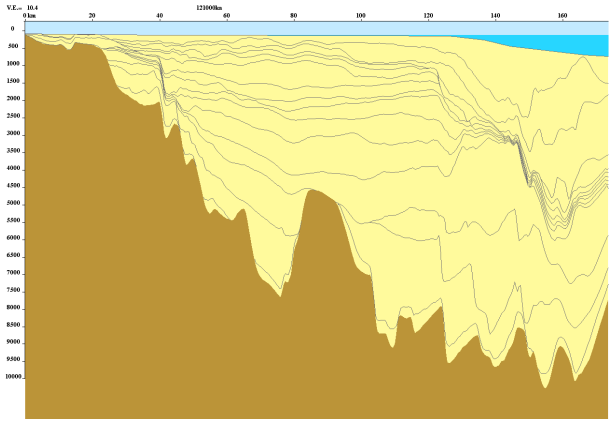

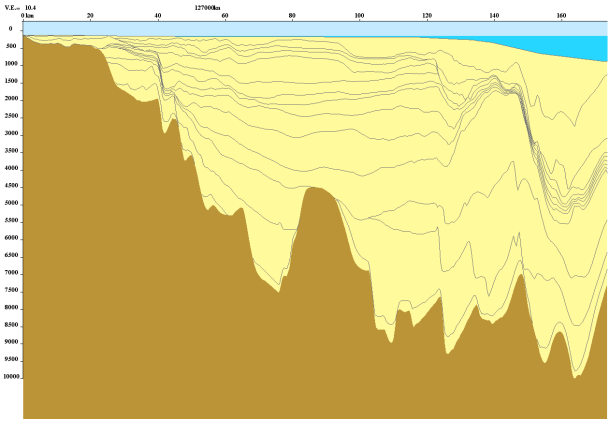

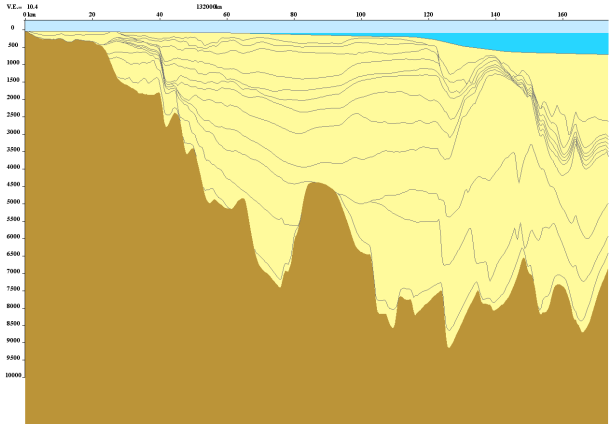

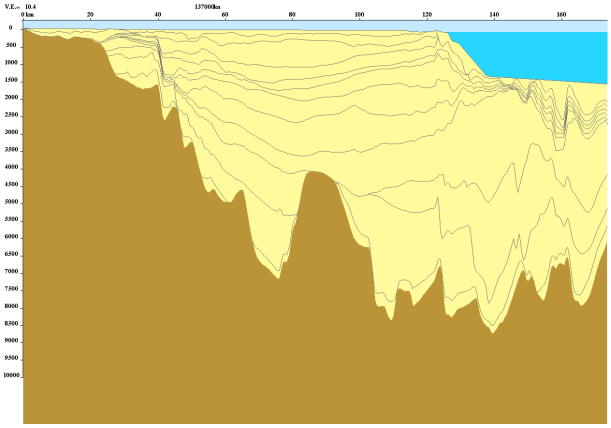

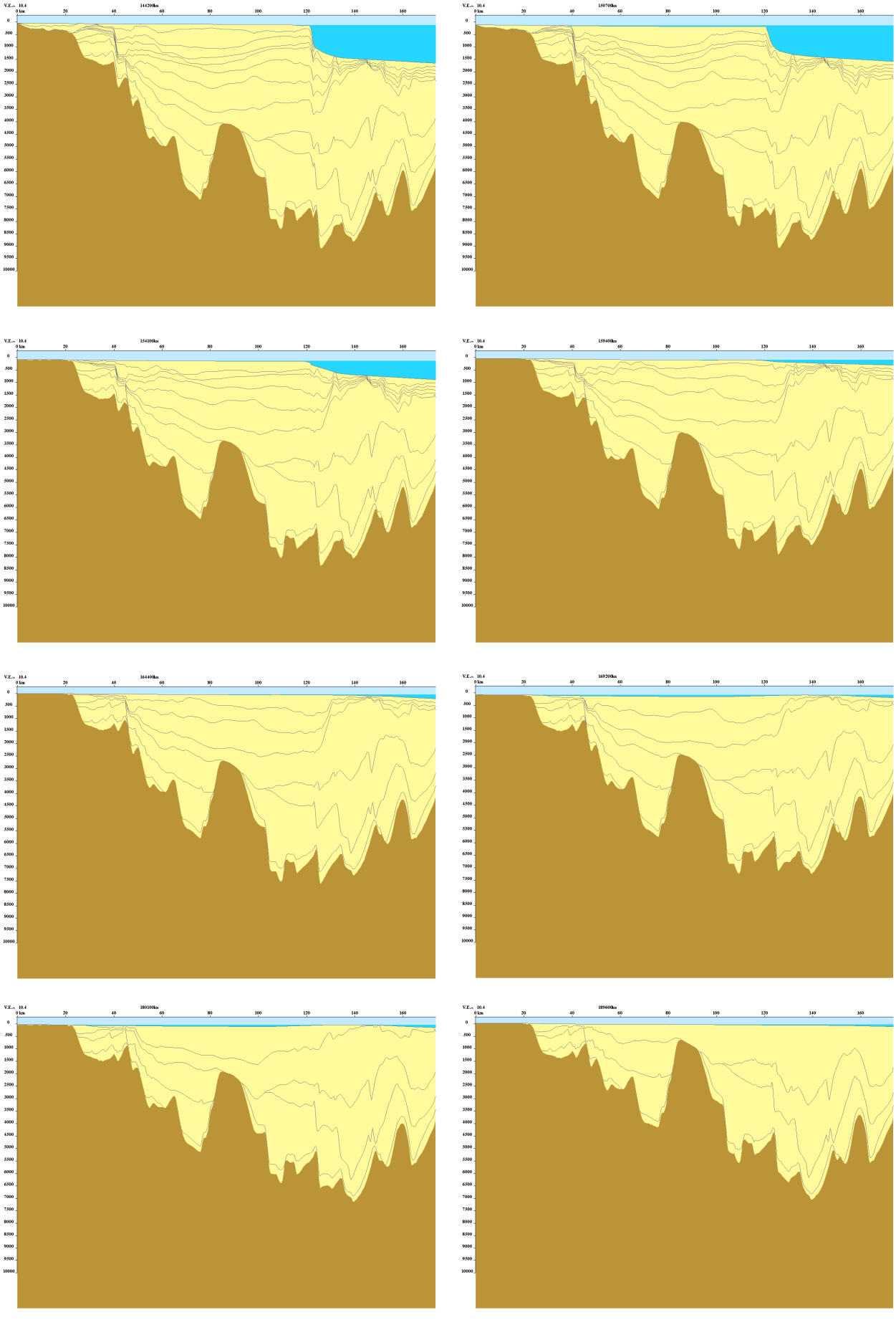

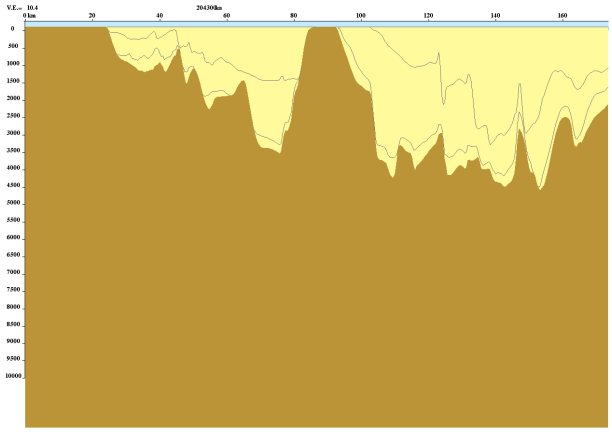
V.E.= 10.4
204300km
0 km
20
40
60
80
100
120
140
160
0
500
1000
1500
2000
2500
3000
3500
4000
4500
5000
5500
6000
6500
7000
7500
8000
8500
9000
9500
10000

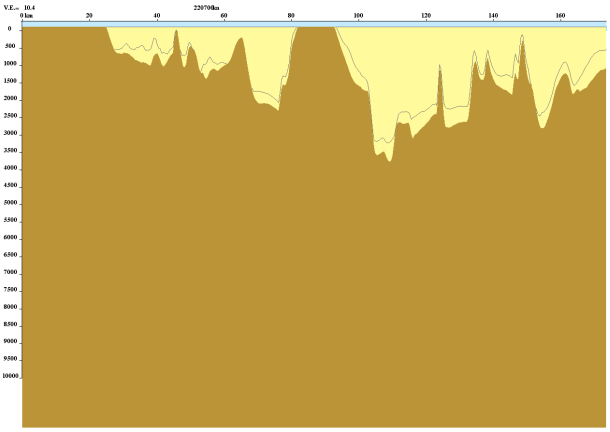
V.E.= 10.4
220700km
0 km
20
40
60
80
100
120
140
160
0
500
1000
1500
2000
2500
3000
3500
4000
4500
5000
5500
6000
6500
7000
7500
8000
8500
9000
9500
10000

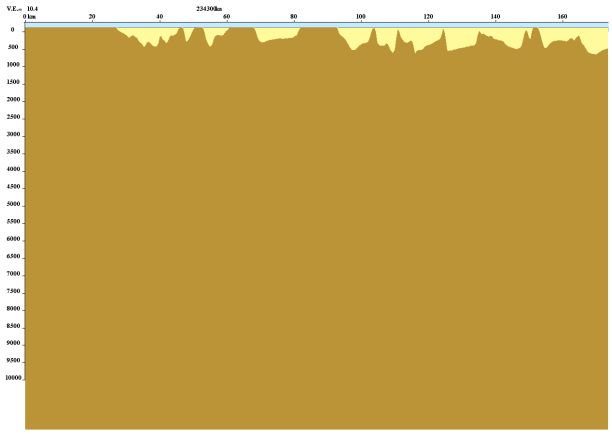
V.E.= 10.4
234300km
0 km
20
40
60
80
100
120
140
160
0
500
1000
1500
2000
2500
3000
3500
4000
4500
5000
5500
6000
6500
7000
7500
8000
8500
9000
9500
10000

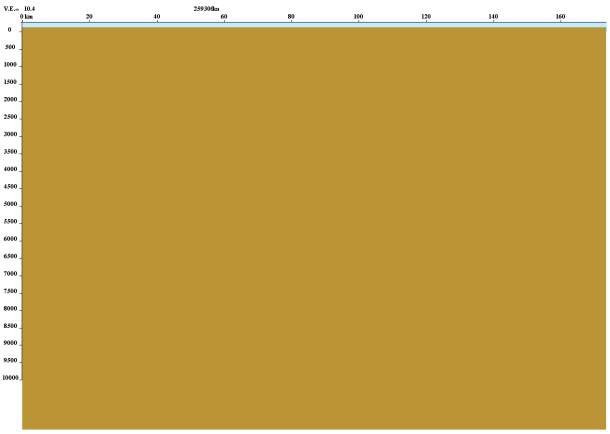
V.E.= 10.4
259300km
0 km
20
40
60
80
100
120
140
160
0
500
1000
1500
2000
2500
3000
3500
4000
4500
5000
5500
6000
6500
7000
7500
8000
8500
9000
9500
10000

Cap Juby transect, present day to Late Permian age in ka, V.E.: vertical exaggeration

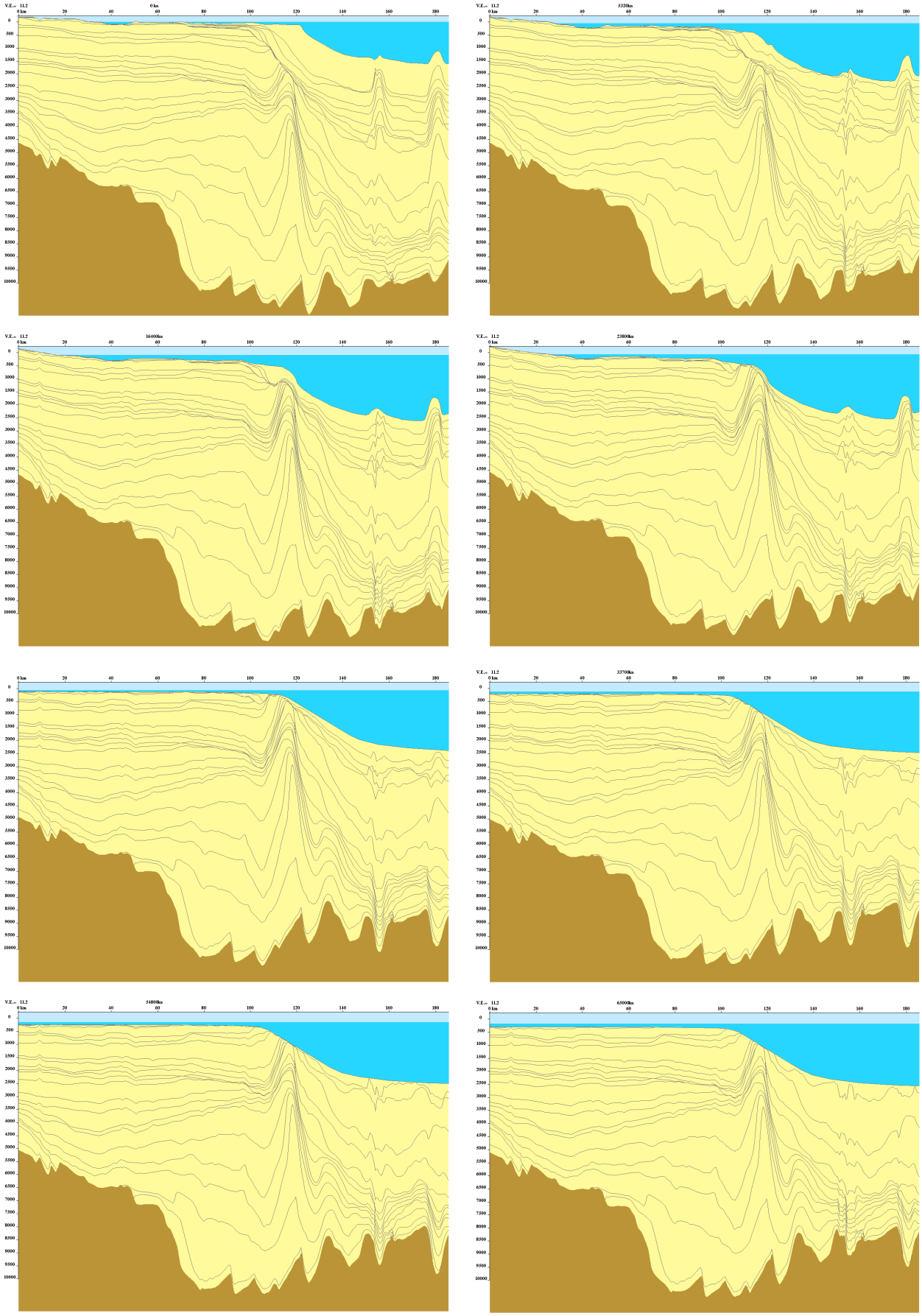

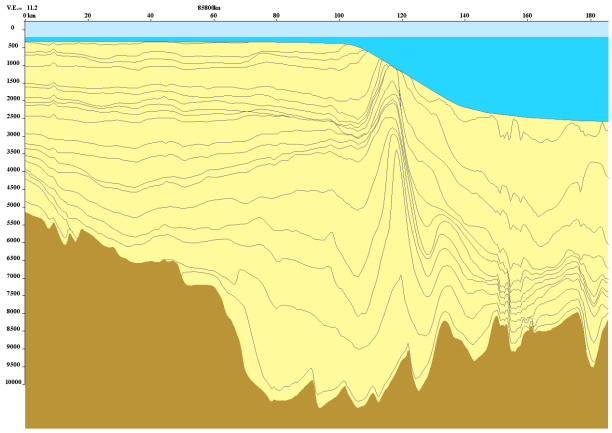

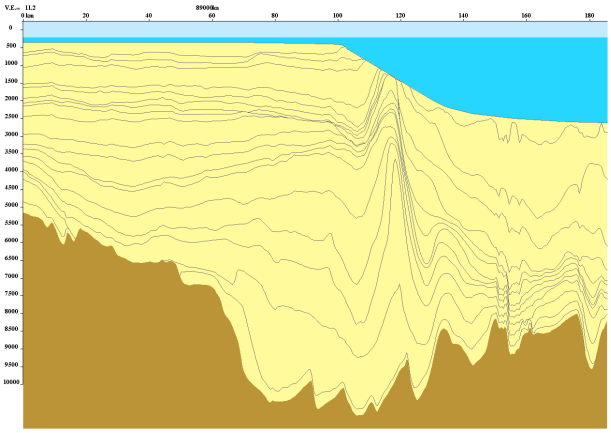

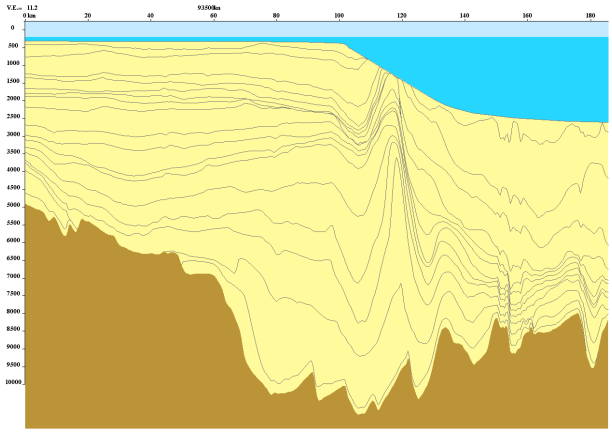

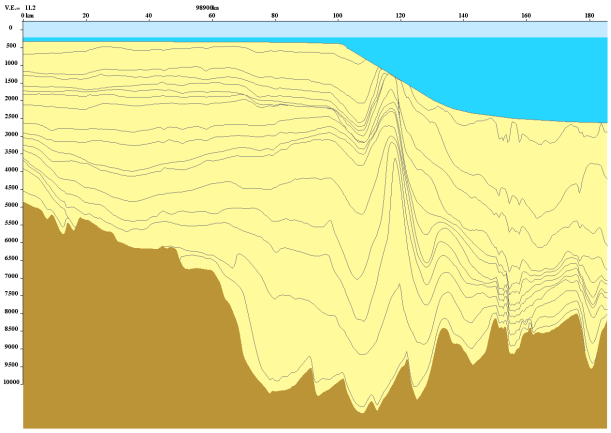

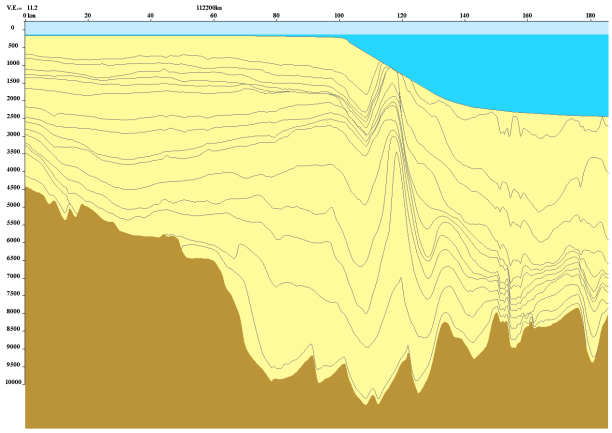

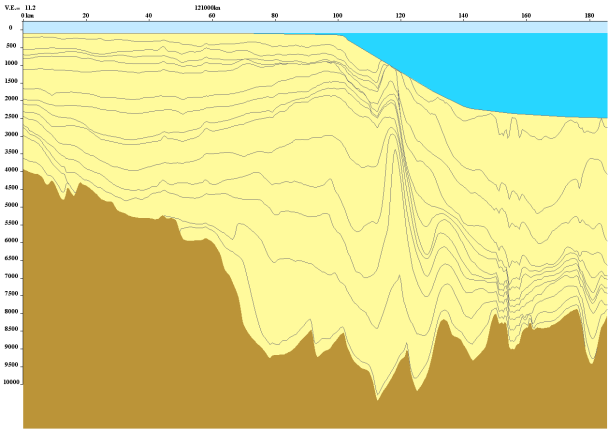

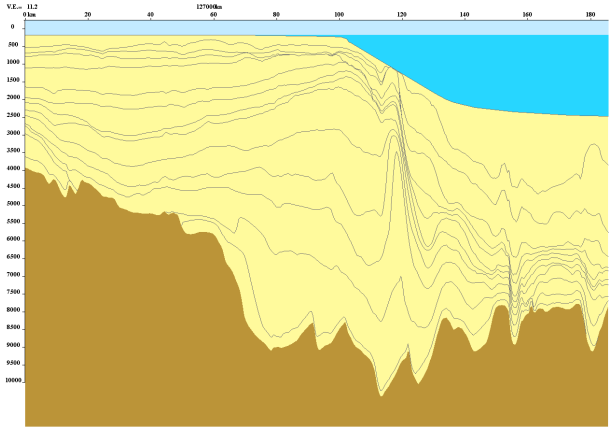

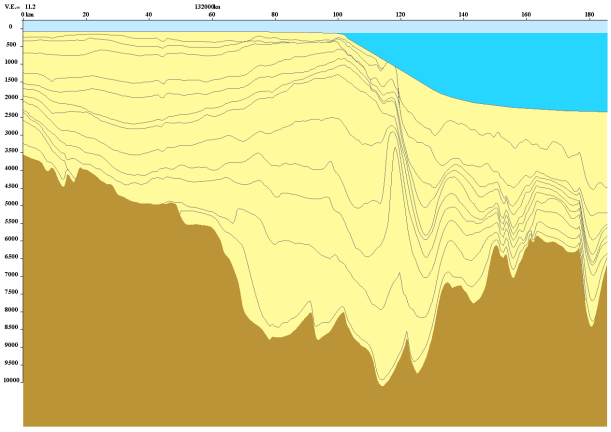

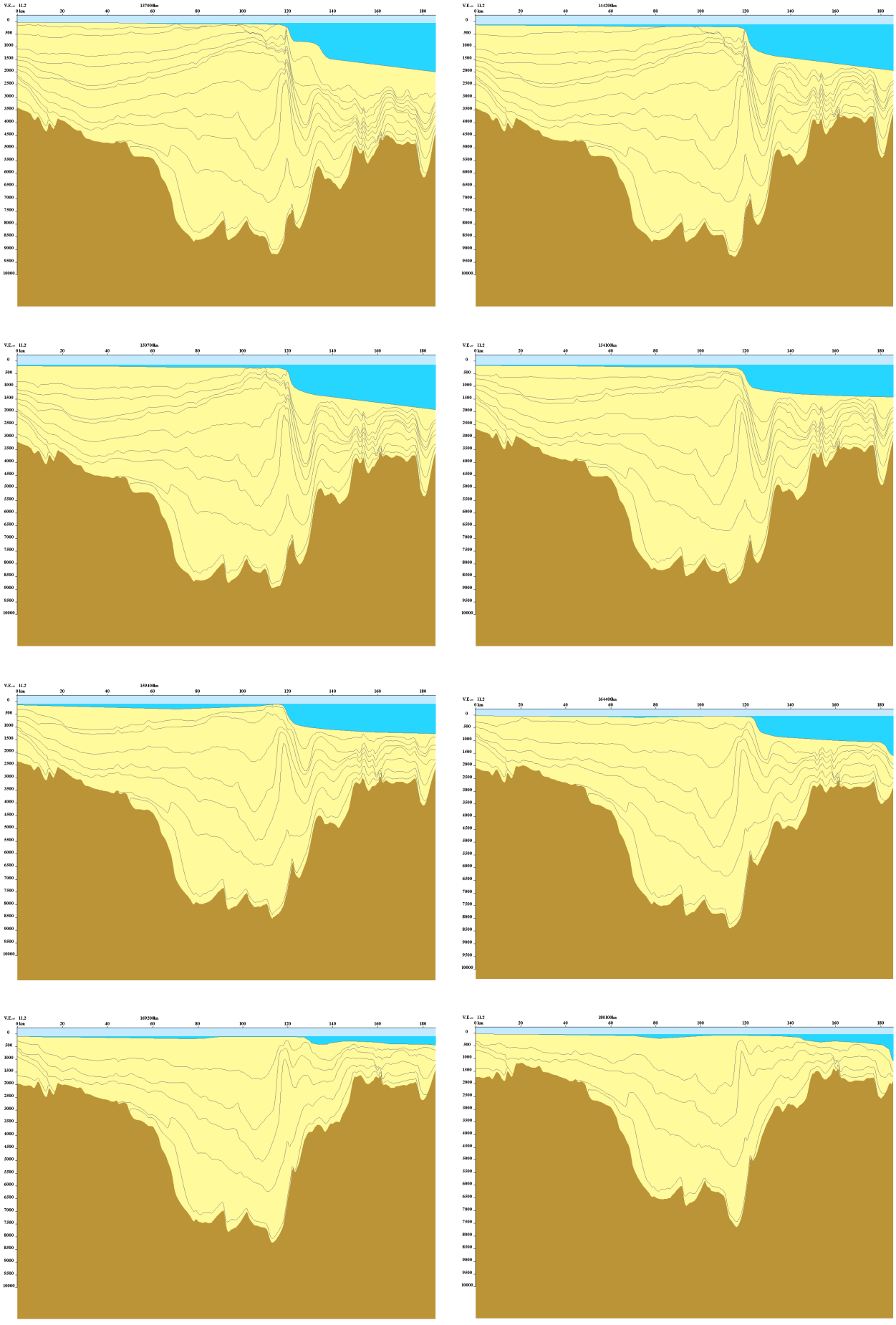

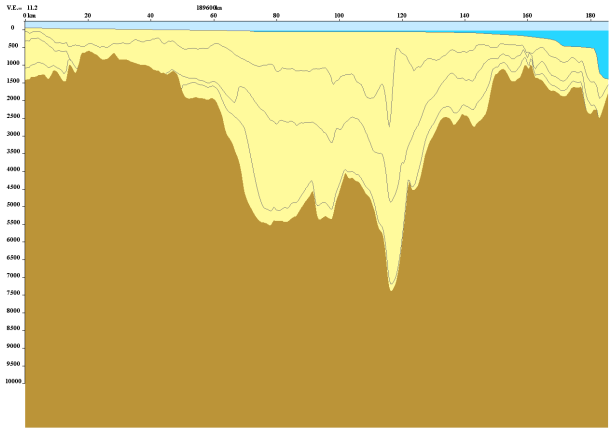

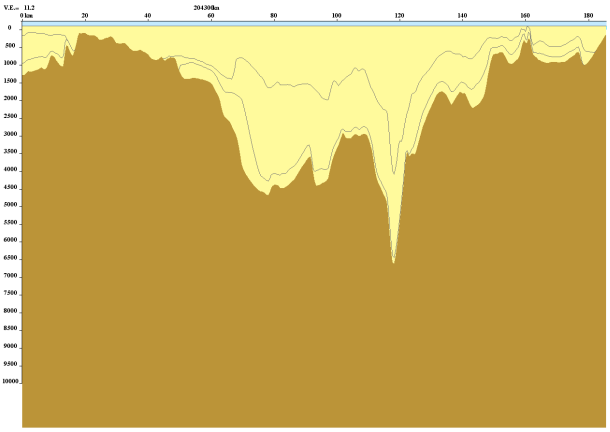

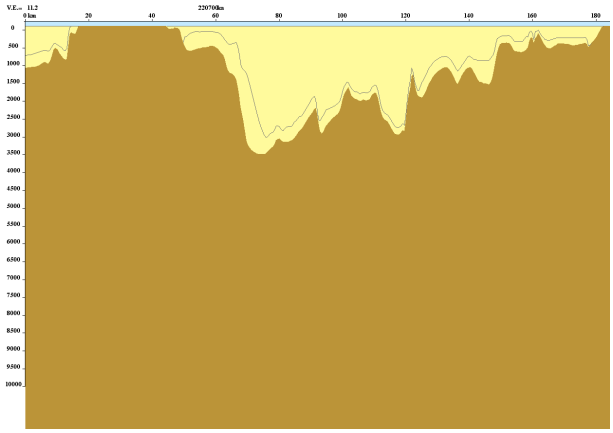

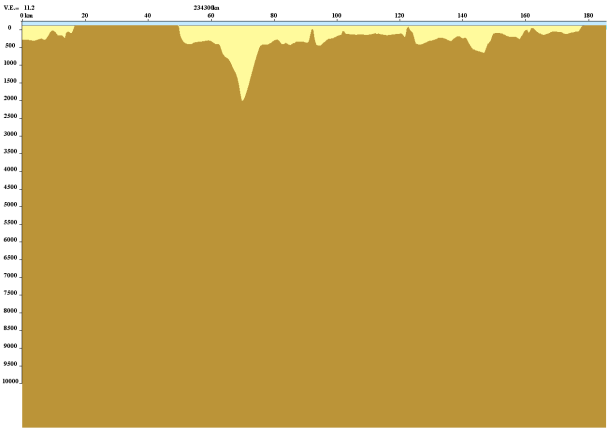

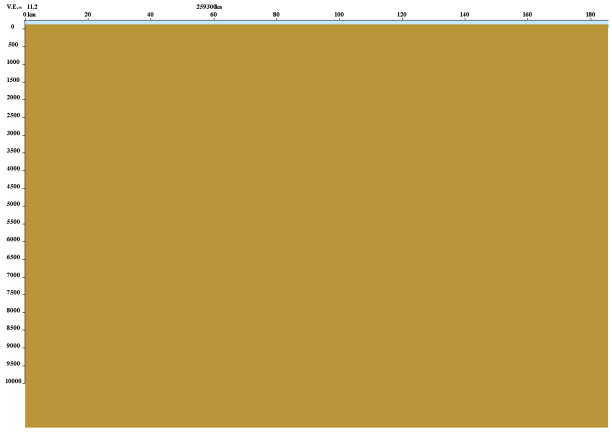

Laâyoune transect, present day to Late Permian age in ka, V.E.: vertical exaggeration

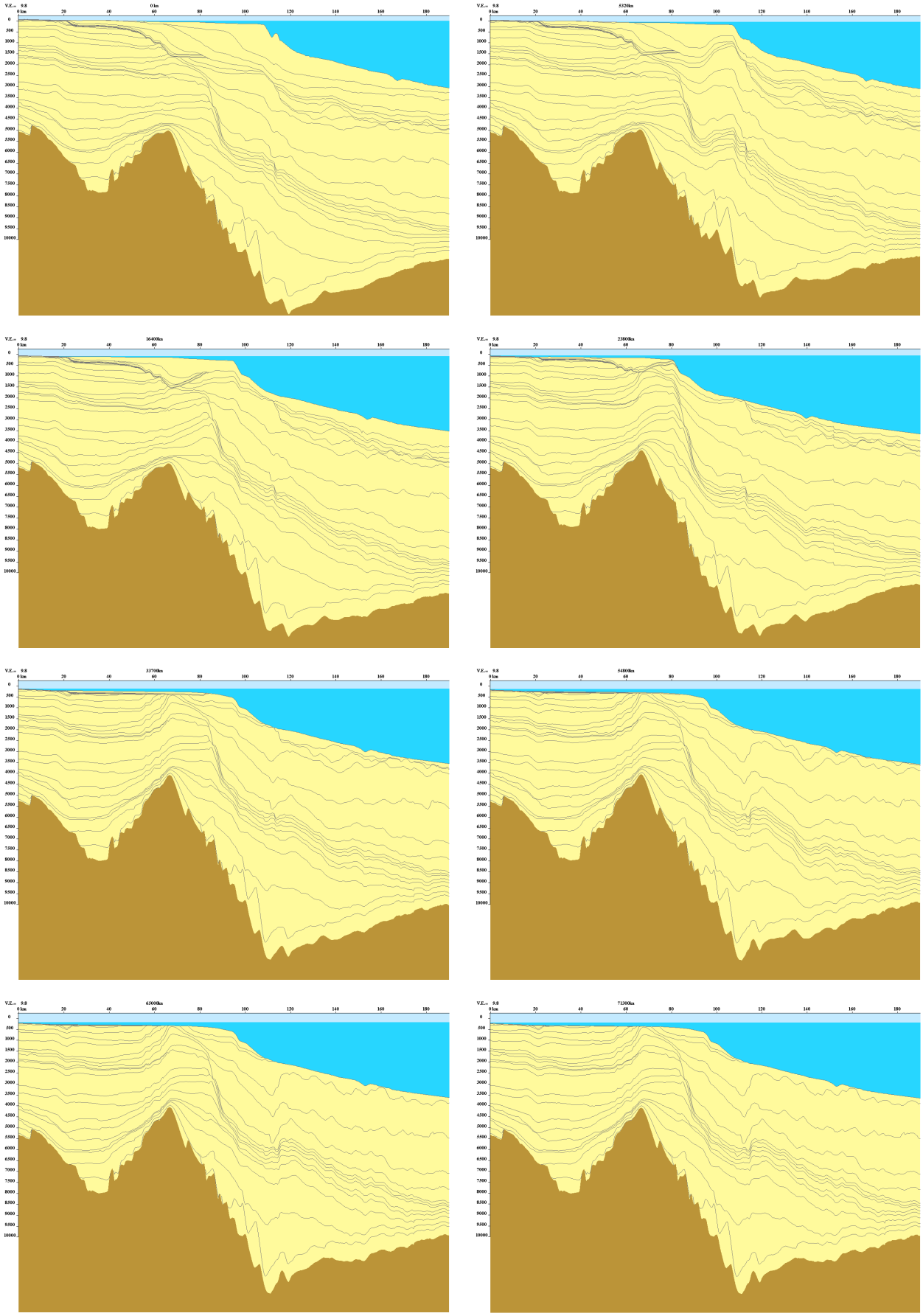

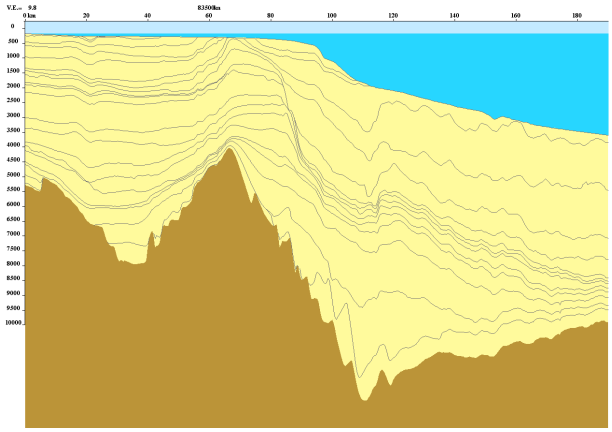

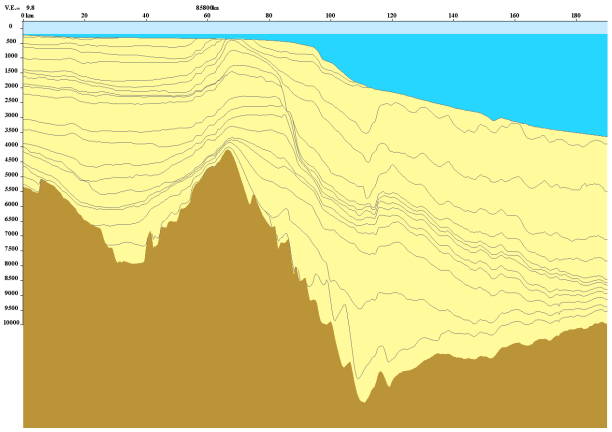

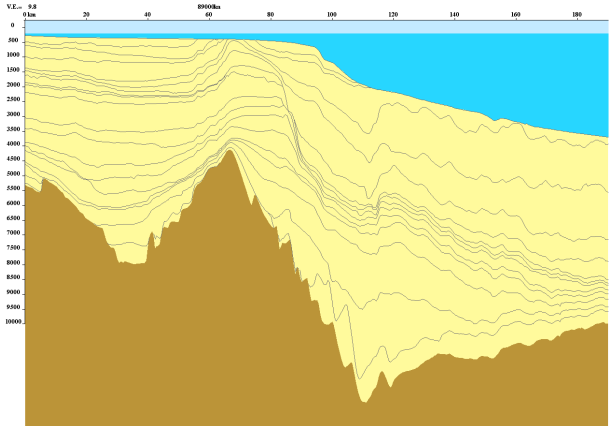

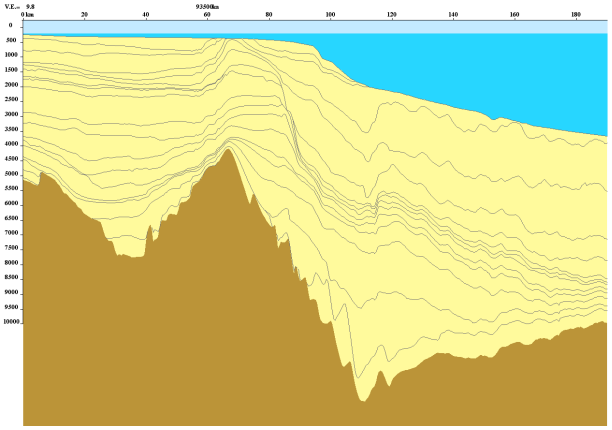

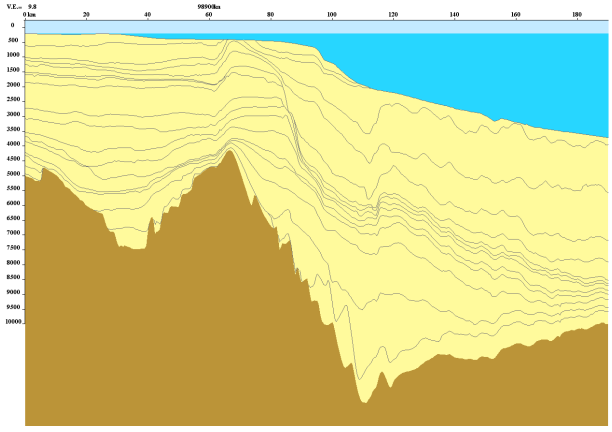

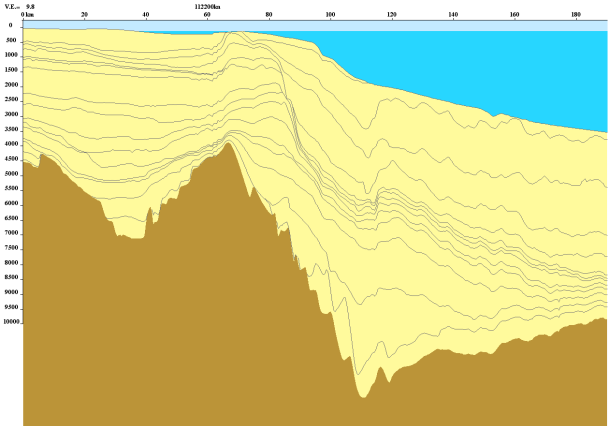

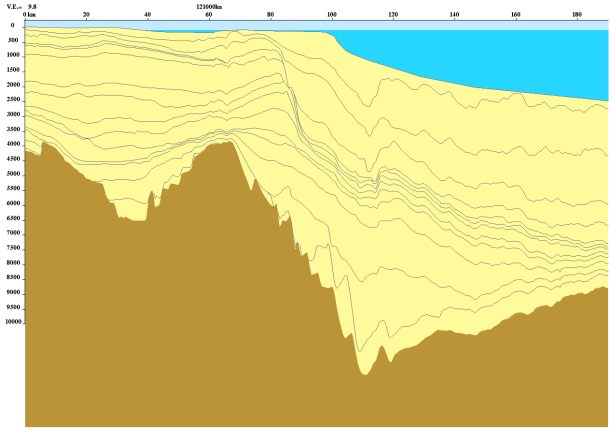

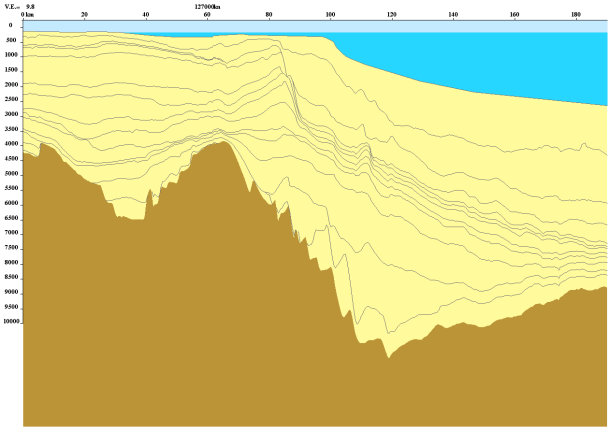

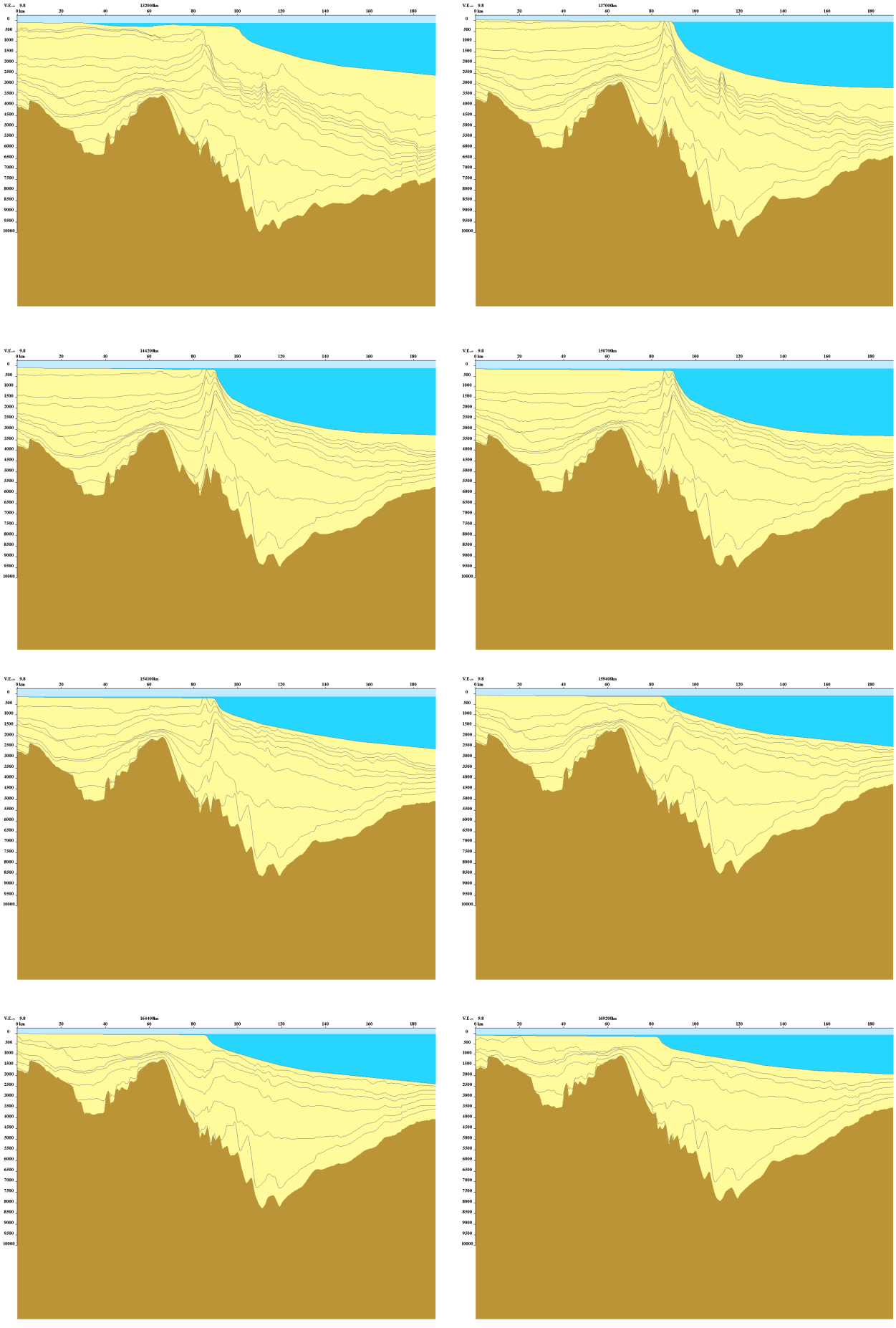

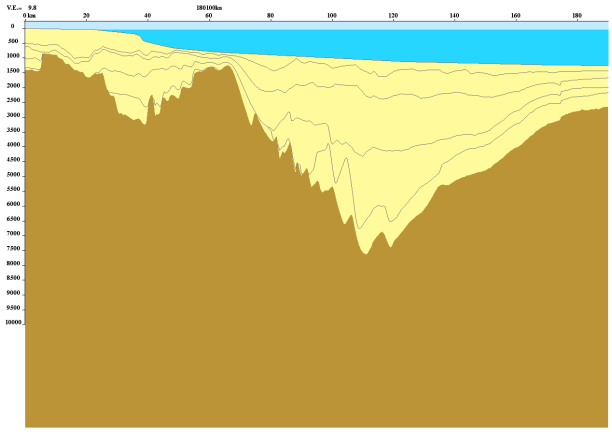

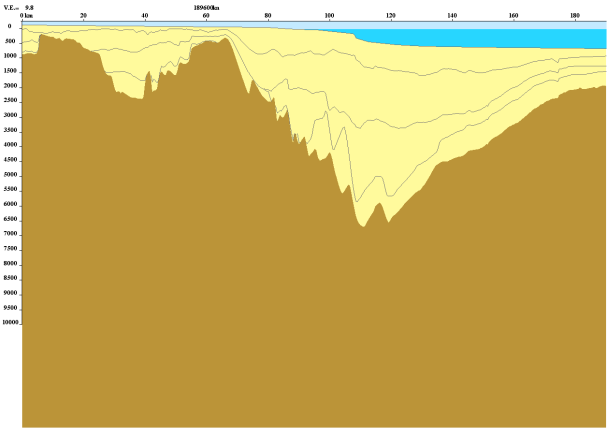

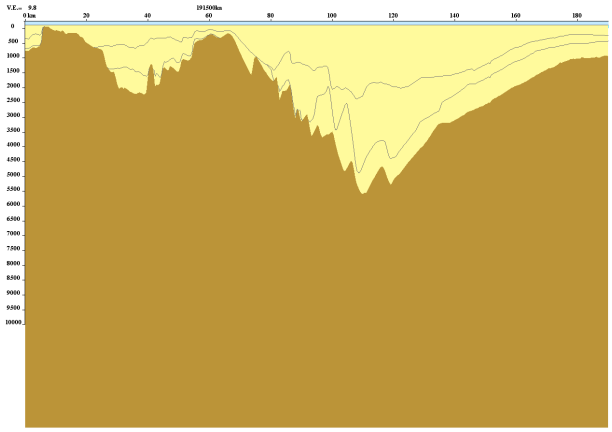

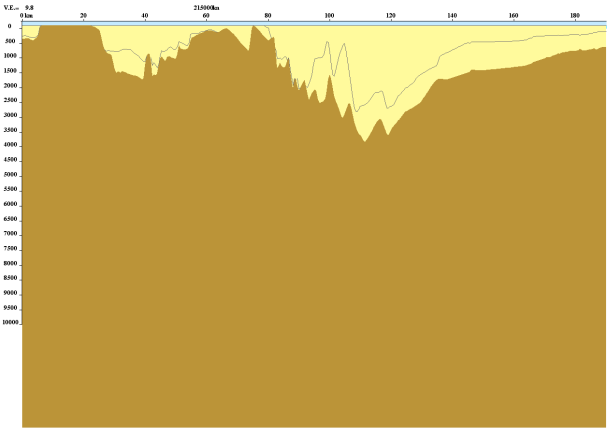

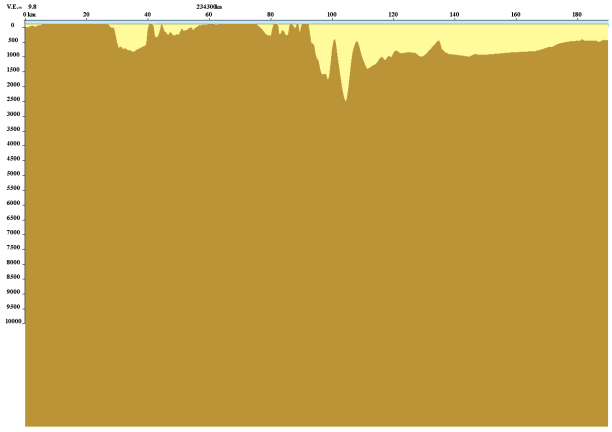

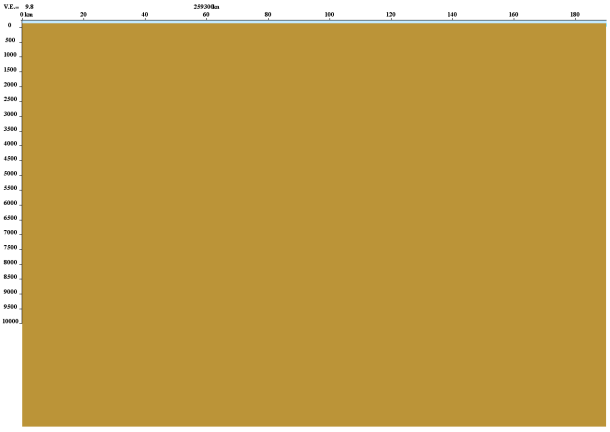

Eidesstattliche Versicherung gemäß § 8 der Promotionsordnung der Naturwissenschaftlich-Mathematischen Gesamtfakultät der Universität Heidelberg

1. Bei der eingereichten Dissertation zu dem Thema

Sequence stratigraphy and basin analysis of the Meso-to Cenozoic Tarfaya-Laâyoune Basins, On- and offshore Morocco

handelt es sich um meine eigenständig erbrachte Leistung.

2. Ich habe nur die angegebenen Quellen und Hilfsmittel benutzt und mich keiner unzulässigen Hilfe Dritter bedient. Insbesondere habe ich wörtlich oder sinngemäß aus anderen Werken übernommene Inhalte als solche kenntlich gemacht.

3. Die Arbeit oder Teile davon habe ich wie folgt/bislang nicht[1)] an einer Hochschule des In- oder Auslands als Bestandteil einer Prüfungs- oder Qualifikationsleistung vorgelegt.

Titel der Arbeit: _____

_____

Hochschule und Jahr: _____

Art der Prüfungs- oder Qualifikationsleistung: _____

4. Die Richtigkeit der vorstehenden Erklärungen bestätige ich.

5. Die Bedeutung der eidesstattlichen Versicherung und die strafrechtlichen Folgen einer unrichtigen oder unvollständigen eidesstattlichen Versicherung sind mir bekannt.

Ich versichere an Eides statt, dass ich nach bestem Wissen die reine Wahrheit erklärt und nichts verschwiegen habe.

Heidelberg, 17.09.14
Ort und Datum

Unterschrift

[1)] Nicht Zutreffendes streichen. Bei Bejahung sind anzugeben: der Titel der andernorts vorgelegten Arbeit, die Hochschule, das Jahr der Vorlage und die Art der Prüfungs- oder Qualifikationsleistung.

12/2012

Addendum

The figures 19 on page 18, as well as 101 and 102 on page 94 have incomplete captions.

The first sentence in the caption of figure 19 reads in the submitted manuscripts as follows:
„Southern Moroccan Basin as a transition between continent and ocean (modified after MICHARD et al. 2008)."
This has to be corrected to:
„Southern Moroccan Basin as a transition between continent and ocean (modified from MIERNIK 2012, after MICHARD et al. 2008).

The first sentence in the caption of figure 101 reads in the submitted manuscripts as follows:
„Chronostratigraphic plot of the Laâyoune transect with sequence stratigraphic interpretation following NEAL& ABREU (2009)."
This has to be corrected to:
„Chronostratigraphic plot of the Laâyoune transect with sequence stratigraphic interpretation following NEAL& ABREU (2009). Modified from MIERNIK, 2012.

The first sentence in the caption of figure 102 reads in the submitted manuscripts as follows:
„Chrono-stratigraphic diagram of the Laâyoune tran. with highlighted source and reservoir facies distribution."
This has to be corrected to:
„Chrono-stratigraphic diagram of the Laâyoune tran. with highlighted source and reservoir facies distribution (modified from MIERNIK, 2012).

One refernece has to be added to the reference list:

MIERNIK, G.J. (2012) Seismic Interpretation and High-Resolution Sequence Stratigraphic Modeling of the Tarfaya-Laâyoune Basin, Morocco. Unpublished Diploma Thesis, Institute of Earth Sciences, Heidelberg University, 63p.